Joint Dynamics and Adaptive Feedforward Control of Lightweight Industrial Robots

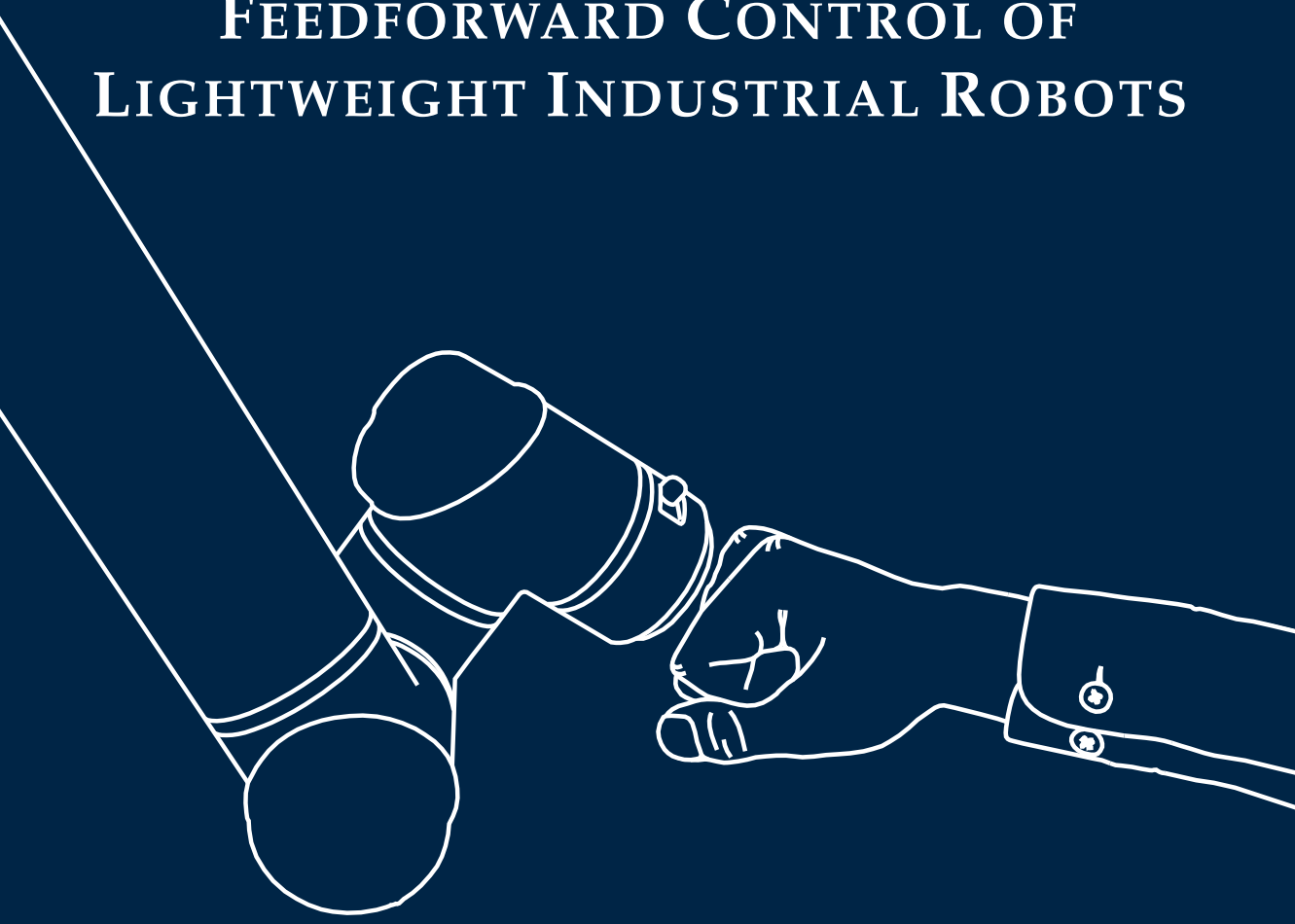

Emil Madsen

Department of Engineering
Aarhus University

A dissertation submitted for the degree of
Philosophiae Doctor

June, 2020

UNIVERSAL ROBOTS

AARHUS UNIVERSITY

PHD DISSERTATION

JOINT DYNAMICS AND ADAPTIVE FEEDFORWARD CONTROL OF LIGHTWEIGHT INDUSTRIAL ROBOTS

Author:
Emil Madsen

Supervisor:
Xuping Zhang

Company Supervisor:
David Brandt

Company Co-supervisor:
Oluf Skov Rosenlund

A dissertation submitted in fulfillment of the requirements for the degree of Philosophiae Doctor

in the

Department of Engineering

June, 2020

ISBN: 978-87-7507-485-3
DOI: 10.7146/aul.384

AARHUS UNIVERSITY

Abstract

Technical Sciences
Department of Engineering

Philosophiae Doctor

Joint Dynamics and Adaptive Feedforward Control of Lightweight Industrial Robots

by Emil Madsen

The use of lightweight strain-wave transmissions in collaborative industrial robots leads to structural compliance and a complex nonlinear behavior of the robot joints. Furthermore, wear and temperature changes lead to variations in the joint dynamics behavior over time. The immediate negative consequences are related to the performance of motion and force control, safety, and lead-through programming.

This thesis introduces and investigates new methods to further increase the performance of collaborative industrial robots subject to complex nonlinear and time-varying joint dynamics behavior. Within this context, the techniques of mathematical modeling, system identification, and adaptive estimation and control are applied. The methods are experimentally validated using the collaborative industrial robots by Universal Robots.

Mathematically, the robot and joint dynamics are considered as two coupled subsystems. The *robot dynamics* are derived and linearly parametrized to facilitate identification of the inertial parameters. Calibrating these parameters leads to improvements in torque prediction accuracy of 16.5 %–28.5 % depending on the motion.

The *joint dynamics* are thoroughly analyzed and characterized. Based on a series of experiments, a comprehensive model of the robot joint is established taking into account the complex nonlinear dynamics of the strain-wave transmission, that is the nonlinear compliance, hysteresis, kinematic error, and friction. The steady-state friction is considered to depend on angular velocity, load torque, and temperature. The dynamic friction characteristics are described by an Extended Generalized Maxwell-Slip (E-GMS) model which describes in a combined framework; hysteresis characteristics

that depend on angular position and Coulomb friction that depend on load torque. E-GMS model-based feedforward control improves the torque prediction accuracy by a factor 2.1 and improve the tracking error by a factor 1.5.

An E-GMS model-based adaptive feedforward controller is developed to address the issue of friction changing with wear and temperature. The adaptive control strategy leads to improvements in torque prediction of 84 % and tracking error of 20 %.

AARHUS UNIVERSITET

Resumé

Technical Sciences
Institut for Ingeniørvidenskab

Philosophiae Doctor

Joint Dynamics and Adaptive Feedforward Control of Lightweight Industrial Robots

af Emil Madsen

Brugen af strain-wave transmissioner i kollaborative industrirobotter fører til strukturel fleksibilitet samt en kompleks, ulineær respons af robotleddene. Endvidere fører slid- og temperaturændringer til variationer i leddynamikens karakteristik over tid. De øjeblikkelige negative konsekvenser er relateret til ydelsen af reguleringskredsløbet, sikkerhed og kinæstetisk læring.

Denne afhandling introducerer og undersøger nye metoder til yderligere at øge ydeevnen af kollaborative industrirobotter med kompleks, ulineær og tidsvarierende leddynamik. I denne sammenhæng anvendes teknikkerne matematisk modellering, systemidentifikation og adaptiv estimering og regulering. Metoderne valideres eksperimentelt ved anvendelse af kollaborative industrirobotter fra virksomheden Universal Robots.

Matematisk set betragtes robot- og leddynamikken som to koblede delsystemer. *Robotdynamikken* er udledt og lineært parametriseret for at lette identifikationen af robottens inertielle parametre. Kalibrering af disse parametre giver forbedringer af momentforudsigelsen på 16,5 %–28,5 % afhængigt af bevægelsen.

Leddynamikken analyseres og karakteriseres grundigt. Baseret på en række eksperimenter etableres en omfattende model af robotled under hensyntagen til den komplekse, ulineære dynamik i strain-wave transmissionen, dvs. ulineær fleksibilitet, hysterese, kinematisk fejl og friktion. Steady-state friktionen anses som afhængig af vinkelhastighed, belastningsmoment og temperatur. De dynamiske friktionsegenskaber er beskrevet ved en udvidet Generalized Maxwell-Slip (E-GMS) model, der kombineret beskriver; hystereseegenskaber, der afhænger af vinkelposition samt Coulomb-friktion,

der afhænger af belastningsmoment. E-GMS modelbaseret fremkobling forbedrer momentforudsigelsen med en faktor 2.1 og banefejlen med en faktor 1.5.

En E-GMS modelbaseret adaptiv fremkoblingsregulator er udviklet til at adressere udfordringen, at friktion ændrer sig med slid og temperatur. Den adaptive reguleringsstrategi fører til forbedringer i momentforudsigelsen på 84 % og banefejlen forbedres 20 %.

Preface

This dissertation is submitted to the Graduate School of Technical Sciences (GSTS) at Aarhus University (AU) in fulfillment of the requirements for the degree of Philosophiae Doctor (PhD). The dissertation is structured as a collection of papers in compliance with official rules and regulations of the GSTS. The dissertation comprises all research findings gathered as a collection of submitted articles in peer reviewed scientific journals and published in conference proceedings.

The research was conducted as an Industrial PhD project under the Industrial Researcher Program by Innovation Fund Denmark[1]. The Industrial PhD is a joint study program between a university and a company or institution in the public or private sector. The Industrial PhD candidate, Emil Madsen, was enrolled at the Department of Engineering, Aarhus University while employed at the company Universal Robots A/S. The project was completely funded by Innovation Fund Denmark under the grant 7038-00058B and the company Universal Robots A/S.

The extent of the research project amounts to 36 months in the period of July 2017–June 2020. The place of work of the PhD candidate was split equally between the company and university, although for a period of 4 months (August 2019–December 2019) the PhD candidate visited the Department of Automatic Control of the Faculty of Engineering (LTH) at Lund University, Sweden.

Aarhus, Denmark

[1] https://innovationsfonden.dk/en

Declaration of Authorship

I, Emil Madsen, declare that this dissertation titled "Joint Dynamics and Adaptive Feedforward Control of Lightweight Industrial Robots" and the work presented in it are my own. I confirm that:

- This work was done wholly or mainly while in candidature for a research degree at this University.
- Where any part of this thesis has previously been submitted for a degree or any other qualification at this University or any other institution, this has been clearly stated.
- Where I have consulted the published work of others, this is always clearly attributed.
- Where I have quoted from the work of others, the source is always given. With the exception of such quotations, this thesis is entirely my own work.
- I have acknowledged all main sources of help.
- Where the thesis is based on work done by myself jointly with others, I have made clear exactly what was done by others and what I have contributed myself.

Acknowledgements

During my PhD studies I enjoyed the privilege of collaborating with a lot of people that I would like to thank. First of all, I would like to thank Esben Hallundbæk Østergaard as the Chief Technology Officer (CTO) of Universal Robots in 2017 for believing in me and providing me with the opportunity of working on such an exciting research project.

I would also like to express my sincere gratitude to my supervisors. Associate Professor Xuping Zhang has been my main supervisor and academic advisor. The door to Prof. Zhang's office was always open and conducting research with him enabled ideas to transform into high-quality results. I want to thank my company supervisor and Technology Officer (TO) of Universal Robots, David Brandt, for his valuable support and for ensuring the industrial relevance of the project. A special thanks goes to my company co-supervisor and Tech Lead Software of Universal Robots, Oluf Skov Rosenlund, for great technical advice and for providing assistance and guidance whenever I ran into a trouble spot or had a question about the robotic system of Universal Robots.

I would also like to thank a number of colleagues at Universal Robots. This includes my manager Anders Billesø Beck whom I would like to thank for our interesting talks regarding a variety of topics in robotics but also for his strategic suggestions in regard to the direction of the PhD project. My PhD trajectory would have been much less smooth without his guidance and suggestions. Further, I would like to thank Innovation Project Coordinator Anne-Kirstine Christensen Spring for kind help and assistance whenever needed and Innovation Lab Manager Morten Boris Højgaard for showing me no mercy in our table tennis matches. Then I would like to thank IPR Manager Morten Fruelund for his highly valued assistance with patents. I also appreciate having the opportunity to work with my skilled colleagues and project partners, Anders Skovgaard Knudsen and Martin Trædholm. I have learned a lot about programming and software engineering from our collaboration. A special thanks goes to my colleague and good friend Dan Kielsholm Thomsen. I have really enjoyed our time together outside and at work. Credit goes to my former colleagues and master's thesis students, Simon Aagaard Timm and Norbert Andras Ujfalusi, whom I thank for their great work and endless efforts during our collaboration.

I would further like to direct my appreciation to friends and office mates at Aarhus University. Oliver T. Filsoof, Frederik F. Foldager, Simon P. H.

Skovsgård, Simon Heide-Jørgensen, Kasper Ringgaard, and Joakim Vester-Petersen have made the last three years outside and at the department particularly enjoyable.

I would also like to express my gratitude to the people at the Department of Automatic Control of Lund University. In particular, I thank Professor Anders Robertsson for allowing me to visit the Robotics Laboratory at Lund University and for our joint development of the "pepparkaka-cobot". I also had the pleasure of meeting Professor Emeritus Karl Johan Åström whom I would like to thank for his great enthusiasm during our talks on dynamic friction models.

Finally, I would like to express my gratitude to my family. I thank my father Poul Nielsen, mother Berit Elise Krarup Madsen, and sister Emma Madsen for their love and support during all these years. In closing, I would like to express my sincere gratitude to my girlfriend Iben Kirstine Lolk Nielsen. Her never-ending patience, encouragement, support, and love is truly appreciated. The wear and tear of me would have been much more severe had it not been for her.

Funding

The research leading to these results was supported financially by Innovation Fund Denmark under grant no. 7038–00058B.

Innovation Fund Denmark

Publications

[Conf. Paper 1] E. Madsen, O. S. Rosenlund, D. Brandt, and X. Zhang, "Model-Based On-line Estimation of Time-Varying Nonlinear Joint Stiffness on an e-Series Universal Robots Manipulator," In *IEEE International Conference on Robotics & Automation*, pp. 8408–8414, May 2019. Doi: `https://doi.org/10.1109/ICRA.2019.8793935` (*Published*)

[Journal Paper 1] E. Madsen, O. S. Rosenlund, D. Brandt, and X. Zhang, "Comprehensive Modeling and Identification of Nonlinear Joint Dynamics for Collaborative Industrial Robot Manipulators," *Control Engineering Practice*, Vol. 101, August 2020. Doi: `https://doi.org/10.1016/j.conengprac.2020.104462` (*Published*)

[Journal Paper 2] E. Madsen, S. A. Timm, N. A. Ujfalusi, O. S. Rosenlund, D. Brandt, and X. Zhang, "Dynamics Parametrization and Calibration of Flexible-Joint Collaborative Industrial Robot Manipulators," *Mathematical Problems in Engineering*, 2020 (*Under Review*)

[Journal Paper 3] E. Madsen, O. S. Rosenlund, D. Brandt, and X. Zhang, "Adaptive Feedforward Control for a Collaborative Industrial Robot Manipulator Using a Novel Extension of the Generalized Maxwell-Slip Friction Model," *Mechanism and Machine Theory*, 2020 (*Under Review*)

[Patent App. 1] EPO, EP 18 19 4683, E. Madsen, "OBTAINING THE GEAR STIFFNESS OF A ROBOT JOINT GEAR OF A ROBOT ARM," September 2018

[Patent App. 2] DKPTO, PA/2019/00470, E. Madsen, "METHOD OF CONTROLLING A ROBOT ARM BASED ON ADAPTIVE FRICTION," April 2019

Oral Presentations

I Internal Briefing at Universal Robots A/S, August 2017, Odense, Denmark
Title: *Joint Dynamics and Adaptive Feedforward Control*

II Innovation Fund Denmark Kick-Off, March 2018, Copenhagen, Denmark
Title: *Joint Dynamics and Adaptive Feedforward Control of Lightweight Industrial Robots*

III IEEE International Conference on Robotics & Automation, May 2019, Montreal, Canada
Title: *Model-Based On-line Estimation of Time-Varying Nonlinear Joint Stiffness on an e-Series Universal Robots Manipulator*

IV DCAMM 17th Internal Symposium, March 2020, Vejle, Denmark
Title: *Joint Dynamics and Adaptive Feedforward Control of Lightweight Industrial Robots*

V Lund University, Research Presentation at the Department of Automatic Control Seminar, November 2019, Lund, Sweden
Title: *Lightweight Industrial Robots – Modeling, Identification, and Control*

Contents

List of Figures

List of Abbreviations

BIBO	**B**ounded-**I**nput, **B**ounded-**O**utput
BP	**B**ase **P**arameters
CAD	**C**omputer **A**ided **D**esign
CCW	**C**ounter-**C**lock**W**ise
CD	**C**entral **D**ifference
CW	**C**lock**W**ise
DH	**D**enavit-**H**artenberg
DKPTO	**D**anish **P**atent and **T**rademark **O**ffice
DNLRX	**D**ynamic **N**on**L**inear **R**egression with direct application of e**X**citation
DOF	**D**egree-**O**f-**F**reedom
EP	**E**ssential **P**arameters
E-GMS	Extended **G**eneralized **M**axwell-**S**lip
EPO	**E**uropean **P**atent **O**ffice
FJR	**F**lexible-**J**oint **R**obot
GMS	**G**eneralized **M**axwell-**S**lip
IDIM	**I**nverse **D**ynamics **I**dentification **M**odel
ISO	**I**nternational **O**rganization for **S**tandardization
LS	**L**east **S**quares
LTP	**L**ead-**T**hrough **P**rogramming
MRAC	**M**odel-**R**eference **A**daptive **C**ontrol
NE	**N**ewton-**E**uler
OLS	**O**rdinary **L**east **S**quares
pHRI	**p**hysical **H**uman-**R**obot **I**nteraction
PMSM	**P**ermanent **M**agnet **S**ynchonous **M**achine
RLS	**R**ecursive **L**east **S**quares
RNE	**R**ecursive **N**ewton-**E**uler
RNEA	**R**ecursive **N**ewton-**E**uler **A**lgorithm
STC	**S**elf-**T**uning **C**ontroller
TCP	**T**ool **C**enter **P**oint
UR	**U**niversal **R**obots
WLS	**W**eighted **L**east **S**quares

Chapter 1

Introduction

"Do the right thing because it is right."

— Immanuel Kant (1724–1804)

Collaborative robot arms need to accurately predict the actuator torques required to complete any desired task. This will ensure a safe operation, lead to increased precision and accuracy, and result in a smooth lead-through programming experience. Predicting accurately the actuator torques requires accurate mathematical models of the robot. However, the wear and tear of the robot and changes in ambient conditions lead to changes in the real robotic system. This dissertation presents new mathematical models and methods to ensure that the models always closely resembles the real robot arm despite changes and variations of the robotic system.

1.1 Background and Motivation

The International Organization for Standardization (ISO) suggests the following definition.

Definition 1 (industrial robot)

> *Automatically controlled, reprogrammable multipurpose manipulator, programmable in three or more axes, which can be either fixed in place or mobile for use in industrial applications.*
>
> *Note: The industrial robot includes the manipulator, consisting of actuators, controller, teach pendant and any communication interface (hardware and software).*
>
> (ISO 8373:2012)

Thus, an *industrial* robot is meant for being use "*in industrial automation applications*". The first industrial robot manipulator was deployed for operation

in 1961 in a General Motors automobile factory to perform spot welding and extract die castings [1]. Since then, the area and application of industrial robots has experienced huge growth. The market for safer, smaller, and more affordable robots is rapidly expanding with sales to the electrical and electronics industry increasing by 24 % on average each year since 2013 [2]. These robots are referred to as *collaborative robots*, or simply *cobots*, because they can work collaboratively with human co-workers unlike traditional industrial robots that need to be fenced off.

1.1.1 Collaborative Robots

The ISO suggests the following definitions.

Definition 2 (collaborative robot)

Robot designed for direct interaction with a human within a defined ***collaborative workspace*** *(Definition 3).*

(ISO 10218–2:2011)

Definition 3 (collaborative workspace)

Workspace within the safeguarded space where the robot and a human can perform tasks simultaneously during production operation.

(ISO 10218–2:2011)

These definitions make a clear distinction in the purpose of a collaborative robot, i.e. "*for direct interaction with a human within the safeguarded space*". Collaborative industrial robots are directed towards industrial manufacturing that includes physical Human–Robot Interaction (pHRI), small-size production, and high production flexibility. Performance criteria relevant to collaborative industrial robots are the precision and accuracy of motion and force control tasks, the safety, and the ability to perform quick and easy robot programming. The next three sections will highlight the importance of having an accurate mathematical description that relates the actuator torques to the manipulator motion – a so-called *dynamic model*.

Safety

Collaborative robots keep humans safe by relying less on physical safeguards and more on inherently safe measures, i.e. properties of the collaborative robot that make it less likely to cause harm. The ISO 10218 [3, 4] and ISO 13849 [5, 6] standards define a set of safety features for collaborative

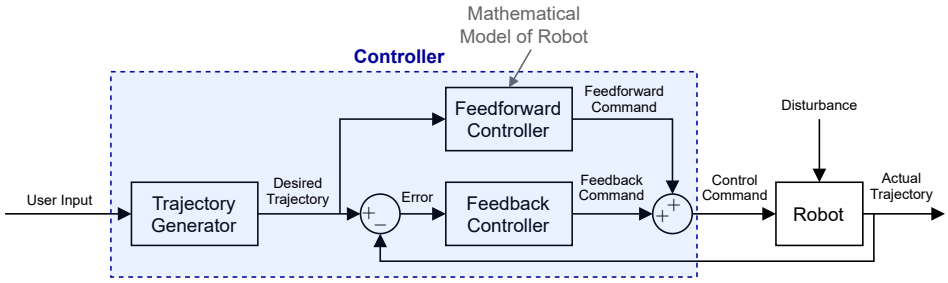

FIGURE 1.1: Schematic representation of a simplified control strategy.

robots and general machinery, respectively. For instance the power and force exerted by the robot to the environment must be limited in magnitude. Rather than measuring the exerted power and force directly, measurements from internal sensing hardware such as absolute rotary encoders and current sensors are mathematically related to the exerted force. Thus, accurate mathematical models of the robot will facilitate identification of external disturbances such as human interference and thereby improves the robot safety [7–9].

Control Precision & Accuracy

The control system for an industrial robot most often consists of a combined feedforward and feedback control strategy. An example of a simplified control structure is presented in Fig. 1.1. The feedforward controller comprises a mathematical model of the robot. If the model perfectly resembles the real robot, the actual trajectory will equal the desired trajectory, i.e. the tracking error will be zero. The mathematical model will never exactly represent the robot and disturbances will affect the system, thus the error correcting feedback controller is necessary. However, a high-fidelity mathematical model combined with feedforward control will improve the control performance because known disturbances can be accounted for before they cause deviations from the desired trajectory or force reference [10, 11].

Lead-Through Programming

In some parts of industry, it is common with short-series production. For the manufacturing to rapidly adapt to changing task specifications and to minimize the down-time, the robot programming must be quick and easy to perform. *Programming by demonstration*, sometimes referred to as *kinesthetic teaching*, is a field where *lead-through programming* (LTP) can be used to reduce the complexity of the robot programming. LTP works by having the user physically moving the robot around to demonstrate the desired robot motion – Fig. 1.2 shows lead-through programming[1] of a UR3e robot. The LTP feature is obtained by using the mathematical model of the robot to compensate gravity, friction, etc. and to detect and estimate the interaction forces applied by the human operator to the manipulator. A more accurate mathematical model of the robot thus allows to identify smaller interaction forces, which minimizes the force required to be exerted by the human operator. Accurate mathematical modeling thus facilitates a smooth LTP experience [12, 13].

FIGURE 1.2: Lead-through programming of a Universal Robots UR3e manipulator.

1.1.2 Dynamics Model Accuracy

For a good robot performance it is necessary to have a dynamic model that accurately relates the actuator torques to the manipulator motion. For collaborative industrial robots, the concerns of safety and production flexibility motivates the use of lightweight components to lower the kinetic energy and ease the relocation of the robot. Thus, strain-wave transmissions are widely used for collaborative robots due to their desirable characteristics of lightweight design yet high torque capacity. For instance they are used in the Universal Robots manipulators [14], Kuka LWR [15], FANUC LR Mate 200i [16], Yaskawa Motoman HP3J [17], DLR 7 DOF robot [18], and Mitsubishi PA–10 [19]. The lightweight design of strain-wave transmissions, however, comes at the expense of inherent complex nonlinear characteristics such as [20, 21]; *flexibility*, *friction*, *hysteresis*, and *kinematic error*. These joint dynamics characteristics must be considered in the mathematical model of the robot to achieve a good robot performance.

[1] The lead-through programming feature by Universal Robots is named *Freedrive*.

When a mathematical model has been established, a set of parameter values need to be determined. Parameters that yield the least model error is naturally desired. Some parameters such as the inertial parameters of the robot are constant throughout the lifetime of the robot and as such they need to be determined just once. Other parameters, for instance those related to the joint dynamics (friction, stiffness, etc.) may change gradually in ways that cannot be accurately predicted from prior knowledge. The causes and effects of gradual changes to the robot dynamics are:

- **Wear.** From a mechanical perspective wear can be defined as "*the progressive removal of material from a body occurring as a result of relative motion between contacting surfaces*" [22]. The wear of a strain-wave transmission leads to; 1) changes in flexibility, most prominent at small deformations [23–25] and 2) changes in friction, most prominent near the end of its lifetime [26, 27].
- **Temperature.** The viscosity of lubricants depends approximately exponentially on temperature [28] and the shear forces for newtonian fluids increase proportionally with viscosity. These facts elucidate the observed dependency of friction on temperature [29, 30]. The effect can be compensated provided the relation between temperature and friction is known and temperature sensing is available. However, due to practical reasons the temperature of a solid body is most often measured rather than the lubricant. The thermal resistance, and consequent time delay, complicates the exact cancellation of the effect [31].

1.2 Literature Review

The complex nonlinear and time-varying joint dynamics characteristics deteriorates the accuracy of the dynamic model and thus the robot performance if not properly compensated. Dynamics modeling, identification, and adaptive estimation and control are techniques to improve the performance of a robot subject to such phenomena. This section presents a review of the literature relevant to dynamic modeling, identification, and adaptive estimation and control of industrial robots with the consideration of joint dynamics.

1.2.1 Dynamics Modeling & Identification

A robot manipulator can be considered as a set of links interconnected by joints that allow for relative motion between the links. With the use of lightweight transmissions elements such as strain-wave transmissions, the usual assumptions of joint rigidity no longer holds. A Flexible-Joint Robot (FJR) manipulator can be described by assigning generalized coordinate to both sides of each of the flexible transmissions.

Robot Dynamics Modeling & Identification

Dynamic models of robot manipulators relate the motion of the robot and the forces and torques that cause the motion. The modeling of Flexible–Joint Robot (FJR) manipulators was advanced by Spong [32], who introduced a set of clever assumptions to simplify the dynamics without much loss of accuracy for robots with reduction gears. The resulting dynamic model allows for a larger set of control strategies to be applied. Today, the most comprehensive literature on robot dynamics modeling is [33] and [34].

Since the mid 80's, much research have been devoted to developing minimal descriptions of the rigid-body dynamics of robot manipulators [35–37]. Gautier and Khalil [38] developed an analytical method to reduce the full set of parameters to a minimal set of *base parameters* (BP). Another approach is to use numerical methods to find a set of *essential parameters* (EP) by imposing a numerical threshold on the influence of the parameters on the dynamics and searching for parameters above the threshold [39, 40]. The number of EP is often less than the number of BP because the numerical methods tend to eliminate parameters that show the least contribution to the manipulator dynamics. This can be unsatisfactory for some applications where high accuracy is required. The methods for robot dynamics identification are generally affected by *measurement noise* and *modeling errors*. The measurement noise is commonly addressed by the use of exciting trajectories and filtering of the noisy measurements [41]. The most common method for robot dynamics identification is a combined Inverse Dynamics Identification Model and Least Squares (IDIM-LS) method. Other methods have been suggested such as the Extended Kalman Filter (EKF) [42, 43], Linear Matrix Inequalities (LMI) [44], Maximum Likelihood (ML) [45], the set membership uncertainty [46], and the Huber's estimator [47]. However, these methods do not improve the accuracy and uncertainty of the IDIM-LS method. The need for tuning the bandpass filter was addressed

in [48–50] by introducing the Direct and Inverse Dynamic Identification Models (DIDIM) and in [51, 52] by introducing the concept of Instrumental Variables (IV). These methods are based on a Closed Loop Output Error (CLOE) method using both the *direct* and *inverse* dynamic models. The direct dynamic model is used to obtain model-based estimates of the angular position, velocity, and acceleration in contrast to the bandpass filtering of the IDIM-LS method. However, with well-tuned bandpass filtering, the accuracy and uncertainty of the DIDIM, IDIM-IV, and CLOE methods do not improve upon the IDIM-LS method [50].

Dynamics identification have been conducted for several industrial robots including the 7 DOF DLR light-weight robot [18], COMAU Smart-3 S2 [53], KUKA KR 15 [54], Mitsubishi PA-10 [55], Staubli RX-60 [56], Staübli TX40 [57], ER-16 [58], SCHUNK Powerball LWA 4P [59], KUKA KR 6-2 [60], KUKA LBR iiwa [61], and Denso VP-6242G [62]. However, the works on robot dynamics identification assume simple models for the joint dynamics which introduce bias to the inertial parameter estimates. Joints are assumed rigid and friction, if included, is described by simple two or three coefficient models with Coulomb friction, linear viscous friction, and friction offset. Even so for the identification of the dynamics for collaborative industrial robots that are known to experience non-negligible joint dynamics effects. Gaz et al. [63] identified the dynamics of the Franka Emika Panda collaborative robot, and Taghbalout et al. [64] identified the dynamics of the 2×7 DOF dual-arm ABB IRB14000 (YuMi) collaborative robot. For the KUKA LWR 4+ collaborative robot, Kolyubin et al. [65] identified the EP while assuming a three-parameter friction model and Shareef et al. [66] and Gaz and Luca [67] did dynamics identification with friction neglected. The works on the KUKA LWR 4+ robot exploited the torque sensor in each joint located on the output side of the transmission and as such the joint dynamics did not affect the measurements. Such sensor hardware is however expensive and rarely found in industrial robots.

Joint Dynamics Modeling & Identification

The modeling and identification of the joint dynamics for industrial robots is for the most works limited to frictional nonlinearities describing the steady-state relationship between friction torque and the angular velocity, temperature, and load torque. Thus, the complex frictional dynamics is most often neglected. The dynamic modeling of nonlinear robot joint dynamics has been considerably advanced by research studies explicitly considering

strain-wave transmissions. This section presents firstly the literature on identification of static nonlinearities of the joints of industrial robots, and lastly the identification of the dynamics of strain–wave transmissions.

Depending on the application for the joint dynamics model, for example control and other on–line calculations or simulations, different properties are needed. Thus, this work focuses on the control oriented model for real-time calculations in contrast to the *Extended Flexible Joint* model developed by Moberg and Hanssen [68] which is meant for simulation.

In [69] the friction of the *ABB IRB 6620* robot was analyzed and the angular velocity, load torque, and temperature were found to be important factors to accurately describe the observed friction characteristics. In [70], the *Comau SMART NS 16 1.65 ARC* was analyzed in terms of the dependency of friction on temperature. In [71] the frictional characteristics for the *ABB IRB 140* and *ABB YuMi* industrial robots were studied in terms of angular position and temperature. In [29] the load torque and temperature effects of friction on the *SIASUN* lightweight industrial robot which comprises Harmonic Drive transmissions was examined. The above-mentioned works made important contributions to characterize the steady-state friction characteristics of industrial robots. Angular velocity, temperature, and load torque are found to be important factors in this regard. However, the more complex frictional dynamics and joint flexibility effects which are known to exist for strain-wave transmissions were not considered which leads to model errors – especially at low velocity. In [72], the Harmonic Drive-based DLR Floating Spring Joint [73] was investigated experimentally to characterize the nonlinear static dependencies of friction on angular velocity and temperature. In [30], their work was extended by utilizing the Generalized Maxwell-Slip (GMS) model to describe the frictional dynamics. Furthermore, an application to external torque estimation was demonstrated. The GMS dynamic friction model [74, 75] has been successfully used to model strain-wave transmissions [76, 77]. In the more general robotics literature – not necessarily considering strain-wave transmissions – the LuGre dynamic friction model [78] has been widely used. However, the LuGre model does not describe hysteresis with non-local memory [79] commonly observed in strain-wave transmissions [77].

Hysteresis

The dynamic modeling of robot joints have been advanced significantly by

works that exclusively consider strain-wave transmissions. In [80] a hysteresis model of the Harmonic Drive was developed. In [81] a mathematical model of a Harmonic Drive was derived based on the gear-tooth geometry. In [21] a complete model of a Harmonic Drive was suggested including simple sub-models of flexibility, hysteresis, and friction. In [82] the mechanical structure of the Harmonic Drive was studied and a control-oriented model was proposed including flexibility with soft wind-up, hysteresis, and friction. In [83] the Harmonic Drive was described by an integro-differential equation through the combination of nonlinear stiffness and damping. In [84] a hysteresis model of the Harmonic Drive was developed using the Preisach model for hysteresis and the GMS model for describing dynamic friction effects. In [85] the hysteresis was described using an extended Bouc-Wen model, and in [86–89] the application of hysteresis modeling was demonstrated in sensor-less torsion control. The above-mentioned studies present results on high-fidelity modeling of Harmonic Drive strain-wave transmissions, but the works are on single-joint systems and they do not consider the known dependencies of friction on temperature and load torque.

Kinematic Error

The kinematic error of strain-wave transmissions is related to the production tolerances and therefore varies between robot joints with the same type of transmission. In [90], compensating the kinematic error in an integral manifold control framework led to increased control performance, and in [91] modeling and compensation of the kinematic error led to reduced vibration of an industrial robot. Characterizing and compensating the kinematic error is thus highly relevant. In [92], a modeling framework was made for the rolling friction with hysteresis attributes and compensation of the kinematic error. In [93] the wave generator shape was analyzed theoretically in terms of the kinematic error.

1.2.2 Adaptive Control

Today, the most comprehensive literature on general nonlinear control is Khalil [94], while Slotine and Li [95] provide many examples on mechanical systems and robots. This section presents a review of literature on adaptive control of industrial robot manipulators subject to time-varying joint dynamics. Friction compensation is a fundamental problem in motion control and thus a huge amount of literature exists. This literature review

focuses on adaptation of dynamic friction models that are able to describe rate-independent hysteresis found in strain-wave transmissions.

In [96], adaptive control strategies was developed based on the LuGre dynamic friction model. In [97], a friction observer was developed for robots with joint torque sensing. Its application was demonstrated on the DLR medical robot. In [98], adaptive estimation of a static friction model was conducted for a robot with linearly elastic joints. In [99], an adaptive model-based friction estimation and compensation method was developed based on an Extended Kalman Filter (EKF) for use in combination with an impedance controller for the DLR-HIT II robot hand. In [100], an adaptive control strategy based on the LuGre dynamic friction model was developed. A few works considered adaptation of friction models based on the GMS model structure. In [101, 102] a switching adaptive controller was developed based on the GMS friction model with a linear parametrization of the Stribeck function. A parameter projection strategy was used to prove stability, and numerical results demonstrated the method. The choice of switching function is however not suited for real systems as noted in [103], where the GMS model identified using the adaptive observer proposed in [104]. The method was validated by simulation. In [105] the method was improve by introducing a filter to the regressor for the requirement of Lipschitz continuity to be respected. In [106, 107] the Dynamic NonLinear Regression with direct application of eXcitation (DNLRX) model was identified adaptively using a recursive least squares estimator with exponential forgetting and used in feedforward control.[2] Results were promising in comparison to a standard PID controller. In [108], an adaptive controller was presented for a Harmonic Drive transmission the Coulomb and viscous friction coefficients and the friction offset. The algorithm relied on sensing of the angular positions at each side of the Harmonic Drive as well as joint torque sensing.

1.3 Universal Robots

Universal Robots (UR) is a Danish company which develops, manufactures, and sells collaborative robots. The three founders of Universal Robots, namely Esben Østergaard, Kasper Støy, and Kristian Kassow, met at the

[2]The DNLRX model is simply a GMS model with its state and input driven through FIR filters

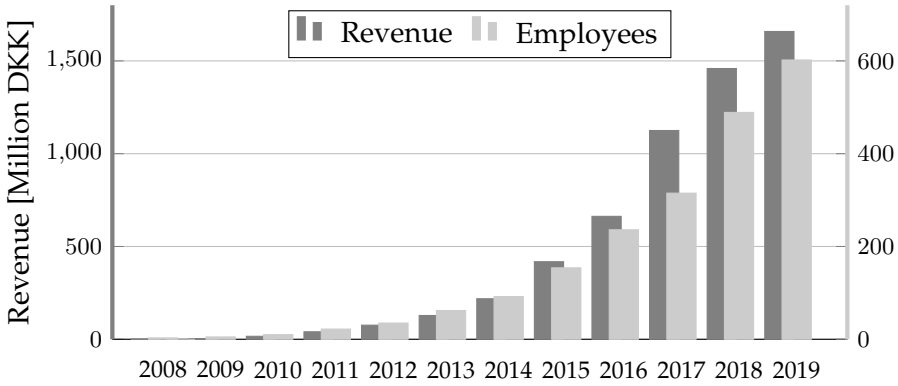

FIGURE 1.3: Universal Robots' revenue and no. of employees since 2008.

	UR3e	**UR5**e	**UR10**e	**UR16**e
Reach	500 mm	850 mm	1300 mm	900 mm
Payload	3 kg	5 kg	10 kg	16 kg
Footprint	Ø128 mm	Ø149 mm	Ø190 mm	Ø190 mm
Weight	11.2 kg	20.6 kg	33.5 kg	33.1 kg

TABLE 1.1: Specifications for the Universal Robots e-Series robots.

University of Southern Denmark (SDU) in 2003.[3] They got the idea of creating a lightweight robot that was easy to install and program. Universal Robots was officially founded in 2005 with the goal of making collaborative robots accessible to small and medium-sized enterprises (SME's). Three years after, in 2008, the first collaborative robot was sold by distributors in Denmark and Germany. Today, Universal Robots is the world leader in collaborative robots, and remarkable rates of growth has propelled Universal Robots' revenue to DKK 1.658 million in 2019 and more than 600 employees. The progress of the revenue and number of employees is shown in Fig. 1.3. The latest series of robot arms by Universal Robots is the e-Series shown in Fig. 1.4 with data listed in Table 1.1.

[3] universal-robots.com/about-universal-robots/our-history/
[4] universal-robots.com

FIGURE 1.4: Universal Robots' e-Series robots, from left to right; UR3e, UR5e, UR16e, and UR10e, named after their rated payload in kilograms.[4]

1.3.1 Experimental System Overview

The experimental system includes a PC and a UR robot consists of three main parts: The robot arm, control box, and teach pendant, illustrated in Fig. 1.5. The desired behavior of the robot arm is specified through the *teach pendant*, which provides a graphical touch interface, or through the PC via a TCP/IP connection from a MATLAB® client. Data logging is performed using a Python client. The *controller* executes the high-level programs provided by the user and sends commands for the *robot arm* to execute. The robot arm also sends back information to the controller. The controller uses this information for instance to evaluate whether the robot should continue its task or stop in case something unexpected happens.

The Robot Arm

The robot arm is a 6 degree-of-freedom (DOF) serial-link articulated robot manipulator which means that the robot links are connected in series and the joints admit rotary motion of the links. Each joint comprise an electric actuator, specifically a three-phase Permanent Magnet Synchronous Machine (PMSM) as well as a strain-wave transmission. The PMSM transmits its high-velocity/low-torque power to the input axle and through the transmission the power is converted to low-velocity/high-torque at the output axle. The sensor hardware of UR e-Series robots provide measurements for each joint of;

[5] `https://universal-robots.com/download/?option=69270#section69029`

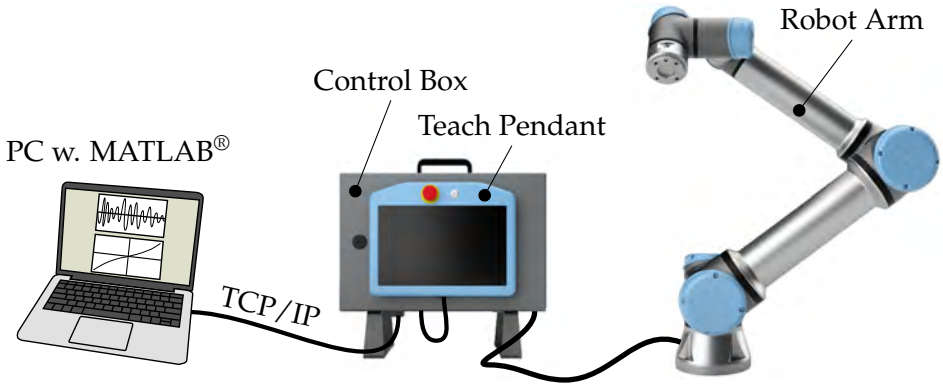

FIGURE 1.5: Experimental setup with a Universal Robots UR5e robot arm, control box, teach pendant, and PC. The PC has a TCP/IP connection to the control box and sends UR script commands[5] – e.g. `movej(·)` – to the controller via a MATLAB® TCP/IP client. MATLAB also has an SSH/SFTP/SCP client [109].

- the angular position of the input axle,
- the angular position of the output axle,
- the phase currents of the PMSM, and
- the temperature.

Additionally, the wrench and acceleration at the TCP is measured.

1.4 Objectives

The aim of this Industrial PhD project is to further increase the performance of collaborative industrial robots through dynamic modeling, identification, and controller design. This strategic goal is achieved through a research framework that synergistically integrates three interrelated sub-objectives, that is:

1) To develop a **dynamic model** of the 6 DOF collaborative industrial robot by Universal Robots considering the joint dynamics effects inherent to the strain-wave transmissions such as flexibility, friction, hysteresis, and kinematic error.

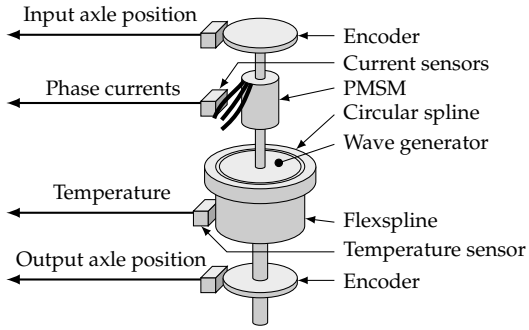

FIGURE 1.6: Schematic illustration of the main components of a Universal Robots e-Series robot joint.

2) To investigate and develop **adaptive estimation and feedforward control** based on the developed dynamic model to effectively estimate and compensate the time-varying joint dynamics due to wear and temperature changes.

3) To establish a testing system, conduct the testing using a Universal Robots collaborative robot, thus **experimentally validate** the dynamic model and adaptive estimation and control algorithms.

1.5 Contributions

Starting from a description of the state-of-the-art on dynamics modeling, identification, and adaptive estimation and control of industrial robots, this dissertation presents new methods and procedures for increasing the performance of collaborative industrial robots. The steps beyond state-of-the-art are:

1) **Adaptive stiffness estimation.** A method for online estimation of the nonlinear robot joint stiffness is developed and validated experimentally. The method expands the state-of-the art by being able to operate online without additional sensing hardware or mechanical fixture and works for arbitrary manipulator configurations and motion trajectories. In 10 seconds, the stiffness is estimated with an accuracy of 95.2 % – comparable to that of offline identification.

2) **Joint dynamics modeling and identification.** A comprehensive mathematical model and identification procedures for robot joints was

developed. The model includes flexibility, kinematic error, hysteresis, and dynamic friction. The state-of-the-art is expanded by:

(a) The choice of temperature model admit a linear parametrization (hence facilitates identification) and is more accurate than models used in prior works.

(b) A new linear regression procedure is developed for identification of Generalized Maxwell-Slip friction model. The procedure improves torque prediction accuracy compared to existing procedures.

(c) Identification of hysteresis characteristics that depend on the joint angular position. This phenomenon is not described previously, but its existence was rendered probable from theoretical analyses.

(d) The Generalized Maxwell-Slip dynamic friction model is extended (E-GMS) to describe in a combined framework; 1) the dependency of the hysteresis characteristics on the angular position and 2) the dependency of friction on the joint torque. The torque prediction accuracy is improved by a factor of 2.1 and the tracking error is reduced by a factor of 1.5. Additionally, discontinuities in the angular velocity is overcome.

3) **Robot dynamics calibration.** A robot dynamics calibration methodology is developed and experimentally validated to calibrate the identifiable (base) parameters and increase the torque prediction accuracy. The state-of-the-art is expanded by compensating the nonlinear joint flexibility and nonlinear rotor dynamics to reduce uncertainty and bias in the parameter estimates from unmodeled dynamics.

4) **Adaptive feedforward control.** A self-tuning feedforward controller is developed based on the proposed E-GMS dynamic friction model to address the challenge of friction that change with; 1) wear and 2) temperature. The adaptive controller is realized by combining a gradient descent parameter estimation scheme and feedforward control. The state-of-the-art is expanded by realizing adaptive control based on the proposed E-GMS dynamic friction model. The torque prediction accuracy is improved 84 % while the tracking error is reduced by 20 %.

1.6 Thesis Overview

The rest of this dissertation is structured in the following chapters.

Chapter 2 presents the theoretical background of this research. First, mathematical modeling of robot manipulators with the consideration of flexible joints is presented. The dynamics inherent to strain-wave transmissions such as nonlinear flexibility, friction, hysteresis, and kinematic error is discussed. Then, system identification procedures are presented with regards to determining the robot and joint dynamics parameters. Lastly, strategies for adaptive estimation and control of industrial robots is discussed. This includes methods for general feedforward and feedback control of flexible-joint robot manipulators.

Chapter 3 presents an adaptive estimation procedure for online identification of the nonlinear robot joint stiffness and includes *Conference Paper 1*. The method relies on the sensing hardware readily available in the Universal Robots manipulators, and in contrast to other robot joint stiffness calibration procedures, the method requires no specially designed trajectory or fixation of the robot end-effector. The perspectives of adaptive joint stiffness estimation are in predictive maintenance and in linearizing and decoupling control strategies.

Chapter 4 presents a comprehensive mathematical model of the robot joint and includes *Journal Paper 1*. The model describes the nonlinear flexibility, hysteresis, and kinematic error. Additionally, the steady-state friction is described in terms of angular velocity, load torque, and temperature. The dynamic friction characteristics are described by the Generalized Maxwell-Slip (GMS) model. The hysteresis characteristics are observed to depend on the angular position.

Chapter 5 presents the robot dynamics calibration procedure and includes *Journal Paper 2*. The robot dynamics calibration procedure is based on the analytic expressions for regrouping the inertial parameters. Our procedure is based on the IDIM-WLS procedure extended with a method to compensate the nonlinear rotor-side dynamics. Improvements in torque prediction accuracy are in the range 16.5 %–28.5 % compared to a model containing CAD model parameters.

Chapter 6 presents an extension to the GMS friction model (E-GMS) and an adaptive feedforward controller. The chapter includes *Journal Paper 3*. The E-GMS model describes in a combined framework the hysteresis characteristics that depend on the joint angular position as well as Coulomb friction torque which depend on the load torque. The adaptive feedforward controller is designed based on the E-GMS model and addresses friction that depend on wear and temperature changes. Improvements in torque prediction accuracy average at 84 % among the joints, while the position error is improved by 20 %.

Chapter 7 concludes the work by summarizing the main contributions of the research project. Finally, the perspectives for further development of the presented methods are presented.

Chapter 2

Theoretical Background

> *"Experience without theory is blind, but theory without experience is mere intellectual play."*
>
> — Immanuel Kant (1724–1804)

To achieve a good robot performance, it is necessary to have a dynamic model that accurately relates the actuator torques to the manipulator motion. However, the use of lightweight strain-wave transmissions introduces complex nonlinear and time-varying dynamics to the robot joints, which deteriorates the robot performance if not properly addressed. The combined techniques of dynamics modeling, identification, and adaptive estimation and control are essential tools to address such issues.

2.1 Dynamic Modeling

The dynamic model of the robot manipulator relates the actuator torques to the motion of the robot manipulator. It contains a set of *kinematic parameters* such as the position and the orientation of the joints and a set of *dynamic parameters* such as masses, center-of-mass positions, and inertia components.

2.1.1 Kinematics

To obtain an inverse dynamics model of a robot manipulator, a forward kinematic model is needed. Thus, the kinematics of robot manipulators will be briefly outlined. The kinematic model describes the relation between joint angles $\mathbf{q}$ and the position and orientation $\mathbf{x}$ of the end-effector. The *forward kinematics* describes the transformation $\boldsymbol{\Gamma}(\cdot)$ from joint angles to the end-effector position and orientation, and the *inverse kinematics* describes the transformation from the end-effector position and orientation to the

		UR3e		**UR5e**		**UR10e**		**UR16e**	
j	α_j	a_j	d_j	a_j	d_j	a_j	d_j	a_j	d_j
1	$\pi/2$	0	0.15185	0	0.1625	0	0.1807	0	0.1807
2	0	-0.24355	0	-0.425	0	-0.6127	0	-0.4784	0
3	0	-0.2132	0	-0.3922	0	-0.57155	0	-0.36	0
4	$\pi/2$	0	0.13105	0	0.1333	0	0.17415	0	0.17415
5	$-\pi/2$	0	0.08535	0	0.0997	0	0.11985	0	0.11985
6	0	0	0.0921	0	0.0996	0	0.11655	0	0.11655

TABLE 2.1: Denavit–Hartenberg parameters of the Universal Robots e-Series robots.[1]

joint angles. The forward kinematics can be represented as

$$\mathbf{x} = \mathbf{\Gamma}(\mathbf{q}) \tag{2.1}$$

and the inverse kinematic is given

$$\mathbf{q} = \mathbf{\Gamma}^{-1}(\mathbf{x}) \tag{2.2}$$

The kinematic model is derived using *Denavit–Hartenberg* (DH) convention or its modified variant [110]. The kinematic parameters of the UR robots are listed in Table 2.1 and illustrated on a UR5e robot in Fig. 2.1 configured in the home position.

2.1.2 Flexible-Joint Robot Manipulator Dynamics

The safety issue is addressed, partly, by the use of lightweight transmission components. Thus, the kinetic energy of the robot is minimized, which reduces the risk of injury in the event of a collision. However, due to the use of flexible transmission elements this assumption no longer holds. In this section, the dynamics of Flexible–Joint Robot (FJR) manipulators is presented.

The dynamic model of the robot manipulator provides a relationship between the joint torques and the motion of the robot manipulator.[2] The dynamics of a robot manipulator can be derived using several methods.

[1] `https://www.universal-robots.com/articles/ur-articles/parameters-for-calculations-of-kinematics-and-dynamics/`

[2] The definition of dynamics is different in general multi–body dynamics literature [111], where *kinetics* covers motion and the forces that cause it and *kinematics* covers the geometric

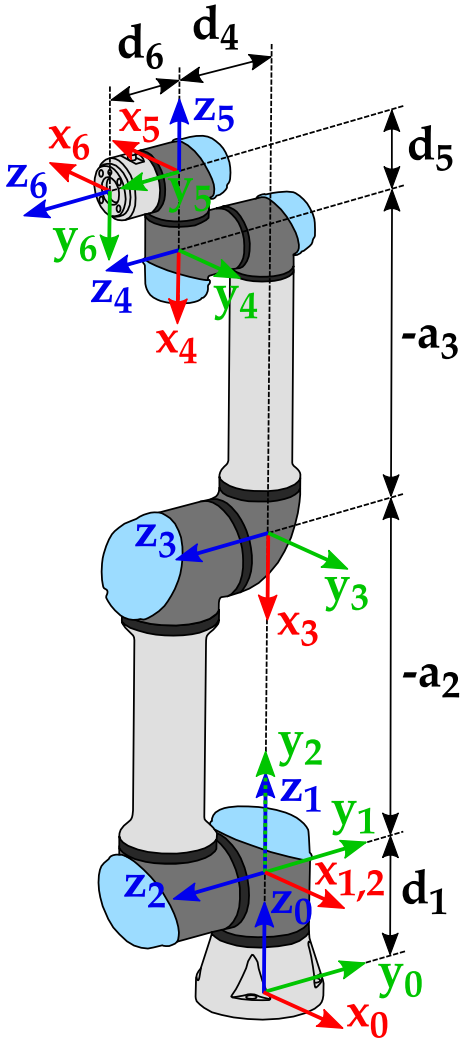

FIGURE 2.1: UR robot arm in its home position with the kinematic parameters provided.

The most common methods are *Lagrange's formulation* [33], the *Newton–Euler formulation* [110], and *Kane's method* [112]. These methods produce the same result but uses different approaches.

The deflection of the transmission elements can be modeled as concentrated at the joints, thus limiting the model complexity. Compared to the rigid manipulator case, the model of an FJR manipulator requires *twice* the number of generalized coordinates to completely characterize the manipulator configuration, i.e. all rigid bodies (rotors and links). This also means, that the control design for FJR manipulators will be more difficult.

An FJR manipulator is considered as an open kinematic chain of $N+1$ rigid bodies, the base and N links, interconnected by N revolute joints undergoing angular deformation around the joint axis of rotation and actuated by N electric actuators. To derive the manipulator dynamics a frame is attached to each of the $2N$ rigid bodies. Let the generalized coordinates

$$\boldsymbol{\Theta} = \begin{pmatrix} \mathbf{q} \\ \boldsymbol{\theta} \end{pmatrix} \in \mathbb{R}^{2N} \tag{2.3}$$

be the angular positions of the links and rotors, $\mathbf{q} \in \mathbb{R}^N$ and $\boldsymbol{\theta} \in \mathbb{R}^N$, respectively. Note that the rotor angular positions $\boldsymbol{\theta}$ are reflected through the gear ratios. Let $\mathbf{R} = \operatorname{diag}(r_1, \ldots, r_N)$ be the diagonal matrix of gear ratios with $r_i > 1 \; \forall \, i$. That is, if the physical rotor angular positions are denoted $\boldsymbol{\theta}_m$, then $\boldsymbol{\theta} = \mathbf{R}^{-1} \, \boldsymbol{\theta}_m$. The following standard assumptions are made.

A1 The motors are axis-balanced, i.e. the rotors are uniform bodies having their center of mass on the joint axis of rotation.

A2 Each motor $j = 1, \ldots, N$ is mounted on link $j-1$ and moves link j, see Fig. 2.2.

Assumption **A1** is a basic requirement for long life of an electric actuator and is thus quite reasonable. This also means that the inertia and gravity terms in the robot dynamic model will be independent of the rotor angular position. The Lagrangian $\mathcal{L}(\boldsymbol{\Theta}, \dot{\boldsymbol{\Theta}}) = \mathcal{T}(\boldsymbol{\Theta}, \dot{\boldsymbol{\Theta}}) - \mathcal{U}(\boldsymbol{\Theta})$ is used to derive the manipulator dynamics through Lagrange's equation

$$\frac{\mathrm{d}}{\mathrm{d}\, t} \left(\frac{\partial \, \mathcal{L}(\boldsymbol{\Theta}, \dot{\boldsymbol{\Theta}})}{\partial \, \dot{\boldsymbol{\Theta}}} \right) - \frac{\partial \, \mathcal{L}(\boldsymbol{\Theta}, \dot{\boldsymbol{\Theta}})}{\partial \, \boldsymbol{\Theta}} = \boldsymbol{\Gamma} \tag{2.4}$$

relations of motion regardless of the forces. Dynamics then includes both kinematics and kinetics.

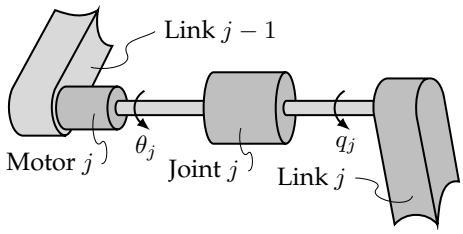

FIGURE 2.2: The FJR manipulator configuration.

where $\mathbf{\Gamma} \in \mathbb{R}^{2N}$ is the non–conservative generalized torque performing work on $\mathbf{\Theta}$. The *kinetic energy* is given by

$$\mathcal{T}(\mathbf{\Theta}, \dot{\mathbf{\Theta}}) = \frac{1}{2}\, \dot{\mathbf{\Theta}}^{\mathsf{T}}\, \boldsymbol{\mathcal{M}}(\mathbf{q})\, \dot{\mathbf{\Theta}} \tag{2.5}$$

and the *potential energy* is given by the sum of a gravitational term, which is a function of $\mathbf{q}$ alone due to assumption **A1**, and a term arising from joint elasticity

$$\mathcal{U}(\mathbf{\Theta}) = \mathcal{U}_g(\mathbf{q}) + \mathcal{U}_e(\mathbf{\Theta}) \tag{2.6}$$

with gravity torques $\boldsymbol{\mathcal{G}}(\mathbf{q}) = (\partial \mathcal{U}_g(\mathbf{q})/\partial\, \mathbf{\Theta})^{\mathsf{T}}$. If linear elasticity is assumed, the elastic energy is

$$\mathcal{U}_e(\mathbf{\Theta}) = \frac{1}{2}\, \mathbf{\Theta}^{\mathsf{T}}\, \boldsymbol{\mathcal{K}}\, \mathbf{\Theta} \tag{2.7}$$

The assumption of linear elasticity can easily be relaxed as shall be evident later. Using (2.5), (2.6), and (2.7) in (2.4) yields the complete dynamic model

$$\boldsymbol{\mathcal{M}}(\mathbf{q})\, \ddot{\mathbf{\Theta}} + \boldsymbol{\mathcal{C}}(\mathbf{\Theta}, \dot{\mathbf{\Theta}})\, \dot{\mathbf{\Theta}} + \boldsymbol{\mathcal{K}}\, \mathbf{\Theta} + \boldsymbol{\mathcal{G}}(\mathbf{q}) = \mathbf{\Gamma} \tag{2.8}$$

with $\boldsymbol{\mathcal{G}}(\mathbf{q}) = (\mathbf{g}^{\mathsf{T}}(\mathbf{q})\ \ \mathbf{0}^{\mathsf{T}})^{\mathsf{T}}$. Since only the motor coordinates are directly actuated $\mathbf{\Gamma} = \left(\mathbf{0}^{\mathsf{T}}\ \ \boldsymbol{\tau}_m^{\mathsf{T}}\right)^{\mathsf{T}}$, $\boldsymbol{\tau}_m \in \mathbb{R}^N$. Non–conservative torques, for instance energy dissipating effects like general nonlinear friction $\boldsymbol{\mathcal{F}}$ and damping $\boldsymbol{\mathcal{D}}\, \dot{\mathbf{\Theta}}$ can easily be added. It should be noted that friction acting on the motor coordinate can be completely compensated by a proper choice of control torque, while this is not true for friction acting on the link coordinate due to the non–collocation.

Model Properties

The following useful properties can be derived [34]

P1 Equation (2.8) admit a linear parametrization in terms of a set of dynamic coefficients (including joint stiffnesses and rotor inertias), which is useful for identification and adaptive control.

P2 The system inertia matrix is symmetric and positive-definite and has the following structure

$$\boldsymbol{\mathcal{M}}(\mathbf{q}) = \begin{bmatrix} \mathbf{M}(\mathbf{q}) & \mathbf{S}(\mathbf{q}) \\ \mathbf{S}^{\mathsf{T}}(\mathbf{q}) & \mathbf{B} \end{bmatrix} \tag{2.9}$$

with $\mathbf{M}(\mathbf{q}) \succ 0 \in \mathbb{R}^{N \times N}$ the symmetric inertia matrix given by

$$\mathbf{M}(\mathbf{q}) = \mathbf{M}_L(\mathbf{q}) + \mathbf{M}_R(\mathbf{q}) + \mathbf{S}(\mathbf{q})\,\mathbf{B}^{-1}\,\mathbf{S}(\mathbf{q})^{\mathsf{T}} \tag{2.10}$$

which consist of contributions from the links and rotors, denoted by subscript $_L$ and $_R$, respectively, and $\mathbf{B} \succ 0 \in \mathbb{R}^{N \times N}$ is the diagonal matrix of rotor inertias.

P3 The matrix $\mathbf{S}(\mathbf{q})$ comprises the inertial coupling between the link and rotor and is always strictly upper-triangular with a cascaded dependence of its nonzero elements, i.e.

$$\mathbf{S}(\mathbf{q}) = \begin{bmatrix} 0 & S_{12}(q_1) & S_{13}(q_1, q_2) & \cdots & S_{1N}(q_1, \ldots, q_{N-1}) \\ 0 & 0 & S_{23}(q_2) & \cdots & S_{2N}(q_2, \ldots, q_{N-1}) \\ \vdots & \vdots & \vdots & \ddots & \vdots \\ 0 & 0 & 0 & \cdots & S_{N-1,N}(q_{N-1}) \\ 0 & 0 & 0 & \cdots & 0 \end{bmatrix} \tag{2.11}$$

and its elements can be obtained as

$$S_{ij}(\mathbf{q}) = \frac{\partial^2 \mathcal{T}(\boldsymbol{\Theta}, \dot{\boldsymbol{\Theta}})}{\partial\, \dot{q}_j\, \partial\, \dot{\theta}_i} \tag{2.12}$$

P4 The elements of $\boldsymbol{\mathcal{C}}(\boldsymbol{\Theta}, \dot{\boldsymbol{\Theta}})$ can always be defined such that $\dot{\boldsymbol{\mathcal{M}}}(\mathbf{q}) - 2\,\boldsymbol{\mathcal{C}}(\boldsymbol{\Theta}, \dot{\boldsymbol{\Theta}})$ is *skew-symmetric*. One feasible choice is provided by the Christoffel symbols of the first kind

$$\boldsymbol{\mathcal{C}}_i(\boldsymbol{\Theta}, \dot{\boldsymbol{\Theta}}) = \frac{1}{2}\,\dot{\boldsymbol{\Theta}}^{\mathsf{T}} \left[\frac{\partial\, \boldsymbol{\mathcal{M}}_i}{\partial\, \boldsymbol{\Theta}} + \left(\frac{\partial\, \boldsymbol{\mathcal{M}}_i}{\partial\, \boldsymbol{\Theta}} \right)^{\mathsf{T}} - \frac{\partial\, \boldsymbol{\mathcal{M}}}{\partial\, \boldsymbol{\Theta}_i} \right] \dot{\boldsymbol{\Theta}} \tag{2.13}$$

where dependencies of $\boldsymbol{\mathcal{M}}$ have been omitted for readability. The decomposition $\boldsymbol{\mathcal{C}}(\boldsymbol{\Theta}, \dot{\boldsymbol{\Theta}}) = \mathbf{C}_A(\mathbf{q}, \dot{\boldsymbol{\theta}}) + \mathbf{C}_B(\mathbf{q}, \dot{\mathbf{q}})$ lets one define

$$\boldsymbol{\mathcal{C}}(\boldsymbol{\Theta}, \dot{\boldsymbol{\Theta}}) = \begin{bmatrix} \mathbf{C}_{A1}(\mathbf{q}, \dot{\boldsymbol{\theta}}) + \mathbf{C}_{B1}(\mathbf{q}, \dot{\mathbf{q}}) & \mathbf{C}_{B2}(\mathbf{q}, \dot{\mathbf{q}}) \\ \mathbf{C}_{B3}(\mathbf{q}, \dot{\mathbf{q}}) & \mathbf{0} \end{bmatrix} \tag{2.14}$$

with elements [113]

$$C_{A1,ij}(\mathbf{q}, \dot{\boldsymbol{\theta}}) = \frac{1}{2} \left(\frac{\partial \mathbf{S}_i(\mathbf{q})}{\partial q_j} - \frac{\partial \mathbf{S}_j(\mathbf{q})}{\partial q_i} \right) \dot{\boldsymbol{\theta}} \tag{2.15}$$

$$C_{B1,ij}(\mathbf{q}, \dot{\mathbf{q}}) = \frac{1}{2} \left(\frac{\partial M_{ij}(\mathbf{q})}{\partial \mathbf{q}} \dot{\mathbf{q}} + \left(\frac{\partial \mathbf{M}_i(\mathbf{q})}{\partial q_j} - \frac{\partial \mathbf{M}_j(\mathbf{q})}{\partial q_i} \right) \dot{\mathbf{q}} \right) \tag{2.16}$$

$$C_{B2,ij}(\mathbf{q}, \dot{\mathbf{q}}) = \frac{1}{2} \left(\frac{\partial S_{ij}(\mathbf{q})}{\partial \mathbf{q}} \dot{\mathbf{q}} - \frac{\partial \left(\mathbf{S}^{\mathsf{T}}(\mathbf{q}) \right)_j}{\partial q_i} \dot{\mathbf{q}} \right) \tag{2.17}$$

$$C_{B3,ij}(\mathbf{q}, \dot{\mathbf{q}}) = \frac{1}{2} \left(\frac{\partial S_{ji}(\mathbf{q})}{\partial \mathbf{q}} \dot{\mathbf{q}} + \frac{\partial \left(\mathbf{S}^{\mathsf{T}}(\mathbf{q}) \right)_i}{\partial q_j} \dot{\mathbf{q}} \right) \tag{2.18}$$

P5 For articulated manipulators (having revolute joints only), the gradient of the gravity vector $\mathbf{g}(\mathbf{q})$ is globally bounded in norm by a constant, i.e.

$$\left\| \frac{\partial \mathbf{g}(\mathbf{q})}{\partial \mathbf{q}} \right\| \leq \alpha \qquad \forall \, \mathbf{q} \tag{2.19}$$

P6 The system stiffness matrix can be defined from the joint stiffness matrix $\mathbf{K} = \mathrm{diag}(k_1, \ldots, k_j, \ldots, k_N)$, $k_j \in \mathbb{R}_+$ being the stiffness of joint j, as

$$\boldsymbol{\mathcal{K}} = \begin{bmatrix} \mathbf{K} & -\mathbf{K} \\ -\mathbf{K} & \mathbf{K} \end{bmatrix} \tag{2.20}$$

Similarly the system damping can be defined in terms of the joint damping $\mathbf{D} = \mathrm{diag}(d_1, \ldots, d_j, \ldots, d_N)$, $d_j \in \mathbb{R}_+$ as

$$\boldsymbol{\mathcal{D}} = \begin{bmatrix} \mathbf{D} & -\mathbf{D} \\ -\mathbf{D} & \mathbf{D} \end{bmatrix} \tag{2.21}$$

The dynamics of an FJR manipulator given assumptions **A1**–**A2** and the before–mentioned properties can be expressed as

$$\begin{bmatrix} \mathbf{M}(\mathbf{q}) & \mathbf{S}(\mathbf{q}) \\ \mathbf{S}^{\mathsf{T}}(\mathbf{q}) & \mathbf{B} \end{bmatrix} \begin{pmatrix} \ddot{\mathbf{q}} \\ \ddot{\boldsymbol{\theta}} \end{pmatrix} + \begin{bmatrix} \mathbf{C}_{A1}(\mathbf{q}, \dot{\boldsymbol{\theta}}) + \mathbf{C}_{B1}(\mathbf{q}, \dot{\mathbf{q}}) & \mathbf{C}_{B2}(\mathbf{q}, \dot{\mathbf{q}}) \\ \mathbf{C}_{B3}(\mathbf{q}, \dot{\mathbf{q}}) & \mathbf{0} \end{bmatrix} \begin{pmatrix} \dot{\mathbf{q}} \\ \dot{\boldsymbol{\theta}} \end{pmatrix} + \begin{pmatrix} \mathbf{g}(\mathbf{q}) \\ \mathbf{0} \end{pmatrix} + \begin{pmatrix} \mathbf{K}\,(\mathbf{q} - \boldsymbol{\theta}) \\ \mathbf{K}\,(\boldsymbol{\theta} - \mathbf{q}) \end{pmatrix} = \begin{pmatrix} \mathbf{0} \\ \boldsymbol{\tau}_m \end{pmatrix} \tag{2.22}$$

For robots with large reduction ratios, the fast spinning of the rotors dominates the angular velocity of the previous links. Thus, it is reasonable to make the following assumption proposed by Spong [32].

A3 The motion of the rotors are pure rotations with respect to an inertial frame, i.e. the angular velocities of the rotors are due only to their own spinning.

Assumption **A3** is equivalent to neglecting the inertial couplings between the rotors and links. In [114] the dynamics of the ABB IRB6700 was analyzed and found that in the most extreme situation, the inertial coupling accounts for < 1 % of the torque originating from angular accelerations, while the model error for the Coriolis coupling effect is < 0.1 % in the most extreme situation. In [114] they conclude: "*Even in a high–fidelity dynamic model these effects do not add much value compared to the computational operations it also introduces.*" Modeling these rotor/link coupling effects is of fundamental interest, however provided the limited gain in model accuracy it is of little practical relevance, in the light of other model uncertainties related to mechanical flexibilities and joint dynamics. Given assumptions **A1**–**A3**, with the linear joint elasticity assumption of (2.7) relaxed, the link and rotor dynamics becomes

$$\mathbf{M}(\mathbf{q})\,\ddot{\mathbf{q}} + \mathbf{C}(\mathbf{q}, \dot{\mathbf{q}})\,\dot{\mathbf{q}} + \mathbf{g}(\mathbf{q}) + \boldsymbol{\tau}_{\text{ext}} = \boldsymbol{\tau}_J \tag{2.23}$$

$$\mathbf{B}\,\ddot{\boldsymbol{\theta}} + \mathbf{f} + \boldsymbol{\tau}_J = \boldsymbol{\tau}_m \tag{2.24}$$

where in the link equation, for simplicity $\mathbf{C}(\mathbf{q}, \dot{\mathbf{q}}) \triangleq \mathbf{C}_{B1}(\mathbf{q}, \dot{\mathbf{q}})$ which is the matrix of Coriolis and centripetal terms with $\dot{q}_j^2$ the centripetal terms and $\dot{q}_j\,\dot{q}_k,\ j \neq k$ the Coriolis terms, $\boldsymbol{\tau}_{\text{ext}}$ is the vector of torques applied externally, and $\boldsymbol{\tau}_J \in \mathbb{R}^N$ is the vector of joint torques which couples the link and rotor equations, and $\mathbf{f} \in \mathbb{R}^N$ is the vector of friction torques. If an external wrench $\mathbf{f}_{\text{ext}} \in \mathbb{R}^N$ is applied at the end–effector, the resulting

torques at the joints are

$$\boldsymbol{\tau}_{\text{ext}} = \mathbf{J}^{\mathsf{T}}(\mathbf{q})\, \mathbf{f}_{\text{ext}} \tag{2.25}$$

with $\mathbf{J}(\mathbf{q})$ the kinematic Jacobian of the manipulator. For free motion $\boldsymbol{\tau}_{\text{ext}} = \mathbf{f}_{\text{ext}} = \mathbf{0}$.

Obtaining the Link Dynamics

The robot manipulator link dynamics is most easily obtained using the Recursive Newton–Euler Algorithm (RNEA) [110]. The RNEA is initialized by specifying constraints for the base joint and the TCP. For the base joint, the angular velocity and angular acceleration (both zero if the robot is fixed statically) and the linear acceleration (g m/s^2 upward if mounted on a table with the direction of the gravitational acceleration parallel to the base joint axis of rotation) are specified. For the TCP, a zero force and zero torque is specified. To admit a linear parametrization of the dynamics, the inertia tensor is defined relative to the joint center axis of rotation (CoR). However, for the RNEA the inertia tensor is described relative to the center of mass (CoM). Thus, the parallel axis theorem (Steiner's law) is used to translate the inertia tensor between reference frames.

$$\boldsymbol{\tau}_J(\mathbf{q}, \dot{\mathbf{q}}, \ddot{\mathbf{q}}, \mathbf{g}) = \text{RNEA}(\mathbf{a}, \mathbf{d}, \boldsymbol{\alpha}, \mathbf{q}, \mathbf{m}, \mathbf{CoM}, \mathbf{I}_{\text{CoM}}, \mathbf{g},) \tag{2.26}$$

From the torque expressions of (2.26) the components of the Euler–Lagrange system can be extracted as follows. The gravity vector is obtained by evaluating the dynamics in zero angular velocity and zero angular acceleration, i.e.

$$\mathbf{g}(\mathbf{q}) = \boldsymbol{\tau}_J(\mathbf{q}, \mathbf{0}, \mathbf{0}, \mathbf{g}) \tag{2.27}$$

Let $\mathbf{e}_i$ denote the i^{th} standard basis vector of $\mathbb{R}^N$, i.e. a vector with a 1 in the i^{th} coordinate and 0's elsewhere, then the i^{th} row of the inertia matrix can be obtained as

$$\mathbf{M}_i(\mathbf{q}) = \boldsymbol{\tau}_J(\mathbf{q}, \mathbf{0}, \mathbf{e}_i, \mathbf{0}) \tag{2.28}$$

Knowing the inertia matrix, the i^{th} row of the Coriolis/centripetal matrix can be defined based on the Christoffel symbols of the first kind as

$$\mathbf{C}_i(\mathbf{q}, \dot{\mathbf{q}}) = \frac{1}{2}\, \dot{\mathbf{q}}^{\mathsf{T}} \left(\frac{\partial\, \mathbf{M}_i}{\partial\, \mathbf{q}} + \left(\frac{\partial\, \mathbf{M}_i}{\partial\, \mathbf{q}} \right)^{\mathsf{T}} - \left(\frac{\partial\, \mathbf{M}}{\partial\, q_i} \right) \right) \dot{\mathbf{q}} \tag{2.29}$$

Thus, from (2.27), (2.28), and (2.29) the link dynamics of (2.23) is obtained.

2.1.3 Joint Dynamics

This section presents the dynamics of the robot joint. Since the joint torques are uncoupled among the joints, the notation in this section is simplified to the single joint case reducing the vector equations to scalar ones.

Invented in the 1950's by C. W. Musser [115] for aerospace applications, strain-wave transmissions are now used in many robot manipulators due to their desirable characteristics of lightweight design and high torque capacity. Strain-wave transmissions are used for instance in the Universal Robots manipulators [14], Kuka LWR [15], FANUC LR Mate 200i [16], Yaskawa Motoman HP3J [17], DLR 7 DOF robot [18], and Mitsubishi PA-10 [19]. The working principle of strain-wave transmissions are based upon the elastic mechanics of metals. One example of a strain-wave transmission is the Harmonic Drive™ shown in Fig. 2.3. It consists of three parts: The *circular spline* (CS), a rigid cylinder with internal toothing; the *flexspline* (FS), a thin-walled cup with outer toothing; and the *wave generator* (WG), an elliptic shaped hub in a ball bearing.

Fig. 2.4 illustrates how the three transmission elements engage and rotate. The flexspline is smaller in diameter and has two fewer teeth compared to the circular spline. The elliptic shape of the wave generator causes the teeth of the flexspline to engage with the teeth of the circular spline at the regions around the major axis of the ellipse. Each 180° rotation of the wave generator results in one tooth relative motion between the flexspline and circular spline. The strain-wave transmission can be operated in different ways depending on the component of input and output rotation. Either the flexspline is fixed and the circular spline is the output or vice versa. The reduction ratio varies slightly depending on the configuration [116].

Strain–wave transmissions are known to possess the following complex nonlinear dynamic characteristics [76]; *flexibility*, *friction*, *hysteresis*, and *kinematic error*. This section presents our approach to dynamic modeling of these characteristics.

Flexibility

The joint torque couples the links and rotor equations, (2.23) and (2.24) respectively. Let $\boldsymbol{\phi} \triangleq \boldsymbol{\theta} - \mathbf{q}$ denote the angular deformation of the transmission and assume that the transmission has the same behavior in the CW and CCW direction and that no torque is transmitted for zero deformation, i.e.

$$\tau_J(\phi) = -\tau_J(-\phi) \quad \forall\, \phi \tag{2.30}$$

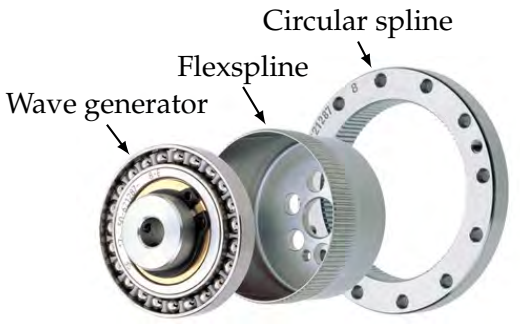

FIGURE 2.3: The Harmonic Drive™ strain-wave transmission consisting of a circular spline, flexspline, and wave generator. The wave generator comprises a thin raced ball bearing which is fitted onto an elliptical hub. `harmonicdrive.net`

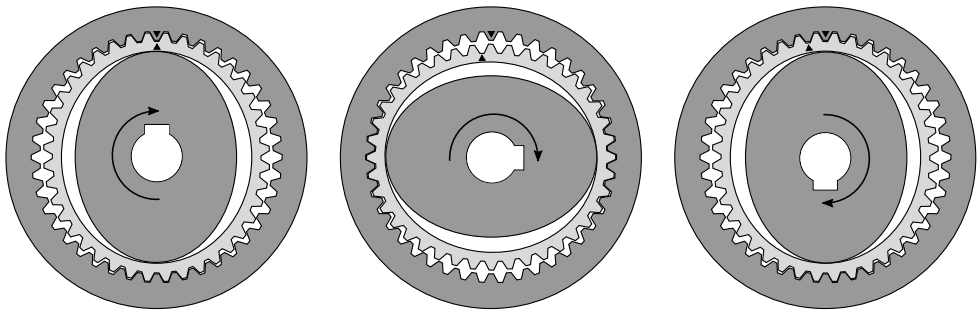

FIGURE 2.4: Working principle of a strain-wave transmission; an input revolution of 180° results in a one tooth relative motion between the circular spline and flexspline as indicated by the triangles.

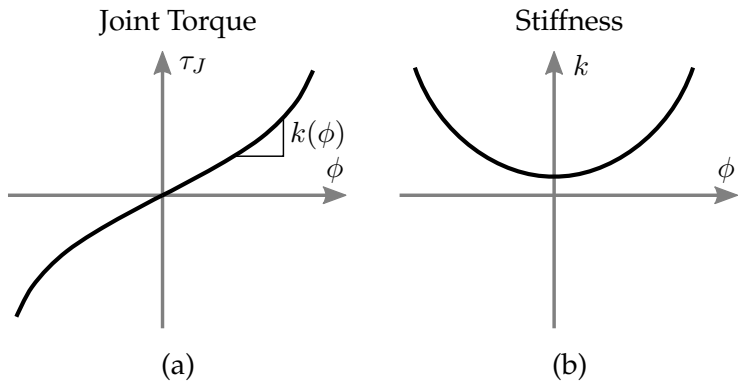

FIGURE 2.5: The stiffening spring characteristics of a strain-wave transmission; (a) the map from angular deformation ϕ to joint torque τ_J, and (b) the angular deformation-dependent stiffness $k(\phi)$.

$$\tau_J(0) = 0 \tag{2.31}$$

The joint stiffness is the change of torque wrt. angular deformation, thus

$$k(\phi) = \frac{\partial \tau_J(\phi)}{\partial \phi} \tag{2.32}$$

Strain–wave transmissions behaves as stiffening springs, i.e. the stiffness increases with the angular deformation. Harmonic Drive™ suggests a model consisting of three linear segments [116]. Such model was used by [117]. In literature, it is most common with a cubic polynomial description [81, 82, 118].

Hysteresis

Hysteresis represents the dependence of the state of a system on its history. For instance, if a solid body is subject to a force and deforms – when the force is released, does the deformation state return to its original shape completely? If not, then the material exhibits hysteresis. Mathematically, hysteresis refers to the input–output behavior of a system, that is the lag of a system's output wrt. its input. If the hysteresis vanishes for slowly varying inputs it is known as *rate-dependent*, and if durable memory is possible the hysteresis is said to be *rate-independent*. Backlash is the clearance

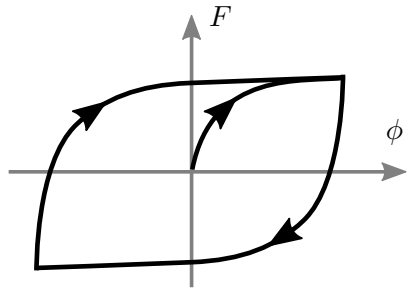

FIGURE 2.6: The hysteresis characteristics of a strain-wave transmission illustrated by the map from deformation to torque.

between mating parts, which is one of many properties of a mechanical system, that can give rise to rate-independent hysteresis characteristics. A comprehensive explanation of general terminology related to hysteresis is given in [119].

Strain-wave transmissions are known to experience hysteresis. Mathematically, the hysteresis phenomenon has been described by different hysteresis models. In [83], a nonlinear differential equations was developed based on the heredity concept of dynamic systems, while a Preisach model was used in [84]. In [85, 88], a Buc-Wen model was used, and the Generalized Maxwell-Slip model was used in [76, 120, 121, 77].

Kinematic Error

Strain-wave transmissions are subject to a periodic positioning error known as kinematic error. The kinematic error is defined as the error between the expected and actual angular output positions for a given input position, that is how much the actual transmission deviates from an ideal one. Kinematic error is caused by several factors including tooth-placement errors on the circular spline and flexspline, misalignment during assembly, and roundness errors in all three transmission components [20]. The error characteristics can have components that are integer multiples of two cycles per wave generator revolution [19] as well as integer multiples of the output-side revolution [122]. Usually, the kinematic error is approximated by a Fourier

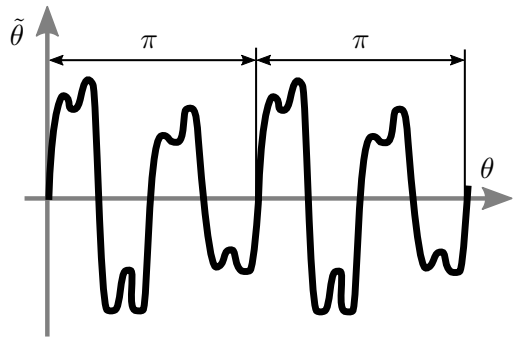

FIGURE 2.7: The kinematic error of a strain-wave transmission with π-periodic behavior in θ.

series [123–125], that is

$$\tilde{\theta}(\theta) = \frac{a_0}{2} + \sum_{n=1}^{k} [\, a_n \cos(\omega_n \theta_i) + b_n \sin(\omega_n \theta_i) \,] \tag{2.33}$$

with a_0 a constant which represents whether the impact of the positive part of the kinematic error is larger than that of the negative part, and

$$a_n = \frac{1}{\pi} \int_0^{2\,\pi} \tilde{\theta}(\theta) \cos(n\,\theta)\ \mathrm{d}\,\theta \qquad b_n = \frac{1}{\pi} \int_0^{2\,\pi} \tilde{\theta}(\theta) \sin(n\,\theta)\ \mathrm{d}\,\theta \tag{2.34}$$

In [123] the mean squared error of the approximation did not improve for $k > 12$ number of Fourier terms.

Friction

Friction affects the robot performance negatively if not properly compensated. The friction phenomenon generally involves elastic and plastic deformations as well as the dynamics of fluids. Consequently most friction models are empirical, i.e. derived from experimental observations rather than the laws of physics. Friction models can be separated into two categories; *static* and *dynamic* friction models. While static models are sufficiently accurate in steady-state conditions, dynamic models are required for capturing the dynamic effects which are especially prominent for velocity reversals.

Friction can be characterized in terms of the relative motion between two surfaces in contact. It can be divided into two regimes; *pre-sliding* and

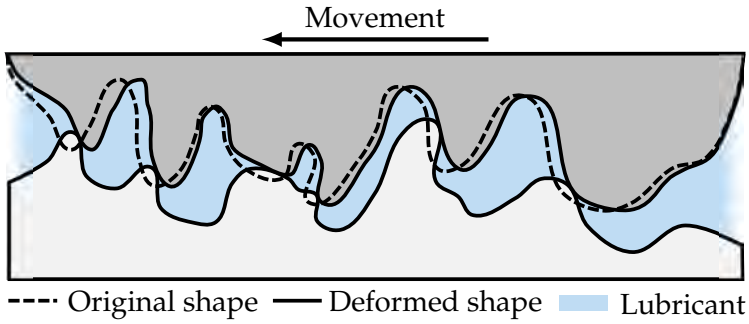

FIGURE 2.8: Friction at micro scale illustrating the pre-sliding regime. The surfaces in contact deforms elastoplastically.

gross sliding (or simply *sliding*). In the pre-sliding regime, the surfaces are in contact and the friction is mainly a function of the relative displacement of the surfaces. In the pre-sliding regime, the surfaces are in contact and deform elasto-plastically, see Fig. 2.8. For increasing displacement, the asperity junctions break and the relative velocity increases, i.e. the friction changes into the sliding regime. Here, the surfaces do not touch each other physically, but slides on a thin layer of lubricant.

2.1.4 Static Friction Models

Static friction models describe the friction as a unique mapping from a dependent variable, such as the velocity, to the friction force. Fig. 2.9 illustrate the most common static friction models. The simplest model of friction is the Coulomb model, which assumes a constant friction force acting in the reverse direction of motion. The viscous model assumes a friction force acting in the reverse direction of motion with a magnitude proportional to the velocity. The stiction model is based on the Coulomb and viscous friction model with an additional friction torque at zero velocity. The Stribeck model is based on the stiction model, however, with the transition from stiction to the sliding regime given by a continuous function. All the presented static models are however discontinuous at zero velocity, which is not an accurate description of the friction of a mechanical system. The discontinuity can be solved by describing the Coulomb friction instead as some function with a well defined derivative at zero velocity such as a

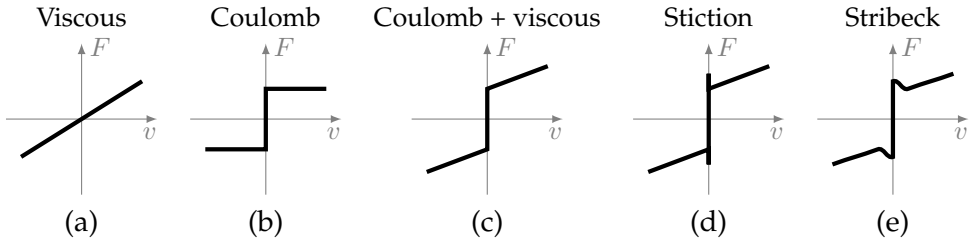

FIGURE 2.9: Illustrations of various static friction models.

hyperbolic tangent function, however such model will still not describe real friction characteristics well at low velocity.

2.1.5 Dynamic Friction Models

Dynamic friction models allow for accurate modeling of friction processes occurring at standstill and at very small velocities. In essence, the Coulomb friction law is replaced by a rate–state law.

The LuGre Model

The LuGre friction model [78] has been widely used in the robotics literature and it is given by a state equation representing the average bristle deflection z, a generalized velocity function $g(\cdot)$, and a friction force F equation, that is

$$F = \sigma_0\, z + \sigma_1\, \dot{z} + f(v) \tag{2.35}$$

$$\dot{z} = v - \frac{\sigma}{g(v)}\, |v|\, z\,, \qquad g(v) = \alpha_0 + \alpha_1\, \mathrm{e}^{(-v/v_0)^2} \tag{2.36}$$

The LuGre model has been widely used in general robotics research. However, it is unable to represent hysteresis with non-local memory, which is observed in strain-wave transmissions, and as such the LuGre model is not well suited for the modeling of strain-wave transmissions.

The Leuven model [126] was proposed as an extension to the LuGre friction model in order to be able to describe non-local hysteresis characteristics. However, practical implementation of the Leuven model resulted in the problem of stack overflow [127]. Thus, the Leuven model finally led to the development of the Generalized Maxwell-Slip model.

The Generalized Maxwell–Slip Model

The Generalized Maxwell–Slip (GMS) friction model [74, 75] differs from the LuGre friction model in multiple ways. Firstly, the GMS model is a multi-state model, i.e. $\mathbf{z} \in \mathbb{R}^M$. Conceptually it can be visualized as a parallel connection of M massless block-spring models/operators each characterized by a stiffness k_i and a maximum spring deformation Δ_i (or a slip-force limit $W_i = k_i \, \Delta_i$). Fig. 2.10 illustrates the model structure mechanically and schematically. The number of states can be chosen arbitrarily, but typically it is in the order of 3 to 5 to yield a proper trade-off between model complexity and performance. The dynamics of each operator $i = 1, \ldots, M$ is described as follows. If the element is sticking

$$\dot{F}_i = k_i \, \omega \tag{2.37}$$

where k_i is the spring stiffness of the i^{th} operator. The operator remains sticking until $F_i > \nu_i \, s(\omega)$ where the fractional parameter ν_i subject to $\Sigma_i \, \nu_i = 1$ determines the maximum force F_i for each element during sticking. If the element is slipping

$$\dot{F}_i = \operatorname{sign}(\omega) \, C_i \left(\nu_i + \frac{F_i}{s(\omega)} \right) \tag{2.38}$$

and the element remains slipping until velocity reversal. The attraction parameter C_i determines how fast $|F_i - \nu_i \, s(\omega)| \to 0$, i.e. how fast the total friction force approaches $s(\omega)$ in sliding.

The GMS friction model captures essentially all observed friction characteristics such as arbitrary shapes of hysteresis loops, non-local memory, rate-independent hysteresis, and frictional lag [128].

2.1.6 Motor Dynamics

The electrical dynamics provides the relation between the electrical quantities such as voltages and currents and the mechanical torque output. For the analyses contained in this work, the electrical dynamics are much faster than the mechanical dynamics and as such they are not taken into account. In the following, they are briefly presented for completeness. The electric actuator is current controlled three–phase permanent magnet synchronous machine (PMSM). The electrical dynamics of a PMSM expressed in the

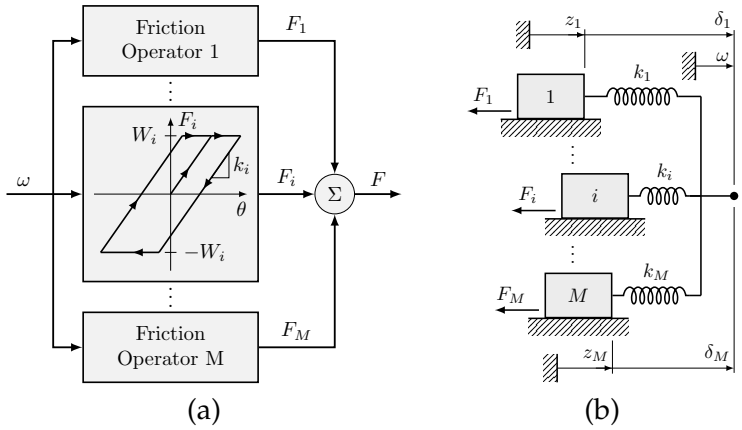

FIGURE 2.10: Schematic (a) and mechanical (b) representation of the Generalized Maxwell–Slip friction model.

Direct–Quadrature (dq) reference frame can be described as [129]

$$\begin{aligned} \frac{\mathrm{d}}{\mathrm{d}\,t}\, i_d &= \frac{1}{L_d}\, v_d - \frac{R}{L_d}\, i_d + \frac{L_q}{L_d}\, p\, \omega\, i_q \\ \frac{\mathrm{d}}{\mathrm{d}\,t}\, i_q &= \frac{1}{L_q}\, v_q - \frac{R}{L_q}\, i_q + \frac{L_d}{L_q}\, p\, \omega\, i_d - \frac{\lambda\, p\, \omega}{L_q} \end{aligned} \tag{2.39}$$

where subscripts $_d$ and $_q$ denote, respectively, quantities in the d and q reference frames, v is the stator voltage, i is the current, L is the inductance, $p \in \mathbb{N} \geq 0$ is the number of stator pole pairs, and λ is the flux linkage of the permanent magnet. The mechanical torque for a single PMSM can be expressed in the d–q rotor reference frame as

$$\tau_m = \frac{3\,p}{2}\left(\Psi\, i_q + (L_d - L_q)\, i_d\, i_q\right) \tag{2.40}$$

in which Ψ is the flux linkage of the permanent magnet. Since inductances L_d and L_q are roughly equal, and the PMSM controller operates to yield zero direct current i_d, the mechanical torque may be well approximated by

$$\tau_m = \frac{3p}{2}\, \Psi\, i_q \tag{2.41}$$

in which the toque constant of the PMSM can be identified as $K_\tau = \frac{3p}{2}\, \Psi$ and the torque-generating quadrature current $i_q \triangleq i$ from this point.

2.1.7 Modeling Summary

The parameters considered in the mathematical model of the robot and joint dynamics are listed in Table 2.2.

Robot Model	Kinematics	DH Parameters
	Dynamics	Mass
		Center of Mass
		Link Inertia
Joint Model	Kinematics	Kinematic Error
		Backlash
	Dynamics	Motor Drive Gain
		Rotor Inertia
		Stiffness
		Friction
		Hysteresis

TABLE 2.2: Kinematic and dynamic parameters for the Flexible-Joint Robot manipulator.

2.2 Identification

System identification is the art of identifying model structures and/or parameter values based on experimental input–output data. For robot manipulators, the experimental data are for instance angular positions and currents. System identification also includes the design of experiments for efficient model identification, i.e. designing the experiment(s) to describe the variation of information under conditions that are expected to reflect the variation. For instance, a robot can be configured to perform a specific motion such that the dynamic model simplifies. For **linear models** of the form

$$\mathbf{y} = \mathbf{\Psi}^{\mathsf{T}} \boldsymbol{\alpha} + \boldsymbol{v} \tag{2.42}$$

with $\mathbf{y} \in \mathbb{R}^{n\times 1}$ the vector of measurements, $\mathbf{\Psi} \in \mathbb{R}^{m\times n}$ the regressor matrix, $\boldsymbol{\alpha} \in \mathbb{R}^{m\times 1}$ the vector of unknown parameters. The least squares solution can be obtained from the *Moore–Penrose generalized inverse* of $\mathbf{\Psi}$, i.e.

$$\boldsymbol{\alpha} = \left(\mathbf{\Psi}^{\mathsf{T}}\mathbf{\Psi}\right)^{-1} \mathbf{\Psi}^{\mathsf{T}}\mathbf{y} \tag{2.43}$$

Numerical methods such as QR decomposition or Cholesky factorization can enhance the numerical stability. For **nonlinear models** of the form

$$\mathbf{f}(\boldsymbol{\alpha}) = \mathbf{0} \tag{2.44}$$

the least squares solution is obtained iteratively using for instance a Newton–Gauss method initiated at $\boldsymbol{\alpha}_0$ and iterating towards the solution as

$$\boldsymbol{\alpha}_{k+1} = \boldsymbol{\alpha}_k + \boldsymbol{\Delta\alpha}_k \tag{2.45}$$

and using the Jacobian matrix $\mathbf{J}(\boldsymbol{\alpha}) = \partial\,\mathbf{f}(\boldsymbol{\alpha})/\partial\,\boldsymbol{\alpha}$ of $\mathbf{f}(\boldsymbol{\alpha})$ to attain the least squares solution by choosing

$$\boldsymbol{\Delta\alpha}_k = -(\mathbf{J}^\mathsf{T}\,\mathbf{J})^{-1}\mathbf{J}^\mathsf{T}\mathbf{f}(\boldsymbol{\alpha}_k) \tag{2.46}$$

A large number of nonlinear programming methods exist for obtaining the solution, see for instance [130] for a overview.

2.2.1 Robot Dynamics Calibration

The minimum number of parameter required to compute the dynamic model is referred to as *base parameters*. These parameters are derived from the (standard) set of inertial parameters through a procedure described in Khalil [94]. Parameters that have no influence on the dynamics are eliminated and parameters that are identifiable only in linear combinations with other parameters are grouped.

If *a priori* knowledge of the kinematic parameters is assumed, the robot dynamics can be parametrized to a system of equations linear in a set of inertial parameters (as noted in property **P1**), thus

$$\boldsymbol{\tau}_J = \mathbf{Y}(\mathbf{q}, \dot{\mathbf{q}}, \ddot{\mathbf{q}})\,\boldsymbol{\gamma} \tag{2.47}$$

with $\mathbf{Y}(\mathbf{q}, \dot{\mathbf{q}}, \ddot{\mathbf{q}}) \in \mathbb{R}^{N \times N_p}$ the regressor of known functions and $\boldsymbol{\gamma} \in \mathbb{R}^{N_p}$ the (unknown) inertial parameters ordered link-wise, i.e.

$$\boldsymbol{\gamma} = [\,\boldsymbol{\gamma}_1^\mathsf{T}\ \cdots\ \boldsymbol{\gamma}_i^\mathsf{T}\ \cdots\ \boldsymbol{\gamma}_N^\mathsf{T}\,]^\mathsf{T} \tag{2.48}$$

A rigid body i has 10 inertial parameters; the mass, three center-of-mass (CoM) positions, and 6 inertia components (the inertia tensor is symmetric).

The inertial parameters are thus

$$\boldsymbol{\gamma}_i = [\, XX_i \;\; XY_i \;\; XZ_i \;\; YY_i \;\; YZ_i \;\; ZZ_i \;\; mX_i \;\; mY_i \;\; mZ_i \;\; m_i \,]^{\mathsf{T}} \tag{2.49}$$

Thus, an N link robot manipulator is described by a total of $N_p = 10N$ inertial parameters. More parameters can easily be added – for instance those related to (linearly parametrized) friction. The next two sections explain how the set of N_p parameters $\boldsymbol{\gamma}$ can be reduced to b_m base parameters $\boldsymbol{\gamma}_B$ to uniquely describe the link dynamics as

$$\boldsymbol{\tau}_J = \mathbf{Y}_B(\mathbf{q}, \dot{\mathbf{q}}, \ddot{\mathbf{q}})\, \boldsymbol{\gamma}_B \tag{2.50}$$

with $\boldsymbol{\gamma}_B \in \mathbb{R}^{b_m}$ the set of base parameters and $\mathbf{Y}_B(\mathbf{q}, \dot{\mathbf{q}}, \ddot{\mathbf{q}}) \in \mathbb{R}^{N \times b_m}$ the corresponding matrix of regressors.

Parameters with no Influence on the Dynamics

Considering the expressions for the kinetic and potential energies, the parameters having no influence on the dynamics satisfy

$$\sum_{i=1}^{N_p} \frac{\partial \mathcal{T}(\boldsymbol{\Theta}, \dot{\boldsymbol{\Theta}})}{\partial \boldsymbol{\gamma}_i} \boldsymbol{\gamma}_i = 0 \qquad \text{and} \qquad \sum_{i=1}^{N_p} \frac{\partial \mathcal{U}(\boldsymbol{\Theta})}{\partial \boldsymbol{\gamma}_i} \boldsymbol{\gamma}_i = 0 \tag{2.51}$$

and are thus excluded from the set of inertial parameters. Parameters that satisfy these conditions are generally related to the links close to the base joint. Parameters that have no influence on the dynamics can be eliminated by considering the zero–columns of the regressor.

Linearly Dependent Parameters

Denote

$$\mathcal{DT}_i = \frac{\partial \mathcal{T}(\boldsymbol{\Theta}, \dot{\boldsymbol{\Theta}})}{\partial \boldsymbol{\gamma}_i} \boldsymbol{\gamma}_i \qquad \text{and} \qquad \mathcal{DU}_i = \frac{\partial \mathcal{U}(\boldsymbol{\Theta})}{\partial \boldsymbol{\gamma}_i} \boldsymbol{\gamma}_i \tag{2.52}$$

A parameter γ_i is identifiable only in linear combinations with other parameters $\gamma_{1i}, \ldots, \gamma_{1k}, \ldots, \gamma_{1r}$ if

$$\mathcal{DT}_i = \sum_{k=1}^{r} \alpha_{ik}\, \mathcal{DT}_{ik} \qquad \text{and} \qquad \mathcal{DU}_i = \sum_{k=1}^{r} \alpha_{ik}\, \mathcal{DU}_{ik} \tag{2.53}$$

with α_{ik} a constant. Evaluating the conditions in (2.53) may be time consuming. Instead, parameters that fulfill these conditions for a robot manipulator with a given kinematic arrangement may be found through the closed-form re-grouping relations derived by Gautier and Khalil [36] or by numerical analysis of the regressor in (2.47) [39].

Performing Dynamics Calibration

To perform the dynamics calibration, the robot manipulator is set to perform the motion specified by a trajectory while actuator currents and angular positions are sampled. The data can be ordered joint-wise, that is $\mathbf{y} = [\,\boldsymbol{\tau}_1^\mathsf{T}, \ldots, \boldsymbol{\tau}_N^\mathsf{T}\,]^\mathsf{T}$ and the regressor $\mathbf{W} = [\,\mathbf{Y}_1^\mathsf{T}, \ldots, \mathbf{Y}_N^\mathsf{T}\,]^\mathsf{T}$ to obtain the system of equations

$$\mathbf{y} = \mathbf{W}\,\boldsymbol{\gamma}_B + \boldsymbol{\rho}\,, \qquad \boldsymbol{\rho} \sim \mathcal{N}(\mathbf{0},\, \boldsymbol{\sigma}^2) \tag{2.54}$$

Several techniques exist for the solution of (2.54) with the Ordinary Least Squares (OLS) and Weighted Least Squared (WLS) being the most common. The WLS solution is

$$\hat{\gamma}_B = \left(\mathbf{W}^\mathsf{T}\,\mathbf{G}\,\mathbf{W}\right)^{-1}\mathbf{W}^\mathsf{T}\,\mathbf{G}\,\mathbf{y} \tag{2.55}$$

with the weighting matrix $\mathbf{G}$ usually chosen as a matrix containing the reciprocal of the standard deviations estimated from the OLS solution.

2.2.2 Joint Dynamics Calibration

The dynamic characteristics of a single robot joint can be identified by providing the robot with an input signal such that the phenomenon of interest contributes the most to the output signal is excited and other contributions to the measured output signal are minimal. For instance, the steady–state friction characteristics can be identified by orienting the robot joint with the axis of rotation parallel to the direction of the gravitational acceleration.

2.3 Adaptive Estimation & Control

In this section, strategies for adaptive estimation and control are presented. Adaptive control is a strategy for the control of systems with unknown but constant or slowly varying parameters [95, 131], for instance systems subject to behavioral changes due to aging, drift, wear, etc. In non-adaptive controllers, the controller parameters are often computed based on a model

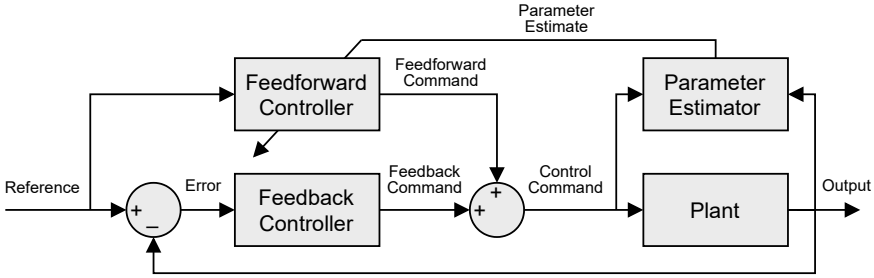

FIGURE 2.11: Schematic illustration of the self-tuning feedforward controller.

of the physical system. Thus, it is intuitive to replace the model parameters by an estimate provided by a parameter estimator. This is the concept of controllers based on the *certainty equivalence principle* such as Self-Tuning Controllers (STC), which consist of a controller combined with a parameter estimator. Fig. 2.11 illustrates schematically a self–tuning feedforward controller in which the parameter estimate is fed back to the feedforward part of the controller.

Other adaptive control strategies include for instance those based on the Model-Reference Adaptive Control (MRAC) concept. MRAC and STC are similar in the way that they comprise an inner loop for control and an outer loop for parameter estimation. MRAC is different from STC in the way that the parameters of MRAC are updated to minimize the tracking error in contrast to the prediction error minimization for STC. In comparison to STC, the MRAC parameter adaptation law depends on the control law while the control and estimation is separated on STC. This separation of control and estimation provides STC with a lot of flexibility [95]. A common model for parameter estimation is the linear parametrization of the output signal

$$y(t) = \boldsymbol{\psi}^{\mathsf{T}}(t)\,\boldsymbol{\alpha} \tag{2.56}$$

with $\boldsymbol{\psi}(t)$ the regressor of known signals and $\boldsymbol{\alpha}$ the parameter vector. If a parameter estimate $\hat{\boldsymbol{\alpha}}(t)$ is available at time t, the output can be predicted as

$$\hat{y}(t) = \boldsymbol{\psi}^{\mathsf{T}}(t)\,\hat{\boldsymbol{\alpha}}(t) \tag{2.57}$$

The difference between the measured and predicted outputs is the prediction error

$$\begin{aligned} \varepsilon(t) &= y(t) - \hat{y}(t) \\ &= y(t) - \boldsymbol{\psi}^{\mathsf{T}}(t)\,\hat{\boldsymbol{\alpha}}(t) \end{aligned} \tag{2.58}$$

Common methods of prediction error based estimation methods include Recursive Least Squares (RLS) and gradient descent. These methods provide adaptation laws for real time updating the parameter estimates. The RLS and gradient descent methods are outlined in the following.

2.3.1 Gradient Descent Estimation

In the gradient descent estimation method, parameters are updated to reduce the prediction error. Specifically, the parameters are updated in the opposite direction of the gradient of the squared prediction error wrt. the parameters. The stability properties of this estimator can be analyzed by considering the Lyapunov function candidate

$$V = \frac{1}{2}\,\tilde{\boldsymbol{\alpha}}^{\mathsf{T}}(t)\,\boldsymbol{\Gamma}^{-1}\,\tilde{\boldsymbol{\alpha}}(t) \tag{2.59}$$

If the parameter update law is chosen as

$$\dot{\hat{\boldsymbol{\alpha}}}(t) = \boldsymbol{\Gamma}\,\boldsymbol{\psi}(t)\,\varepsilon(t) \tag{2.60}$$

and if the real parameters are assumed to change slowly ($\dot{\boldsymbol{\alpha}} = 0$), the time-derivative of V is

$$\begin{aligned} \dot{V} &= -\tilde{\boldsymbol{\alpha}}^{\mathsf{T}}\,\boldsymbol{\Gamma}^{-1}\,\dot{\hat{\boldsymbol{\alpha}}}(t) \\ &= -\tilde{\boldsymbol{\alpha}}^{\mathsf{T}}(t)\,\boldsymbol{\psi}^{\mathsf{T}}(t)\,\boldsymbol{\psi}(t)\,\tilde{\boldsymbol{\alpha}}(t) \leq 0 \end{aligned} \tag{2.61}$$

which implies that the estimator is always stable for the single parameter case and for the multi parameter case the stability depends on the choice of adaptation gain [95]. Parameter convergence always depends on the excitation signal.

2.3.2 Recursive Least Squares Estimation

Time–varying parameters can be estimated by the Recursive Least Squares (RLS) algorithm [132] by the introduction of a forgetting scheme. For a

signal sampled at times $t_k = kT$, $k = 1, 2, \ldots$, the RLS algorithm with exponential forgetting reads

$$\begin{aligned} \hat{\boldsymbol{\alpha}}_{k+1} &= \hat{\boldsymbol{\alpha}}_k + \mathbf{P}_{k+1}\, \boldsymbol{\psi}_{k+1}\, \varepsilon_{k+1} \\ \varepsilon_{k+1} &= y_{k+1} - \boldsymbol{\psi}_{k+1}^{\mathsf{T}}\, \hat{\boldsymbol{\alpha}}_k \\ \mathbf{P}_{k+1} &= \frac{1}{\lambda} \left(\mathbf{P}_k - \frac{\mathbf{P}_k\, \boldsymbol{\psi}_{k+1}\, \boldsymbol{\psi}_{k+1}^{\mathsf{T}} \mathbf{P}_k}{\lambda + \boldsymbol{\psi}_{k+1}^{\mathsf{T}} \mathbf{P}_k \boldsymbol{\psi}_{k+1}} \right) \end{aligned} \tag{2.62}$$

where $\hat{\boldsymbol{\alpha}}$ is the vector of parameter estimates, $\boldsymbol{\varepsilon}$ is the estimation error, $\boldsymbol{\Phi}$ is the regressor of known functions, $\mathbf{P}$ is the parameter covariance matrix, and $0 < \lambda \leq 1$ is the forgetting factor. A value $\lambda = 1$ results in no forgetting, that is the problem simplifies to the usual RLS solution.

During poor excitation conditions, old information is continuously forgotten while little new information is obtained. This may cause the covariance matrix to grow exponentially and the estimator to become unstable. Solutions include to introduce an upper bound to the covariance matrix [133], to use an on/off method with a time-varying forgetting factor [134], resetting the covariance matrix during poor excitation conditions [135]. Kulhavý and Zarrop [136] provides a general discussion on forgetting schemes.

A popular forgetting scheme is *directional forgetting*. This forgetting scheme reduces the possibility of estimator wind-up if the incoming information is non-uniformly distributed in parameter space by performing a selective amplification of the covariance matrix. Hägglund [137] and Kulhavý [138] developed some early versions of the directional forgetting scheme, Bittanti et al. [139] discussed the convergence properties, and Bittanti et al. [140] proposed a modification in terms of a Levenberg-Marquardt regularization of the covariance matrix to ensure exponential convergence.

2.3.3 Control of Flexible-Joint Robots

In this section, the feedforward control problem for an FJR manipulator in comparison to a rigid robot is presented. An FJR manipulator is an example of a differentially flat system [141], i.e. a system where all state variables and control inputs can be expressed as an algebraic function of the flat output (the desired trajectory) and a finite number of its derivatives. However, the order (number of time-derivatives) is higher for FJR manipulators than for rigid manipulators. Differential flatness is equivalent to feedback linearization by static or dynamic state feedback [142].

The feedforward control problem is sometimes referred to as inverse dynamics control or computed–torque control. The feedforward control problem can be formulated as: "*Given a desired trajectory of the robot manipulator, compute the actuator torque required to exactly realize the desired motion*". In practice, inverse dynamics is obtained by evaluating the dynamic model in the desired motion of the generalized coordinates. For rigid manipulators $\boldsymbol{\theta} = \mathbf{q}$ and the dynamic model of (2.23) and (2.24) becomes

$$\boldsymbol{\tau}_m = (\mathbf{M}(\mathbf{q}) + \mathbf{B})\,\ddot{\mathbf{q}} + \mathbf{C}(\mathbf{q}, \dot{\mathbf{q}})\,\dot{\mathbf{q}} + \mathbf{g}(\mathbf{q}) + \mathbf{f} \tag{2.63}$$

Thus, all generalized coordinates are assigned by evaluating the dynamic model in a trajectory containing angular positions, velocities, and accelerations. In other words, the angular position must be $\mathbb{C}^1$ continuous (the angular acceleration must exist).

In the following, feedforward control for FJR manipulators with linear elastic joint is presented. For FJR manipulators, feedforward control is more complex because not all generalized coordinates are assigned directly by specifying the desired trajectory. Let higher order time-derivatives be denoted $x^{[i]} = \mathrm{d}^i\, x / \mathrm{d}\, t^i$ for $i > 2$. The dynamics of an FJR manipulator with linear elastic joints are obtained from (2.23) and (2.24) with $\boldsymbol{\tau}_J = \mathbf{K}(\boldsymbol{\theta} - \mathbf{q})$, i.e.

$$\mathbf{M}(\mathbf{q})\,\ddot{\mathbf{q}} + \mathbf{C}(\mathbf{q}, \dot{\mathbf{q}})\,\dot{\mathbf{q}} + \mathbf{g}(\mathbf{q}) = \mathbf{K}\,(\boldsymbol{\theta} - \mathbf{q}) \tag{2.64}$$

$$\mathbf{B}\,\ddot{\boldsymbol{\theta}} + \mathbf{f} + \mathbf{K}\,(\boldsymbol{\theta} - \mathbf{q}) = \boldsymbol{\tau}_m \tag{2.65}$$

Differentiating the link dynamics of (2.64) twice wrt. time yields

$$\begin{aligned} \mathbf{M}(\mathbf{q})\,\mathbf{q}^{[4]} &+ \Big(2\,\dot{\mathbf{M}}(\mathbf{q}, \dot{\mathbf{q}}) + \mathbf{C}(\mathbf{q}, \dot{\mathbf{q}})\Big)\mathbf{q}^{[3]} \\ &+ \Big(\ddot{\mathbf{M}}(\mathbf{q}, \dot{\mathbf{q}}, \ddot{\mathbf{q}}) + 2\,\dot{\mathbf{C}}(\mathbf{q}, \dot{\mathbf{q}}, \ddot{\mathbf{q}})\Big)\ddot{\mathbf{q}} \\ &+ \ddot{\mathbf{C}}(\mathbf{q}, \dot{\mathbf{q}}, \ddot{\mathbf{q}}, \mathbf{q}^{[3]})\,\dot{\mathbf{q}} + \ddot{\mathbf{g}}(\mathbf{q}, \dot{\mathbf{q}}, \ddot{\mathbf{q}}) = \mathbf{K}\,(\ddot{\boldsymbol{\theta}} - \ddot{\mathbf{q}}) \end{aligned} \tag{2.66}$$

Let

$$\begin{aligned} \mathbf{c}(\mathbf{q}, \dot{\mathbf{q}}, \ddot{\mathbf{q}}, \mathbf{q}^{[3]}) = &\Big(2\,\dot{\mathbf{M}}(\mathbf{q}, \dot{\mathbf{q}}) + \mathbf{C}(\mathbf{q}, \dot{\mathbf{q}})\Big)\,\mathbf{q}^{[3]} \\ &+ \Big(\ddot{\mathbf{M}}(\mathbf{q}, \dot{\mathbf{q}}, \ddot{\mathbf{q}}) + 2\,\dot{\mathbf{C}}(\mathbf{q}, \dot{\mathbf{q}}, \ddot{\mathbf{q}})\Big)\,\ddot{\mathbf{q}} \\ &+ \ddot{\mathbf{C}}(\mathbf{q}, \dot{\mathbf{q}}, \ddot{\mathbf{q}}, \mathbf{q}^{[3]})\,\dot{\mathbf{q}} + \ddot{\mathbf{g}}(\mathbf{q}, \dot{\mathbf{q}}, \ddot{\mathbf{q}}) \end{aligned} \tag{2.67}$$

Solving for $\ddot{\boldsymbol{\theta}}$ in (2.65) and inserting that into (2.66) yields

$$\begin{aligned} \mathbf{M}(\mathbf{q})\,\mathbf{q}^{[4]} + \mathbf{c}(\mathbf{q},\dot{\mathbf{q}},\ddot{\mathbf{q}},\mathbf{q}^{[3]}) \\ = \mathbf{K}\left(\mathbf{B}^{-1}\left(\boldsymbol{\tau}_m - \mathbf{f} - \mathbf{K}\left(\boldsymbol{\theta}-\mathbf{q}\right)\right) - \ddot{\mathbf{q}}\right) \end{aligned} \tag{2.68}$$

Replacing the term $\mathbf{K}\left(\boldsymbol{\theta}-\mathbf{q}\right)$ by the link dynamics of (2.64) yield the actuator torque expressed completely in terms of $\mathbf{q}$ and its time-derivatives, thus the feedforward control law

$$\begin{aligned} \boldsymbol{\tau}_m = \mathbf{B}\left(\mathbf{K}^{-1}\left[\,\mathbf{M}(\mathbf{q})\,\boldsymbol{v} + \mathbf{c}(\mathbf{q},\dot{\mathbf{q}},\ddot{\mathbf{q}},\mathbf{q}^{[3]})\,\right] + \ddot{\mathbf{q}}\right) \\ +\ \left(\mathbf{M}(\mathbf{q}) + \mathbf{B}\right)\ddot{\mathbf{q}} + \mathbf{C}(\mathbf{q},\dot{\mathbf{q}})\,\dot{\mathbf{q}} + \mathbf{g}(\mathbf{q}) + \mathbf{f} \end{aligned} \tag{2.69}$$

leads to the closed–loop system $\mathbf{q}^{[4]} = \boldsymbol{v}$, that is a linear and input–output decoupled system is obtained which leads to N separate chains of four integrators. The implementation of (2.69) requires the trajectory to contain the fourth-order time-derivative of the angular position, that is the angular position must be $\mathbb{C}^3$ continuous (the angular snap must exist). Comparing (2.69) to (2.63), the flexibility contribution is clearly recognized.

Linearization of the FJR manipulator system of (2.22) (without assumption **A3**) required additional smoothness of the desired trajectory, i.e. $2\,(N+1)$-times differentiable trajectories ($\mathbf{q}^{[2N+1]}$ must exist) [143]. The inverse dynamics of FJR manipulators can be realized through a recursive Newton-Euler procedure [144] that has a complexity that grows as $\mathcal{O}(N^3)$. Inverse dynamics for rigid manipulators has linear complexity, that is $\mathcal{O}(N)$.

Feedback Control of FJR Manipulators

The feedforward control law of (2.69) is a function of the linearizing coordinates $(\mathbf{q},\dot{\mathbf{q}},\ddot{\mathbf{q}},\mathbf{q}^{[3]})$. However, a feedback control law may be formulated also in terms of other state variables. The choice of a suitable feedback control strategy depends on the available sensing hardware. Indeed $(\mathbf{q},\dot{\mathbf{q}},\dot{\mathbf{q}},\mathbf{q}^{[3]})$ is a globally defined state representation and thus, the control law

$$\boldsymbol{\tau}_m = \boldsymbol{\tau}_m(\mathbf{q},\dot{\mathbf{q}},\ddot{\mathbf{q}},\mathbf{q}^{[3]},\boldsymbol{v}) \tag{2.70}$$

may be realized as nonlinear static state feedback from the original state. For most robot manipulators, it is not practically feasible to obtain reliable estimates of $\ddot{\mathbf{q}}$ and $\mathbf{q}^{[3]}$. Numerical differentiation of $\mathbf{q}$ may cause critical noise problems. Instead, the controller may be expressed in terms of the

states $(\mathbf{q}, \boldsymbol{\theta}, \dot{\mathbf{q}}, \dot{\boldsymbol{\theta}})$ which is a more suitable representation for the Universal Robots manipulators given the two absolute rotary encoder sensor setup. The link dynamics of (2.64) may be exploited to express $\ddot{\mathbf{q}}$ in terms of $\mathbf{q}$, $\dot{\mathbf{q}}$, and $\boldsymbol{\theta}$, i.e.

$$\ddot{\mathbf{q}} = \mathbf{M}^{-1}(\mathbf{q}) \left(\mathbf{K} \left(\boldsymbol{\theta} - \mathbf{q} \right) - \mathbf{C}(\mathbf{q}, \dot{\mathbf{q}}) \, \dot{\mathbf{q}} - \mathbf{g}(\mathbf{q}) \right) \tag{2.71}$$

The jerk $\mathbf{q}^{[3]}$ may be expressed in terms of $\mathbf{q}$, $\dot{\mathbf{q}}$, $\boldsymbol{\theta}$, and $\dot{\boldsymbol{\theta}}$ by time-differentiation of (2.64) and using the definition of $\ddot{\mathbf{q}}$ in (2.71), thus

$$\begin{aligned} \mathbf{q}^{[3]} = \mathbf{M}^{-1}(\mathbf{q}) \Big(& \mathbf{K} \left(\boldsymbol{\theta} - \mathbf{q} \right) - (\dot{\mathbf{M}}^{-1}(\mathbf{q}, \dot{\mathbf{q}}) + \mathbf{C}(\mathbf{q}, \dot{\mathbf{q}})) \\ & \cdot \left[\mathbf{M}^{-1}(\mathbf{q}) \left(\mathbf{K} \left(\boldsymbol{\theta} - \mathbf{q} \right) - \mathbf{C}(\mathbf{q}, \dot{\mathbf{q}}) \, \dot{\mathbf{q}} - \mathbf{g}(\mathbf{q}) \right) \right] - \dot{\mathbf{C}}(\mathbf{q}, \dot{\mathbf{q}}, \ddot{\mathbf{q}}) \Big) \end{aligned} \tag{2.72}$$

Using (2.71) and (2.72) in (2.69) a feedback linearization is obtained from the state representation $(\mathbf{q}, \dot{\mathbf{q}}, \boldsymbol{\theta}, \dot{\boldsymbol{\theta}})$, i.e.

$$\boldsymbol{\tau}_m = \boldsymbol{\tau}_m(\mathbf{q}, \dot{\mathbf{q}}, \boldsymbol{\theta}, \dot{\boldsymbol{\theta}}, \boldsymbol{v}) \tag{2.73}$$

If torque sensing is available, another possible set of linearizing coordinates are $(\mathbf{q}, \boldsymbol{\theta}, \dot{\boldsymbol{\theta}}, \boldsymbol{\tau}_J)$ as used by the DLR LWR–III lightweight manipulator [145]. Here, magneto-resistive incremental encoders are used for the motor angular positions, a full bridge of strain gauges provides joint torque sensing, and the link angular positions are obtained from a capacitive potentiometer.

A Note on Joint Torque Feedback Control

Joint torque feedback (JTF) is the general term for robot control strategies that utilizes joint torque measurements in a feedback control loop. Joint torque sensors have been widely used in the feedback motion and force control of robot manipulators with promising results [145–147, 97]. Different strategies exist for estimating the joint torque. Conventionally, the robot joints are equipped with commercially available torque sensors, however these are costly and usually takes up much space. Several alternative approaches exist.

One method is to measure the deformation of an elastic member inside the joint transmission, for instance by the use of optical distance sensors [148, 149], strain gauges [108, 150–153] or high-resolution linear encoders [154]. However, the inclusion of additional torque sensing hardware in the robot joints add significant costs to the robot.

Recently, high-resolution absolute position rotary encoders have become

commercially available. This makes it possible to directly measure the deformation of the transmission system by integrating two of these encoders in the robot joints. Combining the measurement of the transmission deformation with an accurate compliance model of the transmission system makes it possible to estimate the joint torque. This was done by Zhang et al. [155, 156]. This however requires to accurately know the robot manipulator's dynamics at all times. Predicting accurately the robot manipulator dynamics solely from math and physical arguments is not feasible since these dynamics depends on many and often unknown and time-varying factors such as temperature and wear. For instance, the robot joint stiffness change with wear [23–25] and the robot joint friction change with wear and temperature [157, 158, 71].

Patent Application 2 in Appendix B describes a method for joint torque feedback control using two absolute rotary encoders and a compliance model of the robot joint in combination with an adaptive friction observer.

Chapter 3

Online Stiffness Estimation [Conf. Paper 1]

Model-Based On-line Estimation of Time-Varying Nonlinear Joint Stiffness on an e-Series Universal Robots Manipulator [14]

"$e^{i\,\pi} + 1 = 0$"

— Leonard Euler (1707–1783)

3.1 Introduction

Strain-wave transmissions such as the Harmonic Drive™ are widely used in collaborative robots due to their desirable characteristics of high torque capacity and low weight. Flexibility commonly exist in these types of transmissions leading to a dynamic time-varying angular displacement between the rotor of the drive actuator and the driven link. Additionally, the wear of the circular spline and flexspline gear meshing leads to a decrease in stiffness, especially for small deformations [23–25]. It is of great value to know the stiffness of a robot joint, for instance in the computation of the feedforward or feedback control action and for estimating the wear of the robot joint. The latter is possible provided a relationship between the stiffness and wear is known. Existing methods for estimating the joint stiffness for industrial robots are of the *calibration* kind, either;

1) the end-effector of the robot is clamped to the environment and known torques are applied by the actuators while measuring the deformation of the joints or end-effector [159, 160], or

2) a single joint at the time is moved in pre-specified motion [18, 161–163].

With these methods it is possible to estimate the stiffness. However, due to the methodological constraints the robot is not productive during the estimation.

3.2 Method

A new method is proposed for on-line estimating the nonlinear and time-varying joint stiffness. The method works for arbitrary serial-link robot manipulators in any static or dynamic configuration which leads to a measurable deformation of the transmission. The method relies on the sensing hardware readily available in the Universal Robots manipulators, i.e. two absolute rotary encoders per joint, one at each side of the transmission, and actuator current sensing hardware. The method is patent pending, see Patent App. 1 in Appendix A.

The method works by using said measurements to generate a virtual measure of the flexibility torque, i.e. the torque that will lead to a deformation of the transmission. The virtual measure of the flexibility torque can be obtained mathematically in two ways; 1) from the motor side and 2) from the link side. In this paper, we use use the motor-side dynamics because of the higher sensor resolution of the motor-side encoder relative to the transmission deformation. It is assumed that the flexibility torque can be approximated well by a polynomial with odd powers in the transmission deformation. The virtual measure and assumed model of the flexibility torque is used in a Recursive Least Squares (RLS) based on-line estimation strategy. To estimate time-varying parameters while ensuring robustness wrt. poor excitation a directional forgetting scheme is used, and exponential convergence is ensured by a *Levenberg–Marquardt* regularization of the covariance matrix.

The on-line estimation method is validated by a comparison to an offline identification procedure, see Fig. 3.1. The offline identification procedure consist of using a force gauge to impose a set of known torques on the robot joint while measuring the transmission deformation – thus obtaining the joint stiffness.

FIGURE 3.1: Experimental setup for offline identification of the joint stiffness of the Universal Robots UR5e robot.

3.3 Findings

The assumed model of the flexibility torque is found to describe the force gauge measurements with a Normalized Root Mean Squared Error of at most 96.9 %, hence this is the maximum accuracy that can be expected from the on-line procedure. The on-line identification procedure was found to yield a slightly lower accuracy of 96.6 % after 35 seconds experiment. The capability of the method to estimate a time-varying stiffness is examined by deliberately changing the signal to half of its original value after a period of 10 seconds. Results show that after 10 seconds, the stiffness is estimated with an NRMSE of 95.2 %, while for the next 15 seconds the stiffness is estimated with an NRMSE of 94.0 %.

3.4 Reflection

With the demonstrated level of accuracy, the proposed on-line stiffness estimation method is well suited for several applications:

1) **Dynamic Calibration**: If a feedforward or feedback controller which makes use of the joint stiffness is developed, the proposed method will help ensure a consistently good controller performance during the lifetime of the robot.

2) **Predictive Maintenance**: Online monitoring the stiffness will provide an indication of the health of the robot joint.

Some additions to the presented method are suspected to further improve its performance and robustness. In particular, this work did not consider the time-variation of the friction characteristics due to the increased level of wear and changing temperature. The disturbance due to inaccurate specification of the payload was also not considered.

3.5 Author's Contribution

The author proposed the method, implemented the method in a MATLAB® environment, performed experiments, and prepared the manuscript with inputs from the co-authors.

2019 International Conference on Robotics and Automation (ICRA)
Palais des congres de Montreal, Montreal, Canada, May 20-24, 2019

Model-Based On-line Estimation of Time-Varying Nonlinear Joint Stiffness on an e-Series Universal Robots Manipulator * §

Emil Madsen[†,1,2], Oluf Skov Rosenlund[1], David Brandt[1], Xuping Zhang[‡,2]

Abstract— **Flexibility commonly exists in the joints of many industrial robots due to the elasticity of the lightweight strain-wave type transmissions being used. This leads to a dynamic time-varying displacement between the position of the drive actuator and that of the driven link. Furthermore, the joint flexibility changes with time due to the material slowly being worn off at the gear meshing. Knowing the stiffness of the robot joints is of great value, e.g. in the design of new model-based feedforward and feedback controllers, and for predictive maintenance in the case of gearing unit failure.**

In this paper, we address on-line estimation of robot joint stiffness using a recursive least squares strategy based on a parametric model taking into account the elastic torques' nonlinear dependency on transmission deformation. Robustness is achieved in the presence of measurement noise and in poor excitation conditions. The method can be easily extended to general classes of serial-link multi-degree-of-freedom robots. The estimation technique uses only feedback signals that are readily available on Universal Robots' e-Series manipulators. Experiments on the new UR5e manipulator demonstrate the effectiveness of the proposed method.

I. INTRODUCTION

Harmonic drives and other strain-wave type transmission elements are widely used in servo systems such as robots due to their desirable characteristics of lightweight design, high torque capacity, and near-zero backlash. Flexibility commonly exists in these types of transmissions leading to a dynamic time-varying displacement between the position of the drive actuator and that of the driven link. Neglecting the flexibility may negatively affect the precision and accuracy of the end-effector.

Significant research efforts have been devoted to accurately identify the dynamic characteristics of the harmonic drive transmission. However, one practical issue when taking into account the joint stiffness in the controller design is that the joint stiffness changes with wear. This is due to the gradual wear of the circular spline and flex spline teeth that will reduce the radial preload and therefore the torsional stiffness, especially in the low-deflection region [1], [2], [3]. So, a robot controller taking into account the joint flexibilities may perform well right after calibration but for a good performance over the lifetime of the robot, the joint stiffness must be estimated on-line. Further, estimating the joint stiffness on-line will allow for predictive maintenance in the case of gear unit failure.

* This work was supported by the company Universal Robots A/S and Innovation Fund Denmark (Ref.no. 7038-00058B)

§ Patent pending (*European Patent Application EP18194683.1*)

[1] Universal Robots A/S, DK-5260 Odense S, Denmark
[2] Dept. of Eng., Aarhus University, DK-8000 Aarhus C, Denmark
Corresponding authors: † ema@eng.au.dk and ‡ xuzh@eng.au.dk

In most cases, no sensor is available for directly measuring the joint stiffness, so the stiffness information is collected by combining an accurate model of the flexibility torque with measurements from the available sensor system, such as position and force/torque sensor measures, either implemented in the robot or by using external hardware.

Estimating the joint stiffness on industrial robots have been accomplished through off-line identification procedures by several researchers. One method is to apply external excitation on one robot joint at a time as in [4], [5], [6], [7], which results in a reduced dynamic model that can easier be identified. Another approach is to evaluate joint stiffness values using an external laser-tracking sensor system to visually track the end effector displacements for a given applied wrench [8]. A third option is to estimate the joint stiffness using a so-called locked-link joint procedure as in [9] where the end-effector is clamped to the environment and using either motor positions measurement and motor torques data or a force/torque sensor to measure the external wrench between the clamped end effector and the environment.

However, very few works are available on the on-line estimation of time-varying nonlinear stiffness. These works are focused towards Variable Stiffness Actuators (VSAs), e.g. the AwAS-II joint [10] and the VSA joints used in the DLR Hand Arm System [11] by the DLR Institute of Robotics and Mechatronics. In 2011, Flacco and De Luca [12] estimated the time-invariant nonlinear stiffness of robot joints using only a motor position sensor by computing a dynamic residual based on the generalized momentum followed by a least squares algorithm to estimate the stiffness parameters. Robustness issues were later addressed in [13] by introducing a kinematic Kalman filter to handle discretization and quantization errors and a modified recursive least squares algorithm was used to better handle poor excitation conditions.

To deal with time-varying nonlinear stiffness, Flacco and De Luca [14] further refined their method by using a Recursive Least Squares method based on a QR decomposition (QR-RLS). A non-causal Savitzky-Golay (SG) filter was used to remove noise on the input/output signals. However, no experiments were conducted to support their findings. Another approach to estimate the time-varying nonlinear stiffness was taken by Ménard et al. [15] who developed an observer capable of on-line estimating the time-varying stiffness of a VSA. The observer performed very well in simulations, but the experimental analysis on the VSA system revealed parameter uncertainties of up to 25 % of the true stiffness. Friction was assumed purely viscous with a single

978-1-5386-6026-3/19/$31.00 ©2019 IEEE

constant coefficient. To the best knowledge of the authors, such friction model is not capable of accurately describing real frictional characteristics of most electromechanical systems.

In this paper, we propose a novel approach to on-line estimate the flexibility torque of a general multi-degree-of-freedom robot manipulator assuming time-varying, nonlinear joint stiffness. The on-line estimate is conducted using position measurements at each side of the joints' flexible transmission and motor torque data calculated from the electric actuator current and the drive gain data. These feedback signals are readily available on Universal Robots' e-Series manipulators.

The method consists of linearly parameterizing the expression of the flexibility torque by a polynomial basis, whose parameters are updated by a recursive least squares (RLS) procedure. The specific RLS procedure chosen is able to handle time-varying parameters and poor excitation conditions. In particular, we use a RLS algorithm with forgetting related to the excited directions in the parameter space and with regularization of the covariance matrix (RLS-DF*). The parametric model is shown to converge to the real stiffness characteristics of the base joint on the UR5e manipulator by Universal Robots (UR). The functional estimation of the stiffness characteristics allows its differential expressions to be directly obtained as needed in the decoupling and linearizing control strategies. Special attention is given to the complex frictional characteristics of the robot joint. The Generalized Maxwell-Slip (GMS) friction model is utilized to describe the hysteresis of the joint, and a nonlinear friction torque/velocity map is constructed based on an initial friction identification.

The rest of this paper is organized as follows. Section II outlines the procedures to the modeling, identification and estimation. Section III and IV describes, respectively, the dynamic models of the flexible joint robot (FJR) manipulator and the flexible joint. Section V describes the initial identification of the flexible robot joint. Section VI presents the on-line least squares estimation method, and Section VII presents the experimental analysis carried out on the UR5e manipulator. Section VIII concludes on the work and discusses possible extensions for further research.

II. PRINCIPLE AND PROCEDURE

We present here the general outline of the procedure to on-line estimate the robot joint stiffness and flexibility torque as shown in Fig. 1. From the robot joint the phase currents i_{abc} through the Permanent Magnet Synchronous Machine (PMSM) coils and the absolute positions q and θ of the link and the motor axle, respectively, are measured. From the phase currents, the torque generating quadrature current i is obtained via the Park Transformation, and the motor torque τ is obtained by multiplying with the torque constant K_τ. The joint deformation $\phi = \theta - q$ is then obtained and corrected for the transmission ratio. The angular velocity of the motor axle $\dot{\theta}$ is obtained by a simple backward difference procedure from which the friction torque F_θ is estimated. Likewise, the deflection velocity $\dot{\phi}$ and the angular acceleration of the rotor is obtained by the backward difference procedure. From these signals, the damping torque and the torque from accelerating the rotor inertia are obtained. The flexibility torque is then calculated. Based on the flexibility torque and the robot joint deformation, the RLS procedure estimates the coefficients $\boldsymbol{\alpha}$ defining the robot joint stiffness from which a smoothed versio À ed.

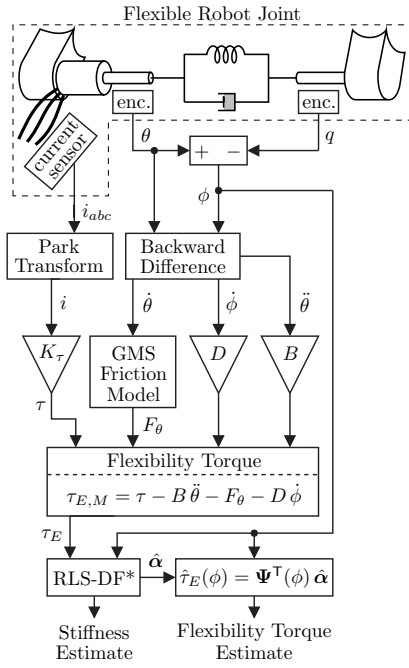

Fig. 1. Principle and procedure of the proposed method for on-line estimating the stiffness and predicting the flexibility torque. The abbreviation *enc.* refers to the term encoder.

III. ROBOT MANIPULATOR MODEL

This section presents the dynamic model of the FJR manipulator. We consider a robot with flexible joints as an open kinematic chain having $N+1$ rigid bodies, the base and the N links, interconnected by N revolute joints undergoing deflection, and actuated by N electrical drives. The following standard assumptions are made.

- **A1** The actuators' rotors are uniform bodies having their mass center on the axis of rotation.
- **A2** Each motor is located on the robot arm in a position preceding the driven link, i.e. motor i is mounted on link $i-1$ and moves link i.

Assumption **A1** is a basic requirement for long life of an electrical drive and also implies that the robot dynamics will be independent of the angular position of the rotors. For the UR5e manipulator, we take advantage of the presence of large reduction ratios and simply assume the following.

A3 The angular velocity of the rotors is due only to their own spinning.

This is equivalent to neglecting energy contributions due to the inertial couplings between the motors and the links and also implies that Coriolis and centripetal terms become independent of the rotors' angular velocity.

To uniquely characterize the manipulator configuration we choose the generalized coordinates $(q\ \theta) \in \mathbb{R}^{2N}$ which are, respectively, the link position and rotor position reflected through the gear ratio. The simplifying modeling assumptions used also by Spong in [16] yield the dynamic model of the FJR manipulator

$$M(\mathbf{q})\,\ddot{\mathbf{q}} + C(\mathbf{q},\dot{\mathbf{q}})\,\dot{\mathbf{q}} + \mathbf{G}(\mathbf{q}) + \mathbf{F_q} + \boldsymbol{\tau}_{\mathbf{ext}} = \boldsymbol{\tau}_{\mathbf{J}} \quad (1)$$

$$B\,\ddot{\boldsymbol{\theta}} + \mathbf{F}_{\boldsymbol{\theta}} + \boldsymbol{\tau}_{\mathbf{J}} = \boldsymbol{\tau} \quad (2)$$

where (1) and (2) are referred to as the link and motor equation, respectively. In the link equation, $M(q)$ is the inertia matrix, $C(\mathbf{q},\dot{\mathbf{q}})$ is the Coriolis and centripetal matrix, $\mathbf{G}(\mathbf{q})$ is the gravity vector, $\mathbf{F_q}$ is friction acting on the link coordinate, and $\boldsymbol{\tau}_{\mathbf{J}}$ is the coupling torque through the flexible transmissions. If the end effector is subject to external forces/torques $\mathbf{F_{ext}}$, the resulting joint torques $\boldsymbol{\tau}_{\mathbf{ext}} = J^{\mathsf{T}}(\mathbf{q})\,\mathbf{F_{ext}}$, where $J(\mathbf{q})$ is the manipulator Jacobian. In the motor equation, B is the positive-definite diagonal matrix of rotor inertias, $\mathbf{F}_{\boldsymbol{\theta}}$ is friction acting on the motor coordinate, and $\boldsymbol{\tau}$ is the torque generated by the motor.

IV. ROBOT JOINT MODEL

This section details the robot joint model as shown in Fig. 2. The joint transmission torques and friction phenomena are uncoupled among the joints, so for notational simplicity we consider in this section a single joint which simplifies the vector equations into scalar equations. The electric actuators

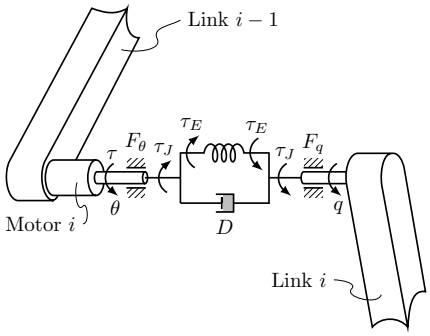

Fig. 2. Kinematic arrangement of motors and links and schematic representation of the flexible robot joint.

are three-phase PMSM with dynamics much faster than that of the manipulator. If the actuators are operated under their current saturation limit, the output torque can simply be modeled as

$$\tau = K_\tau\, i \quad (3)$$

where K_τ is the positive-definite diagonal matrix of torque constants and i is the torque-generating (quadrature) current obtained from the phase currents through the Park Transform.

The joint transmission torque τ_J is modeled as a function of the deflection variable $\phi = \theta - q$ and its time-derivative and consist of a nonlinear elastic term and linear viscosity

$$\tau_J(\phi,\dot{\phi}) = \tau_E(\phi) + D\,\dot{\phi} \quad (4)$$

where $\tau_E(\phi)$ is the nonlinear flexibility torque later to be on-line estimated, and D is the viscous damping. We assume that no flexibility torque exist for the undeformed transmission and that the transmission has the same behavior in compression and extension, thus

$$\tau_E(0) = 0 \qquad \forall\phi \quad (5)$$

$$\tau_E(-\phi) = -\tau_E(\phi) \qquad \forall\phi \quad (6)$$

Further, we assume that the flexibility torque can be approximated by the linearly parametrized polynomial basis

$$\tau_E(\phi) = \boldsymbol{\Psi}^{\mathsf{T}}(\phi)\,\boldsymbol{\alpha} \quad (7)$$

Based on the symmetry assumptions in (5) and (6) we choose specifically the regressor $\boldsymbol{\Psi}(\boldsymbol{\phi})$ to contain only odd powers in ϕ, i.e.

$$\begin{aligned}\boldsymbol{\Psi}(\phi) &= \phi^{2p-1}, \qquad p = 1,2,\ldots,P \\ &= [\,\phi\ \phi^3\ \ldots\ \phi^{2P-1}\,]^{\mathsf{T}}\end{aligned} \quad (8)$$

The stiffness is simply the rate of change of flexibility torque with respect to transmission deformation

$$k(\phi) = \frac{\partial\,\tau_E(\phi)}{\partial\,\phi} \quad (9)$$

hence the parameterization of the stiffness is simply

$$k(\phi) = \boldsymbol{\Omega}^{\mathsf{T}}(\phi)\,\boldsymbol{\alpha}, \quad \boldsymbol{\Omega}(\phi) = \phi^{-1}(2p-1)\,\boldsymbol{\Psi}(\phi) \quad (10)$$

To capture the behavior of friction and the hysteresis in the pre-sliding regime as commonly experienced by strain-wave transmissions [17], [18] we utilize the Generalized Maxwell-Slip (GMS) model [19]. The GMS model is based on three frictional properties; 1) a Stribeck curve for constant velocities, 2) a hysteresis function with nonlocal memory in the pre-sliding regime, and 3) a frictional lag in the sliding regime. The GMS model can be visualized as a parallel connection of M massless block-spring models (see Fig. 3) subject to the same input velocity $\omega = \mathrm{d}\,\theta/\mathrm{d}\,t$. The total friction force is given as the summation of friction forces for each element j, i.e.

$$F_\theta = \sum_{j=1}^{M} F_j \quad (11)$$

The dynamics of each elementary model is represented by the equations (12) and (13). If the element is sticking

$$\frac{\mathrm{d}\,F_j}{\mathrm{d}\,t} = k_j\,\omega \quad (12)$$

where k_j is the spring stiffness of the j^{th} element. The element remains sticking until $F_j > \nu_j\,s(\omega)$ where the

fractional parameter ν_j subject to $\Sigma_j\, \nu_j = 1$ determines the maximum force F_j for each element during sticking. If the element is slipping

$$\frac{\mathrm{d}\, F_j}{\mathrm{d}\, t} = \mathrm{sign}(\omega)\, C \left(\nu_j + \frac{F_j}{s(\omega)} \right) \tag{13}$$

and the element remains slipping until velocity reversal. The attraction parameter C determines how fast the total friction force approaches $s(\omega)$ in sliding.

The nonlinear static map

$$\begin{aligned} s(\omega) = \mathrm{sign}(\omega)(F_C + (F_S - F_C) \\ \cdot \exp[-(|\omega|/v_S)^{\mu}]) \\ + F_{V_1}\, \omega + F_{V_2}\, \mathrm{sign}(\omega)\, \omega^2 + F_{V_3}\, \omega^3 \end{aligned} \tag{14}$$

captures the Stribeck effect and nonlinear viscous friction. F_C, F_S, v_S and μ are, respectively, the Coulomb friction, the stiction, the Stribeck velocity, and the Stribeck shape factor, and $F_{V_{1,2,3}}$ are viscous coefficients of friction.

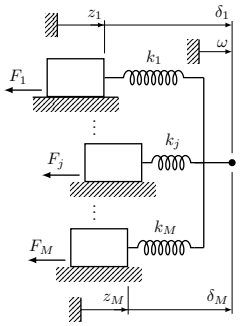

Fig. 3. Schematic representation of the Generalized Maxwell-Slip friction model.

V. OFF-LINE IDENTIFICATION

Before we proceed to the on-line estimation of time-varying nonlinear stiffness, we first conduct off-line identification of the friction and stiffness characteristics for the base joint of the UR5e manipulator. The joint is operated in the vicinity of the gravity torque and in a non-contact application.

Throughout the paper, the quality of a model is evaluated by the Normalized Root Mean Squared Error (NRMSE) expressed as a percentage, i.e.

$$\mathrm{NRMSE} = 100 \cdot \left(1 - \frac{||y - \hat{y}||}{||y - \bar{y}||} \right) \tag{15}$$

where $||\ ||$ denotes the 2-norm, $\hat{}$ denotes the estimate, and $\bar{}$ denotes the mean value.

Friction: The steady-state friction torque/velocity map in Fig. 4 is identified by imposing different signals of constant velocity on the base joint while measuring the actuator current. For constant velocity (1), (2), and (3) yield $F_\theta + F_q = K_\tau\, i$. Additionally, (11) and (13) reduce to $F_\theta = s(\omega)$. Assuming further that friction act on the motor coordinate only, i.e. $F_q = 0$, we have $s(\omega) = K_\tau\, i$. An optimum set of parameters in (14) are found using a Quasi-Newton method with a cubic line search procedure and updating the Hessian matrix approximation by the Broyden-Fletcher-Goldfarb-Shanno (BFGS) method.

In this preliminary study, we do not identify the hysteresis and dynamic friction characteristics but choose the parameters M, ν_j, and k_j in (11), (12), and (13) in a rather ad hoc way. In a subsequent study, we are to conduct the hysteresis identification by imposing a cyclic motion with sufficiently small position and acceleration amplitudes while measuring the actuator current and transmission deformation from which ν_j, k_j, and C can be identified. In this study, it is found, that the accuracy of the GMS model does not improve much beyond five elements so in (11) we choose $M = 5$.

Stiffness: The map from transmission deformation to flexibility torque in Fig. 5 is obtained in a static setting by locking the input shaft and imposing a set of known torques on the output shaft using a Sauter FH–S 500 digital force gage while measuring the transmission deformation. These measurements serves as a baseline for the on-line estimation method. The model fit is obtained as the least squares (LS) solution for a model with two coefficients. In the following we choose $P = 2$ in (8), i.e. $\mathbf{\Psi}(\phi) = [\ \phi\ \ \phi^3\ ]^{\mathsf{T}}$. We note also that the actual stiffness varies significantly compared to the values stated by Harmonic Drive and thus the data sheet values should be used only as a rough approximation.

The stiffening spring characteristics can be explained as the increase in applied torque resulting in more width of the flex spline teeth to engage with the circular spline. The increased load sharing increases the torsional stiffness.

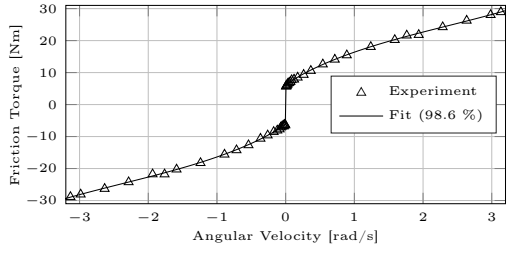

Fig. 4. Friction torque/velocity map obtained by imposing different signals of constant velocity on the base joint while measuring the actuator current.

VI. RECURSIVE LEAST SQUARES ESTIMATION

The flexibility torque cannot be measured directly with the sensor system available. Instead, signals of the flexibility torque are generated from (1), (2), and (4)

$$\boldsymbol{\tau}_{\mathbf{E,L}} = M(\mathbf{q})\, \ddot{\mathbf{q}} + C(\mathbf{q}, \dot{\mathbf{q}})\, \dot{\mathbf{q}} + \mathbf{G}(\mathbf{q}) + \boldsymbol{\tau}_{\mathbf{ext}} - D\, \dot{\boldsymbol{\phi}} \tag{16}$$

$$\boldsymbol{\tau}_{\mathbf{E,M}} = \boldsymbol{\tau} - B\, \ddot{\boldsymbol{\theta}} - \mathbf{F}_{\boldsymbol{\theta}} - D\, \dot{\boldsymbol{\phi}} \tag{17}$$

where subscripts $_L$ and $_M$ denote, respectively, calculations based on the link and motor equation.

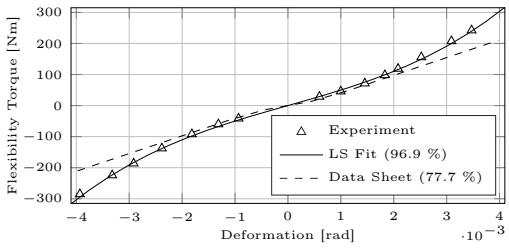

Fig. 5. Flexibility torque/transmission deformation map obtained by imposing a set of known torques using a force gage and measuring the transmission deformation as the difference between absolute encoder readings at each side of the flexible transmission.

Estimating time-varying parameters with the Recursive Least Squares (RLS) approach is obtained by incorporating a forgetting scheme discounting past data. In the present example, the incoming information (the transmission deformation) is nonuniformly distributed over the parameter space. Tracking can only happen in some direction if there is an excitation in that same direction, hence the estimation algorithm tracks time-varying parameters only within the excited subspace. Therefore, inspired by the results in [20] and [21], by a suitable notion of excitation subspace, the parameter vector $\boldsymbol{\alpha}$ in (7) is estimated by the procedure

$$
\begin{aligned}
\varepsilon(k) &= \tau_E(k) - \boldsymbol{\Psi}^{\mathsf{T}}(k)\,\hat{\boldsymbol{\alpha}}(k-1) \\
r(k) &= \boldsymbol{\Psi}^{\mathsf{T}}(k)\,P(k-1)\,\boldsymbol{\Psi}(k) \\
\mathbf{L}(k) &= \frac{P(k-1)\,\boldsymbol{\Psi}(k)}{1+r(k)} \\
\hat{\boldsymbol{\alpha}}(k) &= \hat{\boldsymbol{\alpha}}(k-1) + \mathbf{L}(k)\,\varepsilon(k) \\
\beta(k) &= \begin{cases} \mu - \frac{1-\mu}{r(k)}, \quad \mu \in [0;1] & \text{if } r(k) > 0 \\ 1 & \text{if } r(k) = 0 \end{cases} \\
P(k) &= P(k-1) - \frac{P(k-1)\,\boldsymbol{\Psi}(k)\,\boldsymbol{\Psi}^{\mathsf{T}}(k)\,P(k-1)}{\beta(k)^{-1} + r(k)} + \delta\, I
\end{aligned}
\tag{18}
$$

where $\delta > 0$ enforces an increment of the covariance matrix P improving the algorithm alertness. More alertness is achieved by decreasing μ at the price of an increased sensitivity to disturbances. By setting $\mu = 1$ and $\delta = 0$, (18) reduces to the standard RLS algorithm.

VII. EXPERIMENTS

Generating the flexibility torque signal based on the link equation in (16) results in a noisy signal due to the encoder quantization and time discretization. We proceed by estimating the flexibility torque from (17) only. In the future, one could estimate the flexibility torque using both (16) and (17) by fusing the data.

In the experiment we use the UR5e manipulator by Universal Robots shown in Fig. 6 and move the base joint without the robot making contact with the environment. The flexibility torque in (17) thus becomes

$$
\tau_{E,M_1} = K_{\tau_1}\, i_1 - B\,\ddot{\theta}_1 - F_{\theta_1} - D_1\,\dot{\phi}_1 \tag{19}
$$

where the time-derivatives are approximated by a backward difference procedure. Data is sampled at 1000 Hz.

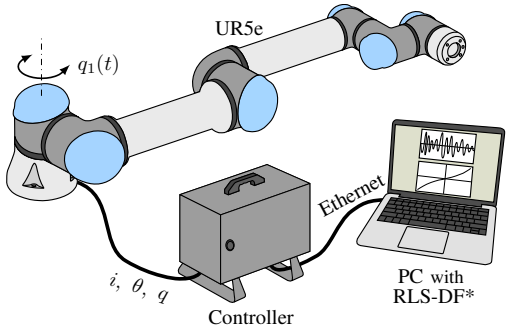

Fig. 6. UR5e manipulator in the configuration used in the experimental analysis.

A. Excitation Signal

The base joint is moved according to the bang-coast-bang joint space trajectory in Fig. 7 with randomly generated waiting times from 0–1 second and angular positions, velocities, and accelerations in intervals ranging from 30 % to 100 % of the maximum allowed values.

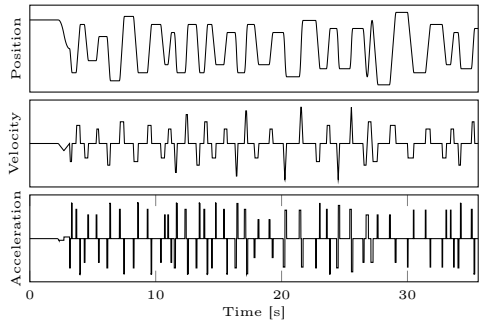

Fig. 7. Joint space trajectory used in the experimental analysis.

B. Results

We initialize the recursive least squares algorithm in (18) with the parameter estimate $\hat{\boldsymbol{\alpha}}(0) = [\ 0\ 0\ ]^{\mathsf{T}}$, covariance matrix $P(0) = diag(1\text{E}9, 1\text{E}18)$, $\delta = 0.1$, and $\mu = 0.99995$.

At the end of the experiment, after 35 s, the map from transmission deformation to flexibility torque is that shown in Fig. 8. We see that the stiffness estimated on-line by the RLS-DF* algorithm is very close to the baseline stiffness curve obtained via the static experiment. Therefore, the proposed method seems promising for on-line estimating the joint transmission stiffness.

The flexibility torque estimated using the proposed method is given in Fig. 9 using (7) to predict the signal in (19). The

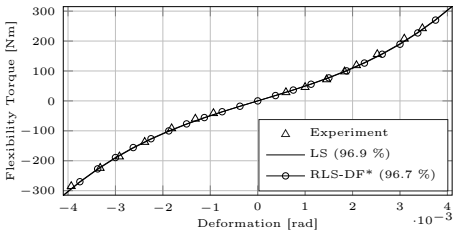

Fig. 8. Off-line identified and on-line estimated map from transmission deformation to flexibility torque.

predicting capability according to the NRMSE is 73.9 % evaluated after the first 15 seconds. Predicting the flexibility torque on-line could for instance be relevant in a compensation scheme, e.g. complemented by a disturbance observer to account for unmodeled dynamics. Inserting the estimated flexibility torque in (1) will allow to more accurately predict the torque from external disturbances, for instance human interference, which is of great concern in terms of safety. The method thus seems reasonable, since in less than one second with excitation the model adapts to predict the flexibility torque from the measured transmission deformation.

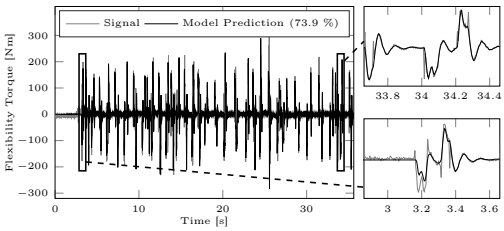

Fig. 9. Signals of the flexibility torque obtained using (19) and predicted by model using the RLS-DF* algorithm in (18) and using (7) to generate the output.

C. Time-Varying Stiffness

It is well known that Harmonic Drives experience a decrease in joint stiffness over time due to the wear and tear of the gear meshing. Within the 35-second experiment the robot manipulator did not experience varying stiffness. Therefore, the experiment did not demonstrate the RLS-DF* algorithms' ability to track time-varying stiffness. It was not possible to run the experiment until a change in stiffness could be observed. Therefore, to demonstrate the capabilities of the proposed method to track time-varying stiffness, we intentionally reduce the amplitude of the flexibility torque signal from (19) after 10 seconds according to the simple linear transformation

$$\tilde{\tau}_{E,M_1} = \begin{cases} \tau_{E,M_1} & \text{if } 0 \leq t \leq 10\,\text{s} \\ 0.5\,\tau_{E,M_1} & \text{if } 10\,\text{s} < t < t_{\text{end}} \end{cases} \tag{20}$$

The map from flexibility torque to transmission deformation therefore change according to Fig. 10. The RLS-DF* algorithm is initialized with the same parameters as before. In 10 seconds we on-line estimate the baseline stiffness curve to a NRMSE of 95.2 %. Changing the signal according to (20) and waiting another 25 seconds yields a NRMSE of 94.0 %. The proposed method is therefore considered to be a reliable method for on-line estimating time-varying stiffness of robot joints.

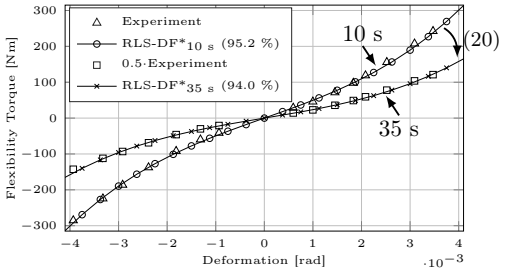

Fig. 10. Map from transmission deformation to flexibility torque at 10 s; just before the transformation in (20), and at 35 s; at the end of the experiment, 25 s after the transformation.

VIII. CONCLUSIONS

In this paper we demonstrated on-line estimation of time-varying and nonlinear robot joint stiffness. The contribution is twofold. First, we propose the method for off-line identification of the nonlinear friction and stiffness characteristics. Second, we propose the on-line estimation method based on the RLS-DF* algorithm. Then we experimentally demonstrate the method for on-line estimating the flexibility torque, which is directly related to the transmission stiffness. In particular, using the RLS-DF* algorithm we achieve robustness in periods of poor excitation and at the same time ensuring reactiveness to parametric changes, i.e. changing stiffness that is known to occur over time.

Monitoring the joints' stiffness characteristics will provide valuable information about the transmissions' health condition. However, additional information is needed relating the robot joint stiffness to the gear unit failure statistics.

On-going research will include the following topics.

1) The robot joint friction is known to change along with the wear and tear of the robot joint and changes in the ambient conditions. Possible future work will therefore include on-line estimating the friction.
2) Thanks to the use of two built-in absolute encoders we demonstrate that we effectively have a joint torque sensor, which leads to the possible future work of conducting decoupling and feedback linearizing control.

ACKNOWLEDGMENT

We would like to acknowledge the valuable support from Universal Robots A/S and Innovation Fund Denmark (Ref.no. 7038-00058B).

REFERENCES

[1] T. W. Nye, "Harmonic Drives: Determining Wear Life Based on Stiffness Considerations," in Proc. of the International Power Transmission and Gearing Conference, Chicago, April 25-28, 1989.

[2] M. R. Johnson et al., "Life Test Failure of Harmonic Gears in a Two-Axis Gimbal for the Mars Reconnaissance Orbiter Spacecraft," Proceedings of the 38th Aerospace Mechanisms Symposium, Langley Research Center, May 17-19, 2006.

[3] J. Mobley and J. Parker, "Harmonic Drive™ Gear Material Selection and Life Testing," Proceedings of the 41th Aerospace Mechanisms Symposium, Jet Propulsion Laboratory, May 16-18, 2012.

[4] A. Albu-Schäffer and G. Hirzinger, "Parameter identification and passivity based joint control for a 7DOF torque controlled light weight robot," in Proc. of IEEE International Conference on Robotics & Automation (ICRA), Seoul, Korea, May 21-26, 2001, pp. 2852–2858.

[5] M. T. Pham et al., "Identification of joint stiffness with bandpass filtering," in Proc. of IEEE International Conference on Robotics & Automation (ICRA), Seoul, Korea, May 21-26, 2001, pp. 2867–2872.

[6] M. Östring et al., "Closed-loop identification of an industrial robot containing flexibilities," in Control Engineering Practice, vol. 11, 2003, pp. 291–300.

[7] M. Gautier et al., "Dynamic Identification of flexible joint manipulators with an efficient closed loop output error method based on motor torque output data," in IEEE International Conference on Robotics and Automation (ICRA), Karlsruhe, Germany, May 6-10, 2013, pp. 2949–2955.

[8] C. Dumas et al., "Joint stiffness identification of six-revolute industrial serial robots," in Robotics and Computer-Integrated Manufacturing, vol. 27, 2011, pp. 881–888.

[9] A. Jubien et al., "Joint Stiffness Identification of a Heavy Kuka Robot with a Low-cost Clamped End-effector Procedure," in Proc. of International Conference on Informatics in Control, Automation and Robotics (ICINCO), Vienna, Austria, Sept. 1-3, 2014, pp. 585–591.

[10] A. Jafari et al., "AwAS-II: A new Actuator with Adjustable Stiffness based on the novel principle of adaptable pivot point and variable lever ratio," in Proc. of IEEE International Conference on Robotics & Automation (ICRA), Shanghai, China, May 9-13, 2011, pp. 4638–4643.

[11] M. Grebenstein et al., "The DLR Hand Arm System," in Proc. of IEEE International Conference on Robotics & Automation (ICRA), Shanghai, China, May 9-13, 2011, pp. 3175–3182.

[12] F. Flacco and A. De Luca, "Residual-based Stiffness Estimation in Robots with Flexible Transmissions," in Proc. of IEEE International Conference on Robotics & Automation (ICRA), Shanghai, China, May 9-13, 2011, pp. 5541–5547.

[13] F. Flacco and A. De Luca, "Robust Estimation of Variable Stiffness in Flexible Joints," in Proc. of IEEE/RSJ International Conference on Intelligent Robots and Systems, San Francisco, CA, USA, September 25-30, 2011, pp. 4026–4033.

[14] F. Flacco and A. De Luca, "A Pure Signal-Based Stiffness Estimation for VSA Devices," in Proc. of IEEE International Conference on Robotics & Automation (ICRA), Hong Kong, China, May 31 - June 7, 2014, pp. 2418–2423.

[15] T. Ménard et al., "A real time robust observer for an Agonist-Antagonist Variable Stiffness Actuator," in Proc. of IEEE International Conference on Robotics & Automation (ICRA), Karlsruhe, Germany, May 6-10, 2013, pp. 3988–3993.

[16] M. W. Spong, "Modeling and Control of Elastic Joint Robots," Journal of Dynamic Systems, Measurement, and Control, vol. 109, no. 4, 1987, pp. 310–319.

[17] R. Dhaouadi et al. "A New Dynamic Model of Hysteresis in Harmonic Drives," IEEE Trans. on Industrial Electronics, vol. 50, no. 6, pp. 1165–1171, 2003.

[18] T. Tjahjowidodo et al., "Theoretical modelling and experimental identification of nonlinear torsional behaviour in harmonic drives," Mechatronics, vol. 23, no. 5, August 2013, pp. 497–504.

[19] V. Lampaert et al., A Generalized Maxwell-Slip Friction Model appropriate for Control Purposes," in IEEE International Conference for Physics and Control, St. Petersburg, Russia, Proceedings, pp. 1170–1177, 2003.

[20] S. Bittanti et al., "Recursive Least-Squares Identification Algorithms with Incomplete Excitation: Convergence Analysis and Application to Adaptive Control," IEEE Trans. Automatic Control, vol. 35, pp. 1371–1373, 1990.

[21] S. Bittanti et al., "Convergence and Exponential Convergence of Identification Algorithms with Directional Forgetting Factor," Automatica, Vol. 26, No. 5, pp. 929–932, 1990.

Chapter 4

Joint Dynamics Modeling [Journal Paper 1]

Comprehensive Modeling and Identification of Nonlinear Joint Dynamics for Collaborative Industrial Robot Manipulators [122]

"Experiment is the sole interpreter of the artifices of nature."

— Leonardo da Vinci (1452–1519)

4.1 Introduction

To obtain a high-fidelity mathematical model, the dynamics of the robot joint must be considered. Existing works on the joint dynamics modeling of industrial robots describe friction in terms of static nonlinearities in the angular velocity, load torque, and temperature [69, 29, 31]. However, strain-wave transmissions are known to experience more complex nonlinear behavior of nonlinear stiffness, hysteresis, and kinematic error [164, 76, 165].

4.2 Method

In this work, a high-fidelity mathematical model of the robot joint dynamics is developed based on extensive experimental analyses on the base joint of

the Universal Robots UR5e manipulator. First, the static nonlinear dependencies of friction on the angular velocity, load torque, and temperature are identified. Then, the kinematic error and hysteresis characteristics are identified. For each identified phenomenon, a mathematical model is proposed to describe the observations.

4.2.1 Experiments

The various experiments are designed to isolate each individual joint dynamics phenomenon. Such isolation simplifies mathematically the otherwise complex and nonlinear robot dynamics, hence facilitate subsequent system identification. In the following, the various experiments designed to isolate each individual joint dynamics phenomenon are described.

1) **Stiffness**: The robot joint is oriented with the axis of rotation oriented parallel to the direction of the gravitational acceleration such that gravity will induce no torque. The joint is subject to a set of torques in the clockwise (CW) and counter-clockwise (CCW) directions using a force gauge with a known perpendicular distance to the joint axis of rotation. The stiffness is identified in two ways; 1) using the force gauge data and 2) using the actuator current data.

2) **Static Friction**: The steady-state friction characteristics are known to depend on angular velocity, load torque, and temperature.

   (a) **Angular Velocity**: The robot joint is oriented with its axis of rotation parallel to the direction of the gravitational acceleration such that there will be no torque induced by gravity. The joint is subject to a set of constant-velocity motions in the CW and CCW directions.

   (b) **Load Torque**: The robot joint is oriented with its axis of rotation perpendicular to the direction of the gravitational acceleration so that gravity will induce a torque on the joint. The joint is subject to a set of constant-velocity motions in the CW and CCW directions. The load torque can be estimated based on the robot dynamics.

   (c) **Temperature**: Prior to the experiment, the robot is cooled down. The robot joint is oriented with its axis of rotation parallel to the direction of the gravitational acceleration to eliminate torques

induced by gravity. The joint is subject to a set of constant-velocity motions in the CW and CCW directions.

3) **Kinematic Error, Backlash & Dynamic Friction**: The kinematic error, backlash, and dynamic friction are identified from the same experiment. The joint is oriented with its axis of rotation parallel to the direction of the gravitational acceleration such that gravity will not induce torque around the joint axis of rotation. The joint is subject to one full revolution over 17 minutes while reversing 240 times with very low angular velocity and acceleration.

   (a) **Backlash**: The backlash for any given angular position is defined as the difference in transmission deformation for CW and CCW motion.

   (b) **Kinematic Error**: The kinematic error for any given angular position is defined as the midpoint/average of the transmission deformations in the CW and CCW directions.

   (c) **Dynamic Friction**: The dynamic friction characteristics is defined as the behavior of the torque during velocity reversals – specifically, the behavior of the friction torque while the direction of motion changes (angular velocity changes sign).

4.2.2 Identification

For each of the above-mentioned experiments, a mathematical (sub)model is proposed to describe each joint dynamics phenomenon individually. The combination of all submodels yields the comprehensive joint dynamics model. The goal is to find mathematical models that are coherent with observations and have a minimum number of describing functions and parameters. Furthermore, the choice of parameterization should be practically suitable for identification, i.e. linear if possible.

4.3 Findings

It is found that the stiffness can be described accurately by two parameters, specifically a linearly parameterized polynomial of the first two odd powers in the transmission deformation. This result is coherent with our experience in [14] and results presented in [81, 82, 118]. The dependency of friction on the angular velocity is modeled by a nonlinear function of seven parameters.

The dependency of friction on load is described by a single parameter times the squared load torque. This model was found more accurate for the UR5e robot compared to the model presented in [29]. The dependency of friction on the temperature is described by a linearly parameterized polynomial of three parameters. The kinematic error depends nonlinearly on the joint angular position, and it is described by linear interpolation between 1 000 equispaced points over one revolution. Existing works identify backlash at a specific angular position and assume the same value for other angular positions [164, 76, 166]. However, as the paper reveals, the amount of backlash depend on the angular position. Such behavior was deemed possible from theoretical and numerical analyses by Dong et al. [167]. The kinematic error and backlash were modeled by linear interpolation between 1 000 equispaced points over one revolution. The dynamic friction is found to be described well by the GMS friction model. Known identification methods for the GMS model are examined including linear and nonlinear regression methods. A new linear regression based identification method which outperforms existing linear regression methods is proposed. For ≥ 4 operators, the performance is comparable to that of the nonlinear regression method, keeping the advantages of fast and robust optimization of the parameters.

4.4 Reflection

The joints of the Universal Robots collaborative robot manipulators comprise strain-wave transmissions. Mathematical models have been proposed to describe various joint dynamics phenomena. The combination of the models constitutes a high-fidelity joint dynamics model. This model may facilitate the improvement of the robot performance in various areas:

- **Safety:** External disturbances can be identified more quickly, thus in the possible event of a collision with a human being, the robot motion may be stopped faster which reduces the risk of injury [7–9].
- **Precision & Accuracy:** Improved model knowledge may allow the robot to follow the motion or force reference with greater accuracy. For instance, the model knowledge can be exploited by introducing a model-based compensation in the feedforward controller to compensate disturbances before they cause deviations from the reference [10, 11].

- **Lead-through Programming:** It allows to more accurately identify the human-applied wrench, leading to a more smooth lead-though programming experience [12].

4.5 Author's Contribution

The author proposed the identification procedures and mathematical models, implemented the models and procedures in a MATLAB® environment, performed experiments, and prepared the manuscript with inputs from the co-authors.

Control Engineering Practice 101 (2020) 104462

Contents lists available at ScienceDirect

Control Engineering Practice

journal homepage: www.elsevier.com/locate/conengprac

Comprehensive modeling and identification of nonlinear joint dynamics for collaborative industrial robot manipulators ☆

Emil Madsen [a,b,*], Oluf Skov Rosenlund [a], David Brandt [a], Xuping Zhang [b,**]

[a] Universal Robots A/S, Energivej 25, DK-5260 Odense S, Denmark
[b] Aarhus University, Inge Lehmanns Gade 10, DK-8000 Aarhus C, Denmark

ARTICLE INFO

Keywords:
Collaborative robots
System identification
Flexible-joint robot manipulators
Strain-wave transmissions
Friction

ABSTRACT

For collaborative robots, the ability to accurately predict the actuator torques required to realize the desired task is highly important. This will improve and guarantee the safety, motion and force control performance, and smooth lead-through programming experience. Thus, this paper presents the investigation towards comprehensive modeling and identification of nonlinear joint dynamics for collaborative robots. The proposed joint dynamics model and identification describes the most dominant dynamic characteristics of robot joints that comprise strain-wave transmissions, such as nonlinear friction, nonlinear stiffness, hysteresis, and kinematic error. Position-dependent backlash characteristics is observed and quantified using our proposed identification method and the Generalized Maxwell-Slip friction model is extended to describe the observed phenomena. The developed dynamic modeling and identification procedures provides insightful guidance for the design and model-based control of collaborative robots.

1. Introduction

In the area of collaborative industrial robots it is important to acquire accurate torque predictions due to several reasons:

1. **(Safety).** It allows to accurately identify external disturbances such as human interference, hence any potentially harmful robot motion can be stopped faster, effectively reducing the risk of injury (Haddadin, Albu-Schaffer, Luca, & Hirzinger, 2008; Luca, Albu-Schaffer, Haddadin, & Hirzinger, 2006). In fact, the level of safety can be generally enhanced in physical Human–Robot Interaction (pHRI) and Human–Robot Collaboration (HRC) tasks.
2. **(Precision & Accuracy).** It allows to accurately follow the trajectory or force reference because disturbances can be accounted for before they affect the robot system and cause deviations from the reference. The compensation is introduced for instance with an additional term in the feed-forward part of the control structure (Bona & Indri, 2005; Olsson, Åström, de Wit, Gäfvert, & Lischinsky, 1998).
3. **(Lead-Through Programming).**[1] It allows to improve the performance of *programming by demonstration* applications by minimizing the force required by the user to move the robot around (Stolt et al., 2015).

Additional benefits include enhanced controller stability, lower energy consumption, and it generally allows to design the robot system using lower-cost components, i.e. less material (for structural rigidity), less accurate sensors, and lower demands on computational resources.

Current advancements in robotics such as industrial robot manipulators tend towards replacing heavy and rigid structures with lightweight structures. The motivation is that the lightweight systems are capable of achieving higher velocity, acceleration, mobility, safety, and energy efficiency. However, the increased structural flexibility of lightweight components complicates the development of such systems.

Accurate modeling of joint dynamics effects pose a major challenge in the control system design for lightweight industrial robots, especially when using lightweight transmission elements such as strain-wave type transmissions. Developed in the 1950's (Musser, 1959) for aerospace applications, strain-wave transmissions such as the Harmonic Drive™are now widely used in lightweight industrial robots due to their desirable characteristics of lightweight design, high torque capacity, and near-zero backlash. However, their inherent dynamic characteristics such as friction, flexibility, hysteresis, and kinematic error complicates the accurate mathematical modeling of robotics systems that employ such transmissions.

In literature, the above-mentioned challenge of accurate mathematical modeling of industrial robots are addressed mainly through

☆ This work was supported by the company Universal Robots A/S, Odense, Denmark and Innovation Fund Denmark [Ref.no. 7038-00058B].
* Corresponding author at: Aarhus University, Inge Lehmanns Gade 10, DK-8000 Aarhus C, Denmark.
** Corresponding author.
E-mail addresses: ema@eng.au.dk (E. Madsen), xuzh@eng.au.dk (X. Zhang).
[1] A robot programming method where the user takes the robot by the hand and guides it — so-called *programming by demonstration*.

https://doi.org/10.1016/j.conengprac.2020.104462
Received 29 January 2020; Received in revised form 11 May 2020; Accepted 16 May 2020
Available online 30 May 2020

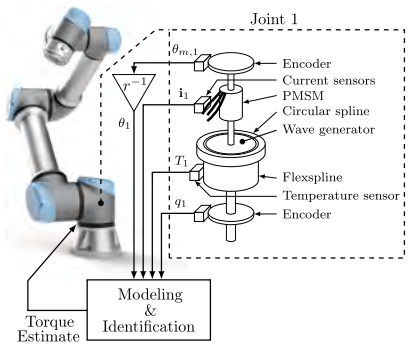

Fig. 1. The Universal Robots UR5e collaborative industrial robot manipulator used in this work having 6 revolute joints each comprising two rotary absolute encoders, a temperature sensor, a current sensor for each electrical phase of the PMSM, and a strain-wave transmission.

modeling and identification of the industrial robots' joint friction. Bittencourt and Gunnarsson (2012) showed that the friction torque of the second joint of the *ABB IRB 6620* robot experienced clear correlation with velocity, load, and temperature, and Simoni, Beschi, Legnani, and Visioli (2015) analyzed the *Comau SMART NS 16 1.65 ARC* industrial robot in terms of the friction's temperature dependency. In Carlson, Robertsson, and Johansson (2015) the position and temperature dependent friction phenomena was estimated on the *ABB YuMi* and *ABB IRB140* industrial robots with a focus on robot joints without built-in temperature sensing hardware. Gao, Yuan, Han, Wang, and Wang (2017) analyzed how load and temperature affected friction on the *SIASUN* lightweight industrial robot comprising Harmonic Drives. The above-mentioned approaches on mathematical modeling and identification of robot joints considered friction to be described by static nonlinearities with no complex frictional dynamics. Also, joint flexibility effects were neglected. This is indeed reasonable for rigid/heavy-duty industrial robots but such assumptions does not hold for lightweight collaborative robots, in particular those that comprise strain-wave transmissions. Wolf and Iskandar (2018) modeled the *DLR Floating Spring Joint* and identified the nonlinear influences of velocity and temperature on the friction torque. Iskandar and Wolf (2019) extended their work by incorporating the Generalized Maxwell-Slip (GMS) model to estimate frictional dynamics and an application to external torque estimation was demonstrated.

The modeling of nonlinear joint characteristics has been significantly advanced by studies explicitly considering strain-wave transmissions. Seyfferth, Maghzal, and Angeles (1995) developed a hysteresis model for harmonic drives in which the hysteresis is related to torsional displacement and velocity. Tuttle and Seering (1996) derived a mathematical model of harmonic drives from the gear-tooth geometry. Taghirad and Bélanger (1996) proposed a harmonic drive model consisting of simple models of compliance, hysteresis, and friction. Kircanski and Goldenberg (1997) described the mechanical structure of the harmonic drive and proposed a control-oriented model with nonlinear stiffness, soft-windup hysteresis, and friction. Dhaouadi, Ghorbel, and Gandhi (2003) described the hysteresis of harmonic drives as an integro-differential equation being the result of nonlinear stiffness and nonlinear damping. Ruderman, Hoffmann, and Bertram (2009) described the hysteresis of harmonic drives using the Preisach model and included dynamic friction effects by the GMS model. Ruderman and Bertram (2012) opted for an extended Bouc–Wen model to capture the hysteresis effect and Ruderman (2019), Ruderman, Bertram, and Iwasaki (2014) demonstrated its application in sensorless torque control. Common to the studies explicitly considering strain-wave transmissions is that they opt for very simple models of the friction that does not incorporate the friction's dependencies on load and temperature. Additionally, the results of this paper suggest that the utilized hysteresis models may be inadequate for describing the position-dependent hysteresis characteristics that can be encountered for systems with the strain-wave transmission being integrated to the robot joint.

Motivated by the above discussion, we will: (1) Develop and experimentally validate a mathematical model of the robot joint taking into account the nonlinear joint stiffness and the nonlinear dependency of friction on velocity, temperature, and load. (2) Propose new models for the dependency of friction on load and temperature which are more accurate when evaluated on the Universal Robots UR5e robotic system. (3) Extend the GMS friction model to handle effectively the position-dependent backlash characteristics which was observed in the system. (4) Develop a new and more accurate Linear Regression method based on the GMS model.

The methods of this work are especially relevant to collaborative robots, which have advanced safety systems that requires accurate knowledge about the robot dynamics. Human interference can thus be more easily identified and any potentially harmful motion can be stopped faster. The developed models can be incorporated in a variety of model-based control strategies, such as the recent advancements in the control of nonlinear systems by Sun, Jianbin, Karimi and Fu (2020), Sun, Liu, Qiu and Feng (2020), Sun, Qiu, Karimi and Gao (2020). Implementing our developed nonlinear models in such nonlinear control schemes could lead to improved tracking performance. Alternatively, using the measured joint deformation in a high-fidelity mathematical model of the joint, may allow to control the joint using torque feedback (Albu-Schäffer et al., 2007; Vischer & Khatib, 1995) without the need of commercially available torque sensing hardware, which are costly and takes up much space.

The remainder of the paper is organized as follows: Section 2 presents the mathematical model of the flexible-joint robot manipulator, and Section 3 details the initial assumptions related to the joint dynamics. Section 4 presents the results of the joint dynamics identification. Firstly, the static nonlinearities are identified such as the torsional stiffness and the dependency of friction on angular velocity, load, and temperature. Then, the kinematic error and position-dependent backlash are identified. Lastly, an extended version of the GMS friction model is proposed to describe the dynamic friction during velocity reversals while subject to position-dependent backlash. Section 5 concludes the work and presents possible further research topics.

Notations. The notation used in the paper is mostly standard. Let $\mathbb{R}$ be the set of real numbers, $\mathbb{N}$ the set of non-negative integers, and $\mathbb{N}^+$ the set of positive integers. Let $\mathbf{x} \in \mathbb{R}^n$ be a vector of n real numbers, then x_i is its i^{th} entry, $\mathbf{x}^\mathsf{T}$ its transpose, $\bar{\mathbf{x}}$ the mean value of the elements of $\mathbf{x}$, and $\|\mathbf{x}\|$ the 2-norm. Let $\hat{\mathbf{x}}$ denote an estimate of $\mathbf{x}$ and $\tilde{\mathbf{x}} \triangleq \mathbf{x} - \hat{\mathbf{x}}$ be the estimation error. Given a function $g : \mathcal{G} \to \mathbb{R}$ let $\text{sgn} : \mathbb{R} \to \{-1, 0, 1\}$ be the *signum function* defined such that $\text{sgn}(g) = -1$ if $g < 0$, $\text{sgn}(g) = 0$ if $g = 0$, and $\text{sgn}(g) = 1$ if $g > 0$. Given a square real matrix $\mathbf{A} \in \mathbb{R}^{n\times n}$ let $\mathbf{A} > 0$ indicate that $\mathbf{A}$ is positive definite, i.e. $\mathbf{x}^\mathsf{T}\mathbf{A}\,\mathbf{x} > 0$ for any non-zero column vector $\mathbf{x}$ of n real numbers. Let $\text{diag} : \mathbb{R}^n \to \mathbb{R}^{n\times n}$ map a vector of n elements to a diagonal matrix with the i^{th} element of the vector on its i^{th} diagonal entry while zero everywhere else. Given N matrices $\mathbf{B}_1, \ldots, \mathbf{B}_N \in \mathbb{R}^{l\times m}$ we denote by $\text{blkdiag}\{\mathbf{B}_1, \ldots, \mathbf{B}_N\}$ (or simply $\text{blkdiag}\{\mathbf{B}_i\}$, where the range of index i can be identified from context) a block diagonal matrix with $\mathbf{B}_1, \ldots, \mathbf{B}_N$ as diagonal elements.

2. Mathematical modeling of a flexible-joint robot

We consider the Flexible-Joint Robot (FJR) manipulator as an open kinematic chain having $N + 1$ rigid bodies; the base and the N links,

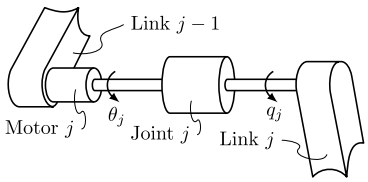

Fig. 2. Kinematic arrangement of motors and links for the FJR manipulator model. Note that θ_j is already scaled by the reduction ratio as indicated also by Fig. 1.

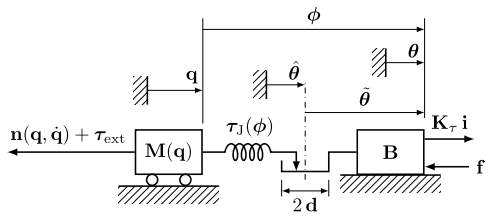

Fig. 3. Visual representation of the mathematical model of the flexible-joint robot manipulator with $\mathbf{n}(\mathbf{q},\dot{\mathbf{q}}) = \mathbf{C}(\mathbf{q},\dot{\mathbf{q}})\,\dot{\mathbf{q}} + \mathbf{g}(\mathbf{q})$ in (1).

interconnected by N revolute joints undergoing deflection, and actuated by N electrical actuators, see Fig. 2. To derive the dynamics of the robot manipulator, the following standard assumptions are made.

A1 The rotors are uniform bodies having their center of mass on the axis of rotation.

A2 Each motor $j = 1, \dots, N$ is mounted on link $j-1$ and moves link j, see Fig. 2.

Assumption **A1** is a basic requirement for long life of an electrical drive and implies that the robot dynamics become independent of the angular position of the rotors. For the UR5e manipulator we take advantage of the presence of large reduction ratios and simply assume the following.

A3 The angular velocity of the rotors is due only to their own spinning.

This simplifying assumption was proposed by Spong (1987) and is equivalent to neglecting energy contributions due to the inertial couplings between the rotors and the links. It also implies that Coriolis and centripetal terms will be independent of the rotors' angular velocity $\boldsymbol{\omega} \triangleq \mathrm{d}\,\boldsymbol{\theta}/\mathrm{d}\,t$.

To uniquely characterize the manipulator configuration we choose the generalized coordinates $(\mathbf{q}\ \boldsymbol{\theta}) \in \mathbb{R}^{2N}$ being, respectively, the positions of the links and rotors reflected through the gear ratios, i.e. the rotor positions are seen in the link space. Given assumptions **A1–A3**, the link and rotor dynamics become, respectively

$$\mathbf{M}(\mathbf{q})\,\ddot{\mathbf{q}} + \mathbf{C}(\mathbf{q},\dot{\mathbf{q}})\,\dot{\mathbf{q}} + \mathbf{g}(\mathbf{q}) + \boldsymbol{\tau}_{\text{ext}} = \boldsymbol{\tau}_{\text{J}} \tag{1}$$

$$\mathbf{B}\,\ddot{\boldsymbol{\theta}} + \mathbf{f} + \boldsymbol{\tau}_{\text{J}} = \mathbf{K}_\tau\,\mathbf{i} \tag{2}$$

where in the link equation, $\mathbf{M}(\mathbf{q}) \succ 0 \in \mathbb{R}^{N\times N}$ is the symmetric inertia matrix, $\mathbf{C}(\mathbf{q},\dot{\mathbf{q}}) \in \mathbb{R}^{N\times N}$ is the Coriolis and centripetal matrix, $\mathbf{g}(\mathbf{q}) \in \mathbb{R}^N$ is the gravity vector, and $\boldsymbol{\tau}_{\text{J}} \in \mathbb{R}^N$ is the vector of joint torques which couple the link and rotor subsystems. In the rotor equation, $\mathbf{B} \succ 0 \in \mathbb{R}^{N\times N}$ is the diagonal matrix of rotor inertias, $\mathbf{f} \in \mathbb{R}^N$ is friction acting on the rotor coordinate, $\mathbf{K}_\tau \succ 0 \in \mathbb{R}^{N\times N}$ is the diagonal matrix of torque constants and $\mathbf{i} \in \mathbb{R}^N$ is the torque-generating (quadrature) current obtained from the phase currents and the *Park Transformation*. If the end effector is subject to an external wrench $\mathbf{f}_{\text{ext}} \in \mathbb{R}^N$, the resulting joint torques

$$\boldsymbol{\tau}_{\text{ext}} = \mathbf{J}^{\text{T}}(\mathbf{q})\,\mathbf{f}_{\text{ext}} \tag{3}$$

where $\mathbf{J}(\mathbf{q}) \in \mathbb{R}^{N\times N}$ is the kinematic Jacobian for the manipulator.

3. Mathematical modeling of the flexible joint

This section presents some initial assumptions on the joint dynamics characteristics in terms of flexibility, friction, and backlash. The mathematical model of the flexible joint robot is illustrated as a translational system in Fig. 3. The definition of the kinematic error $\tilde{\boldsymbol{\theta}} \triangleq \boldsymbol{\theta} - \hat{\boldsymbol{\theta}}$ and the backlash $2\,\mathbf{d}$ (discussed in Section 4.3) is illustrated as well.

The literature on FJR manipulators is not consistent with its terminology related to the terms *backlash* and *hysteresis*. Therefore, we state their definitions in the following.

Definitions (*Backlash*)**.** Backlash, sometimes referred to as lash or play, is understood as the largest distance or angle through which any part of a mechanism may be moved or rotated in one direction without transferring force or torque to the next part in the mechanism.

The backlash can be interpreted as a complete loss of stiffness in some region of deformation.

Definitions (*Hysteresis*)**.** Hysteresis is understood as the lag of a system's output wrt. its input. The hysteresis can be a dynamic lag between input and output that vanishes if the input varies slowly; this is known as *rate-dependent* hysteresis. Similarly, the hysteresis can be *rate-independent* if durable memory is possible.

Backlash will give rise to a rate-independent hysteresis phenomena.

3.1. Joint torque assumptions

The joint torques which couple the link and rotor subsystems are assumed to depend on the joint angular deflections $\boldsymbol{\phi} \triangleq \boldsymbol{\theta} - \mathbf{q}$, i.e.

$$\boldsymbol{\tau}_{\text{J}} = \boldsymbol{\tau}_{\text{J}}(\boldsymbol{\phi}) \tag{4}$$

We further assume that no flexibility torques exist for the undeformed joints and that the joints have the same behavior in compression and extension, thus

$$\boldsymbol{\tau}_{\text{J}}(\mathbf{0}) = \mathbf{0} \tag{5}$$

$$\boldsymbol{\tau}_{\text{J}}(-\boldsymbol{\phi}) = -\boldsymbol{\tau}_{\text{J}}(\boldsymbol{\phi}) \qquad \forall \boldsymbol{\phi} \tag{6}$$

3.2. Joint friction assumptions

Considering a set of states $\mathbf{x}$ and parameters $\boldsymbol{\zeta}$ we assume that the friction torque $\mathbf{f} \triangleq \mathbf{f}(\mathbf{x},\boldsymbol{\zeta})$ can be described as a sum of M functions $\mathbf{f}_i$, i.e.

$$\mathbf{f}(\mathbf{x},\boldsymbol{\zeta}) = \sum_{i=1}^{M} \mathbf{f}_i(\mathbf{x},\boldsymbol{\zeta}) \tag{7}$$

Note, that $\mathbf{f}_i$ is a function not necessarily of $\mathbf{x}_i$ alone.

It is further assumed that the friction torques are uncoupled among the joints, i.e. the states and parameters related to the friction of one joint will affect the friction torque of that joint only.

4. Identification

Strain-wave transmissions are known to experience nonlinear stiffness, nonlinear friction, kinematic error, and backlash (or very low stiffness for small applied loads, sometimes referred to as soft-windup Kennedy & Desai, 2005), that gives rise to hysteresis between the transmission deflection and torque. This section presents the experimental procedures and results of the identification of these joint dynamics phenomena and the models used to describe them. The identification of this paper is restricted to joint 1 of the UR5e manipulator, however

the methodology easily extends to the remaining joints of the UR5e or other industrial robot joints.

Common to all identification procedures is that: (1) Data is sampled at times $t(k) = k\,T_S$, $k = 1, \dots, N_S$, and $T_S = 1$ ms. (2) The parametrization of a model is considered optimum if it minimizes the Mean Squared Error (MSE) between the vector of measurements $\mathbf{y} \in \mathbb{R}^{N_S}$ and the vector of model estimates $\hat{\mathbf{y}} \in \mathbb{R}^{N_S}$, hence the cost function is always

$$\mathcal{J} \triangleq \frac{1}{N_S}\|\mathbf{y} - \hat{\mathbf{y}}\| \tag{8}$$

with the error $\mathbf{y} - \hat{\mathbf{y}}$ assumed to be a stationary zero mean and white sequence. (3) The quality of a model is evaluated by the Normalized Root Mean Squared Error (NRMSE) expressed as a percentage, i.e.

$$\text{NRMSE} = 100\% \cdot \left(1 - \frac{\|\mathbf{y} - \hat{\mathbf{y}}\|}{\|\mathbf{y} - \bar{\mathbf{y}}\|}\right) \tag{9}$$

ranging from $-\infty$ (bad fit) to 1 (perfect fit).

The goal is to find models that are coherent with observations, have a minimum number of describing functions and a low dimension of the parameter space. Furthermore, the choice of describing functions should be practically suitable for identification, i.e. linear if possible. The reason to have a small number of describing functions and parameters is that it will decrease the risk of over-fitting the models, which could result in reduced model performance on new data-sets, i.e. in real-world applications.

4.1. Torsional stiffness

The joint torsional stiffness is identified by exerting a force on the end-effector while the robot is static and the joint of interest is oriented with its axis of rotation parallel to the direction of the gravitational acceleration, thus in the vicinity of gravity torque around the axis of rotation. The described robot configuration simplifies (1) and (3) to

$$\boldsymbol{\tau}_\mathrm{J} = \mathbf{J}^\mathsf{T}(\mathbf{q})\,\mathbf{f}_\text{ext} \tag{10}$$

while (2), when assuming for simplicity $\mathbf{f} = \mathbf{0}$, becomes

$$\boldsymbol{\tau}_\mathrm{J} = \mathbf{K}_\tau\,\mathbf{i} \tag{11}$$

Thereby, the flexibility torque is obtained in two ways; (1) using (10) and measuring $\mathbf{f}_\text{ext}$ using a calibrated Sauter FH-S 500 digital force gauge, and (2) using (11).

Strain-wave transmissions are known to experience stiffening with increasing load due to the increased gear-tooth contact area with increasing loads (Nye, 1989). The stiffness characteristics of the Harmonic Drive has in literature been modeled linearly (Taghirad & Bélanger, 1996), as a cubic polynomial (Gandhi & Ghorbel, 2004; Kircanski & Goldenberg, 1997; Madsen, Rosenlund, Brandt, & Zhang, 2019; Tuttle & Seering, 1996) or functions consisting of piecewise linear segments (Harmonic Drive AG, 2018; Shi, Li, & Liu, 2017).

We assume that the joint torques can be approximated by a linearly parametrized polynomial basis in $\boldsymbol{\phi}$, i.e.

$$\boldsymbol{\tau}_\mathrm{J}(\boldsymbol{\phi}) = \boldsymbol{\Psi}(\boldsymbol{\phi})\,\boldsymbol{\alpha} \tag{12}$$

Based on the symmetry assumptions in (5) and (6) the joint torque model should contain only odd powers in $\boldsymbol{\phi}$, thus

$$\begin{aligned}\boldsymbol{\Psi}(\boldsymbol{\phi}) &= \text{blkdiag}\left\{\,\boldsymbol{\Psi}_j^\mathsf{T}\,\right\} \in \mathbb{R}^{N\times N\,P}, \quad j = 1..N\\ \boldsymbol{\Psi}_j &= \begin{pmatrix}\phi_j & \cdots & \phi_j^{2p-1} & \cdots & \phi_j^{2P-1}\end{pmatrix}^\mathsf{T} \in \mathbb{R}^P\end{aligned} \tag{13}$$

with $\boldsymbol{\Psi}(\boldsymbol{\phi})$ a rectangular block diagonal matrix with its N elements being P-element row vectors $\boldsymbol{\Psi}_j^\mathsf{T}$. In (13) all joints have bases of order P, however it is possible to choose different order bases among the joints. The vector of parameters corresponding to the definition in (13) is

$$\begin{aligned}\boldsymbol{\alpha} &= \begin{pmatrix}\boldsymbol{\alpha}_1^\mathsf{T} & \cdots & \boldsymbol{\alpha}_j^\mathsf{T} & \cdots & \boldsymbol{\alpha}_N^\mathsf{T}\end{pmatrix}^\mathsf{T} \in \mathbb{R}^{N\,P}\\ \boldsymbol{\alpha}_j &= \begin{pmatrix}\alpha_{j,1} & \cdots & \alpha_{j,p} & \cdots & \alpha_{j,P}\end{pmatrix}^\mathsf{T} \in \mathbb{R}^P\end{aligned} \tag{14}$$

i.e. for each joint the map from transmission deformation to joint torque is described by P parameters. The stiffness $\mathbf{K}(\boldsymbol{\phi})$ is simply the rate of change of flexibility torque with respect to transmission deformation

$$\mathbf{K}(\boldsymbol{\phi}) = \frac{\partial}{\partial\,\boldsymbol{\phi}}\,\boldsymbol{\tau}_\mathrm{J}(\boldsymbol{\phi}) \tag{15}$$

hence from (12) and (13) the parametrization of the stiffness is simply

$$\begin{aligned}\mathbf{K}(\boldsymbol{\phi}) &= \boldsymbol{\Omega}(\boldsymbol{\phi})\,\boldsymbol{\alpha}, \quad \boldsymbol{\Omega}(\boldsymbol{\phi}) = \text{diag}\left(\boldsymbol{\phi}^{-1}\right)\boldsymbol{\Psi}(\boldsymbol{\phi})\,\boldsymbol{\Lambda}\\ \boldsymbol{\Lambda} &= \text{blkdiag}\{\underbrace{\boldsymbol{\lambda}^\mathsf{T},\ \dots,\ \boldsymbol{\lambda}^\mathsf{T}}_{N\ \text{elements}}\}\\ \boldsymbol{\lambda} &= \begin{pmatrix}1 & \cdots & 2\,p-1 & \cdots & 2\,P-1\end{pmatrix}^\mathsf{T}, \quad p = 1, \dots, P\end{aligned} \tag{16}$$

The joint torque can be expressed also in terms of P matrices $\mathbf{K}_1, \dots, \mathbf{K}_P$ each of dimension $N\times N$ and each multiplied by a N-element vector

$$\begin{aligned}\boldsymbol{\tau}_\mathrm{J}(\boldsymbol{\phi}) &= \sum_{p=1}^{P}\mathbf{K}_p\,\boldsymbol{\phi}^{2p-1}, \quad \mathbf{K}_p = \text{diag}\begin{pmatrix}\alpha_{1,p} & \cdots & \alpha_{N,p}\end{pmatrix}\\ \boldsymbol{\phi}_{2p-1} &= \begin{pmatrix}\phi_1^{2p-1} & \cdots & \phi_N^{2p-1}\end{pmatrix}^\mathsf{T}\end{aligned} \tag{17}$$

4.1.1. Least squares estimation

From an experiment on joint j let $2\,N_S$ data points $(\phi_j(k), \tau_{J,j,F}(k))$ and $(\phi_j(k), \tau_{J,j,C}(k))$ be available with $k = 1, \dots, N_S$, where subscripts $_F$ and $_C$ denote, respectively, *Force gage* and *Current* to indicate whether the torque is obtained through (10) or (11), respectively. The regressor matrix and vector of measurements are defined, respectively

$$\mathbf{W}_j = \begin{pmatrix}\phi_j(1) & \dots & \phi_j(1)^{2p-1} & \dots & \phi_j(1)^{2P-1}\\ \vdots & \ddots & \vdots & \ddots & \vdots\\ \phi_j(N_S) & \dots & \phi_j(N_S)^{2p-1} & \dots & \phi_j(N_S)^{2P-1}\\ \phi_j(1) & \dots & \phi_j(1)^{2p-1} & \dots & \phi_j(1)^{2P-1}\\ \vdots & \ddots & \vdots & \ddots & \vdots\\ \phi_j(N_S) & \dots & \phi_j(N_S)^{2p-1} & \dots & \phi_j(N_S)^{2P-1}\end{pmatrix} \tag{18}$$

$$\begin{aligned}\mathbf{y}_j &= \begin{pmatrix}y_F(1) & \cdots & y_F(N_S) & y_C(1) & \cdots & y_C(N_S)\end{pmatrix}^\mathsf{T}\\ y_F(k) &= \tau_{J,j,F}(k), \quad y_C(k) = \tau_{J,j,C}(k)\end{aligned} \tag{19}$$

For $2\,N_S > P$ we obtain an over-constrained linear system

$$\mathbf{y}_j = \mathbf{W}_j\,\boldsymbol{\alpha}_j \tag{20}$$

whose least squares solution is obtained using the Moore–Penrose generalized inverse and gives an estimate of the stiffness coefficients for joint j

$$\hat{\boldsymbol{\alpha}}_j = \left(\mathbf{W}_j^\mathsf{T}\,\mathbf{W}_j\right)^{-1}\mathbf{W}_j^\mathsf{T}\,\mathbf{y}_j \in \mathbb{R}^P \tag{21}$$

In Madsen et al. (2019) a cubic polynomial was shown to be adequate for describing the joint torque so we let $P = 2$ in (17), thus from (17) the joint torque model is simply

$$\boldsymbol{\tau}_\mathrm{J}(\boldsymbol{\phi}) = \mathbf{K}_1\,\boldsymbol{\phi} + \mathbf{K}_2\,\boldsymbol{\phi}^3 \tag{22}$$

where $\mathbf{K}_1 \in \mathbb{R}^{N\times N}$ and $\mathbf{K}_2 \in \mathbb{R}^{N\times N}$ are diagonal matrices of, respectively, linear and cubic stiffness coefficients.

Fig. 4 shows the joint torque for joint 1. The chosen cubic polynomial in (22) matches the experimental data with an accuracy of 91.3%. The data sheet values proposed by Harmonic Drive AG (2018) and used by Shi et al. (2017) are accurate to a degree of 74.5%. It is therefore suggested to use cubic polynomial over the linear segments proposed by Harmonic Drive™.

4.2. Friction

For notational simplicity we simplify the vector equations into scalar equations. The terms and definitions in this section are valid for all joints $j = 1, \dots, N$, however we will not denote the joint index j.

The friction torque is commonly described as a combination of various aspects representing the nonlinear friction characteristics in the

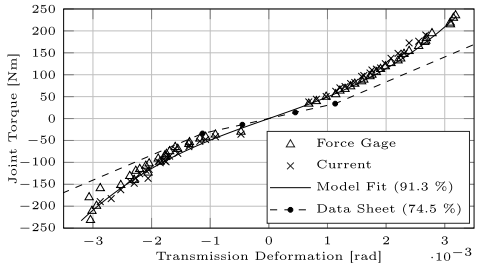

Fig. 4. Joint torque's dependence on transmission deformation for joint 1 obtained experimentally using (10) (triangle), (11) (cross), the model described in (22), and the data sheet for the Harmonic Drive HFUS strain-wave transmission (Harmonic Drive AG, 2018).

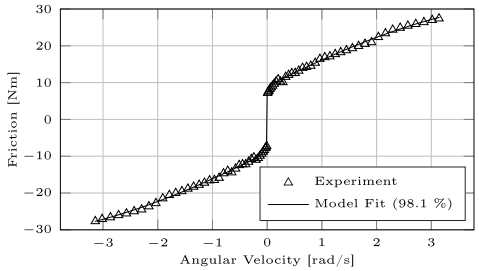

Fig. 5. The dependency of friction on velocity in a no load scenario and with a joint temperature of 35 °C.

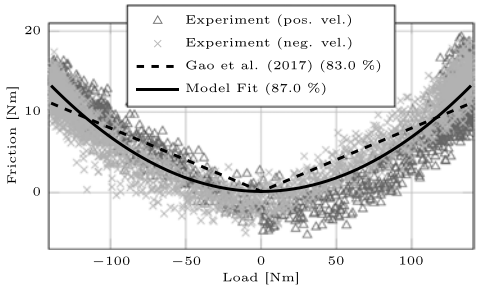

Fig. 6. The dependency of friction on load dependence with the friction for negative velocities being negated and *Model Fit* corresponding to (27). The joint temperature was kept at 35 °C for the entire experiment.

sliding regime such as Coulomb friction, viscous friction, etc. From experiments and empirical observations these friction characteristics are known to depend on the rotor angular velocity, load torque, and joint temperature. This section presents the methodology and results in the identification of the friction's dependency on rotor angular velocity, load torque, and joint temperature, so from (7) the friction torque is described by a summation of the following contributions

$$f = f_v + f_l + f_T \tag{23}$$

with f_v, f_l, and f_T describing, respectively, the dependency of friction on angular velocity, load, and temperature.

4.2.1. Angular velocity

The dependency of friction on velocity is identified by rotating a single robot joint with different constant angular velocities, in the vicinity of external wrench, and the joint axis of rotation being oriented parallel to the direction of the gravitational acceleration. In this case (1) simplifies to $0 = \tau_J$ while (2) becomes

$$f = K_\tau\, i \tag{24}$$

The dependency of friction on angular velocity is modeled similarly to Madsen et al. (2019), i.e.

$$\begin{aligned} f_v = \operatorname{sgn}(\omega)\,\big(F_C + (F_S - F_C)\,\exp[-(V_S^{-1}|\omega|)^\mu]\big) \\ +\; F_{V,1}\,\omega - F_{V,2}\,|\omega|\,\omega + F_{V,3}\,\omega^3 \end{aligned} \tag{25}$$

where $F_C, F_S, V_S, \mu, F_{V,1}, F_{V,2}, F_{V,3} \in \mathbb{R}$ are, respectively, the Coulomb friction coefficient, Stribeck friction coefficient, Stribeck velocity, Stribeck shape factor, and viscous friction coefficients. The results from the identification of the friction's velocity dependency is shown in Fig. 5. The model in (25) is nonlinear in V_S and μ, thus an optimum set of parameters in (25) is found using nonlinear optimization, specifically a Quasi-Newton method with a cubic line search procedure and updating the Hessian matrix approximation by the Broyden–Fletcher–Goldfarb–Shanno (BFGS) method.

4.2.2. Load torque

As indicated by the Coulomb dry friction model, the friction force is proportional to normal force between two surfaces in contact. Thus, it is reasonable to assume that the transmission displays some sort of load-dependent behavior.

The dependency of friction on load torque is identified by rotating a single robot joint at the time with different angular velocities, in the vicinity of external wrench, and the joint axis of rotation being oriented perpendicular to the direction of the gravitational acceleration. This way, the gravity will induce a load. All other joints are kept fixed at a constant angular position. In this case (1) simplifies to $g(q) = \tau_J$, hence (2) can be rewritten

$$f = K_\tau\, i - g(q) \tag{26}$$

in which $g(q)$ is predicted based on the masses and center of mass positions. A payload of 7.5 kg was attached to the robot's end effector to increase the maximum possible load torque. The load dependent friction can be obtained by subtracting the velocity friction in (25) from the total friction described by (26).

One common choice is to model the dependency of friction on load linearly in the magnitude of the load torque (Bittencourt, Wernholt, Sander-Tavallaey, & Brogårdh, 2010; Gao et al., 2017; Hamon, Gautier, & Garrec, 2010), i.e. $f_l = F_l \operatorname{sgn}(\omega)|\tau_l|$. We propose, however, to model the friction's load dependency as

$$f_l = F_l \operatorname{sgn}(\omega)\,\tau_l^2 \tag{27}$$

where $F_l \in \mathbb{R}$ is the load coefficient. The model in (27) can be thought of simply as a scaling of the Coulomb friction with the squared load torque. The model in (27) is linear in F_l and thus the optimum parameter is found by linear least squares using QR decomposition with column pivoting. The results from the identification of the friction's load dependency are shown in Figs. 6 and 7. Fig. 6 shows the isolated effect of load-induced friction while Fig. 7 shows the combined friction effects of velocity and load. The models by Bittencourt et al. (2010), Gao et al. (2017) and Hamon et al. (2010) performs at 83.0% slightly worse compared to 87.0% for our proposed model. Fig. 6 reveals a slight shift between the torques for positive and negative velocities. This could be due to an inaccurate computation of the load (gravity) torque based on inaccurate information related to the masses and center of mass positions of the UR5e manipulator.

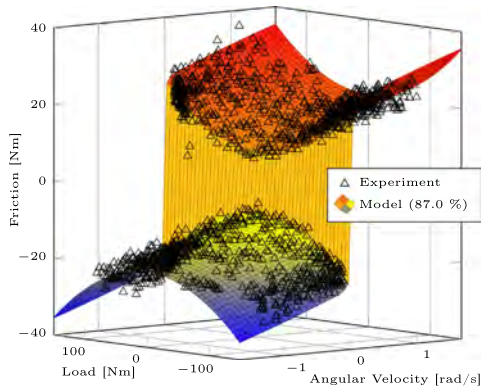

Fig. 7. The dependency of the total friction torque on load and velocity.

4.2.3. Temperature

The viscosity of lubricants approximately has an exponential dependence on temperature, and for newtonian fluids, the shear forces are directly proportional to the viscosity (Seeton, 2006). Thus, it is reasonable to assume that the temperature affects the viscous friction characteristics in some nonlinear fashion.

The dependency of friction on temperature is identified by first cooling the robot to 9 °C, then placing it in an ambient temperature of approximately 20 °C and rotating a single robot joint with different constant angular velocities. The robot joint will naturally heat up. The experiment lasted 1h 56 min. The temperature is measured with a temperature sensor built into the joints. At times where the robot joint rotates with a constant angular velocity the friction torque is simply obtained using (24).

One possible choice for modeling the dependency of friction on temperature is an affine transformation in the temperature multiplied by an exponential function in the temperature and velocity as in Bittencourt et al. (2010) and Gao et al. (2017). This model has four parameters of which two appear nonlinearly.

In this work, we propose for the friction's temperature dependency the following model of three parameters that all appear linearly

$$f_T = \operatorname{sgn}(\omega)\sqrt{|\omega|}\left(F_{T,1} + F_{T,2}\,T + F_{T,3}\,T^{-3}\right) \tag{28}$$

where $F_{T,1}, F_{T,2}, F_{T,3} \in \mathbb{R}$ are temperature coefficients. An optimum set of parameters in (28) is found by linear least squares using QR decomposition with column pivoting. The models by Bittencourt et al. (2010) and Gao et al. (2017) performs at 94.3% slightly worse compared to 95.1% for our proposed model despite its drawbacks of more parameters and nonlinearity.

It should be noted, however, that polynomial descriptions in general do not extrapolate well, which could be relevant in the practical implementation of (28) or temperature compensation of robot joint friction in general.

Fig. 8 shows the temperature over time and Figs. 9 and 10 shows the friction torque as a function of joint angular velocity and temperature. The results show that the temperature only affects the viscous friction, which is coherent with literature on other industrial robots (Bittencourt & Gunnarsson, 2012; Gao et al., 2017).

4.3. Kinematic error & position-dependent backlash

Strain-wave transmissions are known to be subject to kinematic error and backlash (or very low stiffness for small loads, sometimes

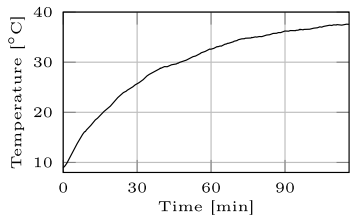

Fig. 8. Joint temperature over time during the temperature experiment.

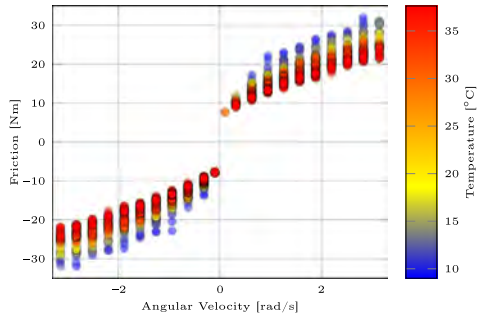

Fig. 9. The dependency of friction on velocity and temperature.

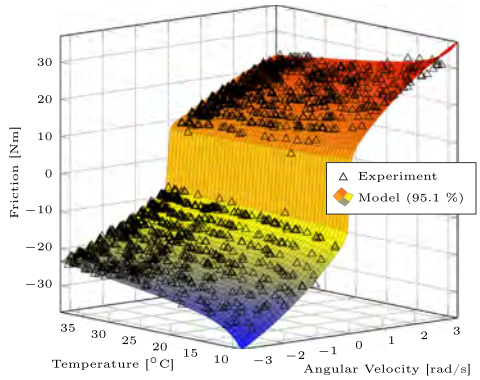

Fig. 10. The dependency of friction on velocity and temperature.

referred to as soft wind-up). The kinematic error and backlash of the robot joint was identified in the same experiment by rotating a single robot joint at the time with reciprocating and very low velocities and accelerations and the joint axis of rotation oriented parallel to the direction of the gravitational acceleration. One full revolution of 240 reversals in approx. 17 min was performed. The trajectory is shown in Fig. 11. Fig. 12 show the variation of the transmission deformation over one full joint revolution.

Neglecting inertial effects and gravity effects, (1) simplifies to $0 = \tau_J$ resulting in the kinematic error-corrected transmission deformation

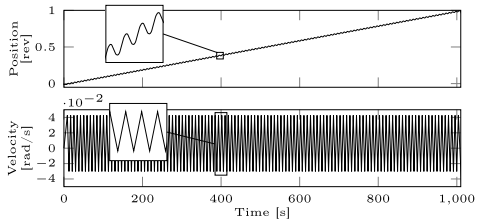

Fig. 11. Trajectory used for identifying the hysteresis characteristics.

being bounded in magnitude by the backlash, i.e.

$$|\phi(t) - \tilde{\theta}(t)| \leq d \quad \forall\, t \tag{29}$$

4.3.1. Kinematic error

Kinematic error is defined as the difference between the expected output position and the actual output position. In strain-wave transmissions kinematic error is a well-known phenomena caused by a number of factors such as tooth-placement errors on both the circular spline and flexspline, out-of-roundness in the three transmission components, and misalignment during assembly (Tuttle & Seering, 1996). If uncompensated, the kinematic error will act as a periodic exciter and cause undesirable vibrations and angular velocity fluctuations during motion. It is therefore desirable to model the kinematic error so it can be compensated.

The kinematic error $\tilde{\theta}$ is defined as the midpoint between transmission deformations for positive and negative velocity denoted with subscripts $_+$ and $_-$, respectively, i.e.

$$\tilde{\theta} = \frac{\phi_+ + \phi_-}{2} \tag{30}$$

The results in Fig. 12 show the kinematic error over one full revolution of the robot joint.

Commonly, the kinematic error is modeled as a Fourier series expansion (Gandhi & Ghorbel, 2002; Ghorbel, Gandhi, & Alpeter, 1998; Preissner, Royston, & Shu, 2012; Zou, Tao, Jiang, Mei, & Wu, 2016) with the angular spatial frequency (measured in kinematic error cycles per wave generator revolution) being integer multiples of the transmission's input-side (wave generator) revolution. As we shall see, the UR5e manipulator is subject to kinematic error behavior that varies with the transmission's output-side revolution, i.e. at a much lower angular spatial frequency.

Let the map $\mathcal{KE}$ from angular position to kinematic error, i.e.

$$\mathcal{KE} : \theta \to \tilde{\theta}, \quad \theta \in [0, 2\pi) \tag{31}$$

be modeled as a lookup table (LUT) with linear interpolation, the table having 240 points $(\theta(t_{ur}), \tilde{\theta}(t_{ur}))$, $t_{ur} = \{t : \omega(t) = 0\}$ over one full revolution defined at the moments of velocity reversal.

4.3.2. Position-dependent backlash

The backlash is defined as the difference in transmission deformation during velocity reversals when no dynamic torques are present. It is extracted from the results by considering the difference in transmission deformation for positive and negative velocities. The results in Fig. 12 show that the amount of backlash depends on the joint's angular position.

It is known that the preload of the flexspline and backlash are inversely related. Dong, Chen, Wang, and Dong (2019) studied theoretically and numerically the effects of wave generator radial offset (input eccentricity error) and found the effects to be uneven distributions of the backlash and flexspline preload over the input angular position.

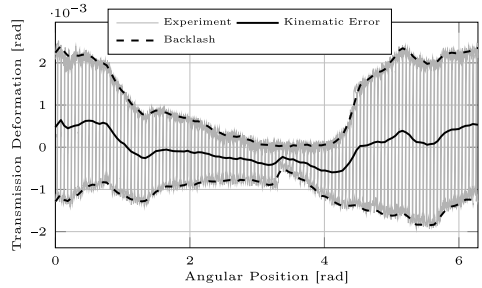

Fig. 12. Experimental results from the reciprocating velocity experiment and the models for the kinematic error and position-dependent backlash, respectively (31) and (32).

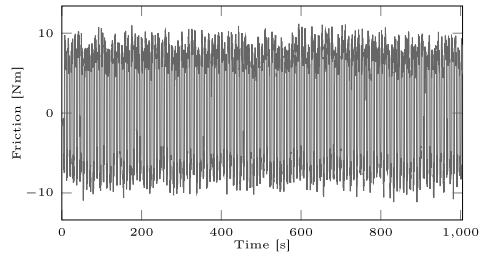

Fig. 13. Motor torque during the reciprocating velocity experiment.

The position-dependent backlash in the UR5e robotic system varies with the output angular position, therefore one explanation is that the flexspline preload varies with the output revolution. This could be caused by imperfect cylindricity of the circular spline combined with either; (1) wave generator radial offset (input eccentricity error) or (2) varying flexspline thickness. Another possible explanation for the position-dependent hysteresis characteristics is if the system was subject to position-dependent dry friction, however such effect would be observable in the motor current which is not the case, see Fig. 13.

Let the smooth and invertible map $\mathcal{D}$ from angular position to backlash, i.e.

$$\mathcal{D} : \theta \to d, \quad \theta \in [0, 2\pi) \tag{32}$$

be modeled as a LUT with linear interpolation.

4.4. Dynamic friction

At times of very low or zero velocities any static nonlinear map will fail to accurately describe the friction characteristics and a dynamic friction model is required. This is obvious from Fig. 14 where the friction torque for a given (near-zero) velocity takes different values depending on the direction of motion. In this pre-sliding regime the friction torque is described more accurately as a continuous function of displacement history rather than velocity. We therefore extend the identified static nonlinearities with a generic dynamic function of internal state $\mathbf{z}$, i.e.

$$f_C = \mathcal{F}(\mathbf{z}, \mathbf{x}), \quad \frac{\mathrm{d}\,\mathbf{z}}{\mathrm{d}\,t} = \mathcal{G}(\mathbf{z}, \mathbf{x}) \tag{33}$$

In other words, the Coulomb friction is no longer described as a discontinuous function in the angular velocity but as a continuous function in the angular position. A common choice in the robotics community is

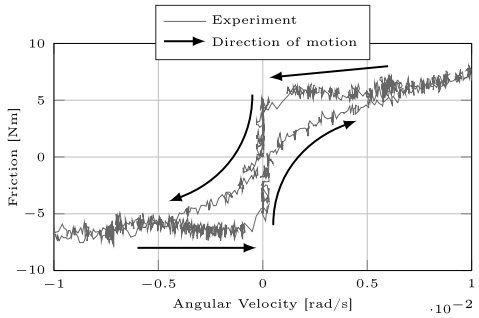

Fig. 14. The friction torque at near-zero velocities depend on the direction of motion, so a static map will fail to describe the friction characteristics in this region.

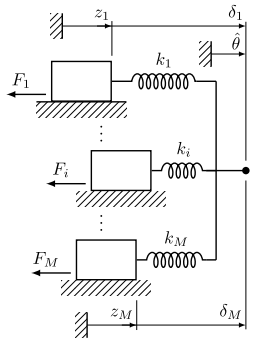

Fig. 15. Schematic representation of the Generalized Maxwell-Slip friction model used to model the effect of hysteresis.

the LuGre model, while for the strain-wave transmissions, models based on the Generalized Maxwell-Slip model structure are favored due to its ability to describe rate-independent hysteresis.

4.4.1. Generalized maxwell-slip model

The Generalized Maxwell-Slip model (Al-Bender, Lampaert, & Swevers, 2005; Lampaert, Al-Bender, & Swevers, 2003) is capable of describing the hysteretic relationship between the displacement and friction force (torque) in the pre-sliding regime and has been used to describe the dynamic friction characteristics of strain-wave transmissions with promising results, see e.g. (Preissner et al., 2012; Tjahjowidodo, Al-Bender, & Van Brussel, 2013). The GMS model can be visualized (Fig. 15) as a parallel connection of $M \in \mathbb{N}^+$ massless elasto-slide operators subject to the same input position $\hat{\theta} \triangleq \theta - \tilde{\theta}$. Each operator $i = 1, \dots, M$ is characterized by its own linear stiffness k_i and either a maximum spring deformation Δ_i or slip force limit $W_i = k_i \Delta_i$. The difference between the input position and the position of the i^{th} operator defines each element's spring deformation

$$\delta_i \triangleq \hat{\theta} - z_i\,, \quad |\delta_i| \le \Delta_i\,, \quad \forall\, i = 1, \dots, M \tag{34}$$

The i^{th} operator remains sticking as long as $|\delta_i| < \Delta_i$ while slipping until the exerted displacement reaches a local extremum, i.e. the exerted velocity goes through zero. The nonlinear state equation of each operator is described compactly by

$$\begin{aligned}\delta_i(k+1) = {} & \operatorname{sgn}(\hat{\theta}(k+1) - \hat{\theta}(k) + \delta_i(k)) \\ & \cdot \min\{|\hat{\theta}(k+1) - \hat{\theta}(k) + \delta_i(k)|, \Delta_i\}\end{aligned} \tag{35}$$

The total friction force is provided as the summation of friction forces for each operator, i.e.

$$f_C = \sum_{i=1}^{M} F_i, \quad F_i = k_i\, \delta_i \tag{36}$$

For convenience, let $\boldsymbol{\delta} \triangleq (\delta_1, \dots, \delta_M)^\mathsf{T}$, $\boldsymbol{\Delta} \triangleq (\Delta_1, \dots, \Delta_M)^\mathsf{T}$, and $\mathbf{k} \triangleq (k_1, \dots, k_M)^\mathsf{T}$.

4.4.2. Extending the GMS model with position-dependent backlash

The GMS model in its original form is unable to describe position-dependent backlash. We extend the GMS model with this capability by enforcing at all times the conditions

$$\frac{\partial \Delta_i}{\partial \theta} \equiv \frac{\partial \mathcal{D}}{\partial \theta}(\theta), \quad \frac{\partial W_i}{\partial \theta} \equiv 0, \quad \forall\, i = 1, \dots, M \tag{37}$$

This corresponds to uniformly scaling the vectors $\boldsymbol{\Delta}$ and $\mathbf{k}$ with, respectively, $\mathcal{D}(\theta)$ and $\mathcal{D}^{-1}(\theta)$. This also implies that the largest of the M spring deformation limits approximately equals 1. The constraints in (37) leads to changes in the state and output equations of the GMS model, specifically

$$\begin{aligned}\delta_i(k+1) = {} & \operatorname{sgn}(\hat{\theta}(k+1) - \hat{\theta}(k) + \delta_i(k)) \\ & \cdot \min\{|\hat{\theta}(k+1) - \hat{\theta}(k) + \delta_i(k)|, \mathcal{D}(\theta)\, \Delta_i\}\end{aligned} \tag{38}$$

$$f_C(k) = \sum_{i=1}^{M} F_i(k), \quad F_i(k) = \mathcal{D}^{-1}(\theta(k))\, k_i\, \delta_i(k) \tag{39}$$

4.4.3. The generalized maxwell-slip (GMS) method

This section presents the Generalized Maxwell-Slip (GMS) method. The GMS method is obtained by preassigning values for the spring deformation limits $\boldsymbol{\Delta}$ and stiffnesses $\mathbf{k}$. The spring deformation limit of each operator is selected such that $\max(\boldsymbol{\Delta}) \equiv 1$ and $\mathbf{k}^\mathsf{T} \boldsymbol{\Delta} \equiv F_C$. Rizos and Fassois (2004) chose to uniformly space the deformation limits. However, motivated by the fact that the curvature of the hysteresis curve is larger for small transmission deformations, we choose the polynomial laws

$$\Delta_i = \left(\frac{i}{M}\right)^{r_\Delta} \tag{40}$$

$$k_i = \frac{F_C}{\Delta_i} \frac{(M+1-i)^{r_k}}{\sum_{i=1}^{M} i^{r_k}} \tag{41}$$

where for $r_\Delta > 1$ the operators' deformation limits are spaced more closely at small spring deformations. The sum of integer powers in (41) is obtained easily by numerical methods, however its analytic solution involves the *Riemann Zeta function* and the *Hurwitz zeta function*. For the special case of $r_k \in \mathbb{N}^+$, Faulhaber's formula gives the sum explicitly in terms of the *Bernoulli numbers*. $r_\Delta = 4$ and $r_k = 2$ are found to yield a good performance.

Defining the GMS model with M operators usually requires the definition of $2M$ parameters; the elements of $\mathbf{k}$ and $\boldsymbol{\Delta}$. However, using (40) and (41), the GMS model can be completely defined by specifying only 4 quantities; F_C, $\mathcal{D}(\theta)$, r_k, and r_Δ, which can be easily identified visually from the proposed identification method. This is equivalent to defining the *shape* of the hysteresis loop from r_k and r_Δ rather than each individual element of $\mathbf{k}$ and $\boldsymbol{\Delta}$.

4.4.4. Identification of the generalized maxwell-slip model

In this section two methods for the extended GMS friction model identification are postulated; (1) The Nonlinear Regression (NLR) method and (2) the Linear Regression (LR) method. They may be thought of as different extensions (or generalizations) of the GMS method (Section 4.4.3), which uses arbitrarily assigned stiffness and threshold vector pre-assignment. The LR method relaxes the stiffness

vector pre-assignment through a linear regression procedure, and the NLR method further relaxes the pre-assignment of the vector of slip force limits through a nonlinear regression procedure.

The experimental data is the data that was also used for identifying the kinematic error and backlash (Figs. 12 and 13). This dataset is divided into a 50.000 sample *estimation dataset* ($k = 10.001, \dots, 60.000$) used for identification, and a 955.493 sample *validation dataset* ($k = 60.001, \dots, 1.015.493$) used for independent evaluation of the model quality (cross validation principle).

In order to avoid problems with the identification due to misspecified initial states, their effects are removed. This is achieved by choosing the starting conditions such that all operators slip, hence in accordance with *Condition C0* in Rizos and Fassois (2004).

The Linear Regression (LR) Linear Spacing Method: Partial identification of the GMS model structure is conducted by preassigning values for the deformation limits $\boldsymbol{\Delta}$ as proposed by Rizos and Fassois (2004). This is achieved using (40) with $r_\Delta = 1$. The nonlinear part of the problem is thereby assumed known resulting in a linear regression type estimator for $\mathbf{k}$. This method is denoted $\text{LR}_{\text{Linear}}$.

The Linear Regression (LR) Polynomial Spacing Method: Partial identification of the GMS model structure is conducted by preassigning values for the deformation limits $\boldsymbol{\Delta}$ according to (40) with $r_\Delta = 4$. This method is denoted $\text{LR}_{\text{Polynomial}}$.

The Nonlinear Regression (NLR) Method: Complete estimation of the GMS model by the minimization of (8) leads to a nonlinear regression-type estimator for the threshold and stiffness vectors, $\boldsymbol{\Delta}$ and $\mathbf{k}$ respectively. The model is nonlinear with respect to $\boldsymbol{\Delta}$ while linear in $\mathbf{k}$ and may thus be realized as a succession of nonlinear and linear regression operations

$$\begin{aligned}(\hat{\mathbf{k}}^\top, \hat{\boldsymbol{\Delta}}^\top)^\top &= \arg\min_{\boldsymbol{\Delta},\mathbf{k}} J(\mathbf{k},\boldsymbol{\Delta}) \\ &= \arg\min_{\boldsymbol{\Delta}} \{\min_{\mathbf{k}} J(\mathbf{k},\boldsymbol{\Delta})\}\end{aligned} \tag{42}$$

The operator thresholds are strictly positive and distinct, i.e. $0 < \Delta_1 < \cdots < \Delta_M$, so linear inequality constraints are defined as $\mathbf{A}\,\boldsymbol{\Delta} \le \mathbf{0}$, $A_{i,i} = -1$ and $A_{i+1,i} = 1$.

$$\begin{aligned}\underset{\mathbf{k},\boldsymbol{\Delta}\in\mathbb{R}^M}{\text{minimize}} \quad & J = \frac{1}{N_S}\sum_{k=1}^{N_S}(y(k)-\hat{y}(k))^2 \\ & y(k) = K_\tau\, i(k) \\ & f_C(k) = D^{-1}(\theta(k))\sum_{i=1}^{M} k_i\,\delta_i(k) \\ \text{subject to} \quad & \\ \delta_i(k+1) = \; & \text{sgn}(\hat{\theta}(k+1)-\hat{\theta}(k)+\delta_i(k)) \\ & \cdot \min\{|\hat{\theta}(k+1)-\hat{\theta}(k)+\delta_i(k)|, D(\theta(k))\,\Delta_i\} \\ & \qquad \forall\, i = 1,\dots,M \\ 0 < \; & \Delta_1 \\ \Delta_{i-1} < \; & \Delta_i \qquad \forall\, i = 2,\dots,M, \quad M \ge 2\end{aligned} \tag{43}$$

The nonlinear regression is realized as a two-phase hybrid optimization using the *Genetic Algorithm* (GA) (Conn, Gould, & Toint, 1997) to explore large areas of parameter space and the *Nelder–Mead Downhill Simplex Algorithm* (Lagarias, Reeds, Wright, & Wright, 1998) to exactly locate the minimum. This two-phase scheme has been shown in Rizos and Fassois (2004) to be able to effectively locate the true global minimum.

4.4.5. Results

In this section, we compare five different friction models; (1) the static nonlinear maps identified in Section 4.2, (2) the GMS model with parameters fixed according to (40) and (41), (3) the $\text{LR}_{\text{Polynomial}}$ method, (4) the $\text{LR}_{\text{Linear}}$ method, and (5) the NLR method (see Fig. 16).

The results of the identification reveal that for $M = 1, \dots, 3$ the NLR method is superior in performance. For $M \ge 4$ the NLR and $\text{LR}_{\text{Polynomial}}$ methods are almost similar in performance with 82.3% and 82.0%, respectively. The proposed polynomial law in (40) for $\boldsymbol{\Delta}$ thus seems reasonable. On the other hand, the $\text{LR}_{\text{Linear}}$ method by Rizos and Fassois (2004) performs for $M = 4$ at 73.7%, i.e. considerably worse than our proposed $\text{LR}_{\text{Polynomial}}$ method. The performance of the $\text{LR}_{\text{Linear}}$ method increases with the number of operators to a maximum of 78.0% for $M = 10$. This is, however, still less than the $\text{LR}_{\text{Polynomial}}$ and GMS methods with $M = 3$, performing at 78.5% and 81.4%, respectively. For 4 operators the GMS method performs at 80.7% slightly worse compared to the $\text{LR}_{\text{Polynomial}}$ method at 82.0%, hence (41) is not quite optimal. The static nonlinear maps identified in Section 4.2 performs at 68.9% worse than all GMS based dynamic friction models with $M > 1$. This shows, that there is a strong motivation for incorporating GMS based dynamic friction models in collaborative robots whose joints comprise strain-wave transmissions.

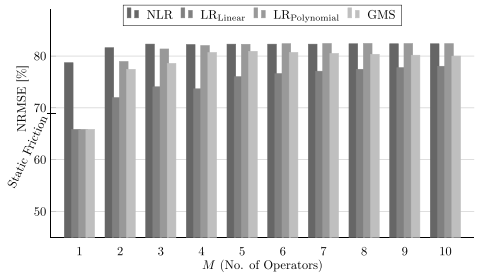

Fig. 16. Performance of the friction models with various number of operators as evaluated on the validation dataset. **NLR** corresponds to complete identification of $\mathbf{k}$ and $\boldsymbol{\Delta}$, $\mathbf{LR_{Linear}}$ corresponds to the method proposed by Rizos and Fassois (2004), i.e. partial identification of $\mathbf{k}$, keeping $\boldsymbol{\Delta}$ fixed through linear spacing of the elements in $\boldsymbol{\Delta}$, $\mathbf{LR_{Polynomial}}$ corresponds to partial identification of $\mathbf{k}$, keeping $\boldsymbol{\Delta}$ fixed according to (40), and **GMS** corresponds to no identification, i.e. $\mathbf{k}$ and $\boldsymbol{\Delta}$ are fixed according to (40) and (41), respectively. **Static Friction** corresponds to the identified static nonlinear maps presented in Section 4.2.

Fig. 17 shows the error torques for the static friction model, the GMS model with 4 operators, the LR_4 method, and the NLR_3 method.

5. Conclusions

Accurate torque estimation is crucial in the development of collaborative robots in order to achieve high performance in terms of safety, accuracy, precision, and lead-through programming. One challenging issue is the dynamic modeling and identification of joint dynamics complicated by and originating mainly from the strain-wave type transmissions.

In this work we applied time domain and nonlinear identification methods on the Universal Robots *UR5e* manipulator. A comprehensive dynamic model has been established and validated through extensive experimental analyses. The methods are valid for serial-link manipulators with rigid links and flexible joints, and the joints are assumed to have the same behavior in both directions. The results of the identification indicate that the applied methodology is very useful for obtaining accurate estimates of the torques, which could be very relevant for joint torque estimation for strain-wave transmissions utilizing two absolute rotary encoders per joint; one at each side of the strain-wave transmission.

The main features of the proposed method is: (1) Enhanced accuracy of torque prediction by extending the Generalized Maxwell-Slip (GMS) friction model to describe the position-dependent backlash characteristics observed in the Universal Robots UR5e manipulator. (2) Easy identification of GMS model; with M the number of Maxwell-Slip operators, one need only specify 4 parameters instead of the usual $2M$ parameters.

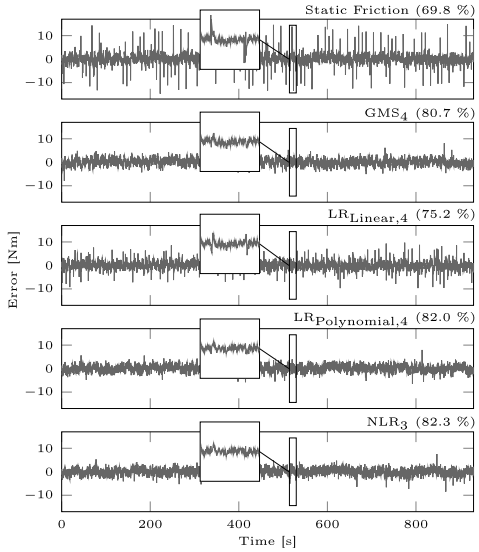

Fig. 17. Error torque over time for the friction models; Static Friction, GMS_4, $LR_{Linear,4}$, $LR_{Polynomial,4}$, and NLR_3. The zoom around 520 s contains two velocity reversals.

The distinguished contributions include: (1) Proposal of more accurate models for the friction's dependency on load and temperature, (2) experimental observation of position-dependent backlash phenomena, and (3) extension of the GMS dynamic friction model to describe position-dependent backlash characteristics. (4) Development of a new and more accurate linear regression method based on the GMS model. The accuracy was improved from an NRMSE of 75.2% to 82.0%.

The established and identified joint dynamics model provides important guidance to the design and control of collaborative robot manipulators and other types of lightweight industrial robot manipulators. Our ongoing research efforts include; (1) implementation of the identified mathematical models in the control and safety systems of the Universal Robots manipulators, and (2) research on practical approaches to the design and implementation of adaptive estimation strategies with a special attention to the safety system of the collaborative robot.

Declaration of competing interest

The authors declare that they have no known competing financial interests or personal relationships that could have appeared to influence the work reported in this paper.

References

Al-Bender, F., Lampaert, V., & Swevers, J. (2005). The generalized maxwell-slip model: A novel model for friction simulation and compensation. *IEEE Transactions on Automatic Control*, *50*(11), 1883–1887. http://dx.doi.org/10.1109/TAC.2005.858676.

Albu-Schäffer, A., Haddadin, S., Ott, C., Stemmer, A., Wimböck, T., & Hirzinger, G. (2007). The DLR lightweight robot: design and control concepts for robots in human environments. In C. Loughlin (Ed.), *Industrial Robot: an International Journal*, *34*(5), 376–385. http://dx.doi.org/10.1108/01439910710774386.

Bittencourt, A. C., & Gunnarsson, S. (2012). Static friction in a robot joint–modeling and identification of load and temperature effects. *Journal of Dynamic Systems, Measurement, and Control*, *134*(5), http://dx.doi.org/10.1115/1.4006589.

Bittencourt, A. C., Wernholt, E., Sander-Tavallaey, S., & Brogårdh, T. (2010). An extended friction model to capture load and temperature effects in robot joints. In *2010 IEEE/RSJ international conference on intelligent robots and systems* (pp. 6161–6167). Taipei, Taiwan: IEEE, http://dx.doi.org/10.1109/IROS.2010.5650358.

Bona, B., & Indri, M. (2005). Friction compensation in robotics: an overview. In *Proceedings of the 44th IEEE conference on decision and control* (pp. 4360–4367). Seville, Spain: IEEE, http://dx.doi.org/10.1109/cdc.2005.1582848.

Carlson, F. B., Robertsson, A., & Johansson, R. (2015). Modeling and identification of position and temperature dependent friction phenomena without temperature sensing. In *2015 IEEE/RSJ international conference on intelligent robots and systems (IROS)* (pp. 3045–3051). Hamburg, Germany: IEEE, http://dx.doi.org/10.1109/IROS.2015.7353797.

Conn, A. R., Gould, N., & Toint, P. L. (1997). A globally convergent Lagrangian barrier algorithm for optimization with general inequality constraints and simple bounds. *Mathematics of Computation*, *66*(217), 261–289. http://dx.doi.org/10.1090/s0025-5718-97-00777-1.

Dhaouadi, R., Ghorbel, F. H., & Gandhi, P. S. (2003). A new dynamic model of hysteresis in harmonic drives. *IEEE Transactions on Industrial Electronics*, *50*(6), 1165–1171. http://dx.doi.org/10.1109/tie.2003.819661.

Dong, H., Chen, T., Wang, D., & Dong, B. (2019). Kinematic model of harmonic drive in robot joints with input eccentricity error. In V. Arakelian, & P. Wenger (Eds.), *ROMANSY 22 – Robot design, dynamics and control* (pp. 134–140). Cham: Springer International Publishing.

Gandhi, P. S., & Ghorbel, F. H. (2002). Closed-loop compensation of kinematic error in harmonic drives for precision control applications. *IEEE Transactions on Control Systems Technology*, *10*(6), 759–768. http://dx.doi.org/10.1109/tcst.2002.804119.

Gandhi, P. S., & Ghorbel, F. H. (2004). Control of hysteresis and kinematic error nonlinearities in harmonic drives for high speed precision control applications. In *Proceedings of the 2004 American control conference* (pp. 1141–1146). Boston, MA, USA: IEEE.

Gao, L., Yuan, J., Han, Z., Wang, S., & Wang, N. (2017). A friction model with velocity, temperature and load torque effects for collaborative industrial robot joints. In *2017 IEEE/RSJ international conference on intelligent robots and systems (IROS)* (pp. 3027–3032). Vancouver, BC, Canada: IEEE, http://dx.doi.org/10.1109/iros.2017.8206141.

Ghorbel, F. H., Gandhi, P. S., & Alpeter, F. (1998). On the kinematic error in harmonic drive gears. *Journal of Mechanical Design*, *123*(1), 90–97. http://dx.doi.org/10.1115/1.1334379.

Haddadin, S., Albu-Schaffer, A., Luca, A. D., & Hirzinger, G. (2008). Collision detection and reaction: A contribution to safe physical human-robot interaction. In *2008 IEEE/RSJ international conference on intelligent robots and systems*. IEEE, http://dx.doi.org/10.1109/iros.2008.4650764.

Hamon, P., Gautier, M., & Garrec, P. (2010). Dynamic identification of robots with a dry friction model depending on load and velocity. In *2010 IEEE/RSJ international conference on intelligent robots and systems* (pp. 6187–6193). Taipei, Taiwan: IEEE, http://dx.doi.org/10.1109/IROS.2010.5649189.

Harmonic Drive AG (2018). Engineering data – HFUS-2UH/2SO/2SH.

Iskandar, M., & Wolf, S. (2019). Dynamic friction model with thermal and load dependency: modeling, compensation, and external force estimation. In *2019 international conference on robotics and automation (ICRA)*. IEEE, http://dx.doi.org/10.1109/icra.2019.8794406.

Kennedy, C. W., & Desai, J. P. (2005). Modeling and control of the mitsubishi PA-10 robot Arm Harmonic drive system. *IEEE/ASME Transactions on Mechatronics*, *10*(3), 263–274. http://dx.doi.org/10.1109/tmech.2005.848290.

Kircanski, N. M., & Goldenberg, A. A. (1997). An experimental study of nonlinear stiffness, hysteresis, and friction effects in robot joints with harmonic drives and torque sensors. *International Journal of Robotics Research*, *16*(2), 214–239. http://dx.doi.org/10.1177/027836499701600207.

Lagarias, J. C., Reeds, J. A., Wright, M. H., & Wright, P. E. (1998). Convergence properties of the Nelder–Mead simplex method in low dimensions. *SIAM Journal on Optimization*, *9*(1), 112–147. http://dx.doi.org/10.1137/s1052623496303470.

Lampaert, V., Al-Bender, F., & Swevers, J. (2003). A generalized maxwell-slip friction model appropriate for control purposes. In *2003 IEEE international workshop on workload characterization (IEEE Cat. No.03EX775)*. IEEE, http://dx.doi.org/10.1109/phycon.2003.1237071.

Luca, A., Albu-Schaffer, A., Haddadin, S., & Hirzinger, G. (2006). Collision detection and safe reaction with the DLR-III lightweight manipulator arm. In *2006 IEEE/RSJ international conference on intelligent robots and systems*. IEEE, http://dx.doi.org/10.1109/iros.2006.282053.

Madsen, E., Rosenlund, O. S., Brandt, D., & Zhang, X. (2019). Model-based on-line estimation of time-varying nonlinear joint stiffness on an e-series universal robots manipulator. In *2019 international conference on robotics and automation (ICRA)*. IEEE, http://dx.doi.org/10.1109/icra.2019.8793935.

Musser, C. W. (1959). Strain wave gearing.

Nye, T. W. (1989). Harmonic drives: Determining wear life based on stiffness considerations. In *Proc. of the international power transmission and gearing conference, Vol. 2* (pp. 867–877). Chicago, USA: American Society of Mechanical Engineers.

Olsson, H., Åström, K. J., de Wit, C. C., Gäfvert, M., & Lischinsky, P. (1998). Friction models and friction compensation. *European Journal of Control*, *4*(3), 176–195. http://dx.doi.org/10.1016/s0947-3580(98)70113-x.

Preissner, C., Royston, T. J., & Shu, D. (2012). A high-fidelity harmonic drive model. *Journal of Dynamic Systems, Measurement, and Control*, *134*(1), 011002. http://dx.doi.org/10.1115/1.4005041.

Rizos, D. D., & Fassois, S. D. (2004). Presliding friction identification based upon the Maxwell slip model structure. *Chaos. An Interdisciplinary Journal of Nonlinear Science*, *14*(2), 431–445. http://dx.doi.org/10.1063/1.1755178.

Ruderman, M. (2019). On stability of virtual torsion sensor for control of flexible robotic joints with hysteresis. *Robotica*, 1–14. http://dx.doi.org/10.1017/s0263574719001358.

Ruderman, M., & Bertram, T. (2012). Modeling and observation of hysteresis lost motion in elastic robot joints. *IFAC Proceedings Volumes*, *45*(22), 13–18. http://dx.doi.org/10.3182/20120905-3-hr-2030.00061.

Ruderman, M., Bertram, T., & Iwasaki, M. (2014). Modeling, observation, and control of hysteresis torsion in elastic robot joints. *Mechatronics*, *24*(5), 407–415. http://dx.doi.org/10.1016/j.mechatronics.2014.02.009.

Ruderman, M., Hoffmann, F., & Bertram, T. (2009). Modeling and identification of elastic robot joints with hysteresis and backlash. *IEEE Transactions on Industrial Electronics*, *56*(10), 3840–3847. http://dx.doi.org/10.1109/tie.2009.2015752.

Seeton, C. J. (2006). Viscosity–temperature correlation for liquids. *Tribology Letters*, *22*(1), 67–78. http://dx.doi.org/10.1007/s11249-006-9071-2.

Seyfferth, W., Maghzal, A. J., & Angeles, J. (1995). Nonlinear modeling and parameter identification of harmonic drive robotic transmissions. In *Proceedings of 1995 IEEE international conference on robotics and automation*. IEEE, http://dx.doi.org/10.1109/robot.1995.525714.

Shi, Z., Li, Y., & Liu, G. (2017). Adaptive torque estimation of robot joint with harmonic drive transmission. *Mechanical Systems and Signal Processing*, *96*, 1–15. http://dx.doi.org/10.1016/j.ymssp.2017.03.041.

Simoni, L., Beschi, M., Legnani, G., & Visioli, A. (2015). Friction modeling with temperature effects for industrial robot manipulators. In *2015 IEEE/RSJ international conference on intelligent robots and systems (IROS)* (pp. 3524–3529). Hamburg, Germany: IEEE, http://dx.doi.org/10.1109/iros.2015.7353869.

Spong, M. W. (1987). Modelling and control of elastic joint robots. *Journal of Dynamic Systems, Measurement, and Control*, *109*(4), 310–319.

Stolt, A., Carlson, F. B., Ardakani, M. M. G., Lundberg, I., Robertsson, A., & Johansson, R. (2015). Sensorless friction-compensated passive lead-through programming for industrial robots. In *2015 IEEE/RSJ international conference on intelligent robots and systems (IROS)*. IEEE, http://dx.doi.org/10.1109/iros.2015.7353870.

Sun, K., Jianbin, Q., Karimi, H. R., & Fu, Y. (2020). Event-triggered robust fuzzy adaptive finite-time control of nonlinear systems with prescribed performance. *IEEE Transactions on Fuzzy Systems*, 1. http://dx.doi.org/10.1109/tfuzz.2020.2979129.

Sun, K., Liu, L., Qiu, J., & Feng, G. (2020). Fuzzy adaptive finite-time fault-tolerant control for strict-feedback nonlinear systems. *IEEE Transactions on Fuzzy Systems*, 1. http://dx.doi.org/10.1109/tfuzz.2020.2965890.

Sun, K., Qiu, J., Karimi, H. R., & Gao, H. (2020). A novel finite-time control for nonstrict feedback saturated nonlinear systems with tracking error constraint. *IEEE Transactions on Systems, Man, and Cybernetics: Systems*, 1–12. http://dx.doi.org/10.1109/tsmc.2019.2958072.

Taghirad, H. D., & Bélanger, P. R. (1996). An experimental study on modelling and identification of harmonic drive systems. In *Proceedings of 35th IEEE conference on decision and control* (pp. 4725–4730). Kobe, Japan: IEEE, http://dx.doi.org/10.1109/CDC.1996.577625.

Tjahjowidodo, T., Al-Bender, F., & Van Brussel, H. (2013). Theoretical modelling and experimental identification of nonlinear torsional behaviour in harmonic drives. *Mechatronics*, *23*(5), 497–504. http://dx.doi.org/10.1016/j.mechatronics.2013.04.002.

Tuttle, T. D., & Seering, W. P. (1996). A nonlinear model of a harmonic drive gear transmission. *IEEE Transactions on Robotics and Automation*, *12*(3), 368–374. http://dx.doi.org/10.1109/70.499819.

Vischer, D., & Khatib, O. (1995). Design and development of high-performance torque-controlled joints. *IEEE Transactions on Robotics and Automation*, *11*(4), 537–544. http://dx.doi.org/10.1109/70.406938.

Wolf, S., & Iskandar, M. (2018). Extending a dynamic friction model with nonlinear viscous and thermal dependency for a motor and harmonic drive gear. In *2018 IEEE international conference on robotics and automation (ICRA)*. IEEE, http://dx.doi.org/10.1109/icra.2018.8460613.

Zou, C., Tao, T., Jiang, G., Mei, X., & Wu, J. (2016). A harmonic drive model considering geometry and internal interaction. *Proceedings of the Institution of Mechanical Engineers, Part C: Journal of Mechanical Engineering Science*, *231*(4), 728–743. http://dx.doi.org/10.1177/0954406215621097.

Chapter 5

Robot Dynamics Calibration [Journal Paper 2]

Dynamics Parametrization and Calibration of Flexible-Joint Collaborative Industrial Robot Manipulators [168]

> *"In the kingdom of ends everything has either a price or a dignity."*
>
> — Immanuel Kant (1724–1804)

5.1 Introduction

The desire for increasing the accuracy of the mathematical model of robot manipulators motivates the calibration of the robot dynamics including the masses, center of mass location, and mass moments of inertia. One promising strategy is a combined Inverse Dynamics Identification Model and Least Squares (IDIM-LS) method [42]. Robot dynamics calibration have been performed for several collaborative industrial robots including the KUKA LBR iiwa [61], ABB IRB14000 (YuMi) [64], and Franka Emika Panda [63]. However, existing methods do not utilize a dual joint encoder sensor

[1] https://creativecommons.org/licenses/by/4.0/

system, of the Universal Robots manipulators, and simple models for the joint friction are assumed.

5.2 Method

In this work, we follow a system identification procedure based on the Inverse Dynamics Identification Model and Weighted Least Squares (IDIM-WLS) method. The usual assumption of rigid joints is relaxed by making use of the two absolute rotary encoders per joint to effectively compensate the flexibility and rotor-side dynamics including nonlinear friction. Thus, the distinction from existing works lies in the technique for compensating the nonlinear flexible-joint dynamics.

First, the robot dynamics are derived using the modified Denavit-Hartenberg kinematics convention and the Recursive Newton-Euler algorithm for the dynamics. Then, the dynamics are linearly parameterized in terms of a vector of unknown parameters and a matrix of known functions in the joint angular positions and their time-derivatives of first and second order. The set of inertial parameters are then reduced to a minimal set of base parameters through the analytic regrouping relations derived in [38]. A trajectory is designed to excite all unknown parameters. The robot is commanded to follow the trajectory while currents and joint angular positions are measured. Based on the measurements, the optimum parameters are chosen in order to minimize the weighted least squares error between the model-predicted and measured currents with the weighting equal to the reciprocal of the standard deviation of the parameter obtained from an ordinary least squares (OLS) solution.

5.3 Findings

The calibration of the robot inertial parameters seems effective for increasing the accuracy of the robot dynamic model. The proposed compensation of rotor dynamics effects including flexibility and nonlinear friction seems like an effective strategy to reduce uncertainty in the parameter estimates.

The presented method of robot dynamics calibration show improvements in the torque prediction accuracy of 16.5 %–28.5 % compared to the parameters obtained from a CAD model. The uncertainty of the parameter estimate is very low for all but two parameters, YZ_4 and ZZR_4, with standard deviations estimated at, respectively, 19 % and 20 %. These are

indications of either; 1) sub-optimality of the chosen trajectory or 2) the parameters do not matter much to the torque computation. YZ_4 is a product moment of inertia (off-diagonal element in the inertia tensor), and as such its influence on the torque is expected to be small. ZZR_4 is a regrouped mass moment of inertia and the uncertainty may be due to insufficient excitation by the chosen trajectory.

5.4 Reflection

Comparing the results of the presented method to the work in [64] indicate improvements in parametric uncertainty. In [64], the number of base parameters is 34 with 25 of those having an uncertainty ≥ 5 %. It is noted that the inaccuracies of the last three joints are influenced by the use of a simple friction model and that the accuracy can be improved by using a more complex friction model.

Thus, the proposed method for robot dynamics calibration with compensation of flexibility and nonlinear friction seems to be effective for increasing the accuracy of the dynamic model. Possible further developments and improvements of the method is summarized in the following.

- The number of identifiable parameters can be increased from 36 to 38 by orienting the base joint of the robot with its axis of rotation non-parallel to the direction of the gravitational acceleration.
- The trajectory used for identification could possibly be optimized through optimization routines.
- The optimization could be constrained to enforce positive definiteness of the inertia matrix using either Sylvester's theorem or Cholesky decomposition. The property of positive-definiteness is relevant in the decoupling and linearizing control strategies elaborated in Chapter 2.

5.5 Author's Contribution

The author supervised the Master's Thesis project, assisted with research and experiments, and prepared the manuscript with inputs from the co-authors.

Hindawi
Mathematical Problems in Engineering
Volume 2020, Article ID 8709870, 13 pages
https://doi.org/10.1155/2020/8709870

Research Article

Dynamics Parametrization and Calibration of Flexible-Joint Collaborative Industrial Robot Manipulators

Emil Madsen,[1,2] **Simon Aagaard Timm**,[1,2] **Norbert Andras Ujfalusi**,[1,2] **Oluf Skov Rosenlund**,[1] **David Brandt**,[1] **and Xuping Zhang**[2]

[1]*Universal Robots A/S, Energivej 25, Odense S DK-5260, Denmark*
[2]*Aarhus University, Inge Lehmanns Gade 10, Aarhus C DK-8000, Denmark*

Correspondence should be addressed to Emil Madsen; emil_madsen@hotmail.com and Xuping Zhang; xuzh@eng.au.dk

Received 1 May 2020; Revised 18 July 2020; Accepted 24 July 2020; Published 17 September 2020

Academic Editor: Jürgen Pannek

Many collaborative robots use strain-wave-type transmissions due to their desirable characteristics of high torque capacity and low weight. However, their inherent complex and nonlinear behavior introduces significant errors and uncertainties in the robot dynamics calibration, resulting in decreased performance for motion and force control tasks and lead-through programming applications. This paper presents a new method for calibrating the dynamic model of collaborative robots. The method combines the known inverse dynamics identification model with the weighted least squares (IDIM-WLS) method for rigid robot dynamics with complex nonlinear expressions for the rotor-side dynamics to obtain increased calibration accuracy by reducing the modeling errors. The method relies on two angular position measurements per robot joint, one at each side of the strain-wave transmission, to effectively compensate the rotor inertial torques and nonlinear dynamic friction that were identified in our previous works. The calibrated dynamic model is cross-validated and its accuracy is compared to a model with parameters obtained from a CAD model. Relative improvements are in the range of 16.5% to 28.5% depending on the trajectory.

1. Introduction

For collaborative industrial robots, it is of crucial importance to acquire accurate predictions of the torques required in order to realize the desired motion or force control task and to ensure a consistently good performance of lead-through programming applications. Being able to accurately predict the torques required to complete the intended task will (1) improve the control performance by being able to react to disturbances before they cause deviations from the reference and (2) improve the robot safety system by being able to more accurately identify external disturbances such as human interference. Accurate torque estimates can be obtained through knowledge about the dynamic properties of the robot. Accurate torque estimates will also improve any possible online estimation procedures such as online estimation of the payload mass and inertia properties [1], friction, and/or wear.

The dynamic model of the robot relates the robot motion to the joint torques and it depends on a set of dynamic parameters being the mass, the first moments, and the mass moments of inertia of each link of the robot. Multiple procedures exist for estimating the dynamic parameters of robot manipulators:

(1) *Physical Experiments.* The robot is disassembled to isolate each link. The mass can be evaluated directly. The first moments can be obtained by evaluating the counterbalanced points of each link. The diagonal elements of the inertia tensor can be evaluated by pendular motions. Such methods are tedious and are not preferred because they require a lot of manual operations to disassemble the robot and carry out the experiments. Furthermore, experiments need to be redone if hardware changes are made to the robot.

(2) *Computer Aided Design (CAD).* The dynamic parameters of each link are found using their nominal

geometric and material characteristics. In the design phase, such investigation can be used in the performance analysis to further improve the design. However, the accuracy of the parameter estimates is reduced because the CAD parts are never identical to the real parts due to the production tolerances.

(3) *System Identification*. The input/output behavior is analyzed on some planned motion. Parameters are estimated by minimizing the difference between the measured output (possibly the current supplied to the electric actuator) and its mathematical model evaluated in the input (possibly the angular positions of the robot joints). Such procedures are preferred because they generally lead to the most accurate results while offering flexibility in the case of robot hardware changes.

For system identification methods, the most common strategy is a combined Inverse Dynamics Identification Model and Least Squares (IDIM-LS) method. For such method, the accuracy of the parameter estimates is generally affected by measurement noise and modeling errors.

The issue of measurement noise is often addressed by generating so-called exciting trajectories and/or filtering the noisy measurements [2]. Other identification techniques have also been suggested such as the Extended Kalman Filter (EKF) [3, 4], algorithms based on Linear Matrix Inequality (LMI) tools [5], maximum likelihood (ML) approaches [6], the Set Membership Uncertainty [7], and Huber's estimator [8]. However, based on the experimental results, these approaches do not improve the IDIM-LS, and they were not validated on 6-degrees-of-freedom (DOF) industrial robots. To eliminate the need for tuning the bandpass filters that are applied to the trajectory data, [9, 10] used the Instrumental Variable (IV) technique, and [11] proposed the Direct and Inverse Dynamic Identification Models (DIDIM) technique. These methods are based on a closed-loop output error (CLOE) method using both the direct and inverse dynamic models of the robot. The direct dynamic model is used to obtain model-based estimates of the position, velocity, and acceleration signals in contrast to the bandpass filtering often coupled with the IDIM-LS method. In [12], the DIDIM and CLOE methods were compared to the IDIM-LS method and it was found that if the IDIM-LS method is coupled with well-tuned bandpass filtering, the DIDIM and CLOE methods do not offer any improvements to the IDIM-LS method. Other methods include identifying the dynamics of a robotics system using neural networks [13].

Modeling errors will generally lead to a bias of the parameter estimates and it is an issue yet unsolved in the system identification for industrial robots. Modeling errors arises mainly from neglecting the complex and nonlinear joint dynamics effects resulting in significant deterministic structural errors that cannot be accounted for by random variables. Such nonlinear joint dynamics come, for instance, due to the use of strain-wave type transmissions such as the Harmonic Drive™ which are often used in collaborative robots due to their desirable characteristics of high torque capacity and low weight.

The works on the identification of dynamic parameters for collaborative robots are limited. In [14], the essential parameters were identified for the KUKA LWR 4+ collaborative robot assuming a three-parameter friction model. In [1, 15], dynamics parameter identification was performed using the KUKA LWR 4+ collaborative robot with friction neglected. The works on the KUKA LWR 4+ collaborative robot exploited the joint torque sensor located on the output side of the transmission; thus the joint dynamics do not affect the measurements. Such sensor hardware is, however, expensive and is rarely found in industrial robots. In [16], the dynamic parameters for the 7 DOF Franka Emika Panda robot were identified with a constrained optimization procedure to ensure the physical consistency of the parameters. In [17], the parameters for the 2×7 DOF ABB IRB 14000 (YuMi) collaborative robot were identified. The fact that very simple models of the friction are employed with Coulomb and linear viscous friction and that joints are assumed rigid are common in the mentioned works. Such assumptions on the joint dynamics characteristics for strain-wave transmissions are serious simplifications of the real dynamic characteristics.

To address the mentioned limitations of the prior art, we propose a new method for estimating the dynamic parameters of collaborative robot manipulators considering the flexible joint dynamics effects. Firstly, the dynamics of the Universal Robots UR5e collaborative robot manipulator are developed in closed form using the modified Denavit-Hartenberg convention and the Recursive Newton–Euler Algorithm. Secondly, the dynamic equations are linearly parametrized and the dimension of the parameter space is reduced to a minimum. Thirdly, the proposed rotor dynamics compensation is introduced to reduce modeling errors. The novelty lies in the rotor dynamics compensation in which *two* built-in rotary encoders are utilized per joint, one at each side of the transmission element, to effectively compensate the complex nonlinear joint dynamics effects of the Universal Robots UR5e robot manipulator identified prior to this work [18,19]. Any unmodeled friction is handled by augmenting the set of dynamic parameters with Coulomb and viscous friction coefficients for each joint. The parameters are then estimated by a WLS procedure with the weighting equal to the inverse of the estimated covariance matrix. Lastly, the calibrated dynamic model is validated on new trajectories that were not used for the estimation (cross-validation principle). The general methodology of the dynamics calibration in this work is illustrated in Figure 1. The two-encoder setup is illustrated by the *Robot* outputting two angular position variables q and θ for the link and rotor, respectively.

The distinguished contributions of this work include the following: (1) a linear parametrization describing the dynamics of the UR5e collaborative robot manipulator has been developed, (2) the complex nonlinear dynamic friction characteristics and rotor inertia have been considered, (3) the minimal set of base parameters that describe the dynamic behavior of the UR5e robot has been accurately estimated, and (4) the performance of the calibrated dynamic model has been validated.

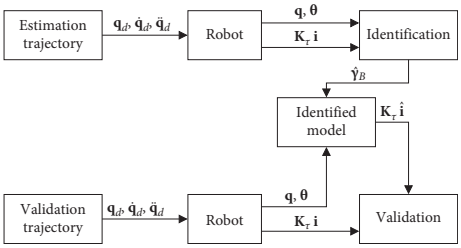

Figure 1: Schematic representation of the methodology of this work showing the interconnection between the identification and validation procedures.

The rest of the paper is organized as follows: Section 2 describes the mathematical model of the Flexible-Joint Robot (FJR) manipulator. In Section 3, the linear parametrization of the dynamics is described. In Section 4, the identification procedure is described and the results of the identification are presented. In Section 5, the calibrated dynamic model is validated and compared to a model obtained with parameters from a CAD model. Section 6 concludes the work and presents the challenges for our ongoing research.

1.1. Notations. The notation used in the paper is mostly standard. Let $\mathbb{R}$ be the set of real numbers, $\mathbb{N}$ be the set of nonnegative integers, and $\mathbb{N}^+$ be the set of positive integers. Let $\mathbf{x} \in \mathbb{R}^n$ be a vector of n real numbers; then x_i is its i^{th} entry, $\mathbf{x}^T$ its transpose, $\overline{\mathbf{x}}$ is the mean value of the elements of $\mathbf{x}$, and $\|\mathbf{x}\|$ is the 2-norm. Let $\hat{\mathbf{x}}$ denote an estimate of $\mathbf{x}$ and let $\tilde{\mathbf{x}} \triangleq \mathbf{x} - \hat{\mathbf{x}}$ be the estimation error. Given a function g: $\mathcal{G} \longrightarrow \mathbb{R}$, let sgn: $\mathbb{R} \longrightarrow \{-1, 0, 1\}$ be the signum function defined such that $\operatorname{sgn}(g) = -1$ if $g < 0$, $\operatorname{sgn}(g) = 0$ if $g = 0$, and $\operatorname{sgn}(g) = 1$ if $g > 0$. If $\mathbf{g}$: $\mathcal{G} \longrightarrow \mathbb{R}^n$ is a vector function, the signum vector function $\mathbf{sgn}(\mathbf{g}) = [\mathbf{sgn}(\mathbf{g}_1) \cdots \mathbf{sgn}(\mathbf{g}_n)]^T$. Given a square real matrix $\mathbf{A} \in \mathbb{R}^{n \times n}$, let $\mathbf{A} > 0$ indicate that $\mathbf{A}$ is positive definite; that is, $\mathbf{x}^T \mathbf{A}\, \mathbf{x} > 0$ for any nonzero column vector $\mathbf{x}$ of n real numbers. Let diag: $\mathbb{R}^n \longrightarrow \mathbb{R}^{n \times n}$ map a vector of n elements to a diagonal matrix with the i^{th} element of the vector on its i^{th} diagonal entry and zero everywhere else. Similarly, let diag^{-1}: $\mathbb{R}^{n \times n} \longrightarrow \mathbb{R}^n$ map the diagonal elements of an $n \times n$ matrix to vector of n elements with the i^{th} diagonal element of the matrix on the i^{th} element of the vector.

2. Mathematical Model

The Flexible-Joint Robot (FJR) manipulator is considered as an open kinematic chain having $N + 1$ rigid bodies; the base and the N links are interconnected by N revolute joints undergoing deflection and actuated by N electrical actuators. To derive the dynamics of the robot manipulator, the following standard assumptions are made:

(i) The rotors are uniform bodies having their center of mass on the axis of rotation

(ii) Each motor $i = 1, \ldots, N$ is mounted on link $i - 1$ and moves link i; see Figure 2

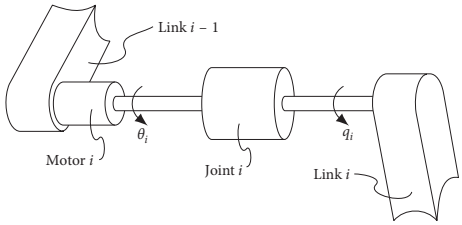

Figure 2: Kinematic arrangement of motors and links for the FJR manipulator model. Note that θ_i is already scaled by the reduction ratio.

Assumption (i) is a basic requirement for long life of an electrical drive and implies that the robot dynamics become independent of the angular position of the rotors. For the UR5e manipulator, we take advantage of the presence of large reduction ratios and simply assume the following.

(iii) The angular velocity of the rotors is due only to their own spinning

This simplifying assumption was proposed by [20] and is equivalent to neglecting energy contributions due to the inertial couplings between the rotors and the links. It also implies that Coriolis and centripetal terms will be independent of the rotors' angular velocity.

To uniquely characterize the manipulator configuration, we choose the generalized coordinates $(\mathbf{q}\, \boldsymbol{\theta}) \in \mathbb{R}^{2N}$ being, respectively, the positions of the links and rotors reflected through the gear ratios; that is, the rotor positions are seen in the link space. Given assumptions (i)–(iii), the link and rotor dynamics become, respectively,

$$\mathbf{M}(\mathbf{q})\ddot{\mathbf{q}} + \mathbf{C}(\mathbf{q}, \dot{\mathbf{q}})\dot{\mathbf{q}} + \mathbf{g}(\mathbf{q}) = \boldsymbol{\tau}_J, \tag{1}$$

$$\mathbf{B}\,\ddot{\boldsymbol{\theta}} + \mathbf{f} + \boldsymbol{\tau}_J = \mathbf{K}_\tau\, \mathbf{i}, \tag{2}$$

where, in the link equation, $\mathbf{M}(\mathbf{q}) > 0 \in \mathbb{R}^{N \times N}$ is the symmetric inertia matrix, $\mathbf{C}(\mathbf{q}, \dot{\mathbf{q}}) \in \mathbb{R}^{N \times N}$ is the Coriolis and centripetal matrix, $\mathbf{g}(\mathbf{q}) \in \mathbb{R}^N$ is the gravity vector, and $\boldsymbol{\tau}_J \in \mathbb{R}^N$ is the vector of joint torques which couple the link and rotor subsystems. In the rotor equation, $\mathbf{B} > 0 \in \mathbb{R}^{N \times N}$ is the diagonal matrix of rotor inertias, $\mathbf{f} \in \mathbb{R}^N$ is friction acting on the rotor coordinate, $\mathbf{K}_\tau > 0 \in \mathbb{R}^{N \times N}$ is the diagonal matrix of torque constants, and $\mathbf{i} \in \mathbb{R}^N$ is the torque-generating (quadrature) current obtained from the phase currents via Park's Transformation. The drive-gain $\mathbf{K}_\tau$ has been calibrated *a priori* with special tests; see, for example, [21].

The dynamic model of the N link robot manipulator is obtained in closed form using the Denavit-Hartenberg (DH) convention [22] with coordinate systems placed as illustrated in Figure 3 to represent the UR5e manipulator and with the parameters in Table 1 and the Recursive Newton–Euler Algorithm (RNEA) [22]. In the RNEA, the position vector ${}^i\mathbf{P}_{i+1} = [a_{i-1} \;\; -d_i \sin(\alpha_{i-1}) \;\; d_i \cos(\alpha_{i-1})]^T$ and the rotation matrix

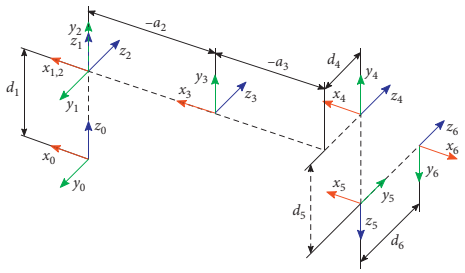

Figure 3: Coordinate systems used for describing the kinematics of the UR5e robot using the Denavit–Hartenberg convention.

Table 1: Denavit–Hartenberg parameters of the UR5e robot.

i	a_i	α_i	d_i	q_i
1	0	$\pi/2$	d_1	q_1
2	a_2	0	0	q_2
3	a_3	0	0	q_3
4	0	$\pi/2$	d_4	q_4
5	0	$-\pi/2$	d_5	q_5
6	0	0	d_6	q_6

$$
{}_{i}^{i+1}\mathbf{R} = \begin{bmatrix} \cos(q_i) & -\sin(q_i) & 0 \\ \sin(q_i)\cos(\alpha_{i-1}) & \cos(q_i)\cos(\alpha_{i-1}) & -\sin(\alpha_{i-1}) \\ \sin(q_i)\sin(\alpha_{i-1}) & \cos(q_i)\sin(\alpha_{i-1}) & \cos(\alpha_{i-1}) \end{bmatrix}. \tag{3}
$$

To allow a parametrization of the dynamics which is linear in the inertial parameters, the inertia tensor for each link is defined relative to the center of rotation (CoR). The RNE algorithm needs the inertia tensor defined relative to the center of mass (CoM), so the parallel axis theorem (Steiner's law) is used for translation; that is,

$$
\mathbf{I}_{\mathrm{CoM},i} = \mathbf{I}_{\mathrm{CoR},i} - m_i\left(\left(\mathbf{P}_{C,i}^T\mathbf{P}_{C,i}\right)\mathbf{E}_3 - \mathbf{P}_{C,i}\mathbf{P}_{C,i}^T\right), \tag{4}
$$

with $\mathbf{E}_3$ being the 3×3 identity matrix, and the vector of center of mass positions $\mathbf{P}_{C,i} = \begin{bmatrix} P_{C,i,x} & P_{C,i,y} & P_{C,i,z} \end{bmatrix}^T$, m_i is the mass of link i, and the symmetric inertia tensor is

$$
\mathbf{I}_{\mathrm{CoR},i} = \begin{bmatrix} \mathrm{XX}_i & \mathrm{XY}_i & \mathrm{XZ}_i \\ \mathrm{XY}_i & \mathrm{YY}_i & \mathrm{YZ}_i \\ \mathrm{XZ}_i & \mathrm{YZ}_i & \mathrm{ZZ}_i \end{bmatrix}. \tag{5}
$$

3. Dynamics Parametrization

The expressions for the torques obtained from the RNE algorithm can be expressed linearly in the inertial parameters:

$$
\boldsymbol{\tau}_J = \mathbf{Y}(\mathbf{q}, \dot{\mathbf{q}}, \ddot{\mathbf{q}})\boldsymbol{\gamma}, \tag{6}
$$

where the inertial parameters are

$$
\begin{aligned}
\boldsymbol{\gamma} &= \left[\boldsymbol{\gamma}_1^T \cdots \boldsymbol{\gamma}_i^T \cdots \boldsymbol{\gamma}_N^T\right]^T, \\
\boldsymbol{\gamma}_i &= \left[\mathrm{XX}_i\ \mathrm{XY}_i\ \mathrm{XZ}_i\ \mathrm{YY}_i\ \mathrm{YZ}_i\ \mathrm{ZZ}_i\ m\mathrm{X}_i\ m\mathrm{Y}_i\ m\mathrm{Z}_i\ m_i\right]^T.
\end{aligned} \tag{7}
$$

For a specific robot manipulator, not all 10 N inertial parameters can be identified. Not all the inertial parameters have an effect on the dynamic model, while others have an effect only in linear combinations. The inertial parameters of a robot can therefore be classified into three groups: fully identifiable, identifiable in linear combinations only, and unidentifiable. This is due to the kinematic arrangement of the joints as well as the orientation of the manipulator's base with respect to gravity. Table 2 shows the 49 inertial parameters that appear in the mathematical model.

For the estimation problem to have a unique solution, the parameters must be linearly independent. The set of linearly independent parameters is called *base parameters*. The number of base parameters b_m is [23]

$$
b_m \leq 7n_r + 4n_p - 3 - \overline{\sigma}_1 - 2n_{g0}, \tag{8}
$$

where n_r is the number of revolute joints, n_p is the number of prismatic joints, and $\overline{\sigma}_1 = 1$ if joint 1 is revolute; otherwise $\overline{\sigma}_1 = 0$; and $n_{g0} = 1$ if the rotation axis of joint 1 is parallel to the direction of the gravitational acceleration; otherwise $n_{g0} = 0$. For a robot manipulator with the kinematic arrangement in Table 1 and the base joint oriented with its rotation axis parallel to the direction of the gravitational acceleration, the number of base parameters $b_m = 36$. Therefore, a number of inertial parameters are grouped into a fewer number of equivalent parameters using the regrouping relations [24]:

Table 2: The 49 inertial parameters that appear in the dynamic model of the UR5e manipulator when mounted such that the rotation axis of the base joint is oriented parallel to the gravitational acceleration.

i	XX_i	XY_i	XZ_i	YY_i	YZ_i	ZZ_i	$m\mathrm{X}_i$	$m\mathrm{Y}_i$	$m\mathrm{Z}_i$	m_i
1	–	–	–	–	–	ZZ_1	–	–	–	–
2	XX_2	XY_2	XZ_2	YY_2	YZ_2	ZZ_2	$m_2P_{C,2,x}$	$m_2P_{C,2,y}$	–	–
3	XX_3	XY_3	XZ_3	YY_3	YZ_3	ZZ_3	$m_3P_{C,3,x}$	$m_3P_{C,3,y}$	$m_3P_{C,3,z}$	m_3
4	XX_4	XY_4	XZ_4	YY_4	YZ_4	ZZ_4	$m_4P_{C,4,x}$	$m_4P_{C,4,y}$	$m_4P_{C,4,z}$	m_4
5	XX_5	XY_5	XZ_5	YY_5	YZ_5	ZZ_5	$m_5P_{C,5,x}$	$m_5P_{C,5,y}$	$m_5P_{C,5,z}$	m_5
6	XX_6	XY_6	XZ_6	YY_6	YZ_6	ZZ_6	$m_6P_{C,6,x}$	$m_6P_{C,6,y}$	$m_6P_{C,6,z}$	m_6

$$
\begin{aligned}
\mathrm{XXR}_i &= \mathrm{XX}_i - \mathrm{YY}_i,\\
\mathrm{XXR}_{i-1} &= \mathrm{XX}_{i-1} + \mathrm{YY}_i + 2d_i m\mathrm{Z}_i + d_i^2 m_i,\\
\mathrm{XYR}_{i-1} &= \mathrm{XY}_{i-1} + a_{i-1}\sin(\alpha_i)m\mathrm{Z}_i + a_{i-1}d_i\sin(\alpha_i)m_i,\\
\mathrm{XZR}_{i-1} &= \mathrm{XZ}_{i-1} - a_{i-1}\cos(\alpha_i)m\mathrm{Z}_i - a_{i-1}d_i\cos(\alpha_i)m_i,\\
\mathrm{YYR}_{i-1} &= \mathrm{YY}_{i-1} + \cos^2(\alpha_i)\mathrm{YY}_i + 2d_i\cos^2(\alpha_i)m\mathrm{Z}_i + \left(a_{i-1}^2 + d_i^2\cos^2(\alpha_i)\right)m_i,\\
\mathrm{YZR}_{i-1} &= \mathrm{YZ}_{i-1} + \cos(\alpha_i)\sin(\alpha_i)\mathrm{YY}_i + 2d_i\cos(\alpha_i)\sin(\alpha_i)m\mathrm{Z}_i + d_i^2\cos(\alpha_i)\sin(\alpha_i)m_i,\\
\mathrm{ZZR}_{i-1} &= \mathrm{ZZ}_{i-1} + \sin^2(\alpha_i)\mathrm{YY}_i + 2d_i\sin^2(\alpha_i)m\mathrm{Z}_i + \left(a_{i-1}^2 + d_i^2\sin^2(\alpha_i)\right)m_i,\\
m\mathrm{XR}_{i-1} &= m\mathrm{X}_{i-1} + a_{i-1}m_i,\\
m\mathrm{YR}_{i-1} &= m\mathrm{Y}_{i-1} - \sin(\alpha_i)m\mathrm{Z}_i - d_i\sin(\alpha_i)m_i,\\
m\mathrm{ZR}_{i-1} &= m\mathrm{Z}_{i-1} + \cos(\alpha_i)m\mathrm{Z}_i + d_i\cos(\alpha_i)m_i,\\
m\mathrm{R}_{i-1} &= m_{i-1} + m_i.
\end{aligned}
\tag{9}
$$

This results in the set of base parameters in Table 3.

The joint torque is expressed as

$$\boldsymbol{\tau}_J = \mathbf{Y}_b(\mathbf{q}, \dot{\mathbf{q}}, \ddot{\mathbf{q}})\boldsymbol{\gamma}_b, \tag{10}$$

with the vector of base parameters

$$\boldsymbol{\gamma}_b = \left[\mathrm{ZZR}_1\ \mathrm{XXR}_2\ \cdots\ m\mathrm{Y}_6\right]^T \in \mathbb{R}^{b_m}. \tag{11}$$

3.1. Including the Rotor Dynamics. Combining (2) and (10) yields

$$\mathbf{K}_\tau\,\mathbf{i} - \mathbf{B}\,\ddot{\boldsymbol{\theta}} - \mathbf{f} = \mathbf{Y}_b(\mathbf{q}, \dot{\mathbf{q}}, \ddot{\mathbf{q}})\boldsymbol{\gamma}_b. \tag{12}$$

Friction torques are considered as a sum of estimates and error terms. From experience and empirical observations, the error $\tilde{\mathbf{f}} \triangleq \mathbf{f} - \hat{\mathbf{f}}$ is assumed to contain Coulomb and viscous friction contributions; that is, $\tilde{\mathbf{f}} = \tilde{\mathbf{F}}_C\,\mathrm{sgn}(\dot{\boldsymbol{\theta}}) + \tilde{\mathbf{F}}_V\,\dot{\boldsymbol{\theta}}$. The nonlinear estimates, as presented in [19], describe the friction torques in terms of the angular velocities, load torques, and temperatures. Rotor inertias $\mathbf{B}$ are considered to be known; however, they could be easily estimated by augmenting the regressor with the angular acceleration of the rotors. The system formulated in terms of base parameters and augmented with the rotor dynamics and friction discrepancy is

$$\boldsymbol{\tau}_J = \mathbf{Y}_B(\mathbf{q}, \dot{\mathbf{q}}, \ddot{\mathbf{q}})\boldsymbol{\gamma}_B + \boldsymbol{\rho}, \tag{13}$$

$$\boldsymbol{\tau}_J = \mathbf{K}_\tau\mathbf{i} - \mathbf{B}\,\ddot{\boldsymbol{\theta}} - \hat{\mathbf{f}}, \tag{14}$$

$$\mathbf{Y}_B(\mathbf{q}, \dot{\mathbf{q}}, \ddot{\mathbf{q}}) = \left[\mathbf{Y}_b(\mathbf{q}, \dot{\mathbf{q}}, \ddot{\mathbf{q}})\ \ \mathrm{diag}\left(\mathbf{sgn}(\dot{\boldsymbol{\theta}})\right)\ \ \mathrm{diag}(\dot{\boldsymbol{\theta}})\right], \tag{15}$$

$$\boldsymbol{\gamma}_B = \left[\boldsymbol{\gamma}_b^T\ \ \mathrm{diag}^{-1}\left(\tilde{\mathbf{F}}_C\right)^T\ \mathrm{diag}^{-1}\left(\tilde{\mathbf{F}}_V\right)^T\right]^T, \tag{16}$$

where the noise $\boldsymbol{\rho}$ due to model errors and measurement noise is assumed to have zero mean, be serially uncorrelated, and be heteroskedastic, that is, having a diagonal covariance matrix.

4. Identification

This section presents the experimental setup, identification procedure, and results. The experiment is carried out using the setup shown in Figure 4. The system consists of the *UR5e* collaborative robot manipulator, Teach Pendant, Control Box, and PC. The estimation trajectory is generated using the Teach Pendant and is sent to the Control Box. The Control Box generates torque commands and sends them to the UR5e, and the measurements of actual values ($\mathbf{q}$, $\boldsymbol{\theta}$, and $\mathbf{i}$) are sent back from the UR5e to the Control Box. All the data are then logged by the PC.

The identification procedure is illustrated schematically in Figure 5.

Table 3: The 36 base parameters for the UR5e manipulator when mounted such that the rotation axis of the base joint is oriented parallel to the gravitational acceleration.

i	XX_i	XY_i	XZ_i	YZ_i	ZZ_i	mX_i	mY_i
1	–	–	–	–	ZZR_1	–	–
2	XXR_2	XY_2	XZR_2	YZ_2	ZZR_2	mXR_2	mY_2
3	XXR_3	XY_3	XZ_3	YZ_3	ZZR_3	mXR_3	mY_3
4	XXR_4	XY_4	XZ_4	YZ_4	ZZR_4	mX_4	mYR_4
5	XXR_5	XY_5	XZ_5	YZ_5	ZZR_5	mX_5	mYR_5
6	XXR_6	XY_6	XZ_6	YZ_6	ZZ_6	mX_6	mY_6

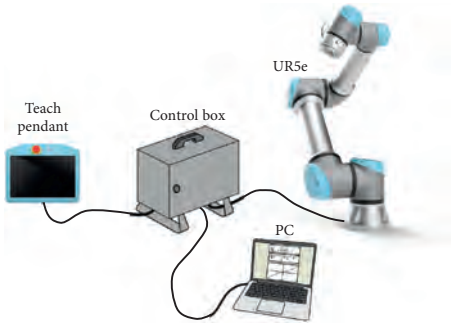

Figure 4: Experimental setup used for the dynamics identification.

Data is sampled at times $t(k) = kT_S, k = 1, 2, \ldots, M$, where $T_S = 1$ ms is the sampling period, and the sampling frequency $f_S = 1$ kHz.

4.1. Joint Position, Velocity, and Acceleration Estimation. The measured trajectory data $\mathbf{q}$ and $\boldsymbol{\theta}$ are filtered by a 4th-order Butterworth filter in both the forward and reverse directions to eliminate lag of the filtered trajectories $\widehat{\mathbf{q}}$ and $\widehat{\boldsymbol{\theta}}$. To keep the useful signal of the robot dynamics in the filter bandwidth, the cutoff frequency of the filter is chosen to be 5 times the frequency of the robot dynamics; that is, $5f_{\text{dyn}} = 50$ Hz. Angular velocities and accelerations $\dot{\widehat{\mathbf{q}}}$, $\ddot{\widehat{\mathbf{q}}}$, $\dot{\widehat{\boldsymbol{\theta}}}$, and $\ddot{\widehat{\boldsymbol{\theta}}}$, respectively, are obtained through a central difference procedure. The combination of the two-pass Butterworth filter and central difference is referred to as the band-pass filtering process.

4.2. Parallel Filtering and Downsampling. The sampling frequency is much higher than the frequencies of interest in the dynamics, so to reduce the required computational resources the data is parallel-filtered and then decimated/downsampled. Firstly, the samples $k = 1, \ldots, M$ are ordered in the measurement vector $\mathbf{y}_i$ and observation matrix $\mathbf{W}_i$ for each joint $i = 1, \ldots, N$ individually; that is,

$$\begin{aligned}\overline{y}_i &= \left[\tau_{J,i,1} \cdots \tau_{J,i,k} \cdots \tau_{J,i,M}\right]^T,\\ \overline{\mathbf{W}}_i &= \left[\mathbf{W}_{i,1}^T \cdots \mathbf{W}_{i,k}^T \cdots \mathbf{W}_{i,M}^T\right]^T,\\ \mathbf{W}_{i,k} &= \mathbf{Y}_{B,i}\left(\widehat{\mathbf{q}}_k, \dot{\widehat{\mathbf{q}}}_k, \ddot{\widehat{\mathbf{q}}}_k\right),\end{aligned} \tag{17}$$

with $\mathbf{Y}_{B,i}(\widehat{\mathbf{q}}_k, \dot{\widehat{\mathbf{q}}}_k, \ddot{\widehat{\mathbf{q}}}_k)$ being the i^{th} row of the regressor evaluated in the k^{th} sample of the filtered trajectory. The parallel filtering of the measurement vector and observation matrix for each joint is conducted by passing the signals through a 4th-order Butterworth filter in both the forward and reverse directions having a cut-off frequency of $2f_{\text{dyn}} = 20$ Hz. The downsampling factor is $0.8f_S/(4f_{\text{dyn}}) = 20$ [10]; that is, every 20th sample is used for parameter estimation. The filtering and downsampling of $\overline{\mathbf{y}}_i$ and $\overline{\mathbf{W}}_i$ produce estimates $\mathbf{y}_i$ and $\mathbf{W}_i$, respectively.

4.3. Torque Computation. The filtered and downsampled data are ordered joint-wise in the measurement vector and observation matrix as

$$\begin{aligned}\mathbf{y} &= \left[\mathbf{y}_1^T \cdots \mathbf{y}_i^T \cdots \mathbf{y}_N^T\right]^T \in \mathbb{R}^{N \cdot M},\\ \mathbf{W} &= \left[\mathbf{W}_1^T \cdots \mathbf{W}_i^T \cdots \mathbf{W}_N^T\right]^T \in \mathbb{R}^{N \cdot M \times b_m}.\end{aligned} \tag{18}$$

The base parameters are estimated by solving the WLS problem:

$$\begin{aligned}\widehat{\boldsymbol{\gamma}}_B &= \arg\min_{\boldsymbol{\gamma}_B} \left\|\mathbf{W}^T\mathbf{G}\left(\mathbf{y} - \mathbf{W}\boldsymbol{\gamma}_B\right)\right\|^2\\ &= \left(\mathbf{W}^T\mathbf{G}\mathbf{W}\right)^{-1}\mathbf{W}^T\mathbf{G}\mathbf{y},\end{aligned} \tag{19}$$

where each weight in $\mathbf{G}$ is equal to the reciprocal of the estimated standard deviation of the error.

$$\begin{aligned}&\mathbf{G} = \operatorname{diag}(\mathbf{S}),\\ &\mathbf{S} = [\mathbf{S}_1 \ \ldots \ \mathbf{S}_i \ \ldots \ \mathbf{S}_N],\\ &\mathbf{S}_i = \left[\frac{1}{\widehat{\sigma}_{i,1}} \cdots \frac{1}{\widehat{\sigma}_{i,j}} \cdots \frac{1}{\widehat{\sigma}_{i,b_{m,i}}}\right], \quad j = 1, \ldots, b_{m,i},\\ &\widehat{\sigma}_{i,j}^2 = \frac{\left\|\boldsymbol{\tau}_i - \mathbf{Y}_{B,i}\widehat{\boldsymbol{\gamma}}_{B,i}\right\|^2}{M - b_{m,i}},\end{aligned} \tag{20}$$

with $b_{m,i}$ being the number of base parameters related to link i. Such weighting operation normalizes the error terms in (13).

4.4. Trajectory. The trajectory used for parameter estimation should allow complete identification of the system; that is, for positive constants α and β, it should satisfy some persistently exciting condition:

$$\beta\mathbf{E} \geq \int_0^T \mathbf{W}^T\mathbf{W}\mathrm{d}t \geq \alpha\mathbf{E}, \tag{21}$$

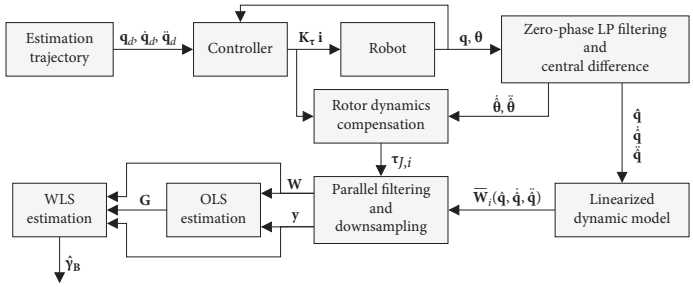

Figure 5: Schematic representation of the Inverse Dynamics Identification Model with Weighted Least Squares (IDIM-WLS) estimation and *rotor dynamics compensation* procedure. The estimation trajectory sends desired angular positions $\mathbf{q}_d, \dot{\mathbf{q}}_d, \ddot{\mathbf{q}}_d$ to the *controller*, which generates torque commands $\mathbf{K}_\tau \mathbf{i}$ to the robot. The angular positions of the links and rotors, $\mathbf{q}$ and $\boldsymbol{\theta}$, respectively, are measured and then filtered to generate smoothed estimates $\hat{\mathbf{q}}$ and time-derivatives $\dot{\hat{\mathbf{q}}}$, $\ddot{\hat{\mathbf{q}}}$, $\dot{\hat{\boldsymbol{\theta}}}$, and $\ddot{\hat{\boldsymbol{\theta}}}$. The rotor quantities are passed to the *Rotor dynamics compensation*, and the link quantities are passed to the *Linearized dynamic model*. The *Rotor dynamics compensation* augments the measured current with the rotor dynamics based on (15) to estimate joint torques $\boldsymbol{\tau}_J$. The *Linearized dynamic model* generates regressors $\overline{\mathbf{W}}_i$ for each joint i. The joint torque estimates and regressors are filtered and downsampled to generate, respectively, the measurement vector $\mathbf{y}$ and observation matrix $\mathbf{W}$. The measurement vector and observation matrix are passed to the *OLS Estimation* and *WLS estimation* procedures. The OLS procedure produces the weighting matrix $\mathbf{G}$ used in the WLS procedure. Finally, the *WLS estimation* provides the dynamic parameters estimates $\hat{\boldsymbol{\gamma}}_B$.

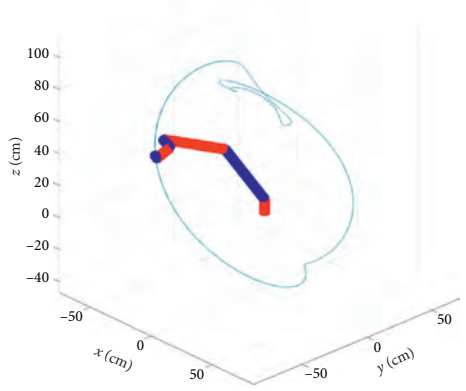

Figure 6: Trajectory used for the parameter estimation yielding a low condition number of the regressor matrix $\text{cond}(\mathbf{W}) = 66$.

where α is the degree of excitation and β/α is the condition number of $\mathbf{W}^T\mathbf{W}$. The trajectory in Figure 6 is used for yielding a condition number for the regressor $\text{cond}(\mathbf{W}) = 66$. The trajectory is 31 seconds long; hence, with a sampling frequency of 1000 Hz and a downsampling factor of 20, the total number of samples is 1550. Another approach to the trajectory design is to optimize the condition number of the regressor with respect to the trajectory subject to kinematic and dynamic constraints, for example, position, velocity, acceleration, and current.

4.5. Model Quality Metric. The model quality is evaluated by the sum of each joint's mean squared error normalized by its average torque magnitude; that is,

$$\text{NMSE} = \sum_{j=1}^{N} \sum_{k=1}^{M} \frac{\left(\tau_{J,i,k} - \hat{\tau}_{J,i,k}\right)^2}{\left|\tau_{J,i,k}\right|}. \tag{22}$$

4.6. Results. Values of the identified base parameters are shown in Table 4. The effectiveness of the method is demonstrated by considering the accuracy of the dynamic model with the optimized parameters compared to our baseline, a model with parameters obtained through CAD software. The model accuracy improves 81.4% from a NMSE of 506.8 Nm to that of 94.5 Nm.

The parameters are generally well estimated with small relative standard deviations, which demonstrates the

Table 4: Estimated values and relative standard deviation of the 36 base parameters obtained by solving the WLS problem with rotor dynamics compensation.

Base param.	Value	$\%\sigma_{\widehat{\gamma_B}}$
ZZR_1	2.1981	0.099
XXR_2	−1.6552	0.130
XY_2	−0.0405	1.975
XZR_2	0.3734	0.210
YZ_2	0.1278	1.367
ZZR_2	−4.1774	0.198
mXR_2	−0.0132	0.001
mY_2	−0.7336	0.141
XXR_3	−0.1563	0.166
XY_3	0.1302	0.225
XZ_3	−0.1714	0.249
YZ_3	0.0212	0.433
ZZR_3	−1.8774	2.908
mXR_3	0.0428	0.001
mY_3	−0.0428	0.030
XXR_4	−0.0454	0.609
XY_4	0.0144	0.422
XZ_4	0.0166	0.767
YZ_4	0.0005	18.894
ZZR_4	−0.0005	20.082
mX_4	−0.0112	0.043
mYR_4	−0.1866	0.001
XXR_5	0.0239	0.450
XY_5	−0.0391	0.055
XZ_5	0.0194	0.080
YZ_5	0.0065	0.286
ZZR_5	0.0315	0.076
mX_5	−0.0013	0.137
mYR_5	0.0442	0.005
XXR_6	0.0187	0.132
XY_6	0.0059	0.107
XZ_6	0.0187	0.054
YZ_6	−0.0002	3.825
ZZ_6	0.0209	0.157
mX_6	0.0036	0.040
mY_6	−0.0043	0.041

effectiveness of the identification procedure. The values of parameters YZ_4 and ZZR_4 are, however, subject to relative standard deviations of 19% and 20%, respectively. This is an indication of either (1) suboptimality of the chosen trajectory or (2) the parameter being of no big value to the torque computation. YZ_4 is a product moment of inertia (off-diagonal element in the inertia tensor) and is therefore likely to be less important in the dynamics. ZZR_4 is a mass moment of inertia (diagonal element in the inertia tensor) and the reduced accuracy in its estimation is likely due to insufficient excitation by the chosen trajectory.

5. Validation

The purpose of the dynamic model calibration is to improve the torque estimation accuracy for arbitrary trajectories. Thus, we evaluate the accuracy of our calibrated model on three trajectories different from the one used for parameter estimation. The measured joint torques are compared to the torques output by the calibrated dynamic model as well as relative to our CAD model baseline. Improvements in NMSE and improvements relative to our baseline are shown in Table 5. The results show a relative improvement of the calibrated dynamic model compared to the dynamic model

Table 5: Normalized Mean Squared Error (NMSE) of the dynamic models; CAD model with parameters obtained from a CAD model of the robot and calibrated with parameters estimated through the WLS procedure with rotor dynamics compensation. Improvements in NMSE and relative to CAD model for three different trajectories.

Traj.	NMSE CAD model	NMSE calibrated	Relative improvement (%)
1	325.9	233.0	28.5
2	1245.7	1040.4	16.5
3	334.0	250.9	24.9

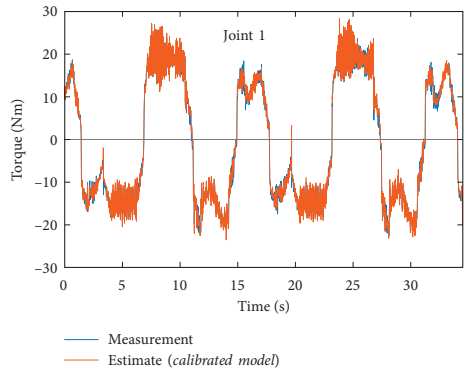

Figure 7: Results of measurement and estimate using the calibrated parameters on the validation trajectory.

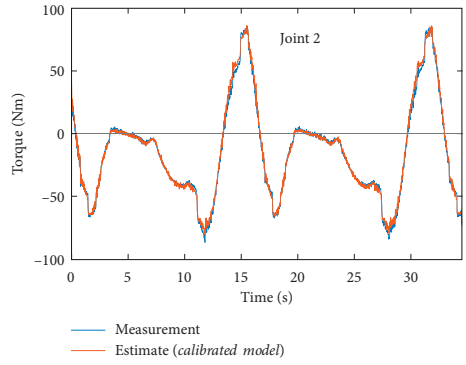

Figure 8: Results of measurement and estimate for joint no. 2 with the calibrated parameters.

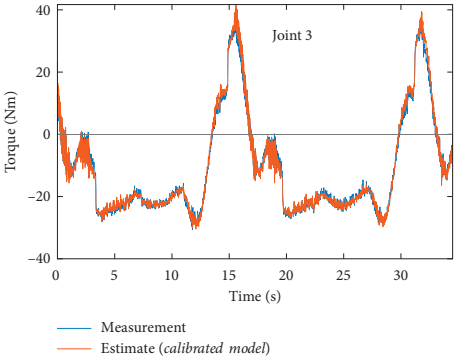

Figure 9: Results of measurement and estimate for joint no. 3 with the calibrated parameters.

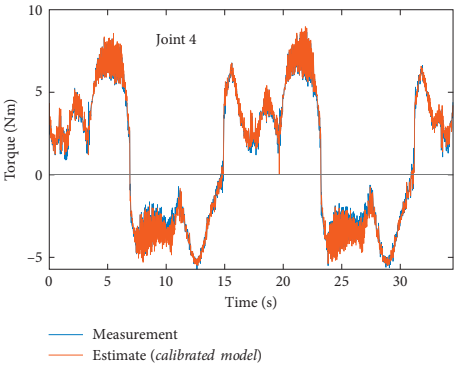

Figure 10: Results of measurement and estimate for joint no. 4 with the calibrated parameters.

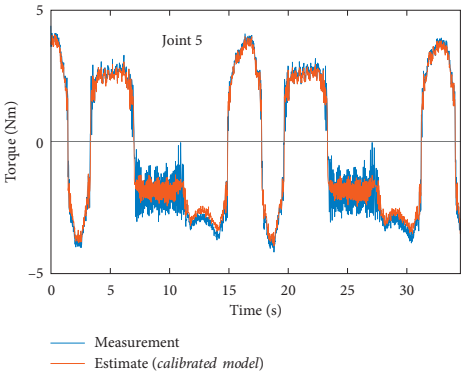

Figure 11: Results of measurement and estimate for joint no. 5 with the calibrated parameters.

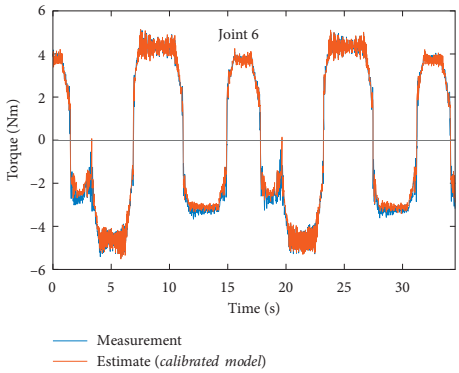

Figure 12: Results of measurement and estimate for joint no. 6 with the calibrated parameters.

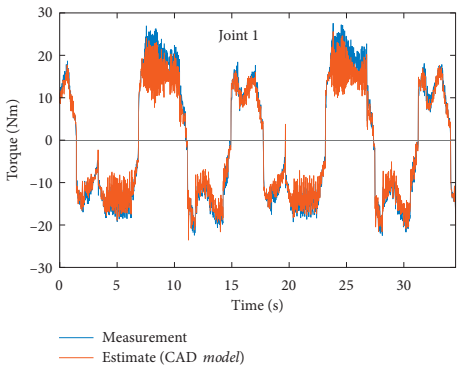

Figure 13: Results of measurement and estimate for joint no. 1 with the CAD model parameters.

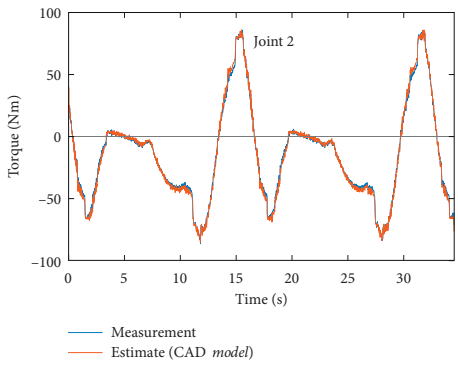

Figure 14: Results of measurement and estimate for joint no. 2 with the CAD model parameters.

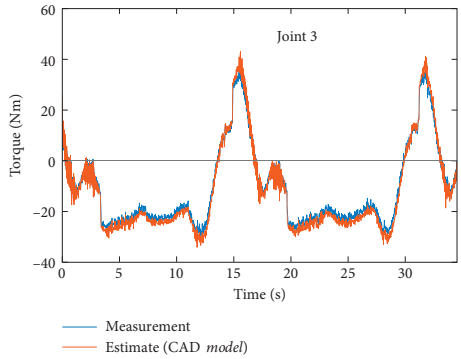

Figure 15: Results of measurement and estimate for joint no. 3 with the CAD model parameters.

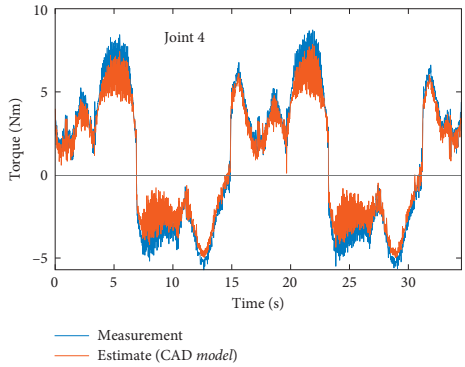

Figure 16: Results of measurement and estimate for joint no. 4 with the CAD model parameters.

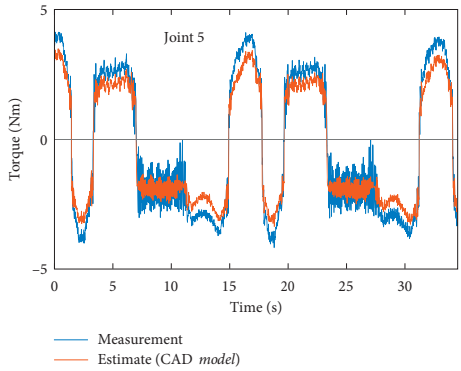

Figure 17: Results of measurement and estimate for joint no. 5 with the CAD model parameters.

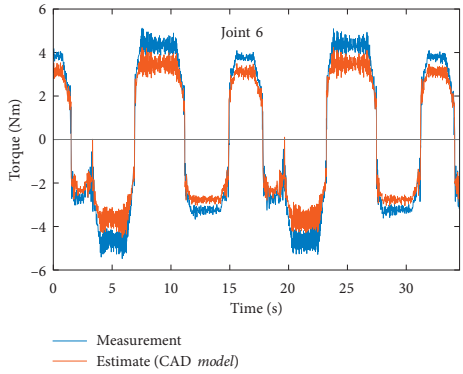

Figure 18: Results of measurement and estimate for joint no. 6 with the CAD model parameters.

with CAD parameters of 16.5%–28.5% depending on the trajectory. Time-series torque data for each of the joints of the UR5e dynamic model with calibrated parameters are shown in Figures 7–12 for trajectory no. 1. Time-series torque data for each of the joints of the *UR5e* dynamic model with CAD model parameters are shown in Figures 13–18 for trajectory no. 1. The reduction in torque prediction error (NMSE) of 16.5%–28.5% of the calibrated dynamic model compared to the dynamic model with CAD model parameters together with the time-series torque data in Figures 7–18 validates the effectiveness of the calibration procedure.

6. Conclusion

Collaborative industrial robots often utilize strain-wave type transmissions due to their desirable characteristics of high torque capacity and low weight. However, their inherent complex nonlinear behavior introduces significant errors and uncertainties in the robot dynamics calibration, resulting in decreased performance for motion and force control tasks and lead-through programming applications.

This paper presented a new method for the dynamics parametrization and calibration of collaborative industrial robot manipulators. The method combines the IDIM-WLS method for rigid robot dynamics with complex nonlinear expressions for the rotor-side dynamics to obtain increased calibration accuracy. Two angular position measurements per robot joint are utilized, one at each side of the strain-wave transmission, to effectively compensate the rotor inertial torques and nonlinear dynamic friction that were identified in our previous works.

The effectiveness of the method was demonstrated by the application to the Universal Robots UR5e collaborative robot manipulator. The results were very accurate estimates of the dynamic parameters. Relative improvement of 16.5% to 28.5% compared to a CAD model baseline was experienced.

The distinguished contributions of this work can be summarized as follows: (1) a linear parametrization describing the dynamics of the UR5e collaborative robot manipulator has been developed, (2) the complex nonlinear dynamic friction characteristics and rotor inertia have been considered, (3) the minimal set of base parameters that describe the dynamic behavior of the UR5e robot has been accurately estimated, and (4) the performance of the calibrated dynamic model has been validated.

Our ongoing work that we are going to challenge consists of the following:

(1) The number of identifiable parameters can be increased by two (from 36 to 38) if the robot is mounted with the base joint axis of rotation not being parallel to the direction of the gravitational acceleration.

(2) The trajectory used for parameter optimization could possibly be optimized through the use of some optimization procedures. Such trajectory optimization procedures were discussed generally in [25] and applied in [26] on a KUKA 361 IR industrial robot.

(3) The optimization problem could be constrained to enforce the positive-definiteness of the inertia matrix using either Sylvester's theorem or Cholesky decomposition. This will ensure invertibility of the inertia matrix, which is useful for model-based control design. From Sylvester's theorem, it is possible to find conditions for the parameters [27], whereas, for Cholesky decomposition, a tolerance is defined and it takes the noise and measurement error into account [28].

Data Availability

Data are not available due to confidentiality and third-party rights.

Conflicts of Interest

The authors declare that they have no conflicts of interest reported in this paper.

Acknowledgments

This work was supported by the company Universal Robots A/S, Odense, Denmark, and Innovation Fund Denmark (Ref. no. 7038-00058B).

References

[1] C. Gaz and A. D. Luca, "Payload estimation based on identified coefficients of robot dynamics — with an application to collision detection," in *Proceedings of the 2017 IEEE/RSJ International Conference on Intelligent Robots and Systems (IROS)*, pp. 3033–3040, IEEE, Vancouver, Canada, September 2017.

[2] K. Kozlowski, *Modelling and Identification in Robotics*, Springer, London, UK, 1998.

[3] P. Poignet and M. Gautier, "Comparison of weighted least squares and extended Kalman filtering methods for dynamic identification of robots," in *Proceedings of the 2000 ICRA, IEEE International Conference on Robotics and Automation. Symposia Proceedings (Cat. No.00CH37065)*, April 2000.

[4] M. Gautier and P. Poignet, "Extended Kalman filtering and weighted least squares dynamic identification of robot," *Control Engineering Practice*, vol. 9, no. 12, pp. 1361–1372, 2001.

[5] G. Calafiore and M. Indri, "Robust calibration and control of robotic manipulators," in *Proceedings of the 2000 American Control Conference. ACC (IEEE Cat. No.00CH36334)*, June 2000.

[6] M. M. Olsen, J. Swevers, and W. Verdonck, "Maximum likelihood identification of a dynamic robot model: implementation issues," *The International Journal of Robotics Research*, vol. 21, no. 2, pp. 89–96, 2002.

[7] N. Ramdani and P. Poignet, "Robust dynamic experimental identification of robots with set membership uncertainty," *IEEE/ASME Transactions on Mechatronics*, vol. 10, no. 2, pp. 253–256, 2005.

[8] A. Janot, P. O. Vandanjon, and M. Gautier, "Using robust regressions and residual analysis to verify the reliability of LS estimation: application in robotics," in *Proceedings of the 2009 IEEE/RSJ International Conference on Intelligent Robots and Systems*, October 2009.

[9] A. Janot, P. O. Vandanjon, and M. Gautier, "Identification of 6 DOF rigid industrial robots with the instrumental variable method," *IFAC Proceedings*, vol. 45, no. 16, pp. 1659–1664, 2012.

[10] A. Janot, P.-O. Vandanjon, and M. Gautier, "A generic instrumental variable approach for industrial robot identification," *IEEE Transactions on Control Systems Technology*, vol. 22, no. 1, pp. 132–145, 2014.

[11] M. Gautier, A. Janot, and P.-O. Vandanjon, "A new closed-loop output error method for parameter identification of robot dynamics," *IEEE Transactions on Control Systems Technology*, vol. 21, no. 2, pp. 428–444, 2013.

[12] A. Janot, M. Gautier, A. Jubien, and P. O. Vandanjon, "Comparison between the CLOE method and the DIDIM method for robots identification," *IEEE Transactions on Control Systems Technology*, vol. 22, no. 5, pp. 1935–1941, 2014.

[13] K. K. Kumbla and M. Jamshidi, "Neural network based identification of robot dynamics used for neuro-fuzzy controller," in *Proceedings of the International Conference on Robotics and Automation*, April 1997.

[14] S. A. Kolyubin, A. S. Shiriaev, and A. Jubien, "Refining dynamics identification for Co-bots: case study on KUKA LWR4+ ∗ ∗this work was supported by the government of the Russian federation, GOSZADANIE no. 8.8885.2017/BP and grant 074-U01," *IFAC-PapersOnLine*, vol. 50, no. 1, pp. 14626–14631, 2017.

[15] Z. Shareef, P. Mohammadi, and J. Steil, "Improving the inverse dynamics model of the KUKA LWR IV+ using independent joint learning∗ ∗Z. Shareef received funding from the German federal ministry of education and research (BMBF) within the leading-edge cluster competition. P. Mohammadi received funding from the European community's horizon 2020 robotics program ICT-23-2014 under grant agreement 644727 - CogIMon," *IFAC-PapersOnLine*, vol. 49, no. 21, pp. 507–512, 2016.

[16] C. Gaz, M. Cognetti, A. Oliva, P. Robuffo Giordano, and A. De Luca, "Dynamic identification of the Franka Emika Panda robot with retrieval of feasible parameters using penalty-based optimization," *IEEE Robotics and Automation Letters*, vol. 4, no. 4, pp. 4147–4154, 2019.

[17] M. Taghbalout, J. F. Antoine, and G. Abba, "Experimental dynamic identification of a YuMi collaborative robot," *IFAC-PapersOnLine*, vol. 52, no. 13, pp. 1168–1173, 2019.

[18] E. Madsen, O. S. Rosenlund, D. Brandt, and X. Zhang, "Model-based on-line estimation of time-varying nonlinear joint stiffness on an e-series universal robots manipulator," in *Proceedings of the 2019 International Conference on Robotics and Automation (ICRA)*, May 2019.

[19] E. Madsen, O. S. Rosenlund, D. Brandt, and X. Zhang, "Comprehensive modeling and identification of nonlinear joint dynamics for collaborative industrial robot manipulators," *Control Engineering Practice*, vol. 101.

[20] M. W. Spong, "Modeling and control of elastic joint robots," *Journal of Dynamic Systems, Measurement, and Control*, vol. 109, no. 4, pp. 310–318, 1987.

[21] P. P. Restrepo and M. Gautier, "Calibration of drive chain of robot joints," in *Proceedings of the International Conference on Control Applications*, September 1995.

[22] J. J. Craig, *Introduction to Robotics*, Pearson Education Limited, London, UK, 2013.

[23] M. Gautier and W. Khalil, "Direct calculation of minimum set of inertial parameters of serial robots," *IEEE Transactions on Robotics and Automation*, vol. 6, no. 3, pp. 368–373, 1990.

[24] M. Gautier and W. Khalil, "A direct determination of minimum inertial parameters of robots," in *Proceedings of the 1988 IEEE International Conference on Robotics and Automation*, pp. 1682–1687, Philadelphia, PA, USA, 1988.

[25] B. Armstrong, "On finding 'exciting' trajectories for identification experiments involving systems with non-linear dynamics," in *Proceedings of the 1987 IEEE International Conference on Robotics and Automation*, March-April 1987.

[26] J. Swevers, C. Ganseman, D. B. Tukel, J. de Schutter, and H. Van Brussel, "Optimal robot excitation and identification,"

IEEE Transactions on Robotics and Automation, vol. 13, no. 5, pp. 730–740, 1997.

[27] K. Yoshida and W. Khalil, "Verification of the positive definiteness of the inertial matrix of manipulators using base inertial parameters," *The International Journal of Robotics Research*, vol. 19, no. 5, pp. 498–510, 2000.

[28] M. Gautier and G. Venture, "Identification of standard dynamic parameters of robots with positive definite inertia matrix," in *Proceedings of the 2013 IEEE/RSJ International Conference on Intelligent Robots and Systems*, November 2013.

Chapter 6

Adaptive Feedforward Control [Journal Paper 3]

Adaptive Feedforward Control for a Collaborative Industrial Robot Manipulator Using a Novel Extension of the Generalized Maxwell-Slip Friction Model [169]

6.1 Introduction

The complex nonlinear behavior of strain-wave transmissions motivates the use of dynamic friction models. In particular, the GMS friction model [74, 75] has been successfully applied to describe the characteristics of strain-wave transmissions [76, 77]. The Coulomb friction torque is known to depend on the load torque. However, existing strategies which seek to describe this dependency are discontinuous at zero velocity [170, 69, 29]. As such, they do not accurately describe the real load torque dependent friction phenomena. Furthermore, the friction changes with the lubricant temperature and the wear and tear of the robot joint – both of which are difficult to estimate accurately. The temperature affects the viscous friction [28] and the wear and tear affects the Coulomb friction [171]. The above-mentioned challenges motivates the development of a *new torque-dependent dynamic friction model* and *adaptive friction compensation*.

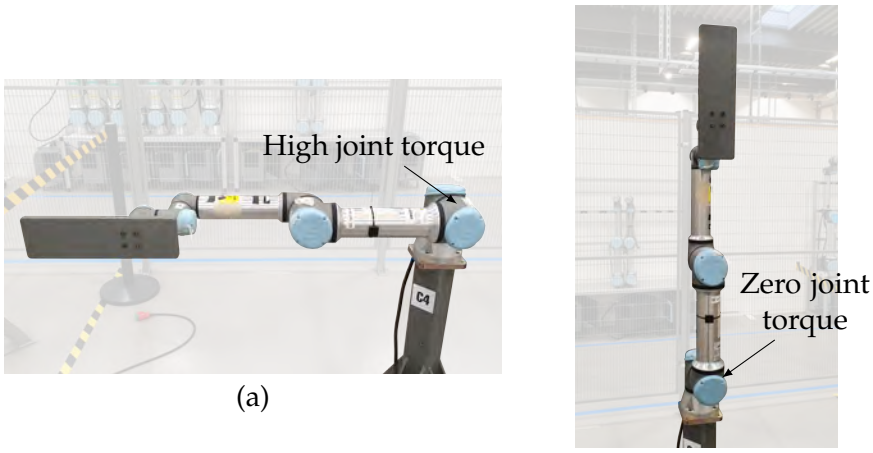

(a) (b)

FIGURE 6.1: Robot manipulator configurations resulting in high (a) and zero (b) torque of the second joint.

6.2 Method

First, an extension to the GMS (E-GMS) is proposed to handle in a combined framework; 1) torque dependent friction characteristics and 2) hysteresis characteristics that depend on the angular position. The E-GMS combines a unit hysteresis model with a function that describes the Coulomb friction in terms of the load torque. Thus, the discontinuity at zero-velocity of existing strategies is overcome. We prove that the E-GMS model, as desired, provides a steady-state output equal to that of the GMS model. The map from load torque to Coulomb friction torque is generated by conducting a robot joint motion with several velocity reversals in different configurations that explore different values of load torque, see Fig. 6.1.

Then, an E-GMS based adaptive feedforward control strategy is proposed to compensate the effects of wear and tear of the robot joint as well as inaccurate temperature compensation. The Coulomb friction and excess viscous friction is estimated using a gradient-type adaptive law with a quadratic cost function. Robustness is addressed by parameter projection and a conditional statement to ensure the regressor be persistently exciting. The stability of the method is proven in the sense of Bounded-Input, Bounded-Output (BIBO).

6.3 Findings

For the experimental validation the E-GMS model is compared to the existing strategy of compensating load-torque dependent friction. A trajectory is designed which includes velocity reversals with the gravity torque varying from zero to a large torque (>150 Nm). It is found that the torque prediction performance is improved by a factor 2.1 and the tracking error is improved by a factor 1.5.

The adaptive feedforward controller is proven stable in the sense of Bounded-Input, Bounded-Output (BIBO). Experimental validation is conducted by comparing the adaptive controller to a non-adaptive controller with parameters that are known to be off but are close enough to not cause the safety system to protectively stop the robot. The validation trajectory consist of the waypoints illustrated in Fig. 6.2. The results show the torque prediction to be improved by 84 % and the tracking control is improved by 20 %.

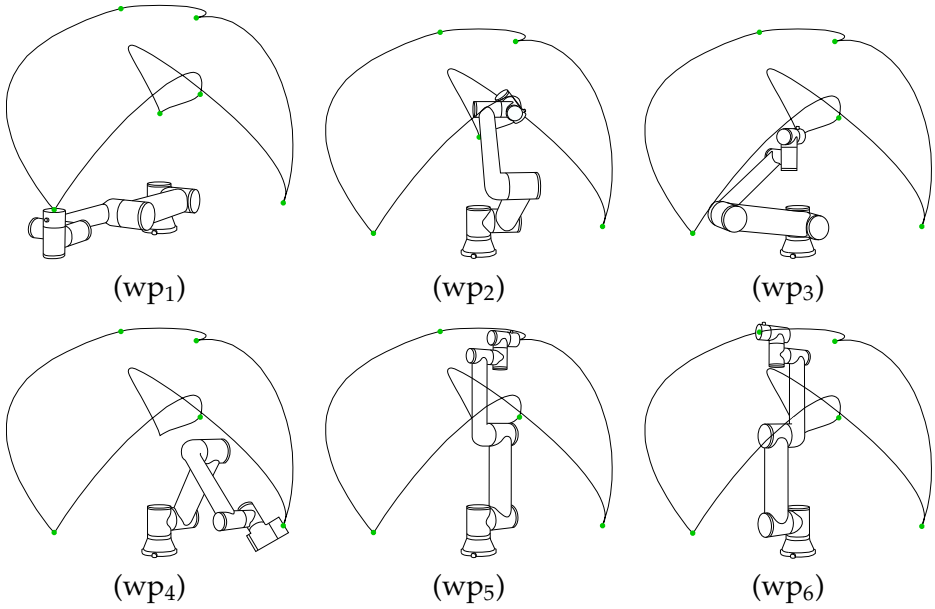

FIGURE 6.2: Waypoints used in the validation of the adaptive feedforward control. A 7.5 kg payload was attached at the end-effector.

6.4 Reflection

The results validate the principle of the E-GMS model and its implementation in UR robots. With the improvements in torque prediction and tracking control of 84 % and 20 %, respectively, the method seems effective for industrial robot manipulators with strain-wave transmissions.

The E-GMS based adaptive feedforward controller provides a method for compensating the effects of wear and inaccurate temperature estimation. The improvements in torque prediction and tracking control (84 % and 20 %, respectively) underlines its effectiveness.

In addition to tracking control, the method has perspectives in terms of safety and lead through programming. In terms of safety, the adaptation can modify the mathematical model used by the robot to compute the torque reference of the safety system. Thus, the adaptive controller must be certified similarly to other safety features of UR robots, i.e. according to applicable standards ISO 13849 and ISO 10218 [3–6]. Generally, it is not a problem certifying adaptive controllers [172].

6.5 Author's Contribution

The author proposed the method, implemented the method in the existing UR robot controller with assistance from UR employees Martin Trædholm and Anders S. Knudsen, performed experiments, and prepared the manuscript with inputs from the co-authors.

Mechanism and Machine Theory 155 (2021) 104109

Contents lists available at ScienceDirect

Mechanism and Machine Theory

journal homepage: www.elsevier.com/locate/mechmachtheory

Research paper

Adaptive feedforward control of a collaborative industrial robot manipulator using a novel extension of the Generalized Maxwell-Slip friction model☆

Emil Madsen[a,b,*], Oluf Skov Rosenlund[a], David Brandt[a], Xuping Zhang[b,**]

[a] Universal Robots A/S, Energivej 25, 5260 Odense S, Denmark
[b] Aarhus University, Inge Lehmanns Gade 10, 8000 Aarhus C, Denmark

ARTICLE INFO

Article history:
Received 24 May 2020
Revised 16 September 2020
Accepted 17 September 2020

Keywords:
Robotics
Adaptive feedforward control
Dynamic friction model
Generalized Maxwell-Slip

ABSTRACT

Collaborative industrial robots often use strain-wave transmissions which display a highly nonlinear behavior. In particular, the friction torque depend on the load torque and the hysteresis characteristics were recently found to depend on the joint angular position.
This paper presents a novel extension of the Generalized Maxwell-Slip friction model to describe said phenomena in a combined framework. The method overcomes the discontinuity around zero velocity of existing models. Experiments on the Universal Robots UR5e manipulator show superior performance in terms of torque prediction accuracy and tracking performance of the proposed method.
An adaptive feedforward friction compensator is proposed based on the extended Generalized Maxwell-Slip friction model to compensate the time-variations of the Coulomb and viscous friction due to, respectively, wear and mispredictions of the lubricant temperature. The adaptive estimator relies on the sensing hardware readily available in the joints of the Universal Robots manipulators, i.e. two absolute rotary encoders; one at each side of the transmission, current sensing for the electric actuator, and a temperature sensor. Results show a considerable reduction of the torque prediction error and tracking error.

1. Introduction

For industrial robot manipulators, and in particular collaborative robots, the ability to accurately predict the actuator torques required to realize the desired task is highly important. An increased accuracy of torque predictions generally lead to improved robot performance, specifically enhanced accuracy in motion and force control tasks [1,2], smoother lead-through programming[1] experience [3,4], and increased performance of robot safety systems [5–7]. Additional benefits include lower energy consumption and the possibility to use hardware of reduced cost, e.g. less accurate sensors.

Collaborative robots most often utilize strain-wave type transmissions such as the Harmonic Drive™ [8] due to their desirable characteristics of high torque capacity and low weight. However, their inherent complex nonlinear friction and hysteresis characteristics complicates the accurate mathematical modeling and thus leads to decreased robot performance if not modeled and properly compensated.

☆ This work was supported by Innovation Fund Denmark [Ref. no. 7038-00058B] and the company *Universal Robots A/S*, located in Odense, Denmark.
* Corresponding author at: Aarhus University, Inge Lehmanns Gade 10, 8000 Aarhus C, Denmark.
** Co-corresponding author.
E-mail addresses: ema@eng.au.dk (E. Madsen), xuzh@eng.au.dk (X. Zhang).
[1] A robot programming concept where the user takes the robot by the hand and guides it – also known as *programming by demonstration* or *kinesthetic teaching*.

https://doi.org/10.1016/j.mechmachtheory.2020.104109
0094-114X/

In addition to the challenge of accurate joint dynamics modeling exists another challenge in which the changes in ambient temperature and the wear and tear of the robot joints cause time-variation of the friction characteristics and thus introduce errors and uncertainties to the mathematical models, which leads to decreased robot performance if uncompensated. The temperature affects the viscous friction [9] while the wear and tear affects the Coulomb friction [10].

The above-mentioned challenges of accurate joint dynamics modeling and time-varying friction characteristics motivates the use of: 1) *Dynamic friction compensation* to compensate the complex nonlinear dynamics of the strain-wave transmissions, and 2) *adaptive control* to continuously learn from the inaccuracies of the mathematical models and adapt the models to better represent the real robotic system. Such compensation is typically introduced in the feedforward part of the control structure [11], i.e. eliminating the frictional effects by *adaptive feedforward dynamic friction compensation*.

Friction is by nature a complex fluid dynamic phenomenon. To accurately describe the frictional behavior at near-zero velocities, dynamic friction models are required. While the LuGre model [12] have attained much interest in the general robotics community, the Generalized Maxwell-Slip (GMS) model [13,14] have proven especially useful for modeling the friction and hysteresis characteristics of strain-wave transmissions [15,16] due to its ability to describe the rate-independent hysteresis phenomenon. Among others, the GMS model has proven successful for describing the dynamic friction characteristics of the Universal Robots manipulators, see [17,18].

Several studies have been conducted to characterize the dynamics of strain-wave transmissions. The steady-state friction characteristics of a strain-wave transmission is known to depend on the angular velocity, temperature, and load torque. However, existing dynamic friction models with load torque dependency does not solve the discontinuity around zero-velocity. Also, in Dong et al. [19] the effects of wave generator radial offset was investigated theoretically and the consequent effects were uneven distributions of the backlash and flexspline preload over the angular position. In [18] the magnitude of the backlash was indeed observed to depend on the angular position of the Universal Robots UR5e manipulator.

Some works presented adaptive friction compensation based on the GMS friction model. Nilkhamhang and Sano [20,21] developed a switching adaptive controller based on the GMS model with linearized Stribeck friction function. Stability was ensured by parameter projection and numerical simulations demonstrated parameter convergence. However the choice of switching function is not suited for implementation in real systems as noted by Grami and Bigras [22]. Grami and Bigras identified the GMS friction model using the robust adaptive observer developed by [23]. The observer was verified by numerical simulation of a single-operator GMS model. In [24] their method was further improved by filtering the regressor to respect the requirement of Lipschitz continuity. However, the issue of the ideal switch was not solved. In [25,26] a recursive least squares estimator with exponential forgetting was proposed to adapt the DNLRX[2] model – a GMS friction model combined with FIR filters for the state vector and input position. Experimental results on an *XY* positioning stage showed great performance for the adaptive DNLRX model compared to a standard PID controller. To further enhance the tracking performance of GMS based feedforward control systems, Jamaludin et al. [27] designed an inverse model-based disturbance observer. Such strategy is indeed effective for increasing the tracking control performance. However, since the robot does not learn from the time-varying friction characteristics and on-line update the friction model, the disturbance observer strategy does not improve the robot performance in terms of safety. Other observers relevant for state estimation includes high-gain observers [28], sliding-mode observers

The aforementioned studies does not solve all challenges related to accurate actuator torque prediction for collaborative industrial robot manipulators. The immediate negative consequences are related to the robot safety, motion and force control performance, and lead-through programming experience.

In this paper, we present an extension to the GMS friction model to handle in a combined framework the load torque dependent Coulomb friction and the dependency of backlash on the joint angular position. We prove that the steady-state response of the extended GMS model is equivalent to that of the original GMS model. The nonlinear viscous friction is considered to depend on angular velocity and temperature. Additionally, a new gradient-based adaptive control strategy is proposed based on the extended GMS friction model to address the time variation of the friction characteristics. The extended GMS model and adaptive feedforward compensator are validated on the Universal Robots UR5e collaborative robot manipulator.

The organization of this paper is as follows: Section 2 presents the adaptive feedforward dynamic friction compensation strategy. Next, the mathematical model of the robot manipulator is presented in Section 3, and in Section 4 the mathematical model of the robot joint dynamics is detailed. Section 5 presents the Extended GMS friction model which is allowed to depend on the joint torque and backlash. The friction model is validated on the Universal Robots UR5e robot manipulator. In Section 6 the adaptive estimator is presented, and its effectiveness is demonstrated on the UR5e robot. Section 7 concludes on the work and presents our ideas for future research.

1.1. Notations

Let $\mathbb{R}$ be the set of real numbers, $\mathbb{Z}$ the set of integers, and $\mathbb{N}$ the set of non-negative integers, denote then $\mathbb{R}_+ = \{x \in \mathbb{R} : x \geq 0\}$ and $\mathbb{N}_+ = \{x \in \mathbb{N} : x > 0\}$; $|\cdot|$ denotes the absolute value and $||\cdot||$ is the 2-norm; $\mathbf{x} \in \mathbb{R}^n$ is a vector of n real numbers, x_i is the ith entry of $\mathbf{x}$, $\mathbf{x}^T$ its transpose, $\bar{\mathbf{x}}$ the mean value the elements of $\mathbf{x}$, let then $\hat{\mathbf{x}}$ be an estimate of $\mathbf{x}$ and define the

[2] Dynamic NonLinear Regression with direct application of eXitation.

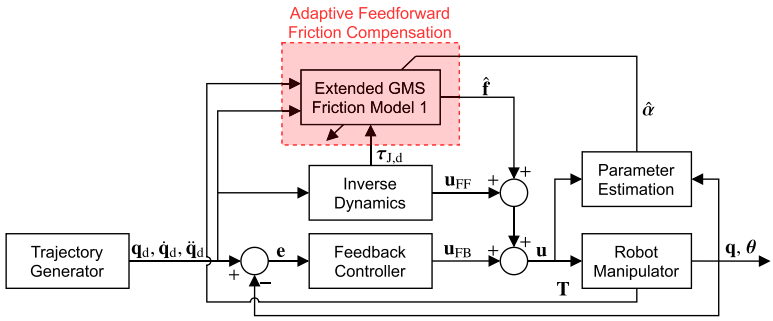

Fig. 1. Model-based control structure with adaptive feedforward dynamic friction compensation.

error vector $\tilde{\mathbf{x}} \triangleq \mathbf{x} - \hat{\mathbf{x}}$; given a square real matrix $\mathbf{A} \in \mathbb{R}^{n\times n}$ let $\mathbf{A} \succ 0$ indicate that $\mathbf{A}$ is positive definite, i.e. $\mathbf{x}^T\mathbf{A}\mathbf{x} > 0$ for any non-zero column vector $\mathbf{x}$ of n real numbers; let diag : $\mathbb{R}^n \to \mathbb{R}^{n\times n}$ map a vector of n elements to a diagonal matrix with the ith element of the vector on its ith diagonal entry and zero everywhere else.

2. Adaptive feedforward control

The friction characteristics cannot be predicted accurately by time-invariant models, hence an adaptive controller is designed and implemented to maintain and improve the accurate torque prediction capabilities during the lifetime of the robot while subject to time-varying friction characteristics due to the wear and tear of the robot joint as well as temperature mispredictions. This section outlines our proposed strategy for adaptive feedforward dynamic friction compensation.

The control strategy is illustrated schematically in Fig. 1. It includes static and adaptive feedforward and PID feedback control with feedback gains scaled by the inertia matrix, i.e. the combined feedforward and feedback control strategy constitute the well-known Computed-Torque Controller (CTC). The *adaptive feedforward friction compensation* is realized by the implementation of two identical Extended GMS friction models. While *Extended GMS Friction Model 1* operates as a feedforward inverse model, the *Parameter Estimation* works in parallel to the *Robot Manipulator* and comprises an identical friction model to calculate the model errors. The model errors are used to drive the adaptation of the linear model parameters by a gradient-based adaptive law.

3. Flexible-joint robot manipulator model

The articulated Flexible-Joint Robot (FJR) manipulator is considered as an open kinematic chain having $N+1$ rigid bodies; the base and the N links, interconnected by N revolute joints undergoing angular deformation due to joint flexibility around the axes of rotation, each joint being actuated by an electric actuator. The manipulator configuration (Fig. 2) is characterized by the generalized coordinates $(\mathbf{q}\ \boldsymbol{\theta}) \in \mathbb{R}^{2N}$ being, respectively, the angular position of the links and rotors (reflected through the gear ratio). From the standard assumptions proposed by Spong [29], the dynamics are

$$\vec{M}(\vec{q})\,\ddot{\vec{q}} + \vec{C}(\vec{q},\dot{\vec{q}})\,\dot{\vec{q}} + \vec{g}(\vec{q}) = \boldsymbol{\tau}_{\mathrm{J}} \tag{1}$$

$$\vec{B}\ddot{\boldsymbol{\theta}} + \vec{f} + \boldsymbol{\tau}_{\mathrm{J}} = \vec{K}_\tau\,\vec{i} \tag{2}$$

where in the link equation, $\mathbf{M}(\mathbf{q}) \succ 0 \in \mathbb{R}^{N\times N}$ is the symmetric inertia matrix, $\mathbf{C}(\mathbf{q},\dot{\mathbf{q}}) \in \mathbb{R}^{N\times N}$ is the matrix of Coriolis and centripetal terms, $\mathbf{g}(\mathbf{q}) \in \mathbb{R}^N$ is the vector of gravity torques, and $\boldsymbol{\tau}_{\mathrm{J}} \in \mathbb{R}^N$ is the vector of joint torques, which couple the link

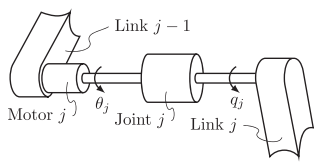

Fig. 2. Kinematic arrangement of motors and links for the Flexible-Joint Robot (FJR) manipulator model. The rotor angular position θ_j is already scaled by the reduction ratio.

and rotor subsystems. Some references refer to this torque as the *load torque* experienced by the motor. The joint torques $\boldsymbol{\tau}_\mathrm{J}$ can be expressed in terms of the joint deformation $\boldsymbol{\theta} - \mathbf{q}$ if the joint flexibility properties are known. Such flexible properties are needed for the inverse dynamics of a flexible-joint robot manipulator, however not if rigid joints are assumed. In the rotor equation, $\mathbf{B} \succ 0 \in \mathbb{R}^{N\times N}$ is the diagonal matrix of rotor inertias reflected to the output-side of the transmission, $\mathbf{f} \in \mathbb{R}^N$ is the vector of friction torques acting on the rotor coordinate, $\mathbf{K}_\tau \succ 0 \in \mathbb{R}^{N\times N}$ is the diagonal matrix of electric actuator torque constants multiplied by the transmission ratios, and $\mathbf{i} \in \mathbb{R}^N$ is the torque-generating (quadrature) current obtained from the phase currents via *Park's Transformation*. In the context of control, the control input $\mathbf{u} = \mathbf{K}_\tau\,\mathbf{i}$, i.e. the motor torque.

4. Robot joint friction & hysteresis model

This section presents the mathematical modeling of the joint friction and hysteresis. The joint transmission torques and friction phenomena are uncoupled among the joints, so for simplicity of notation we consider in this section a single joint which simplifies the vector equations into scalar equations. Indices to denote the arbitrary joint are omitted. Let the rotor angular velocity $\omega \triangleq \mathrm{d}\,\theta/\mathrm{d}\,t$, $t \in \mathbb{R}_+$, the joint temperature $T \in \mathbb{R}$, and the joint torque $\tau_J \in \mathbb{R}$.

The friction torque is considered a summation of a Coulomb friction torque $\mathcal{F}_C : \mathbb{R}^M \times \mathbb{R} \times \mathbb{R} \to \mathbb{R}$ and a nonlinear viscous friction torque $\mathcal{F}_v : \mathbb{R} \times \mathbb{R} \to \mathbb{R}$, i.e.

$$f \triangleq \mathcal{F}_C(\vec{z}, \omega, \tau_J) + \mathcal{F}_v(\omega, T) \tag{3}$$

in which $\mathbf{z} \in \mathbb{R}^M$ is an internal state. In this work, the term *Coulomb friction torque* is used to describe the part of the friction torque that exist in the transition between the stiction regime and sliding regime – sometimes referred to as *dry friction*. The viscous friction torque is modeled as a continuous function with the same sign as its first argument, i.e.

$$\omega\,\mathcal{F}_v(\omega, T) > 0 \quad \forall\,\omega \neq 0 \tag{4}$$

The Coulomb friction torque is considered a multiplication of; 1) a hysteretic function $\mathcal{H} : \mathbb{R}^M \times \mathbb{R} \to \mathbb{R}$ of the internal state $\mathbf{z}$ and ω, and 2) a Coulomb friction coefficient function $\mathcal{F} : \mathbb{R} \to \mathbb{R}$ of the joint torque τ_J, i.e.

$$\mathcal{F}_C(\vec{z}, \omega, \tau_J) \triangleq \mathcal{F}(\tau_J)\,\mathcal{H}(\vec{z}, \omega)\,, \qquad \frac{\mathrm{d}\,\vec{z}}{\mathrm{d}\,t} \triangleq \mathcal{G}(\vec{z}, \omega) \tag{5}$$

in which the state equation $\mathcal{G}(\cdot)$ describes the dynamics of the internal state vector $\mathbf{z}$ as a first-order differential equation of a general form similar to that of the original GMS model [14]. The function $\mathcal{H}$ is a hysteretic function with nonlocal memory characteristics which is at most unitary in magnitude, i.e.

$$-1 \leq \mathcal{H}(\vec{z}, \omega) \leq 1 \quad \forall\,\vec{z} \tag{6}$$

and the Coulomb friction coefficient is an even and positive function, i.e.

$$\mathcal{F}(-\tau_J) = \mathcal{F}(\tau_J) > 0 \quad \forall\,\tau_J \tag{7}$$

Some limiting conditions on the functions $\mathcal{H}(\cdot)$ and $\mathcal{G}(\cdot)$ apply, namely, for constant non-zero velocities, the steady-state friction torque is a function of the angular velocity and joint torque alone and

$$\mathcal{G}(\vec{z}, \omega) = 0 \quad \text{and} \quad |\omega|\,\mathcal{H}(\vec{z}, \omega) = \omega \tag{8}$$

In other words, $\mathcal{H}(\mathbf{z}, \omega) = -1$ if $\omega < 0$ and $\mathcal{H}(\mathbf{z}, \omega) = 1$ if $\omega > 0$, thus

$$f = \mathcal{F}(\tau_J)\,\omega/|\omega| + \mathcal{F}_v(\omega, T) \tag{9}$$

4.1. Identification of no-load coulomb friction and viscous friction

The dependency of the no-load friction torque on angular velocity and temperature is identified by cooling the robot to 9 °C, then placing it in an ambient temperature of approximately 20 °C and rotating a single robot joint with different constant angular velocities with no external wrench applied and with the joint axis of rotation oriented parallel to the direction of the gravitational acceleration. The robot joint will naturally heat up while the constant angular velocity motions are performed.

In this case, (1) simplifies to $\mathbf{0} = \boldsymbol{\tau}_\mathrm{J}$, hence (2) becomes $\mathbf{f} = \mathbf{K}_\tau\,\mathbf{i}$ and due to $\mathbf{K}_\tau$ being diagonal we have for each joint $f = K_\tau\,i$. Further, using (9) in $K_\tau\,i = f$ leads to

$$K_\tau\,i = \mathcal{F}(0)\,\omega/|\omega| + \mathcal{F}_v(\omega, T) \tag{10}$$

The model for the viscous friction torque is defined such that for some temperature $T = T_0$ the contribution from the model

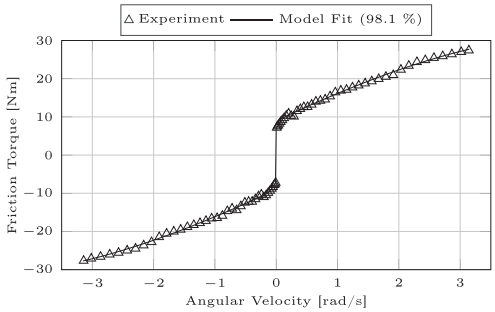

Fig. 3. No-load Coulomb friction and viscous friction in terms of the angular velocity and with a fixed temperature for $T = T_0 = 20$ °C for the base joint of the Universal Robots UR5e robot manipulator.

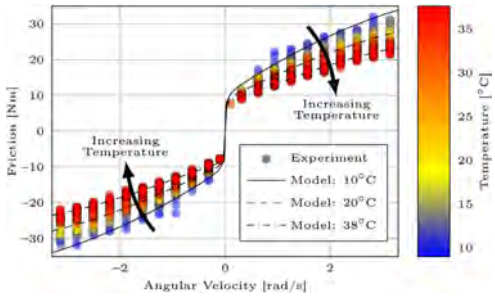

Fig. 4. No-load Coulomb friction and viscous friction in terms of the angular velocity and temperature for the base joint of the Universal Robots UR5e robot manipulator.

for the temperature dependency equals zero, thus

$$\mathcal{F}_v(\omega, T) = \operatorname{sgn}(\omega)\Big((F_S - \mathcal{F}(0)) \exp[-(|\omega|/V_S)^{\mu}] + \sqrt{|\omega|}\big(F_{T,1}\,(T - T_0) + F_{T,2}\,(T - T_0)^{-3}\big)\Big) + F_{V,1}\,\omega + F_{V,2}|\omega|\,\omega + F_{V,3}\,\omega^3 \tag{11}$$

where $F_S, V_S, \mu, F_{V,1}, F_{V,2}, F_{V,3}, F_{T,1}, F_{T,2} \in \mathbb{R}$ are, respectively, the Stribeck friction coefficient, Stribeck velocity, Stribeck shape factor, velocity friction coefficients, and temperature friction coefficients.

The friction torque of the base joint of the UR5e robot manipulator is shown in Fig. 3 in terms of the angular velocity with the temperature $T = T_0 = 20$ °C fixed, and shown in Fig. 4 in terms of both the angular velocity and temperature.

The set of optimum parameters are found through iterative nonlinear optimization. In particular, we used a Quasi-Newton method with a cubic line search procedure and updating the Hessian matrix approximation by the Broyden-Fletcher-Goldfarb-Shanno (BFGS) method. The set of optimum parameters is assumed to be a global optimum because the exact same parameter values are found for different starting points.

Figs. 3 and 4 show levels of friction torques comparable to the levels found in the SIASUN 7-axis robot [30], which is also equipped with strain-wave transmissions, as well as in our previous works on the UR5e robot [17,18]. The level of friction should be seen in view of the max rated torque of the joint; that is, a 30 N m friction torque corresponds to 20% of the max rated torque of 150 N m for the size 3 joint of the Universal Robots UR5e robot.

5. Joint torque and position dependent generalized Maxwell-Slip friction model

The Generalized Maxwell-Slip (GMS) friction model [13,14] has been successfully applied to model the friction characteristics of strain-wave transmissions [15,16]. However, the friction torque of robot joints that comprise strain-wave transmissions have been shown to experience an increase in Coulomb friction with the load torque [18,30–32], which the GMS friction model does not describe. In the existing works, this issue is addressed by *adding* a term describing the dependence of Coulomb friction on joint torque, such as the linear dependence $F_{C,L}\operatorname{sgn}(\omega)|\tau_J|$ [32,33] or squared dependency $F_{C,L}\operatorname{sgn}(\omega)\,\tau_J^2$ [18,34], where $F_{C,L} > 0$, however such extensions makes the friction model discontinuous around $\omega = 0$ due

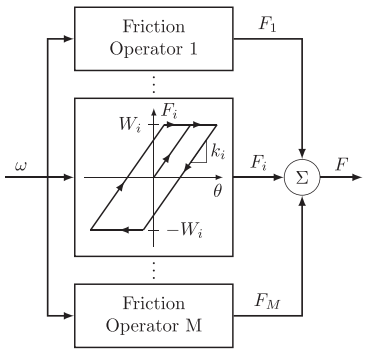

Fig. 5. Schematic representation of the Generalized Maxwell-Slip friction model.

to the sgn(·) term. In this work, we propose an extension to the GMS friction model for it to describe the load dependent friction characteristics.

In [19] the response of strain-wave transmissions subject to certain geometric inaccuracies was investigated analytically and through numerical simulations. It was found that the backlash could depend on the angular position provided eccentricity errors were present between the wave-generator and the circular spline. In [18] we showed that the strain-wave transmissions of the Universal Robots UR5e manipulator do indeed experience such behavior. Thus, the dependency of backlash on the angular position is modeled by $\mathcal{H}(\cdot)$.

The GMS model can be visualized (see Fig. 5) as a parallel connection of $M \in \mathbb{N}_+$ massless block-spring models subject to the same input (displacement θ or velocity ω). Each operator $i = 1, \dots, M$ is characterized by its own spring stiffness k_i and a maximum spring deformation Δ_i (or equivalently a slip-force limit $W_i = k_i \Delta_i$). Let the smooth, 2π-periodic, and invertible function $\mathcal{B} : \mathbb{R} \to \mathbb{R}_+$, $\mathcal{B}(x + 2n\pi) = \mathcal{B}(x)$, $\forall\ n \in \mathbb{Z}$ describe the backlash in terms of θ. The function $\mathcal{B}(\cdot)$ is incorporated into the GMS model simply as a scaling of the spring deformation limits and output equation. The spring deformation of operator i is defined

$$\delta_i \triangleq \theta - z_i\,, \quad |\delta_i| \leq \mathcal{B}(\theta)\,\Delta_i\,, \quad \forall\ i = 1, \dots, M \tag{12}$$

When operator i sticks δ_i changes proportionally to θ and when operator i slips $|\delta_i| = \mathcal{B}(\theta)\,\Delta_i$, thus

$$\frac{\mathrm{d}\,\delta_i}{\mathrm{d}\,t} = \begin{cases} \omega & \text{(stick)} \\ \frac{\partial \mathcal{B}}{\partial \theta}\,\frac{\partial \theta}{\partial t} & \text{(slip)} \end{cases} \tag{13}$$

The ith operator remains sticking as long as $|\delta_i| < \mathcal{B}(\theta)\,\Delta_i$ while slipping until the exerted displacement θ reaches a local extremum, i.e. the exerted velocity ω crosses zero. If data is sampled at times $t(k) = k\,T_S$, $k \in \mathbb{N}$ and T_S the sampling period, the nonlinear state equation of each operator can be described in terms of the change in the exerted displacement. Applying a forward difference scheme on (12) and (13) gives

$$\delta_i(k+1) = \operatorname{sgn}(\theta(k+1) - \theta(k) + \delta_i(k)) \cdot \min\{|\theta(k+1) - \theta(k) + \delta_i(k)|, \mathcal{B}(\theta(k+1))\,\Delta_i\} \tag{14}$$

The total hysteretic function output is the summation of friction forces for each element multiplied by the inverse of $\mathcal{B}(\cdot)$, i.e.

$$\mathcal{H}(\vec{z}, \omega) = \mathcal{B}^{-1}(\theta) \sum_{i=1}^{M} F_i\,, \quad F_i = k_i\,\delta_i \tag{15}$$

Proposition 1. *Modifying the GMS friction model with the smooth, 2π-periodic, and invertible function $\mathcal{B} : \mathbb{R} \to \mathbb{R}_+$, i.e. $\mathcal{B}(x + 2n\pi) = \mathcal{B}(x) > 0$, $\forall\ n \in \mathbb{Z}$, $x \in \mathbb{R}$ according to the nonlinear state (14) and output (15) will, for the slip regime, yield an output identical to that of the original GMS model ($\partial\,\mathcal{B}/\partial\,\theta \equiv 0$) in Rizos and Fassois [35], thus $\mathcal{H}(\cdot)$ will obey (6), effectively making the steady state output invariant to the backlash.*

Proof. In the slip regime $|\delta_i| = \mathcal{B}(\theta)\,\Delta_i$. The sign of δ_i is provided by (14). $\delta_i(k+1) = \mathcal{B}(\theta(k+1))\,\Delta_i$ if $\theta(k+1) - \theta(k) \geq 0$ and $\delta_i(k+1) = -\mathcal{B}(\theta(k+1))\,\Delta_i$ if $\theta(k+1) - \theta(k) \leq 0$. Because $\mathcal{B}(\theta) > 0\ \forall\,\theta$, the output provided by (15) yields the steady-state output to be $\mathcal{H}(\vec{z}, \omega) = \sum_{i=1}^{M} k_i\,\delta_i$ which is equivalent to that of the original GMS model. □

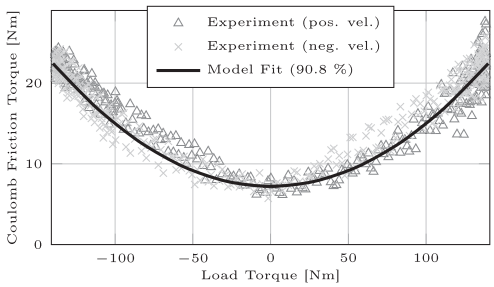

Fig. 6. Coulomb friction torque as a function of the joint torque for the second joint of the Universal Robots UR5e robot manipulator.

Based on the constraint in (6), the slip-force limits are constrained such as to yield a friction output, see (15), which is at most unitary in magnitude, i.e.

$$\sum_{i=1}^{M} W_i = 1, \quad W_i = k_i \, \Delta_i \tag{16}$$

The spring deformation limit and stiffness of each operator is selected so that the constraint of (16) is satisfied. In [35] the deformation limits were spaced uniformly, however in Madsen et al. [18] polynomial laws were found to yield better performance. Such polynomial laws subject to the constraint of (16) results in

$$\Delta_i = \left(\frac{i}{M} \right)^{r_\Delta} \tag{17}$$

$$k_i = \frac{1}{\Delta_i} \frac{(M+1-i)^{r_k}}{\sum_{i=1}^{M} i^{r_k}} \tag{18}$$

where for $r_\Delta > 1$ the deformation limits are spaced more closely for small spring deformations. The sum of integer powers in (18) is obtained easily by numerical methods, however its analytic solution involves the *Riemann Zeta function* and the *Hurwitz zeta function*. For the special case of $r_k \in \mathbb{N}_+$, *Faulhaber's formula* gives the sum explicitly in terms of the *Bernoulli numbers*. $r_\Delta = 4$ and $r_k = 2$ are found to yield a good performance. Fig. 7 shows the experimentally identified and model estimated hysteresis characteristics, the model using (17) and (18).

5.1. Identification of joint torque dependent coulomb friction

The dependency of the Coulomb friction on joint torque is identified by rotating a single joint at the time with an angular velocity of 0.05 rad/s with no external wrench applied and the joint axis of rotation oriented perpendicular to the direction of the gravitational acceleration, thus making the gravity-induced torque act as load torque. To identify the dependency of friction on load torque for *all* joints, the UR5e robot is mounted differently depending on the joint of interest. For joint 1, the robot is "*wall mounted*", i.e. with the joint 1 (base joint) axis of rotation oriented perpendicular to the direction of the gravitational acceleration. For joint 2 to 6, the robot is "*table mounted*", i.e. with the joint 1 (base joint) axis of rotation oriented parallel to the direction of the gravitational acceleration.

In this case, (1) reduces to $\mathbf{g}(\mathbf{q}) = \boldsymbol{\tau}_\mathrm{J}$, hence (2) becomes $\mathbf{f} = \mathbf{K}_\tau \, \mathbf{i} - \mathbf{g}(\mathbf{q})$ and due to $\mathbf{K}_\tau$ being diagonal we have for each joint $f = K_\tau \, i - g(\mathbf{q})$ where $g(\mathbf{q})$ is the scalar gravity torque exerted to the joint subject to testing. Using (8) in (3) leads to

$$|\omega|/\omega(K_\tau \, i - g(\vec{q}) - \mathcal{F}_v(\omega, T)) = \mathcal{F}(g(\vec{q})) \tag{19}$$

in which the gravity-induced joint torque $g(\mathbf{q})$ is predicted based on the measurement of $\mathbf{q}$ and known values of the masses and center of mass positions of the links distal to the joint subject to testing. A payload of 7.5 kg was attached to the robot's end effector to further increase the gravity-induced joint torque.

The dependency of the Coulomb friction torque on the joint torque is described by the polynomial model

$$\mathcal{F}(\tau_J) = F_{C,0} + F_{C,1} \tau_J^2 \tag{20}$$

in which $F_{C,0}$ is the Coulomb friction coefficient for no load and $F_{C,1}$ is the Coulomb friction coefficient to the squared joint torque.

Fig. 6 shows the Coulomb friction in terms of the joint torque for the second joint of the Universal Robots UR5e robot manipulator.

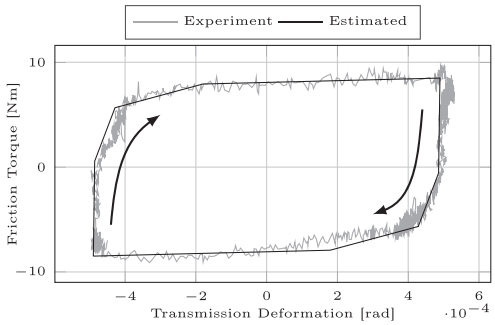

Fig. 7. Hysteretic behavior of the strain-wave transmission of the base joint of the UR5e robot manipulator; experimentally identified and estimated by the Generalized Maxwell-Slip friction model using (17) and (18) with $M = 4$.

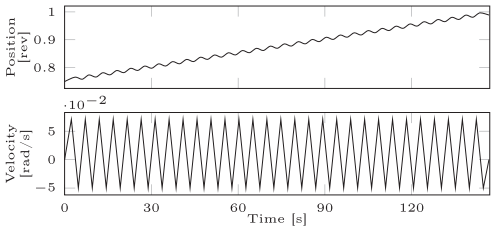

Fig. 8. Trajectory of the second joint used for validating the load-dependent Generalized Maxwell-Slip friction model.

5.2. Identification of generalized Maxwell-Slip friction

The GMS friction model is identified by rotating a single robot joint with reciprocating and very low velocities and accelerations such that inertial effects can be neglected. The joint axis of rotation is oriented parallel to the direction of the gravitational acceleration, i.e. gravity does not induce torque around the joint axis of rotation. The well-known kinematic error nonlinearity [15,36,37] has been identified and compensated *a priori* as described in Madsen et al. [18]. The joint is driven by the signal

$$\ddot{q} = \begin{cases} a & \text{for } t_0 < t \leq t_1 \\ -a & \text{for } t_1 < t \leq t_2 \end{cases}, \quad t_1 - t_0 > t_2 - t_1 \tag{21}$$

with $a = 0.05$ rad/s^2 and the net motion during one cycle $q(t_1) - q(t_0) - (q(t_1) - q(t_2)) = 3^\circ$, i.e. 240 velocity reversals for one complete revolution of the output side. Neglecting inertial effects and gravity effects, (1) simplifies to $0 = \tau_J$ (for each joint) resulting in the transmission deformation being bounded in magnitude by the backlash, i.e.

$$|\theta(t) - q(t)| \leq \mathcal{B}(\theta(t)) \quad \forall t \tag{22}$$

The hysteretic behavior of the strain-wave transmission is shown in Fig. 7 for a single hysteresis loop. The number of operators needed for an accurate model is $M = 4$ [18], and the optimum value of the backlash $\mathcal{B}$ is found to be 0.001 rad.

5.3. Validation of the extended GMS model

We compare the Extended GMS model of (14) and (15) to a baseline model in which the joint torque dependent Coulomb friction is compensated by the common method [30,32–34,38] of which the load dependent friction is modeled and compensated by the term $\text{sgn}(\omega)\mathcal{F}(\tau_J)$ with $\mathcal{F}(\tau_J)$ defined in (20). Thus, this method results in a discontinuity around zero velocity due to the $\text{sgn}(\omega)$ term. The joint torque dependent GMS friction model is validated by implementing the models in the feedforward controller and performing the motion shown in Fig. 8. The motion includes velocity reversals and the load torque varies from zero to a large value – thus, a large subspace of the total load torque space is explored and the validation of the Extended GMS model is enhanced. This is done by starting out with the shoulder joint of the UR5e robot manipulator oriented such that the robot arm is in the vertical orientation (no load) and slowly moving towards the horizontal orientation (maximum load) while reversing multiple times. A 7.5 kg payload is attached to the end-effector. The torque corresponding to the trajectory in Fig. 8 is shown in Fig. 9. The actuator torque is obtained by measuring the phase

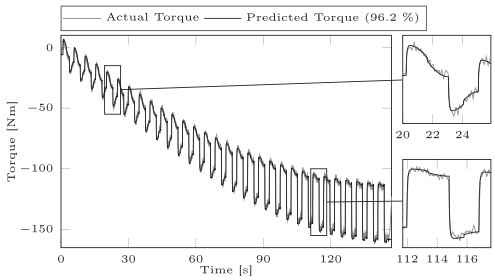

Fig. 9. Torque corresponding to the trajectory shown in Fig. 8; actual torque and torque predicted by the load-dependent Generalized Maxwell-Slip friction model.

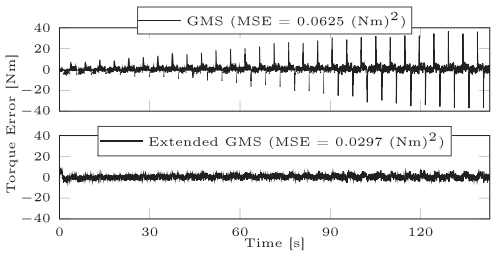

Fig. 10. Torque prediction error for the discontinuous joint torque dependent Coulomb friction model and our proposed joint torque dependent Generalized Maxwell-Slip (GMS) friction model.

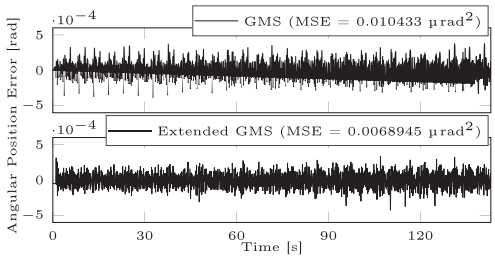

Fig. 11. Angular position error for the static friction model and the joint torque dependent Generalized Maxwell-Slip (GMS) friction model.

currents of the PMSM and using *Park's transformation* and the drive gains to obtain the actuator torque. The torque prediction error of the Extended GMS model and the baseline model is shown in Fig. 10. The difference between the methods is most significant during velocity reversals with large load torque, where the jumps in torque prediction due to the discontinuous sgn(ω) term in the baseline model causes large prediction errors of up to almost 40 N m, while this is not the case for our proposed joint torque dependent Extended GMS friction model. The Mean Squared Error (MSE) of the torque prediction is improved by a factor of 2.1 – from 0.0625 (N m)^2 to 0.0297 (N m)^2. The trajectory tracking performance is evaluated by implementing the Extended GMS model and the original GMS model in the feedforward part of the robot controller. The angular position errors for the Extended GMS model and the original GMS model are shown in Fig. 11. The trajectory tracking performance is improved by a factor of 1.5 – from 0.010433 rad^2 to 0.0068945 rad^2.

6. Adaptive feedforward friction compensation

The friction characteristics of robot joints are known to vary statistically between similar robot joints and also change with; 1) lubricant temperature and 2) the level of wear and tear of the robot joint. To maintain the accurate torque prediction capabilities during the lifetime of the robot, we propose the following prediction error-based parameter estimation scheme in Fig. 12, which will, in the combination with the adaptive control strategy in Fig. 1, ensure a consistently good

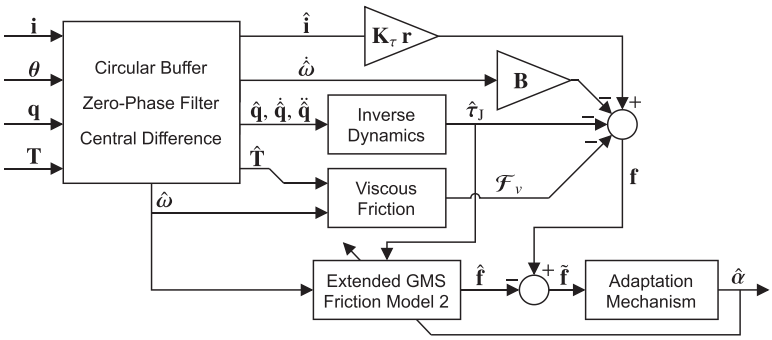

Fig. 12. Parameter estimation scheme.

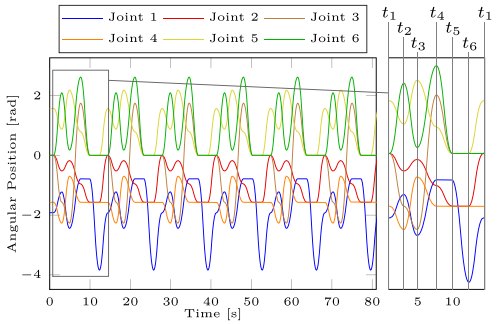

Fig. 13. Trajectory used for the validation of the adaptive feedforward joint torque dependent Generalized Maxwell-Slip friction model compensation.

tracking performance despite changes in the robot friction characteristics. However, other uses of the parameter estimates may be relevant at a later stage such as wear estimation for predictive maintenance.

The adaptation is parametrized based on the facts that; 1) the wear and tear of the robot joint will lead to an increase in Coulomb friction torque [10], and 2) the thermal resistance between the lubricant of the strain-wave transmission and the location of the temperature measurement will lead to an uncompensated time delay in the temperature compensation [34] which will lead to inaccurate predictions of the viscous friction torques.

6.1. State estimation

The utilized measurements includes; the angular positions, $\boldsymbol{\theta}$ and $\mathbf{q}$, of the rotors and links, respectively, the joint temperatures $\mathbf{T}$, and the torque-generating currents $\mathbf{i}$ of the PMSMs. In reality, the phase currents are measured, while the torque-generating (quadrature) currents are obtained from the phase currents using *Park's transformation*.

Common methods for state estimation includes mathematical estimators such as high-gain observers [28], sliding mode observers, etc. The estimation quality can be evaluated by considering the error signal and evaluating the some error norm such as L_2, L_∞, etc. [39].

In this work, we obtain the state estimates through a simple approach without causing phase shifts between the various measured quantities and their time-derivatives. Circular buffers are used to store the measurements for the Savitzky-Golay [40] Finite Impulse Response (FIR) Low-Pass (LP) filters to operate on, and the Central Difference (CD) procedure is used to estimate the time-derivatives $\dot{\vec{q}}$ and $\ddot{\vec{q}}$ from the measurement of $\mathbf{q}$. The first and second order central difference for a signal sampled with a fixed sampling period is unambiguously defined. The CD procedure is a standard result in numerical analysis and is not detailed in this paper. The circular buffers of measurements are of $n_{\text{LP}} \in \mathbb{N}_+$ entries, hence a delay of $(n_{\text{LP}} - 1)/2$ samples are obtained. The smoothed values are stored in circular buffers of $n_{\text{CD}} \in \mathbb{N} > 2$ entries for the central difference procedure to operate causing a total delay of $(n_{\text{LP}} - n_{\text{CD}} - 2)/2$ samples. For the specific *UR5e* robotic system at hand, $n_{\text{LP}} = 101$ and $n_{\text{CD}} = 3$ were used resulting in a total delay of 51 samples, i.e. 0.051 s for the sampling rate of 1 kHz.

6.2. Friction estimation

Common methods for estimating the friction torque includes observer-based disturbance estimation [41].

The general estimation methodology in this paper is to; 1) generate a (virtual) measure of the signal to be estimated based on the available measurements, and 2) use this signal to drive the adaptive estimation. The virtual measures of the friction torques are obtained by the combination of (1), (2), and (11), thus

$$\vec{f} = \vec{K}_\tau \hat{\vec{i}} - \vec{B}\dot{\hat{\boldsymbol{\omega}}} - \hat{\boldsymbol{\tau}}_J(\hat{\vec{q}}, \dot{\hat{\vec{q}}}, \ddot{\hat{\vec{q}}}) - \mathcal{F}_v(\hat{\boldsymbol{\omega}}, \hat{\vec{T}}) \tag{23}$$

where (1) provides the joint torque estimate as $\hat{\boldsymbol{\tau}}_J(\hat{\mathbf{q}}, \dot{\hat{\mathbf{q}}}, \ddot{\hat{\mathbf{q}}}) = \mathbf{M}(\hat{\mathbf{q}})\ddot{\hat{\mathbf{q}}} - \mathbf{C}(\hat{\mathbf{q}}, \dot{\hat{\mathbf{q}}})\dot{\hat{\mathbf{q}}} - \mathbf{g}(\hat{\mathbf{q}})$. The friction measure of (23) can thus be interpreted as the total friction torque minus the identified nonlinear viscous friction torque. Coupling (1) and (2) through the joint torque means that the joint flexibility is accounted for without the need of a joint compliance model. This is possible due to the Universal Robots manipulators having two absolute rotary encoders per joint – one at each side of the strain-wave transmission. The adaptive estimator is formulated at joint level. Thus, for notational simplicity let f be the friction measure for any single joint. The adaptation captures the time-variation of the Coulomb and viscous friction torques, hence the friction model estimate $\hat{f}$ for any joint is given by

$$\begin{aligned}\hat{f} &= \vec{Y}^{\mathsf{T}}(\hat{\tau}_J, \hat{\omega})\,\hat{\boldsymbol{\alpha}} \\ &= \begin{bmatrix} \mathcal{F}(\tau_J) \sum_{i=1}^{M} k_i \delta_i & \hat{\omega} \end{bmatrix} \cdot \begin{bmatrix} \hat{\alpha}_1 \\ \hat{\alpha}_2 \end{bmatrix}\end{aligned} \tag{24}$$

with $\mathbf{Y}$ the regressor and $\hat{\boldsymbol{\alpha}}$ the vector of parameter estimates. The first term in the regressor is output of the Extended GMS model. Thus, the Coulomb friction is estimated with the regressor and its time-derivative being locally Lipschitz continuous for all t without the need of filtering. The prediction error for any joint is defined

$$\tilde{f} = f - \hat{f} \tag{25}$$

The adaptive law is the *gradient method* [42] with a quadratic error cost function, i.e.

$$\dot{\hat{\boldsymbol{\alpha}}} = \boldsymbol{\Gamma}\,\vec{Y}(\hat{\tau}_J, \hat{\omega})\,\tilde{f} \tag{26}$$

with $\boldsymbol{\Gamma} = \mathrm{diag}([\gamma_1 \;\; \gamma_2]^{\mathsf{T}}) \succ 0 \in \mathbb{R}^{2\times 2}$ the diagonal matrix of adaptation gains. The stability and convergence of this estimator depend on the estimation gain $\boldsymbol{\Gamma}$. Generally, larger estimation gain means faster convergence. However, after some point, further increasing the estimation gain leads to oscillatory behavior, slower convergence, and even instability. Also, parameter convergence is ensured only if the regressor is persistently exciting. For the detailed stability analysis of the gradient estimator, the reader is referred to literature such as [42]. In this paper, we do not provide the stability analysis with details due to the limited space.

6.3. Robustness

To increase robustness with respect to disturbances and ensure the overall safety and stability of the robotic system the adaptation law is modified. Several choices of well-known modifications exist such as *leakage* and *shifted-leakage*, fixed σ-modification, switching σ-modification, ϵ_1-modification, and projection. In this work, we use a combination of projection in the parameter space and monitoring conditional logic to ensure that the regressor is persistently exciting.

6.3.1. Parameter projection

The parameter projection method [43] is used to confine the estimated parameters to a bounded convex region, which is assumed to contain the true parameters, i.e.

$$\hat{\alpha}_1 \in [\,\alpha_{1,\min}\,;\,\alpha_{1,\max}\,], \quad \hat{\alpha}_2 \in [\,\alpha_{2,\min}\,;\,\alpha_{2,\max}\,] \tag{27}$$

with $\alpha_{1,\min} = 0.4$, $\alpha_{1,\max} = 1.5$, $\alpha_{2,\min} = -5$ cN m s, and $\alpha_{2,\max} = 5$ cN m s.

6.3.2. Persistence of excitation

To ensure that the regressor is persistently exciting at all time, adaptation is disabled if the rotor angular velocity remains below $\omega_{\min}$ for time t^*, hence the adaptive law of (26) could be expressed as

$$\dot{\hat{\boldsymbol{\alpha}}} = \begin{cases} 0 & \text{if } \omega_{\min} > \max\limits_{t-t^* \le t} |\omega(t)| \\ \boldsymbol{\Gamma}\,\vec{Y}(\hat{\tau}_J, \hat{\omega})\,\tilde{f} & \text{otherwise} \end{cases} \tag{28}$$

with $\omega_{\min} = 0.01$ rad/s and $t^* = 0.05$ s.

Table 1
The six joint space waypoints ($\vec{wp}_l$) in degrees for each of the six joints (q_j) used by the trajectory generator to generate the trajectory shown in Fig. 13.

	q_1	q_2	q_3	q_4	q_5	q_6
$\mathbf{wp}_1$	−110	0	0	−90	90	0
$\mathbf{wp}_2$	−70	−30	−90	−130	50	120
$\mathbf{wp}_3$	−140	−10	−130	−40	125	10
$\mathbf{wp}_4$	−45	−55	100	−90	45	150
$\mathbf{wp}_5$	−45	−90	0	−90	0	0
$\mathbf{wp}_6$	−220	−90	0	−90	0	0

6.4. Feedforward friction compensation

The adaptive feedforward joint torque dependent GMS friction model compensation is obtained at joint level by evaluating the friction model in the desired velocity $\dot{q}_\mathrm{d}$, the nominal joint torque $\tau_{J,\mathrm{d}}$, and the parameter estimate $\hat{\boldsymbol{\alpha}}$, i.e.

$$\hat{f} = \vec{Y}^\mathsf{T}(\tau_{J,\mathrm{d}}, \dot{q}_\mathrm{d})\,\hat{\boldsymbol{\alpha}} \tag{29}$$

The combined control law is a combined feedback $\mathbf{u}_\mathrm{FB}$, feedforward $\mathbf{u}_\mathrm{FF}$, and adaptive feedforward $\hat{\mathbf{f}}$, i.e.

$$\begin{aligned}\vec{u} = \;& \hat{\vec{f}} + \vec{u}_\mathrm{FF} + \vec{u}_\mathrm{FB} \\ = \;& \hat{\vec{f}} + \vec{M}(\vec{q}_\mathrm{d})\,\ddot{\vec{q}}_\mathrm{d} + \vec{C}(\vec{q}_\mathrm{d}, \dot{\vec{q}}_\mathrm{d})\,\dot{\vec{q}}_\mathrm{d} + \vec{g}(\vec{q}_\mathrm{d}) + \vec{\mathcal{F}}_v(\dot{\vec{q}}_\mathrm{d}, \vec{T}) \\ & + \vec{M}(\vec{q}_\mathrm{d})\left(-\vec{K}_\mathrm{d}\,\dot{\vec{e}} - \vec{K}_\mathrm{p}\,\vec{e} - \vec{K}_\mathrm{i}\int_0^t \vec{e}'\,\mathrm{d}\,t'\right)\end{aligned} \tag{30}$$

in which the feedforward $\mathbf{u}_\mathrm{FF} = \mathbf{M}(\mathbf{q}_\mathrm{d})\,\ddot{\mathbf{q}}_\mathrm{d} + \mathbf{C}(\mathbf{q}_\mathrm{d}, \dot{\mathbf{q}}_\mathrm{d})\,\dot{\mathbf{q}}_\mathrm{d} + \mathbf{g}(\mathbf{q}_\mathrm{d}) + \mathcal{F}_v(\dot{\mathbf{q}}_\mathrm{d}, \mathbf{T})$ and $\mathbf{u}_\mathrm{FB} = \mathbf{M}(\mathbf{q}_\mathrm{d})(-\mathbf{K}_\mathrm{d}\,\dot{\mathbf{e}} - \mathbf{K}_\mathrm{p}\,\mathbf{e} - \mathbf{K}_\mathrm{i}\int_0^t \mathbf{e}\,\mathrm{d}\,t')$ is the feedback term. Thus, the combined feedforward and feedback controller constitute the well-known Computed-Torque Control (CTC) strategy. The temperature T is the actual measured temperature used to linearize the model through feedback. For safety reasons this value is bounded simply by confining the value to the region $T \in [T_\mathrm{min};\, T_\mathrm{max}]$.

6.5. Stability

This section presents some statements of stability of the adaptive feedforward compensation. We show that the friction compensation is stable in the sense of BIBO (Bounded Input, Bounded Output). A system is BIBO stable if it has bounded gain [44]. The feedforward friction compensation is given by (29). The critical values for the gain are $\tau_{J,\mathrm{d}}$, $\dot{q}_\mathrm{d}$, and T. The desired angular positions, velocities, and accelerations are bounded by the trajectory generator, hence $\tau_{J,\mathrm{d}}$ is bounded. The hysteretic function $\mathcal{H}(\cdot)$ is also bounded, see (6), and so is the measured temperature, thus the Coulomb friction torque $\mathcal{F}_C(\cdot)$ is bounded. The estimated parameter vector $\hat{\boldsymbol{\alpha}}$ is also bounded (see Section 6.3.1), hence the output of the feedforward friction compensation is bounded.

6.6. Validation

The adaptive controller is validated by specifying initial conditions for the friction that are known to be wrong but still verifies the conditions of (27), and considering the adaptation of the parameters as well as the prediction and tracking performance. The parameter values are kept fixed for the first 30 s and then allowed to change. The torque prediction error and the position tracking error should both decrease. A 7.5 kg payload is attached to the end effector of the robot.

6.6.1. Trajectory

The trajectory used to validate the adaptive feedforward dynamic friction compensation is chosen to contain periods of motion and standstill for all joints. The trajectory is generated based on six waypoints $\mathbf{wp}_l$, $l = 1, \ldots, 6$, with specific joint angular positions listed in Table 1. A linear joint space motion is constructed between the waypoints from 1 to 6 and then repeated, i.e. $\mathbf{wp}_1 \to \mathbf{wp}_2 \to \cdots \to \mathbf{wp}_6 \to \mathbf{wp}_1 \to \ldots$. The cycle time from starting at $\mathbf{wp}_1$ to reaching $\mathbf{wp}_1$ again is 13,458 ms. At all times the maximum angular velocity and acceleration for any joint are constrained to be, respectively, $\max(|\dot{\mathbf{q}}_\mathrm{d}|) = \pi$ rad/s and $\max(|\ddot{\mathbf{q}}_\mathrm{d}|) = 2\pi/3$ rad/s^2. The angular velocities at the waypoints are zero, i.e. $\dot{\mathbf{q}}_\mathrm{d}(t_l) = \mathbf{0}$, $t_l = \{t : \mathbf{q}_\mathrm{d}(t) = \mathbf{wp}_l\}$, $l = 1, \ldots, 6$.

6.6.2. Results & discussion

Parameter estimates $\hat{\alpha}_1$ and $\hat{\alpha}_2$ for each joint are shown in Figs. 14 and 15, respectively. The parameters start out at initial values, $\hat{\alpha}_1 = 0.47$ and $\hat{\alpha}_2 = 0.04$ respectively, and converges within the next 50 s – most of them considerably faster. Fig. 16 show the measured and predicted torques, while Fig. 17 show their difference, i.e. the torque prediction error. Evaluating

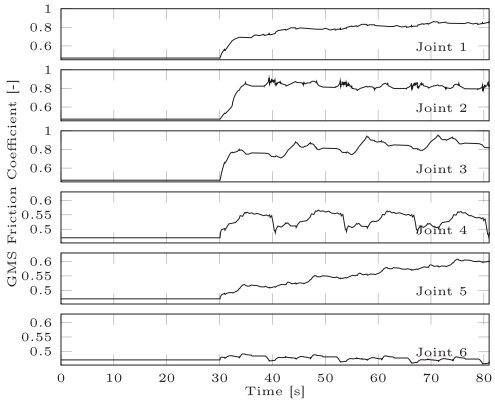

Fig. 14. Adaptation of $\hat{\alpha}_1$; the joint torque dependent Generalized Maxwell-Slip friction model coefficient (the nominal model is obtained for $\hat{\alpha}_1 = 1$).

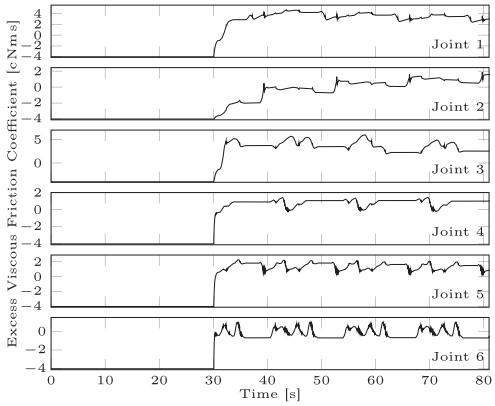

Fig. 15. Adaptation of $\hat{\alpha}_2$; excess viscous friction coefficient (the nominal model is obtained for $\hat{\alpha}_2 = 0$).

Table 2
Results of the adaptive feedforward friction compensation for each joint and the average relative improvement. The performance measured in Mean Squared Error (MSE) of torque prediction (Fig. 17) and trajectory tracking (Fig. 18) evaluated for two full cycles (26,916 ms) while; 1) adaptation is disabled (900 ms to 27,816 ms) and 2) adaptation is enabled (55,075 ms to 81,991 ms).

Description	Controller	Joint 1	Joint 2	Joint 3	Joint 4	Joint 5	Joint 6	Average
Torque MSE [(N m)^2]	Non-Adaptive	0.8173	0.5303	1.2329	0.1009	0.1803	0.3039	0.5276
	Adaptive	0.0693	0.1286	0.1554	0.0347	0.0168	0.0181	0.0705
Improvement		91.5%	75.7%	87.4%	65.6%	90.7%	94.0%	84.2%
Position MSE [rad^2]	Non-adaptive	0.3525	0.0870	0.2593	0.0831	0.1193	0.2662	0.1946
	Adaptive	0.2033	0.0515	0.2038	0.0791	0.1158	0.2460	0.1499
Improvement		42.3%	40.8%	21.4%	4.8%	2.9%	7.6%	20.0%

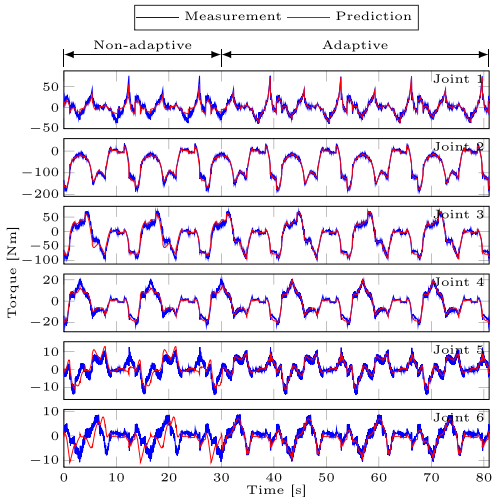

Fig. 16. Measured and predicted torques for each joint.

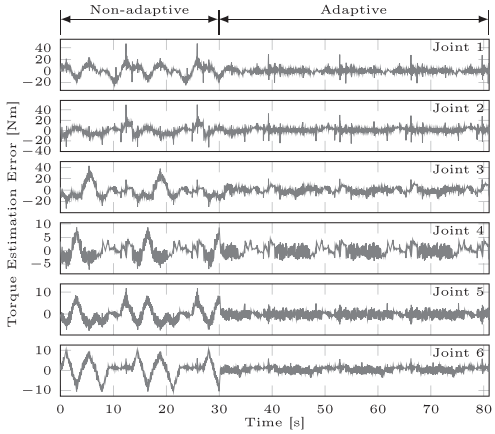

Fig. 17. Torque error for each joint.

two cycles of the trajectory ($2 \times 13,458 = 26,916$ ms) while; 1) adaptation is disabled (900 ms to 27,816 ms) and 2) while adaptation is enabled (55,075 ms to 81,991 ms) yield the torque prediction errors and trajectory tracking errors listed in Table 2. The MSE of the torque prediction is reduced by 84.2% in average and the MSE of the position tracking error is reduced by 20.0% in average. This validates our proposed adaptive feedforward friction compensation.

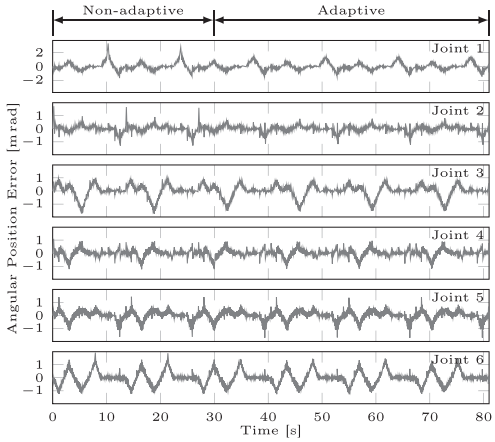

Fig. 18. Trajectory tracking performance; angular position error for each joint.

7. Conclusions

Accurate knowledge of the complex nonlinear dynamics of strain-wave transmissions is important in many areas of robot control, particularly in physical Human-Robot Interaction (pHRI) and other tasks relevant to collaborative robots.

This paper presented an extension to the Generalized Maxwell-Slip (GMS) friction model for it to describe the well-known load torque dependency and angular-position dependency of strain-wave transmissions in a combined framework. The method combines a load torque model and a hysteresis model to overcome the discontinuity around zero velocity of existing implementations of torque dependent friction models. The MSE of the torque prediction accuracy is improved by a factor 2.1 and tracking performance was improved by a factor 1.5.

To address the well-known time-variation of the friction characteristics, we developed and demonstrated an adaptive control strategy based on the proposed extended GMS friction model. For any sufficiently smooth desired trajectory, a feedforward input that is adapted to the identified dynamics of the system can be calculated. For robot manipulators with absolute rotary encoders at each side of the strain-wave transmission, such as the Universal Robots manipulators, the adaptive control strategy allows for automatic recalibration of the control input at any point in time provided the robot joint is non-stationary. The estimation strategy is useful in continuous operation scenarios where the friction parameters may drift due to temperature changes and/or wear and tear of the robot joint by estimating the friction characteristics orders of magnitude faster than any expected real-world changes. The MSE of the torque prediction is improved by 84% and tracking performance is improved by 20%.

Thus, the contributions of this work can be summarized as: 1) extending the GMS friction model to describe in a combined framework the position dependent hysteresis and the dependency of friction on joint torque, and 2) developing an adaptive feedforward controller based on the Extended GMS friction model to effectively compensate for wear and inaccurate estimation of the lubricant temperature.

In our ongoing work that we are going to challenge consists of:

1) Using our high-fidelity model of the joint torque in terms of the transmission deformation to improve the lead-through programming experience of collaborative robots.
2) For the developed feedforward adaptive controller we will investigate strategies to certify its safety according to EN/ISO 10218-1:2011 and 13849-1:2015, Category 3.

Declaration of Competing Interest

The authors declare that they have no known competing financial interests or personal relationships that could have appeared to influence the work reported in this paper.

Acknowledgments

The authors would like to thank Anders Skovgaard Knudsen and Martin Trædholm for their commitment and efforts in the evaluation of the various control laws on the Universal Robots manipulator.

References

[1] B. Bona, M. Indri, Friction compensation in robotics: an overview, in: Proceedings of the 44th IEEE Conference on Decision and Control, IEEE, Seville, Spain, 2005, pp. 4360–4367, doi:10.1109/cdc.2005.1582848.

[2] A. Wahrburg, J. Bos, K.D. Listmann, F. Dai, B. Matthias, H. Ding, Motor-current-based estimation of cartesian contact forces and torques for robotic manipulators and its application to force control, IEEE Trans. Autom. Sci. Eng. 15 (2) (2018) 879–886, doi:10.1109/tase.2017.2691136.

[3] A. Stolt, F.B. Carlson, M.M.G. Ardakani, I. Lundberg, A. Robertsson, R. Johansson, Sensorless friction-compensated passive lead-through programming for industrial robots, in: 2015 IEEE/RSJ International Conference on Intelligent Robots and Systems (IROS), IEEE, 2015, doi:10.1109/iros.2015.7353870.

[4] M. Capurso, M.M.G. Ardakani, R. Johansson, A. Robertsson, P. Rocco, Sensorless kinesthetic teaching of robotic manipulators assisted by observer-based force control, in: 2017 IEEE International Conference on Robotics and Automation (ICRA), IEEE, 2017, doi:10.1109/icra.2017.7989115.

[5] A. Luca, A. Albu-Schaffer, S. Haddadin, G. Hirzinger, Collision detection and safe reaction with the DLR-III lightweight manipulator arm, in: 2006 IEEE/RSJ International Conference on Intelligent Robots and Systems, IEEE, 2006, doi:10.1109/iros.2006.282053.

[6] S. Haddadin, A. Albu-Schaffer, A. De Luca, G. Hirzinger, Collision detection and reaction: a contribution to safe physical human-robot interaction, in: 2008 IEEE/RSJ International Conference on Intelligent Robots and Systems, IEEE, 2008, doi:10.1109/iros.2008.4650764.

[7] B. Yao, Z. Zhou, L. Wang, W. Xu, Q. Liu, Sensor-less external force detection for industrial manipulators to facilitate physical human-robot interaction, J. Mech. Sci. Technol. 32 (10) (2018) 4909–4923, doi:10.1007/s12206-018-0939-5.

[8] C.W. Musser, Strain wave gearing, 1959.

[9] C.J. Seeton, Viscosity–temperature correlation for liquids, Tribol. Lett. 22 (1) (2006) 67–78, doi:10.1007/s11249-006-9071-2.

[10] A.C. Bittencourt, P. Axelsson, Y. Jung, T. Brogårdh, Modeling and identification of wear in a robot joint under temperature uncertainties, IFAC Proc. Vol. 44 (1) (2011) 10293–10299, doi:10.3182/20110828-6-it-1002.01078.

[11] H. Olsson, K.J. Åström, C.C. de Wit, M. Gäfvert, P. Lischinsky, Friction models and friction compensation, Eur. J. Control 4 (3) (1998) 176–195, doi:10.1016/s0947-3580(98)70113-x.

[12] C.C. de Wit, H. Olsson, K.J. Astrom, P. Lischinsky, A new model for control of systems with friction, IEEE Trans. Autom. Control 40 (3) (1995) 419–425, doi:10.1109/9.376053.

[13] V. Lampaert, F. Al-Bender, J. Swevers, A generalized Maxwell-Slip friction model appropriate for control purposes, 2003 IEEE International Workshop on Workload Characterization (IEEE Cat. No.03EX775), IEEE, 2003, doi:10.1109/phycon.2003.1237071.

[14] F. Al-Bender, V. Lampaert, J. Swevers, The generalized Maxwell-Slip model: anovel model for friction simulation and compensation, IEEE Trans. Autom Control 50 (11) (2005) 1883–1887, doi:10.1109/TAC.2005.858676.

[15] C. Preissner, T.J. Royston, D. Shu, A high-fidelity harmonic drive model, J. Dyn. Syst. Meas. Control 134 (1) (2012) 011002, doi:10.1115/1.4005041.

[16] T. Tjahjowidodo, F. Al-Bender, H. Van Brussel, Theoretical modelling and experimental identification of nonlinear torsional behaviour in harmonic drives, Mechatronics 23 (5) (2013) 497–504, doi:10.1016/j.mechatronics.2013.04.002.

[17] E. Madsen, O.S. Rosenlund, D. Brandt, X. Zhang, Model-based on-line estimation of time-varying nonlinear joint stiffness on an e-series universal robots manipulator, in: 2019 International Conference on Robotics and Automation (ICRA), IEEE, 2019, doi:10.1109/icra.2019.8793935.

[18] E. Madsen, O.S. Rosenlund, D. Brandt, X. Zhang, Comprehensive modeling and identification of nonlinear joint dynamics for collaborative industrial robot manipulators, Control Eng. Pract. 101 (2020) 104462, doi:10.1016/j.conengprac.2020.104462.

[19] H. Dong, T. Chen, D. Wang, B. Dong, Kinematic model of harmonic drive in robot joints with input eccentricity error, in: V. Arakelian, P. Wenger (Eds.), ROMANSY 22 – Robot Design, Dynamics and Control, Springer International Publishing, Cham, 2019, pp. 134–140.

[20] I. Nilkhamhang, A. Sano, Adaptive compensation of a linearly-parameterized GMS friction model with parameter projection, in: Proceedings of the 45th IEEE Conference on Decision and Control, IEEE, 2006, doi:10.1109/cdc.2006.377695.

[21] I. Nilkhamhang, A. Sano, Model-based adaptive friction compensation for accurate position control, in: 2008 47th IEEE Conference on Decision and Control, IEEE, 2008, doi:10.1109/cdc.2008.4739109.

[22] S. Grami, P. Bigras, Identification of the GMS friction model based on a robust adaptive observer, Int. J. Model. Ident. Control 5 (4) (2008) 297, doi:10.1504/ijmic.2008.023514.

[23] R. Marine, G.L. Santosuosso, P. Tomei, Robust adaptive observers for nonlinear systems with bounded disturbances, IEEE Trans. Autom. Control 45 (6) (2001) 967–972, doi:10.1109/9.928609.

[24] S. Grami, H. Aissaoui, Filtering approaches for online identification of GMS friction model, in: 2011 IEEE EUROCON - International Conference on Computer as a Tool, IEEE, Lisbon, Portugal, 2011, doi:10.1109/eurocon.2011.5929150.

[25] A. Amthor, S. Zschaeck, C. Ament, High precision position control using an adaptive friction compensation approach, IEEE Trans. Autom. Control 55 (1) (2010) 274–278, doi:10.1109/tac.2009.2036307.

[26] S. Zschack, S. Buchner, A. Amthor, C. Ament, Maxwell Slip based adaptive friction compensation in high precision applications, in: IECON 2012 - 38th Annual Conference on IEEE Industrial Electronics Society, IEEE, 2012, doi:10.1109/iecon.2012.6388877.

[27] Z. Jamaludin, H.V. Brussel, J. Swevers, Design of a disturbance observer and model-based friction feedforward to compensate quadrant glitches, in: Motion and Vibration Control, Springer Netherlands, 2009, pp. 143–154.

[28] H.K. Khalil, L. Praly, High-gain observers in nonlinear feedback control, Int. J. Robust Nonlinear Control 24 (6) (2013) 993–1015, doi:10.1002/rnc.3051.

[29] M.W. Spong, Modelling and control of elastic joint robots, J. Dyn. Syst. Meas. Control 109 (4) (1987) 310–319.

[30] L. Gao, J. Yuan, Z. Han, S. Wang, N. Wang, A friction model with velocity, temperature and load torque effects for collaborative industrial robot joints, in: 2017 IEEE/RSJ International Conference on Intelligent Robots and Systems (IROS), IEEE, Vancouver, BC, Canada, 2017, pp. 3027–3032, doi:10.1109/iros.2017.8206141.

[31] A.C. Bittencourt, E. Wernholt, S. Sander-Tavallaey, T. Brogårdh, An extended friction model to capture load and temperature effects in robot joints, in: 2010 IEEE/RSJ International Conference on Intelligent Robots and Systems, IEEE, Taipei, Taiwan, 2010, pp. 6161–6167, doi:10.1109/IROS.2010.5650358.

[32] P. Hamon, M. Gautier, P. Garrec, Dynamic identification of robots with a dry friction model depending on load and velocity, in: 2010 IEEE/RSJ International Conference on Intelligent Robots and Systems, IEEE, Taipei, Taiwan, 2010, pp. 6187–6193, doi:10.1109/IROS.2010.5649189.

[33] A.C. Bittencourt, S. Gunnarsson, Static friction in a robot joint—modeling and identification of load and temperature effects, J. Dyn. Syst. Meas. Control 134 (5) (2012), doi:10.1115/1.4006589.

[34] M.N. Nevmerzhitskiy, B.S. Notkin, A.V. Vara, K.V. Zmeu, Friction model of industrial robot joint with temperature correction by example of KUKA KR10, J. Robot. 2019 (2019) 1–11, doi:10.1155/2019/6931563.

[35] D.D. Rizos, S.D. Fassois, Presliding friction identification based upon the Maxwell Slip model structure, Chaos 14 (2) (2004) 431–445, doi:10.1063/1.1755178.

[36] P.M. Sammons, L. Ma, K. Embry, L.H. Armstrong, D.A. Bristow, R.G. Landers, Modeling and compensation of backlash and harmonic drive-induced errors in robotic manipulators, Volume 2: Processing, American Society of Mechanical Engineers, 2014, doi:10.1115/msec2014-4123.

[37] C. Zou, T. Tao, G. Jiang, P. Zeng, H. Du, Measurement and modeling of kinematic error and clearance in harmonic drives, in: Proceedings of the 2015 Joint International Mechanical, Electronic and Information Technology Conference, Atlantis Press, Chongqing, China, 2015, pp. 102–109, doi:10.2991/jimet-15.2015.20.

[38] A. Wahrburg, S. Klose, D. Clever, T. Groth, S. Moberg, J. Styrud, H. Ding, Modeling speed-, load-, and position-dependent friction effects in strain wave gears, in: 2018 IEEE International Conference on Robotics and Automation (ICRA), IEEE, 2018, doi:10.1109/icra.2018.8461043.

[39] A.D. Rosas, V.K. Velazquez, F.L. Olivares, T.A. Camacho, I. Williams, Methodology to assess quality of estimated disturbances in active disturbance rejection control structure for mechanical system, ISA Trans. 70 (2017) 238–247, doi:10.1016/j.isatra.2017.05.013.

[40] A. Savitzky, M.J.E. Golay, Smoothing and differentiation of data by simplified least squares procedures, Anal. Chem. 36 (8) (1964) 1627–1639, doi:10.1021/ac60214a047.

[41] A. Mohammadi, M. Tavakoli, H.J. Marquez, F. Hashemzadeh, Nonlinear disturbance observer design for robotic manipulators, Control Eng. Pract. 21 (3) (2013) 253–267, doi:10.1016/j.conengprac.2012.10.008.
[42] J.-J.E. Slotine, W. Li, Applied Nonlinear Control, Pearson Education, Upper Saddle River, New Jersey, 1991.
[43] G. Tao, P.V. Kokotovic, Adaptive Control of Systems with Actuator and Sensor Nonlinearities, John Wiley & Sons, 1996.
[44] K.J. Åström, B. Wittenmark, Adaptive Control, second ed., Prentice Hall, 1994.

Chapter 7

Conclusions & Outlook

This industrial PhD research project addresses the overall issue of obtaining accurate estimates of the dynamics for collaborative industrial robots under conditions of mechanical wear and temperature changes. Furthermore, the project addresses how the dynamics can be used for improving the robot performance. This thesis discusses challenges related to robot dynamics modeling, identification, and adaptive estimation and control. The thesis seeks to fill the gap between robotics research in academia and industry by using a real collaborative industrial robot and providing solutions that are experimentally validated and useful for industrial robots in general.

The first contribution of the research is related to adaptive estimation of the robot joint stiffness. A recursive least squares-based estimation strategy is used in combination with the rotor dynamics model to estimate the nonlinear stiffness characteristics online without the need of additional sensing hardware or mechanical fixture of the end-effector. The estimation strategy works for arbitrary manipulator configurations. Within 10 seconds, the stiffness of the UR5e base joint is estimated with an accuracy of 95.2 %. The accuracy of the parameter estimate is directly related to the accuracy of the joint dynamics model, which led to the second contribution.

The second contribution is related to the modeling and identification of the robot joint dynamics. The steady-state friction torque of strain-wave transmissions is known to depend on angular velocity, load torque, and lubricant temperature. Furthermore, strain-wave transmissions are known to experience nonlinear flexibility, hysteresis, and kinematic error. These characteristics are analyzed and modeled based on experimental observations. A model for the dependency of friction on temperature is proposed, which is linear in parameters – hence facilitates identification – and provides increased accuracy compared to existing works. A linear regression procedure is developed for the Generalized Maxwell-Slip (GMS) friction model, which improves the torque prediction accuracy compared to existing

procedures. The hysteresis characteristics is observed to depend on the joint angular position. This phenomenon is not previously described, although rendered probable from theoretical studies. The GMS friction model is extended (E-GMS) to describe in a combined framework; 1) the dependency of the hysteresis characteristics on angular position, and 2) the dependency of friction on the load torque. The torque prediction accuracy is improved by a factor of 2.1 and incorporating the model in the feedforward controller results in the tracking error being reduced by a factor of 1.5. Additionally, discontinuities in the angular velocity is overcome, which is relevant in feedback linearizing control strategies.

Since the gravitational and inertial effects contributes significantly to the actuator torques, the third contribution is related to calibration of the robot dynamics including masses, center-of-mass positions, and inertial components. The set of physical parameters is reduced to a minimal set of base parameters that uniquely defines the robot dynamics. The Universal Robots collaborative robots comprise two absolute rotary encoders per joint – one at each side of the strain-wave transmission. This fact is utilized to effectively compensate joint flexibility and nonlinear rotor dynamics effects and reduce the uncertainty and bias of the parameter estimates. The model accuracy is improved by 16.5 % to 28.5 % depending on the evaluation trajectory.

The last contribution is related to the adaptive control for robots under the conditions of wear and friction model-based temperature compensation inaccuracies. These conditions leads to unmodeled Coulomb and viscous friction. A gradient-based adaptive parameter estimation scheme is implemented based on the E-GMS dynamic friction model. The torque prediction accuracy is improved 84 % and the tracking error is reduced by 20 % compared to a friction model that is off but complies with the safety system.

7.1 Summary of Contributions

The main contributions of the research project is summarized in the following.

1) A new **adaptive joint stiffness estimation** procedure is proposed and validated experimentally on a Universal Robots UR5e collaborative industrial robot. Utilizing the two absolute encoders in each joint, the method demonstrates that the robot joint stiffness can be adaptively estimated without the need for fixing the end-effector – common for

existing joint stiffness estimation strategies. Within 10 seconds, the stiffness is estimated with an NRMSE accuracy of 95.2 %.

2) A comprehensive **joint dynamics model** is proposed based on a series of experiments using the Universal Robots UR5e robot. The model combines a set of nonlinear sub-models of flexibility, kinematic error, hysteresis, and dynamic friction with static dependencies on angular velocity, load torque, and temperature. The hysteresis characteristics are observed to depend on the angular position, which is not previously described albeit rendered plausible theoretically. An extension to the Generalized Maxwell-Slip friction model (E-GMS) is proposed to describe in a combined framework the dependencies of; 1) hysteresis on angular position and 2) friction on load torque. E-GMS based feedforward control yield improvements of; 1) torque prediction accuracy by a factor of 2.1 and 2) tracking error by a factor of 1.5.

3) A **robot dynamics calibration** procedure is proposed to increase the accuracy of the robot dynamics model. The double joint encoder setup of the Universal Robot manipulators is utilized for compensating nonlinear rotor dynamics and joint flexibility to reduce bias and uncertainty in the parameter estimates. The model accuracy is improved by 16.5 % to 28.5 % depending on the evaluation trajectory.

4) An **E-GMS based adaptive feedforward controller** is designed to compensate the effects of wear and friction model-based temperature compensation inaccuracies. The torque prediction accuracy is improved by 84 % and the tracking error is improved by 20 % compared to a non-adaptive E-GMS model which is known to be off but still within the limits of safety.

7.2 Outlook & Perspectives

The performance improvement for collaborative industrial robots by means of dynamic modeling, identification, and adaptive estimation and control is an open field for research. Some relevant extensions of the research presented in this thesis are summarized in the following.

1) **Predictive maintenance.** The stiffness and the level of friction of a strain-wave transmission are known to be related to the mechanical

wear and tear. Thus, if accurate estimates of the stiffness and friction are available at all times, the level of wear can be continuously predicted provided the relations between stiffness, friction, and wear are known. Thus, an extension of the presented research could involve the development of predictive maintenance strategies. Unnecessary maintenance actions are thus avoided in contrast to *preventive scheduled maintenance*, which is determined from the estimated lifespan of robot components with considerable margins.

2) **Model-based control.** The stiffness of robot joints is used in the decoupling and linearizing control strategies of flexible-joint robot manipulators as elaborated in Chapter 2. Adaptive stiffness estimation combined with a feedback linearizing control strategy based on a flexible-joint robot model could potentially ensure a consistently good controller performance despite gradual change of flexibility from wear.

3) **Adaptive payload estimation.** For the Universal Robots manipulators, the payload inertial properties are specified by the operator, possibly with the help of the *payload and center of gravity estimation wizard*. A well-calibrated dynamic model of the robot may admit accurate adaptive estimation of the payload inertial properties to use for control or online sanity checking of the user-provided payload parameters.

Bibliography

[1] Lars Westerlund. *The Extended Arm of Man — A History of the Industrial Robot*. Informationsförlaget, Stockholm, 2000. ISBN 9789177364672.

[2] IFR. World Robotics 2019 Industrial Robots. Report, International Federation of Robotics, October 2019.

[3] ISO 10218-1:2011 - Robots and robotic devices – Safety requirements for industrial robots – Part 1: Robots, 2011.

[4] ISO 10218-2:2011 - Robots and robotic devices – Safety requirements for industrial robots – Part 2: Robot systems and integration, 2011.

[5] ISO 13849-1:2015 - Safety of machinery – Safety-related parts of control systems – Part 1: General principles for design, 2015.

[6] ISO 13849-2:2015 - Safety of machinery – Safety-related parts of control systems – Part 2: Validation, 2015.

[7] Alessandro Luca, Alin Albu-Schaffer, Sami Haddadin, and Gerd Hirzinger. Collision Detection and Safe Reaction with the DLR-III Lightweight Manipulator Arm. In *2006 IEEE/RSJ International Conference on Intelligent Robots and Systems*. IEEE, oct 2006. doi: 10.1109/iros.2006.282053.

[8] Sami Haddadin, Alin Albu-Schaffer, Alessandro De Luca, and Gerd Hirzinger. Collision Detection and Reaction: A Contribution to Safe Physical Human-Robot Interaction. In *2008 IEEE/RSJ International Conference on Intelligent Robots and Systems*. IEEE, sep 2008. doi: 10.1109/iros.2008.4650764.

[9] Bitao Yao, Zude Zhou, Lihui Wang, Wenjun Xu, and Quan Liu. Sensor-less external force detection for industrial manipulators to facilitate physical human-robot interaction. *Journal of Mechanical Science and Technology*, 32(10):4909–4923, oct 2018. doi: 10.1007/s12206-018-0939-5.

[10] H. Olsson, K. J. Åström, C. Canudas de Wit, M. Gäfvert, and P. Lischinsky. Friction Models and Friction Compensation. *European Journal of Control*, 4(3):176–195, jan 1998. doi: 10.1016/s0947-3580(98)70113-x.

[11] B. Bona and M. Indri. Friction Compensation in Robotics: an Overview. In *Proceedings of the 44th IEEE Conference on Decision and Control*, pages 4360–4367, Seville, Spain, December 2005. IEEE. doi: 10.1109/cdc.2005.1582848.

[12] Andreas Stolt, Fredrik Bagge Carlson, M. Mahdi Ghazaei Ardakani, Ivan Lundberg, Anders Robertsson, and Rolf Johansson. Sensorless friction-compensated passive lead-through programming for industrial robots. In *2015 IEEE/RSJ International Conference on Intelligent Robots and Systems (IROS)*. IEEE, sep 2015. doi: 10.1109/iros.2015.7353870.

[13] Matteo Ragaglia, Andrea Maria Zanchettin, Luca Bascetta, and Paolo Rocco. Accurate sensorless lead-through programming for lightweight robots in structured environments. *Robotics and Computer-Integrated Manufacturing*, 39:9–21, jun 2016. doi: 10.1016/j.rcim.2015.11.002.

[14] Emil Madsen, Oluf Skov Rosenlund, David Brandt, and Xuping Zhang. Model-Based On-line Estimation of Time-Varying Nonlinear Joint Stiffness on an e-Series Universal Robots Manipulator. In *2019 International Conference on Robotics and Automation (ICRA)*. IEEE, may 2019. doi: 10.1109/icra.2019.8793935.

[15] A. Jubien, M. Gautier, and A. Janot. Dynamic identification of the Kuka LWR robot using motor torques and joint torque sensors data. *IFAC Proceedings Volumes*, 47(3): 8391–8396, 2014. doi: 10.3182/20140824-6-za-1003.01079.

[16] Le Ma, Patrick Bazzoli, Patrick M. Sammons, Robert G. Landers, and Douglas A. Bristow. Modeling and calibration of high-order joint-dependent kinematic errors for industrial robots. *Robotics and Computer-Integrated Manufacturing*, 50:153–167, April 2018. doi: 10.1016/j.rcim.2017.09.006.

[17] Masayoshi Iwatani and Ryo Kikuuwe. An identification procedure for rate-dependency of friction in robotic joints with limited motion ranges. *Mechatronics*, 36: 36–44, jun 2016. doi: 10.1016/j.mechatronics.2016.04.002.

[18] A. Albu-Schäffer and G. Hirzinger. Parameter identification and passivity based joint control for a 7 DOF torque controlled light weight robot. In *Proceedings 2001 ICRA. IEEE International Conference on Robotics and Automation (Cat. No.01CH37164)*, pages 2852–2858, Seoul, South Korea, May 2001. IEEE. doi: 10.1109/robot.2001.933054.

[19] C. W. Kennedy and J. P. Desai. Modeling and Control of the Mitsubishi PA-10 Robot Arm Harmonic Drive System. *IEEE/ASME Transactions on Mechatronics*, 10(3):263–274, jun 2005. doi: 10.1109/tmech.2005.848290.

[20] Timothy D. Tuttle. Understanding and Modeling the Behavior of a Harmonic Drive Gear Transmission. Technical Report AI-TR 1365, MIT Artificial Intelligence Labratory, 1992.

[21] H. D. Taghirad and P. R. Bélanger. An Experimental Study on Modelling and Identification of Harmonic Drive Systems. In *Proceedings of 35th IEEE Conference on Decision and Control*, pages 4725–4730, Kobe, Japan, December 1996. IEEE. doi: 10.1109/CDC.1996.577625.

[22] A. R. Lansdown, A. L. Price, and Jorn Larsen-Basse. Materials to Resist Wear—A Guide to their Selection and Use. *Journal of Tribology*, 109(2):379–380, apr 1987. doi: 10.1115/1.3261375.

[23] T. W. Nye. Harmonic Drives: Determining Wear Life Based on Stiffness Considerations. In *Proc. of the International Power Transmission and Gearing Conference*, volume 2, pages 867–877, Chicago, USA, April 1989. American Society of Mechanical Engineers.

[24] Michael R. Johnson, Russ Gehling, and Ray Head. Failure of Harmonic Gears in a Two-Axis Gimbal for the Mars Reconnaissance Orbiter Spacecraft. In *Proceedings of the 38th Aerospace Mechanisms Symposium*, Langley Research Center, May 2006. URL https://ntrs.nasa.gov/archive/nasa/casi.ntrs.nasa.gov/20060028245.pdf.

[25] J. Mobley and J. Parker. Harmonic Drive™Gear Material Selection and Life Testing. In *Proceedings of the 41th Aerospace Mechanisms Symposium*, Jet Propulsion Labratory, May 2012. URL http://esmats.eu/amspapers/pastpapers/pdfs/2012/mobley.pdf.

[26] Emyr W. Roberts, Paul Bridgeman, Markus Jansson, Matthias Schulke, and Adam Tvaruzka. The Performance and Life of Fluid-Lubricated Harmonic Drive® Gears. In *16th European Space Mechanisms and Tribology Symposium*, volume 737, Bilbao, Spain, September 2015. 16th European Space Mechanisms and Tribology Symposium. ISBN 9789292213022.

[27] Caixia Zhang, Zhiqiong Song, Zhifeng Liu, Qiang Cheng, Yongsheng Zhao, Congbin Yang, and Mengmeng Liu. Wear mechanism of flexspline materials regulated by novel amorphous/crystalline oxide form evolution at frictional interface. *Tribology International*, 135:335–343, jul 2019. doi: 10.1016/j.triboint.2019.03.023.

[28] Christopher J. Seeton. Viscosity–temperature correlation for liquids. *Tribology Letters*, 22(1):67–78, apr 2006. doi: 10.1007/s11249-006-9071-2.

[29] Liming Gao, Jianjun Yuan, Zhedong Han, Shuai Wang, and Ning Wang. A friction model with velocity, temperature and load torque effects for collaborative industrial robot joints. In *2017 IEEE/RSJ International Conference on Intelligent Robots and Systems (IROS)*, pages 3027–3032, Vancouver, BC, Canada, September 2017. IEEE. doi: 10.1109/iros.2017.8206141.

[30] Maged Iskandar and Sebastian Wolf. Dynamic friction model with thermal and load dependency: modeling, compensation, and external force estimation. In *2019 International Conference on Robotics and Automation (ICRA)*. IEEE, may 2019. doi: 10.1109/icra.2019.8794406.

[31] Maksim N. Nevmerzhitskiy, Boris S. Notkin, Andrey V. Vara, and Konstantin V. Zmeu. Friction Model of Industrial Robot Joint with Temperature Correction by Example of KUKA KR10. *Journal of Robotics*, 2019:1–11, January 2019. doi: 10.1155/2019/6931563.

[32] Mark W. Spong. Modelling and Control of Elastic Joint Robots. *Journal of Dynamic Systems, Measurement, and Control*, 109(4):310–319, December 1987.

[33] Mark Spong, Seth Hutchinson, and Mathukumalli Vidyasagar. *Robot Modeling and Control*. John Wiley & Sons Inc, 2005. ISBN 0471649902. URL https://www.ebook.de/de/product/5124811/mark_spong_seth_hutchinson_mathukumalli_vidyasagar_robot_modeling_and_control.html.

[34] Bruno Siciliano and Oussama Khatib, editors. *Springer Handbook of Robotics, 2nd Edition*. Springer-Verlag GmbH, 2016. ISBN 3319325523. URL `https://www.ebook.de/de/product/27988962/springer_handbook_of_robotics.html`.

[35] Christopher G. Atkeson, Chae H. An, and John M. Hollerbach. Estimation of Inertial Parameters of Manipulator Loads and Links. *The International Journal of Robotics Research*, 5(3):101–119, sep 1986. doi: 10.1177/027836498600500306.

[36] M. Gautier and W. Khalil. A direct determination of minimum inertial parameters of robots. In *Proceedings. 1988 IEEE International Conference on Robotics and Automation*, pages 1682–1687, Philadelphia, PA, USA, April 1988. IEEE Comput. Soc. Press. doi: 10.1109/robot.1988.12308.

[37] M. Gautier and W. Khalil. On the identification of the inertial parameters of robots. In *Proceedings of the 27th IEEE Conference on Decision and Control*. IEEE, 1988. doi: 10.1109/cdc.1988.194738.

[38] M. Gautier and W. Khalil. Direct calculation of minimum set of inertial parameters of serial robots. *IEEE Transactions on Robotics and Automation*, 6(3):368–373, June 1990. doi: 10.1109/70.56655.

[39] M. Gautier. Numerical calculation of the base inertial parameters of robots. In *Proceedings., IEEE International Conference on Robotics and Automation*, pages 1020–1025, Cincinnati, OH, USA, May 1990. IEEE Comput. Soc. Press. doi: 10.1109/robot.1990.126126.

[40] C. M. Pham and M. Gautier. Essential parameters of robots. In *[1991] Proceedings of the 30th IEEE Conference on Decision and Control*. IEEE, 1991. doi: 10.1109/cdc.1991.261862.

[41] Krzysztof Kozlowski. *Modelling and Identification in Robotics*. Springer London, 1998. doi: 10.1007/978-1-4471-0429-2.

[42] P. Poignet and M. Gautier. Comparison of weighted least squares and extended Kalman filtering methods for dynamic identification of robots. In *Proceedings 2000 ICRA. Millennium Conference. IEEE International Conference on Robotics and Automation. Symposia Proceedings (Cat. No.00CH37065)*. IEEE, 2000. doi: 10.1109/robot.2000.845296.

[43] M. Gautier and Ph. Poignet. Extended Kalman filtering and weighted least squares dynamic identification of robot. *Control Engineering Practice*, 9(12):1361–1372, December 2001. doi: 10.1016/s0967-0661(01)00105-8.

[44] G. Calafiore and M. Indri. Robust calibration and control of robotic manipulators. In *Proceedings of the 2000 American Control Conference. ACC (IEEE Cat. No.00CH36334)*. IEEE, 2000. doi: 10.1109/acc.2000.879552.

[45] Martin M. Olsen, Jan Swevers, and Walter Verdonck. Maximum Likelihood Identification of a Dynamic Robot Model: Implementation Issues. *The International Journal of Robotics Research*, 21(2):89–96, feb 2002. doi: 10.1177/027836402760475379.

[46] N. Ramdani and P. Poignet. Robust Dynamic Experimental Identification of Robots With Set Membership Uncertainty. *IEEE/ASME Transactions on Mechatronics*, 10(2): 253–256, apr 2005. doi: 10.1109/tmech.2005.844703.

[47] A. Janot, P. O. Vandanjon, and M. Gautier. Using robust regressions and residual analysis to verify the reliability of LS estimation: Application in robotics. In *2009 IEEE/RSJ International Conference on Intelligent Robots and Systems*. IEEE, oct 2009. doi: 10.1109/iros.2009.5354469.

[48] M. Gautier, A. Janot, and P. O. Vandanjon. DIDIM: A new method for the dynamic identification of robots from only torque data. In *2008 IEEE International Conference on Robotics and Automation*. IEEE, may 2008. doi: 10.1109/robot.2008.4543520.

[49] Maxime Gautier, Alexandre Janot, and Pierre-Olivier Vandanjon. A New Closed-Loop Output Error Method for Parameter Identification of Robot Dynamics. *IEEE Transactions on Control Systems Technology*, 21(2):428–444, mar 2013. doi: 10.1109/tcst.2012.2185697.

[50] Alexandre Janot, Maxime Gautier, Anthony Jubien, and Pierre Olivier Vandanjon. Comparison Between the CLOE Method and the DIDIM Method for Robots Identification. *IEEE Transactions on Control Systems Technology*, 22(5):1935–1941, sep 2014. doi: 10.1109/tcst.2014.2299544.

[51] Alexandre Janot, Pierre Olivier Vandanjon, and Maxime Gautier. An instrumental variable approach for rigid industrial robots identification. *Control Engineering Practice*, 25:85–101, April 2014. doi: 10.1016/j.conengprac.2013.12.009.

[52] Alexandre Janot, Pierre-Olivier Vandanjon, and Maxime Gautier. A Generic Instrumental Variable Approach for Industrial Robot Identification. *IEEE Transactions on Control Systems Technology*, 22(1):132–145, jan 2014. doi: 10.1109/tcst.2013.2246163.

[53] B. Bona and A. Curatella. Identification of Industrial Robot Parameters for Advanced Model-Based Controllers Design. In *Proceedings of the 2005 IEEE International Conference on Robotics and Automation*. IEEE, 2005. doi: 10.1109/robot.2005.1570355.

[54] Jan Swevers, Walter Verdonck, and Joris De Schutter. Dynamic Model Identification for Industrial Robots. *IEEE Control Systems*, 27(5):58–71, October 2007. doi: 10.1109/mcs.2007.904659.

[55] Nikolaos A. Bompos, Panagiotis K. Artemiadis, Apollon S. Oikonomopoulos, and Kostas J. Kyriakopoulos. Modeling, full identification and control of the mitsubishi PA-10 robot arm. In *2007 IEEE/ASME international conference on advanced intelligent mechatronics*. IEEE, 2007. doi: 10.1109/aim.2007.4412421.

[56] Zafer Bingül and Oğuzhan Karahan. Dynamic identification of Staubli RX-60 robot using PSO and LS methods. *Expert Systems with Applications*, 38(4):4136–4149, apr 2011. doi: 10.1016/j.eswa.2010.09.076.

[57] A. Janot, P. O. Vandanjon, and M. Gautier. Identification of 6 DOF Rigid Industrial Robots with the Instrumental Variable Method. *IFAC Proceedings Volumes*, 45(16): 1659–1664, July 2012. doi: 10.3182/20120711-3-be-2027.00058.

[58] Li Ding, Hongtao Wu, Yu Yao, and Yuxuan Yang. Dynamic Model Identification for 6-DOF Industrial Robots. *Journal of Robotics*, 2015:1–9, 2015. doi: 10.1155/2015/471478.

[59] Amirhossein H. Memar and Ehsan T. Esfahani. Modeling and Dynamic Parameter Identification of the SCHUNK Powerball Robotic Arm. In *Volume 5C: 39th Mechanisms and Robotics Conference*. American Society of Mechanical Engineers, aug 2015. doi: 10.1115/detc2015-47703.

[60] Peter Stueckelmaier, Martin Grotjahn, and Carsten Fraeger. Identification of the Inverse Dynamics of a Serial Robot for Robot Drive Control. In *10. ETG/GMM-Symposium Innovative Small Drives and Micro-Motor Systems*, Cologne, Germany, September 2015. VDE-Verlag. ISBN 9783800740727.

[61] Yvonne R. Stürz, Lukas M. Affolter, and Roy S. Smith. Parameter Identification of the KUKA LBR iiwa Robot Including Constraints on Physical Feasibility. *IFAC-PapersOnLine*, 50(1):6863–6868, jul 2017. doi: 10.1016/j.ifacol.2017.08.1208.

[62] Abdelkrim Bahloul, Sami Tliba, and Yacine Chitour. Dynamic Parameters Identification of an Industrial Robot: A Constrained Nonlinear WLS Approach. In *2018 26th Mediterranean Conference on Control and Automation (MED)*. IEEE, jun 2018. doi: 10.1109/med.2018.8442630.

[63] Claudio Roberto Gaz, Marco Cognetti, Alexander Antonio Oliva, Paolo Robuffo Giordano, and Alessandro De Luca. Dynamic Identification of the Franka Emika Panda Robot with Retrieval of Feasible Parameters Using Penalty-based Optimization. *IEEE Robotics and Automation Letters*, 4(4):4147–4154, July 2019. doi: 10.1109/lra.2019.2931248.

[64] Meryem Taghbalout, Jean François Antoine, and Gabriel Abba. Experimental Dynamic Identification of a YuMi Collaborative Robot. *IFAC-PapersOnLine*, 52(13):1168–1173, 2019. doi: 10.1016/j.ifacol.2019.11.354.

[65] Sergey A. Kolyubin, Anton S. Shiriaev, and Anthony Jubien. Refining Dynamics Identification for Co-Bots: Case Study on KUKA LWR4+. *IFAC-PapersOnLine*, 50(1):14626–14631, jul 2017. doi: 10.1016/j.ifacol.2017.08.1741.

[66] Zeeshan Shareef, Pouya Mohammadi, and Jochen Steil. Improving the Inverse Dynamics Model of the KUKA LWR IV+ using Independent Joint Learning. *IFAC-PapersOnLine*, 49(21):507–512, 2016. doi: 10.1016/j.ifacol.2016.10.653.

[67] Claudio Gaz and Alessandro De Luca. Payload estimation based on identified coefficients of robot dynamics — With an application to collision detection. In *2017 IEEE/RSJ International Conference on Intelligent Robots and Systems (IROS)*, pages 3033–3040, Vancouver, BC, Canada, September 2017. IEEE. doi: 10.1109/iros.2017.8206142.

[68] Stig Moberg and Sven Hanssen. On Feedback Linearization for Robust Tracking Control of Flexible Joint Robots. *IFAC Proceedings Volumes*, 41(2):12218–12223, July 2008. doi: 10.3182/20080706-5-kr-1001.02069.

[69] André Carvalho Bittencourt and Svante Gunnarsson. Static Friction in a Robot Joint—Modeling and Identification of Load and Temperature Effects. *Journal of Dynamic Systems, Measurement, and Control*, 134(5), July 2012. doi: 10.1115/1.4006589.

[70] Luca Simoni, Manuel Beschi, Giovanni Legnani, and Antonio Visioli. Friction modeling with temperature effects for industrial robot manipulators. In *2015 IEEE/RSJ International Conference on Intelligent Robots and Systems (IROS)*, pages 3524–3529, Hamburg, Germany, September 2015. IEEE. doi: 10.1109/iros.2015.7353869.

[71] Fredrik Bagge Carlson, Anders Robertsson, and Rolf Johansson. Modeling and Identification of Position and Temperature Dependent Friction Phenomena without Temperature Sensing. In *2015 IEEE/RSJ International Conference on Intelligent Robots and Systems (IROS)*, pages 3045–3051, Hamburg, Germany, September 2015. IEEE. doi: 10.1109/IROS.2015.7353797.

[72] Sebastian Wolf and Maged Iskandar. Extending a Dynamic Friction Model with Nonlinear Viscous and Thermal Dependency for a Motor and Harmonic Drive Gear. In *2018 IEEE International Conference on Robotics and Automation (ICRA)*. IEEE, may 2018. doi: 10.1109/icra.2018.8460613.

[73] Sebastian Wolf, Oliver Eiberger, and Gerd Hirzinger. The DLR FSJ: Energy based design of a variable stiffness joint. In *2011 IEEE International Conference on Robotics and Automation*. IEEE, may 2011. doi: 10.1109/icra.2011.5980303.

[74] V. Lampaert, F. Al-Bender, and J. Swevers. A generalized Maxwell-slip friction model appropriate for control purposes. In *2003 IEEE International Workshop on Workload Characterization (IEEE Cat. No.03EX775)*. IEEE, 2003. doi: 10.1109/phycon.2003.1237071.

[75] F. Al-Bender, V. Lampaert, and J. Swevers. The Generalized Maxwell-Slip Model: A Novel Model for Friction Simulation and Compensation. *IEEE Transactions on Automatic Control*, 50(11):1883–1887, November 2005. doi: 10.1109/TAC.2005.858676.

[76] Curt Preissner, Thomas J. Royston, and Deming Shu. A High-Fidelity Harmonic Drive Model. *Journal of Dynamic Systems, Measurement, and Control*, 134(1):011002, January 2012. doi: 10.1115/1.4005041.

[77] T. Tjahjowidodo, F. Al-Bender, and H. Van Brussel. Theoretical Modelling and Experimental Identification of Nonlinear Torsional Behaviour in Harmonic Drives. *Mechatronics*, 23(5):497–504, aug 2013. doi: 10.1016/j.mechatronics.2013.04.002.

[78] C. Canudas de Wit, H. Olsson, K. J. Astrom, and P. Lischinsky. A new model for control of systems with friction. *IEEE Transactions on Automatic Control*, 40(3):419–425, mar 1995. doi: 10.1109/9.376053.

[79] V. Lampaert, J. Swevers, and F. Al-Bender. Comparison of model and non-model based friction compensation techniques in the neighbourhood of pre-sliding friction. In *Proceedings of the 2004 American Control Conference*, pages 1121–1126, Boston, MA, USA, June 2004. IEEE. doi: 10.23919/acc.2004.1386722.

[80] W. Seyfferth, A. J. Maghzal, and J. Angeles. Nonlinear modeling and parameter identification of harmonic drive robotic transmissions. In *Proceedings of 1995 IEEE International Conference on Robotics and Automation*. IEEE, 1995. doi: 10.1109/robot.1995.525714.

[81] T. D. Tuttle and W. P. Seering. A Nonlinear Model of a Harmonic Drive Gear Transmission. *IEEE Transactions on Robotics and Automation*, 12(3):368–374, June 1996. doi: 10.1109/70.499819.

[82] Nenad M. Kircanski and Andrew A. Goldenberg. An Experimental Study of Nonlinear Stiffness, Hysteresis, and Friction Effects in Robot Joints with Harmonic Drives and Torque Sensors. *The International Journal of Robotics Research*, 16(2):214–239, April 1997. doi: 10.1177/027836499701600207.

[83] R. Dhaouadi, F. H. Ghorbel, and P. S. Gandhi. A new dynamic model of hysteresis in harmonic drives. *IEEE Transactions on Industrial Electronics*, 50(6):1165–1171, dec 2003. doi: 10.1109/tie.2003.819661.

[84] Michael Ruderman and Torsten Bertram. Feed-forward compensation of hysteresis compliance using inverse Preisach model. *IFAC Proceedings Volumes*, 42(6):243–248, 2009. doi: 10.3182/20090616-3-il-2002.00042.

[85] Michael Ruderman and Torsten Bertram. Modeling and observation of hysteresis lost motion in elastic robot joints. *IFAC Proceedings Volumes*, 45(22):13–18, 2012. doi: 10.3182/20120905-3-hr-2030.00061.

[86] Michael Ruderman, Torsten Bertram, and Makoto Iwasaki. Modeling, observation, and control of hysteresis torsion in elastic robot joints. *Mechatronics*, 24(5):407–415, aug 2014. doi: 10.1016/j.mechatronics.2014.02.009.

[87] Michael Ruderman and Makoto Iwasaki. On identification and sensorless control of nonlinear torsion in elastic robotic joints. In *IECON 2014 - 40th Annual Conference of the IEEE Industrial Electronics Society*. IEEE, oct 2014. doi: 10.1109/iecon.2014.7048909.

[88] Michael Ruderman and Makoto Iwasaki. Sensorless Torsion Control of Elastic-Joint Robots With Hysteresis and Friction. *IEEE Transactions on Industrial Electronics*, 63(3):1889–1899, mar 2016. doi: 10.1109/tie.2015.2453415.

[89] Michael Ruderman. On Stability of Virtual Torsion Sensor for Control of Flexible Robotic Joints with Hysteresis. *Robotica*, pages 1–14, sep 2019. doi: 10.1017/s0263574719001358.

[90] P. S. Gandhi and F. Ghorbel. High-speed precision tracking with harmonic drive systems using integral manifold control design. *International Journal of Control*, 78(2):112–121, jan 2005. doi: 10.1080/00207170500036225.

[91] Makoto Iwasaki and Hiroyuki Nakamura. Vibration Suppression for Angular Transmission Errors in Harmonic Drive Gearings and Application to Industrial Robots. *IFAC Proceedings Volumes*, 47(3):6831–6836, 2014. doi: 10.3182/20140824-6-za-1003.00659.

[92] Makoto Iwasaki, Masafumi Yamamoto, Hiromu Hirai, Yoshifumi Okitsu, Kozo Sasaki, and Toshio Yajima. Modeling and compensation for angular transmission error of harmonic drive gearings in high precision positioning. In *2009 IEEE/ASME International Conference on Advanced Intelligent Mechatronics*. IEEE, jul 2009. doi: 10.1109/aim.2009.5229935.

[93] Federico Gravagno, Victor Hugo Mucino, and Ettore Pennestrì. Influence of wave generator profile on the pure kinematic error and centrodes of harmonic drive. *Mechanism and Machine Theory*, 104:100–117, oct 2016. doi: 10.1016/j.mechmachtheory.2016.05.005.

[94] Hassan K. Khalil. *Nonlinear Systems*. Prentice Hall, Inc., Upper Saddle River, NJ, third edition, 2001.

[95] Jean-Jacques E. Slotine and Weiping Li. *Applied Nonlinear Control*. Pearson Education, Upper Saddle River, New Jersey, 1991. ISBN 978-0130408907. URL `https://www.ebook.de/de/product/3659352/jean_jacques_slotine_applied_nonlinear_control.html`.

[96] C. Canudas de Wit and P. Lischinsky. Adaptive friction compensation with partially known dynamic friction model. *International Journal of Adaptive Control and Signal Processing*, 11(1):65–80, December 1998.

[97] L. Le Tien, A. Albu-Schäffer, A. De Luca, and G. Hirzinger. Friction observer and compensation for control of robots with joint torque measurement. In *2008 IEEE/RSJ International Conference on Intelligent Robots and Systems*, pages 3789–3795, Nice, France, September 2008. IEEE. doi: 10.1109/iros.2008.4651049.

[98] Luc Le-Tien and Alin Albu-Schaffer. Adaptive friction compensation in trajectory tracking control of DLR medical robots with elastic joints. In *2012 IEEE/RSJ International Conference on Intelligent Robots and Systems*. IEEE, oct 2012. doi: 10.1109/iros.2012.6385609.

[99] Zhaopeng Chen, Neal Y. Lii, Thomas Wimböck, Shaowei Fan, and Hong Liu. Experimental Evaluation of Cartesian and Joint Impedance Control with Adaptive Friction Compensation for the Dexterous Robot Hand DLR-Hit II. *International Journal of Humanoid Robotics*, 08(04):649–671, dec 2011. doi: 10.1142/s0219843611002605.

[100] P. Tomei. Robust adaptive friction compensation for tracking control of robot manipulators. *IEEE Transactions on Automatic Control*, 45(11):2164–2169, 2000. doi: 10.1109/9.887661.

[101] Itthisek Nilkhamhang and Akira Sano. Adaptive Compensation of a Linearly-Parameterized GMS Friction Model with Parameter Projection. In *Proceedings of the 45th IEEE Conference on Decision and Control*. IEEE, 2006. doi: 10.1109/cdc.2006.377695.

[102] Itthisek Nilkhamhang and Akira Sano. Model-based adaptive friction compensation for accurate position control. In *2008 47th IEEE Conference on Decision and Control*. IEEE, 2008. doi: 10.1109/cdc.2008.4739109.

[103] Said Grami and Pascal Bigras. Identification of the GMS friction model based on a robust adaptive observer. *International Journal of Modelling, Identification and Control*, 5 (4):297, 2008. doi: 10.1504/ijmic.2008.023514.

[104] R. Marine, G. L. Santosuosso, and P. Tomei. Robust adaptive observers for nonlinear systems with bounded disturbances. *IEEE Transactions on Automatic Control*, 45(6): 967–972, jun 2001. doi: 10.1109/9.928609.

[105] S. Grami and H. Aissaoui. Filtering approaches for online identification of GMS friction model. In *2011 IEEE EUROCON - International Conference on Computer as a Tool*, Lisbon, Portugal, April 2011. IEEE. doi: 10.1109/eurocon.2011.5929150.

[106] A. Amthor, S. Zschaeck, and C. Ament. High Precision Position Control Using an Adaptive Friction Compensation Approach. *IEEE Transactions on Automatic Control*, 55(1):274–278, jan 2010. doi: 10.1109/tac.2009.2036307.

[107] Stephan Zschack, Steffen Buchner, Arvid Amthor, and Christoph Ament. Maxwell Slip based adaptive friction compensation in high precision applications. In *IECON 2012 - 38th Annual Conference on IEEE Industrial Electronics Society*. IEEE, oct 2012. doi: 10.1109/iecon.2012.6388877.

[108] Wen-Hong Zhu, Erick Dupuis, and Michel Doyon. Adaptive Control of Harmonic Drives. *Journal of Dynamic Systems, Measurement, and Control*, 129(2):182–193, August 2007. doi: 10.1115/1.2431813.

[109] David Freedman. SSH/SFTP/SCP For Matlab (v2) (https://www.mathworks.com/matlabcentral/fileexchange/35409-ssh-sftp-scp-for-matlab-v2). *MATLAB Central File Exchange*, June 2020.

[110] John J. Craig. *Introduction to Robotics: Pearson New International Edition*. Pearson Education Limited, 2013.

[111] Ahmed Shabana. *Dynamics of multibody systems*. Cambridge University Press, New York, 2014. ISBN 9781107337213.

[112] Thomas R. Kane and David A. Levinson. *Dynamics: Theory and Applications*. McGraw-Hill College, 1985.

[113] Carlos Canudas de Wit, Bruno Siciliano, and Georges Bastin. *Theory of Robot Control*. Springer London, 1996. ISBN 978-1-4471-1501-4. doi: 10.1007/978-1-4471-1501-4. URL `https://www.ebook.de/de/product/25251233/theory_of_robot_control.html`.

[114] Anton Niglis and Per Öberg. Modelling High-Fidelity Robot Dynamics. Master's thesis, Linköping University, Automatic Control, 2015.

[115] C. Walton Musser. Strain wave gearing, September 1959.

[116] Harmonic Drive AG. Engineering Data – HFUS-2UH/2SO/2SH, December 2018.

[117] Zhiguo Shi, Yuankai Li, and Guangjun Liu. Adaptive torque estimation of robot joint with harmonic drive transmission. *Mechanical Systems and Signal Processing*, 96:1–15, November 2017. doi: 10.1016/j.ymssp.2017.03.041.

[118] P. S. Gandhi and F. H. Ghorbel. Control of hysteresis and kinematic error nonlinearities in harmonic drives for high speed precision control applications. In *Proceedings of the 2004 American Control Conference*, pages 1141–1146, Boston, MA, USA, June 2004. IEEE.

[119] Giorgio Bertotti. *Hysteresis in Magnetism*. Elsevier, 1998. doi: 10.1016/b978-0-12-093270-2.x5048-x.

[120] Christiano C. Casanova, Edson R. De Pieri, Ubirajara F. Moreno, and Eugĕnio B. Castelan. Friction Compensation in Flexible Joints Robot with GMS Model: Identification, Control and Experimental Results. *IFAC Proceedings Volumes*, 41(2):11793–11798, July 2008. doi: 10.3182/20080706-5-KR-1001.01997.

[121] M. Ruderman, F. Hoffmann, and T. Bertram. Modeling and Identification of Elastic Robot Joints With Hysteresis and Backlash. *IEEE Transactions on Industrial Electronics*, 56(10):3840–3847, October 2009. doi: 10.1109/tie.2009.2015752.

[122] Emil Madsen, Oluf Skov Rosenlund, David Brandt, and Xuping Zhang. Comprehensive Modeling and Identification of Nonlinear Joint Dynamics for Collaborative Industrial Robot Manipulators. *Control Engineering Practice*, 101:104462, April 2020. doi: 10.1016/j.conengprac.2020.104462.

[123] Fathi H. Ghorbel, Prasanna S. Gandhi, and Friedhelm Alpeter. On the Kinematic Error in Harmonic Drive Gears. *Journal of Mechanical Design*, 123(1):90–97, October 1998. doi: 10.1115/1.1334379.

[124] Chuang Zou, Tao Tao, Gedong Jiang, Pengfei Zeng, and Hongyang Du. Measurement and modeling of kinematic error and clearance in harmonic drives. In *Proceedings of the 2015 Joint International Mechanical, Electronic and Information Technology Conference*, pages 102–109, Chongqing, China, 2015. Atlantis Press. doi: 10.2991/jimet-15.2015.20.

[125] Chuang Zou, Tao Tao, Gedong Jiang, Xuesong Mei, and Junhui Wu. A harmonic drive model considering geometry and internal interaction. *Proceedings of the Institution of Mechanical Engineers, Part C: Journal of Mechanical Engineering Science*, 231(4):728–743, aug 2016. doi: 10.1177/0954406215621097.

[126] J. Swevers, F. Al-Bender, C. G. Ganseman, and T. Projogo. An integrated friction model structure with improved presliding behavior for accurate friction compensation. *IEEE Transactions on Automatic Control*, 45(4):675–686, apr 2000. doi: 10.1109/9.847103.

[127] V. Lampaert, J. Swevers, and F. Al-Bender. Modification of the Leuven integrated friction model structure. *IEEE Transactions on Automatic Control*, 47(4):683–687, April 2002. doi: 10.1109/9.995050.

[128] Max Boegli, Tinne De Laet, Joris De Schutter, and Jan Swevers. A Smoothed GMS Friction Model Suited for Gradient-Based Friction State and Parameter Estimation.

IEEE/ASME Transactions on Mechatronics, 19(5):1593–1602, October 2014. doi: 10.1109/tmech.2013.2288944.

[129] Paul C. Krause, Oleg Wasynczuk, Scott D. Sudhoff, and Steven Pekarek. *Analysis of Electric Machinery and Drive Systems*. John Wiley & Sons, 2013. ISBN 978-1118024294. URL https://www.ebook.de/de/product/19579645/krause_steven_pekarek_sudhoff_analysis_electric_machinery_3e.html.

[130] Andrzej Ruszczynski. *Nonlinear Optimization*. Princeton University Press, 2006. ISBN 0691119155. URL https://www.ebook.de/de/product/5256800/andrzej_ruszczynski_nonlinear_optimization.html.

[131] Karl Johan Åström and Björn Wittenmark. *Adaptive Control (2nd Edition)*. Prentice Hall, 1994. ISBN 0201558661.

[132] Rolf Johansson. *System modeling and identification*. Prentice Hall, Englewood Cliffs, NJ, 1993. ISBN 9780134823089.

[133] T. R. Fortescue, L. S. Kershenbaum, and B. E. Ydstie. Implementation of self-tuning regulators with variable forgetting factors. *Automatica*, 17(6):831–835, nov 1981. doi: 10.1016/0005-1098(81)90070-4.

[134] N. Rao Sripada and D. Grant Fisher. Improved least squares identification. *International Journal of Control*, 46(6):1889–1913, dec 1987. doi: 10.1080/00207178708934023.

[135] Mario Salgado, Graham Goodwin, and Richard Middleton. Modified least squares algorithm incorporating exponential resetting and forgetting. *International Journal of Control*, 47(2):477–491, feb 1988. doi: 10.1080/00207178808906026.

[136] R. Kulhavý and M. B. Zarrop. On a general concept of forgetting. *International Journal of Control*, 58(4):905–924, oct 1993. doi: 10.1080/00207179308923034.

[137] T. Hägglund. Recursive Estimation of Slowly Time-Varying Parameters. *IFAC Proceedings Volumes*, 18(5):1137–1142, jul 1985. doi: 10.1016/s1474-6670(17)60715-8.

[138] R. Kulhavý. Restricted Exponential Forgetting in Real-Time Identification. *IFAC Proceedings Volumes*, 18(5):1143–1148, jul 1985. doi: 10.1016/s1474-6670(17)60716-x.

[139] S. Bittanti, P. Bolzern, and M. Campi. Recursive least-squares identification algorithms with incomplete excitation: convergence analysis and application to adaptive control. *IEEE Transactions on Automatic Control*, 35(12):1371–1373, 1990. doi: 10.1109/9.61020.

[140] S. Bittanti, P. Bolzern, and M. Campi. Convergence and Exponential Convergence of Identification Algorithms with Directional Forgetting Factor. *Automatica*, 26(5): 929–932, September 1990. doi: 10.1016/0005-1098(90)90012-7.

[141] P. Rouchon, M. Fliess, J. Levine, and P. Martin. Flatness, motion planning and trailer systems. In *Proceedings of 32nd IEEE Conference on Decision and Control*. IEEE, 1993. doi: 10.1109/cdc.1993.325686.

[142] Michiel J. Van Nieuwstadt and Richard M. Murray. Real-time trajectory generation for differentially flat systems. *International Journal of Robust and Nonlinear Control*, 8 (11):995–1020, sep 1998. doi: 10.1002/(sici)1099-1239(199809)8:11⟨995::aid-rnc373⟩3.0.co;2-w.

[143] A. De Luca and P. Lucibello. A general algorithm for dynamic feedback linearization of robots with elastic joints. In *Proceedings of the IEEE International Conference on Robotics & Automation*, pages 504–510, Leuven, Belgium, May 1998. IEEE. doi: 10.1109/robot.1998.677024.

[144] Gabriele Buondonno and Alessandro De Luca. A recursive Newton-Euler algorithm for robots with elastic joints and its application to control. In *2015 IEEE/RSJ International Conference on Intelligent Robots and Systems (IROS)*. IEEE, sep 2015. doi: 10.1109/iros.2015.7354160.

[145] A. Albu-Schäffer, S. Haddadin, C. Ott, A. Stemmer, T. Wimböck, and G. Hirzinger. The DLR lightweight robot: design and control concepts for robots in human environments. *Industrial Robot: An International Journal*, 34(5):376–385, August 2007. doi: 10.1108/01439910710774386.

[146] M. Hashimoto. Robot motion control based on joint torque sensing. In *International Conference on Robotics and Automation*, pages 256–261, Scottsdale, AZ, USA, May 1989. IEEE Comput. Soc. Press. doi: 10.1109/robot.1989.99998.

[147] F. Aghili, M. Buehler, and J. M. Hollerbach. Motion control systems with /spl Hscr//-sup /spl infin// positive joint torque feedback. *IEEE Transactions on Control Systems Technology*, 9(5):685–695, September 2001. doi: 10.1109/87.944464.

[148] D. Vischer and O. Khatib. Design and development of high-performance torque-controlled joints. *IEEE Transactions on Robotics and Automation*, 11(4):537–544, 1995. doi: 10.1109/70.406938.

[149] D. Tsetserukou, R. Tadakuma, H. Kajimoto, and S. Tachi. Optical torque sensors for implementation of local impedance control of the arm of humanoid robot. In *Proceedings 2006 IEEE International Conference on Robotics and Automation, 2006. ICRA 2006.*, pages 1674–1679, Orlando, FL, USA, May 2006. IEEE. doi: 10.1109/robot.2006.1641947.

[150] M. Hashimoto, Y. Kiyosawa, and R. P. Paul. A torque sensing technique for robots with harmonic drives. *IEEE Transactions on Robotics and Automation*, 9(1):108–116, February 1993. doi: 10.1109/70.210802.

[151] H. D. Taghirad and P. R. Bélanger. Torque ripple and misalignment torque compensation for the built-in torque sensor of harmonic drive systems. *IEEE Transactions on Instrumentation and Measurement*, 47(1):309–315, 1998. doi: 10.1109/19.728840.

[152] I. Godler, M. Horiuchi, M. Hashimoto, and T. Ninomiya. Accuracy improvement of built-in torque sensing for Harmonic Drives. *IEEE/ASME Transactions on Mechatronics*, 5(4):360–366, December 2000. doi: 10.1109/3516.891047.

[153] J. W. Sensinger and R. F. ff. Weir. Improved torque fidelity in harmonic drive sensors through the union of two existing strategies. *IEEE/ASME Transactions on Mechatronics*, 11(4):457–461, aug 2006. doi: 10.1109/tmech.2006.878540.

[154] Tomohiro Kawakami, Ko Ayusawa, Hiroshi Kaminaga, and Yoshihiko Nakamura. High-fidelity joint drive system by torque feedback control using high precision linear encoder. In *2010 IEEE International Conference on Robotics and Automation*, pages 3904–3909, Anchorage, AK, USA, May 2010. IEEE. doi: 10.1109/robot.2010.5509625.

[155] Hongwei Zhang, Saleh Ahmad, and Guangjun Liu. Torque Estimation Technique of Robotic Joint with Harmonic Drive Transmission. In *2013 IEEE International Conference on Robotics and Automation*, pages 3034–3039, Karlsruhe, Germany, May 2013. IEEE. doi: 10.1109/icra.2013.6630998.

[156] Hongwei Zhang, Saleh Ahmad, and Guangjun Liu. Torque Estimation for Robotic Joint With Harmonic Drive Transmission Based on Position Measurements. *IEEE Transactions on Robotics*, 31(2):322–330, apr 2015. doi: 10.1109/tro.2015.2402511.

[157] A. C. Bittencourt, E. Wernholt, S. Sander-Tavallaey, and T. Brogårdh. An Extended Friction Model to Capture Load and Temperature Effects in Robot Joints. In *2010 IEEE/RSJ International Conference on Intelligent Robots and Systems*, pages 6161–6167, Taipei, Taiwan, October 2010. IEEE. doi: 10.1109/IROS.2010.5650358.

[158] André Carvalho Bittencourt and Patrik Axelsson. Modeling and Experiment Design for Identification of Wear in a Robot Joint Under Load and Temperature Uncertainties Based on Friction Data. *IEEE/ASME Transactions on Mechatronics*, 19(5):1694–1706, October 2014. doi: 10.1109/tmech.2013.2293001.

[159] Claire Dumas, Stéphane Caro, Sébastien Garnier, and Benoît Furet. Joint stiffness identification of six-revolute industrial serial robots. *Robotics and Computer-Integrated Manufacturing*, 27(4):881–888, aug 2011. doi: 10.1016/j.rcim.2011.02.003.

[160] A. Jubien, G. Abba, and M. Gautier. Joint Stiffness Identification of a Heavy Kuka Robot with a Low-cost Clamped End-effector Procedure. In *Proceedings of the 11th International Conference on Informatics in Control, Automation and Robotics*. SCITEPRESS - Science and and Technology Publications, 2014. doi: 10.5220/0005115805850591.

[161] M. T. Pham, M. Gautier, and P. Poignet. Identification of joint stiffness with bandpass filtering. In *Proceedings 2001 ICRA. IEEE International Conference on Robotics and Automation (Cat. No.01CH37164)*. IEEE, 2001. doi: 10.1109/robot.2001.933056.

[162] Måns Östring, Svante Gunnarsson, and Mikael Norrlöf. Closed-loop identification of an industrial robot containing flexibilities. *Control Engineering Practice*, 11(3):291–300, mar 2003. doi: 10.1016/s0967-0661(02)00114-4.

[163] M. Gautier, A. Jubien, A. Janot, and P. Ph. Robet. Dynamic identification of flexible joint manipulators with an efficient closed loop output error method based on motor torque output data. In *2013 IEEE International Conference on Robotics and Automation*. IEEE, may 2013. doi: 10.1109/icra.2013.6630986.

[164] R. Dhaouadi and F. H. Ghorbel. Modelling and Analysis of Nonlinear Stiffness, Hysteresis and Friction in Harmonic Drive Gears. *International Journal of Modelling and Simulation*, 28(3):329–336, jan 2008. doi: 10.1080/02286203.2008.11442485.

[165] Xiaoli Shi, Yong Han, Jianhua Wu, and Zhenhua Xiong. An FFT-based Method for Analysis, Modeling and Identification of Kinematic Error in Harmonic Drives. In *Intelligent Robotics and Applications*, pages 191–202. Springer International Publishing, 2019. doi: 10.1007/978-3-030-27541-9_17.

[166] Patrick M. Sammons, Le Ma, Kyle Embry, Levi H. Armstrong, Douglas A. Bristow, and Robert G. Landers. Modeling and Compensation of Backlash and Harmonic Drive-Induced Errors in Robotic Manipulators. In *Volume 2: Processing*. American Society of Mechanical Engineers, June 2014. doi: 10.1115/msec2014-4123.

[167] Huimin Dong, Tianhang Chen, Delun Wang, and Bo Dong. Kinematic Model of Harmonic Drive in Robot Joints with Input Eccentricity Error. In Vigen Arakelian and Philippe Wenger, editors, *ROMANSY 22 – Robot Design, Dynamics and Control*, pages 134–140, Cham, 2019. Springer International Publishing. ISBN 978-3-319-78963-7.

[168] E. Madsen, S. A. Timm, N. A. Ujfalusi, O. S. Rosenlund, D. Brandt, and X. Zhang. Dynamics Parametrization and Calibration of Flexible-Joint Collaborative Industrial Robot Manipulators. *Mathematical Problems in Engineering*, 2020:1–13, sep 2020. doi: 10.1155/2020/8709870.

[169] E. Madsen, O. S. Rosenlund, D. Brandt, and X. Zhang. Adaptive Feedforward Control for a Collaborative Industrial Robot Manipulator Using a Novel Extension of the Generalized Maxwell-Slip Friction Model. *Mechanism and Machine Theory*, 2020.

[170] P. Hamon, M. Gautier, and P. Garrec. Dynamic Identification of Robots with a Dry Friction Model Depending on Load and Velocity. In *2010 IEEE/RSJ International Conference on Intelligent Robots and Systems*, pages 6187–6193, Taipei, Taiwan, October 2010. IEEE. doi: 10.1109/IROS.2010.5649189.

[171] André Carvalho Bittencourt, Patrik Axelsson, Ylva Jung, and Torgny Brogårdh. Modeling and Identification of Wear in a Robot Joint under Temperature Uncertainties. *IFAC Proceedings Volumes*, 44(1):10293–10299, jan 2011. doi: 10.3182/20110828-6-it-1002.01078.

[172] Benjamin Navarro, Andrea Cherubini, Aicha Fonte, Robin Passama, Gerard Poisson, and Philippe Fraisse. An ISO10218-compliant adaptive damping controller for safe physical human-robot interaction. In *2016 IEEE International Conference on Robotics and Automation (ICRA)*. IEEE, may 2016. doi: 10.1109/icra.2016.7487468.

Appendix A

Patent Application: Stiffness Estimation [Pat. App. 1]

Obtaining the Gear Stiffness of a Robot Joint Gear of a Robot Arm

Title	OBTAINING THE GEAR STIFFNESS OF A ROBOT JOINT GEAR OF A ROBOT ARM
Intl. App. No.	EP/18/19/4683
Priority Date	September 14, 2018
Applicant	Universal Robots A/S
Inventor	Emil Madsen
Agent	Morten Fruelund

A.1 Contribution

The author developed and described the methods. The agent prepared the application by instruction from the author.

OBTAINING THE GEAR STIFFNESS OF A ROBOT JOINT GEAR OF A ROBOT ARM

FIELD OF THE INVENTION

[0001] The present invention relates to robot joint gears for robot arms comprising a plurality of robot joints connecting a robot base and a robot tool flange.

BACKGROUND OF THE INVENTION

[0002] Robot arms comprising a plurality of robot joints and links where motors can rotate the joints in relation to each other are known in the field of robotics. Typically, the robot arm comprises a robot base which serves as a mounting base for the robot arm and a robot tool flange where to various tools can be attached. A robot controller is configured to control the robot joints to move the robot tool flange in relation to the base. For instance, in order to instruct the robot arm to carry out a number of working instructions.

[0003] Typically, the robot controller is configured to control the robot joints based on a dynamic model of the robot arm, where the dynamic model defines a relationship between the forces acting on the robot arm and the resulting accelerations of the robot arm. Often, the dynamic model comprises a kinematic model of the robot arm, knowledge about inertia of the robot arm and other parameters influencing the movements of the robot arm. The kinematic model defines a geometric relationship between the different parts of the robot arm and may comprise information of the robot arm such as, length, size of the joints and links and can for instance be described by Denavit-Hartenberg parameters or the like. The dynamic model makes it possible for the controller to determine which torques the joint motors shall provide in order to move the robot joints for instance at specified velocity, acceleration or in order to hold the robot arm in a static posture.

[0004] On many robot arms it is possible to attach various end effectors to the robot tool flange, such as grippers, vacuum grippers, magnetic grippers, screwing machines, welding equipment, dispensing systems, visual systems etc.

[0005] In some robots the robot joint comprises a joint motor having a motor axle configured to rotate an output axle via a robot joint gear. Typically, the output axle is connected to and configured to rotate parts of the robot arm

in relation to each other. The robot joint gear forms a transmission system configured to transmit torque provided by the motor axle to the output axle for instance to provide a gear ratio between the motor axle and the output axle. The robot joint gear can for instance be provided as a spur gears, planetary gears, bevel gears, worm gears, strain wave gears or other kind of transmission systems. Commonly flexibility exist in the transmissions used for industrial robots due to the elasticity various type of transmissions. This flexibility may lead to an undesired dynamic time-varying displacement between the position of parts of the robot arm.

[0006] Taking into account the gear flexibility in the dynamic model makes the dynamic model more accurately resemble the dynamics of the real robot arm because the robot joint torque originating from the gear deformation can be known. A more accurate dynamic model can for instance allow the robot controller to control the robot arm with greater accuracy and precision. A more accurate dynamic model can also allow the robot controller to more accurately identify external disturbances, for instance human interference which is of great concern in terms of safety.

[0007] Research have been devoted to accurately identify the dynamic characteristics of the robot gear systems. However, one practical issue when taking into account the joint stiffness in the robot controller design is that the joint stiffness changes with wear due to material being worn off at the gear meshing [1], [2], [3].

[0008] Estimating the joint stiffness on industrial robots have been accomplished through off-line identification procedures by several researchers. Off-line identification procedures are not well suited for solving the problem of time-varying joint stiffness. Such procedures would have to be re-run from time to time to keep the joint stiffness information up to date. While the off-line identification procedure is running the robot is unable to conduct any other task with clear negative consequences to the user. Despite the shortcomings of the off-line calibration procedures for joint stiffness estimation a number of references will be given to such off-line identification procedures applied to solve the robot joint stiffness estimation problem. For the off-line identification of joint stiffness, one method is to apply external excitation on one robot joint at a time resulting in a reduced dynamic model hence easier identification as in [4], [5], [6], [7].

[0009] Another option is to evaluate joint stiffness values using an external laser-tracking sensor system to visually track the end effector displacements for a given applied wrench as in [8] and [9], where the applied wrench is equal to the applied forced and torques at the end effector. A third option is to incorporate two absolute position rotary encoders in the robot joint to enable direct measurement of the joint deflection and then manually impose a known force at the end-effector and using the kinematic model (the Jacobian) of the robot arm to calculate the joint torques as in [9]. Such procedure however requires external and known loading of the end-effector and the robot is not allowed to move during the procedure. A fourth option is to estimate the joint stiffness using a so-called locked-link joint procedure as in [10] where the end-effector is clamped to the environment and using either motor positions measurement and motor torques data or a force/torque sensor to measure the external wrench between the clamped end effector and the environment.

[0010] Very few works are available on the on-line estimation of time-varying nonlinear stiffness e.g. AwAs-II joint [11]. These works are focused towards Variable Stiffness Actuators (VSAs) as found in in the DLR Hand Arm System [12] by the DLR Institute of Robotics and Mechatronics, however most industrial robots do not comprise a VSA. In 2011, Flacco and De Luca [13] estimated the nonlinear stiffness of robot joints using only a motor position sensor by computing a dynamic residual based on the generalized momentum followed by a least squares algorithm to estimate the stiffness parameters.

[0011] Robustness issues were later addressed in [14] by introducing a kinematic Kalman filter to handle discretization and quantization errors and a modified recursive least squares algorithm was used to better handle poor excitation conditions. The stiffness parameters were however assumed time-invariant. Further refinements of their method were carried out in [15] modifying the stiffness estimation algorithm to deal with time-varying stiffness by using a Recursive Least Squares method based on a QR decomposition (QR-RLS) able to handle time-varying stiffness characteristics. A non-causal Savitzky-Golay (SG) filter was used to remove noise on the input/output signals. No experiments did however support their findings.

[0012] In May 2013, Ménard et al. [16] developed an observer capable of on-line estimating the time-varying stiffness of a VSA. Experimental analysis on the VSA system revealed parameter uncertainties of up to 25 % of the true

stiffness. Friction was assumed purely viscous with a single constant coefficient. Such friction model is not capable of accurately describing real frictional characteristics of most electromechanical systems, as well-known frictional characteristics such as Coulomb friction and the Stribeck effect is then neglected completely.

[0013] In July 2013, Cirillo et al. [17] demonstrated online stiffness estimation of a VSA by measuring the elastic energy using an optoelectronic sensor built into the robot joint.

SUMMARY OF THE INVENTION

[0014] The objective of the present invention is to address the above described limitations with the prior art or other problems of the prior art. This is achieved by a method of obtaining the gear stiffness of a robot joint gear as defined by the independent claim. The dependent claims describe possible embodiments of the method according to the present invention. The advantages and benefits of the present invention are described in the detailed description of the invention. Further the objective of the present invention is addressed by a method of controlling a robot arm based on the obtained gear stiffness and a robot arm with a controller configured to control the robot arm based on the obtained gear stiffness.

[0015] A robot controller taking into account the joint flexibilities may perform well right after calibration but for a good performance over the lifetime of the robot, the joint stiffness must be estimated on-line. Further, estimating the joint stiffness on-line will allow for predictive maintenance in the case of gear unit failure. In most cases, no sensor is available for directly measuring the joint stiffness, so the stiffness information is collected by combining an accurate model of the flexibility torque with the measurements available, such as position and force/torque sensor measures, either implemented in the robot or by using external hardware.

[0016] The invention provides a simple method of obtaining the gear stiffness of a robot joint gear of a robot arm without the need to integrate expensive force/torque sensors, as the joint gear stiffness of the robot joint gear can be determined based on sensors commonly used in industrial robots, which also makes it possible to integrate such method into existing industrial robots having such sensors. Additionally, the gear stiffness can be obtained online

during use of the robot and thus used as an input to the dynamic model controlling the robot whereby a more accurate controlling of the robot can be provided. Consequently, vibrations and inaccuracies of the robot's movements due to gear stiffness can be accounted for when controlling the robot. Additionally, the gear stiffness changes over time primarily due to wear of the robot joint gear and obtaining the gear stiffness online makes it possible to control the robots based on changes of gear stiffness whereby the accuracy of the robot over time is maintained/improved. Further obtaining the gear stiffness online over time makes it possible to predict failure of the robot joint gear as the gear stiffness can be used to indicate when the robot joint gear is about to fail. Consequently, the robot joint gear can be sent to service in order to exchange/repair the robot joint gear whereby unplanned downtime of the robot can be reduced.

BRIEF DESCRIPTION OF THE DRAWINGS

Fig. 1 illustrates a robot arm configured to obtain the gear stiffness of the robot joint gears;

fig. 2 illustrates a schematic cross-sectional view of a robot joint;

fig. 3 illustrates a model of a robot joint gear;

fig. 4 illustrates a simplified structural diagram of a robot arm;

fig. 5 illustrates a flow chart of a method of obtaining the gear stiffness of a robot joint gear of a robot joint of a robot arm;

fig. 6 illustrates a flow chart of another method of obtaining the gear stiffness of a robot joint gear of a robot joint of a robot arm;

fig. 7 illustrates a robot arm in a pose used in an experimental analysis of the method according to the present invention;

fig. 8 illustrates a friction torque/velocity map obtained by imposing different signals of constant velocity on the base joint of a robot arm, while measuring the joint motor current;

fig. 9 illustrates a flexibility torque/transmission deformation map obtained by imposing a set of known torques to the tool flange of a robot arm using a force

gage and measuring the deformation as the difference between absolute joint encoder readings at each side of the robot joint gear;

fig. 10 illustrates angular position, angular velocity and angular acceleration of the base joint of the robot arm used in the experimental analysis;

fig. 11 illustrates a schematic representation of the Generalized Maxwell-Slip friction model;

fig. 12 illustrates a flexibility torque/transmission deformation map obtained by the method according to the present invention;

fig. 13 illustrates gear stiffness of the robot joint gear obtained in the experimental analysis,

DETAILED DESCRIPTION OF THE INVENTION

[0017] The present invention is described in view of exemplary embodiments only intended to illustrate the principles of the present invention. The skilled person will be able to provide several embodiments within the scope of the claims. Throughout the description, the reference numbers of similar elements providing similar effects have the same last two digits. Further it is to be understood that in the case that an embodiment comprises a plurality of the same features then only some of the features may be labeled by a reference number.

[0018] The invention can be embodied into a robot arm and is described in view of the robot arm illustrated in fig. 1. The robot arm 101 comprises a plurality of robot joints 103a, 103b, 103c, 103d, 103e, 103f and robot links 104b, 104c, 104d connecting a robot base 105 and a robot tool flange 107. A base joint 103a is connected directly with a shoulder joint and is configured to rotate the robot arm around a base axis 111a (illustrated by a dashed dotted line) as illustrated by rotation arrow 113a. The shoulder joint 103b is connected to an elbow joint 103c via a robot link 104b and is configured to rotate the robot arm around a shoulder axis 111b (illustrated as a cross indicating the axis) as illustrated by rotation arrow 113b. The elbow joint 103c connected to a first wrist joint 103d via a robot link 104c and is configured to rotate the robot arm around an elbow axis 111c (illustrated as a cross indicating the axis) as

illustrated by rotation arrow 113c. The first wrist joint 103d connected to a second wrist joint 103e via a robot link 104d and is configured to rotate the robot arm around a first wrist axis 111d (illustrated as a cross indicating the axis) as illustrated by rotation arrow 113d. The second wrist joint 103e is connected to a robot tool joint 103f and is configured to rotate the robot arm around a second wrist axis 111e (illustrated by a dashed dotted line) as illustrate by rotation arrow 113e. The robot tool joint 103f comprising the robot tool flange 107, which is rotatable around a tool axis 111f (illustrated by a dashed dotted line) as illustrated by rotation arrow 113f. The illustrated robot arm is thus a six-axis robot arm with six degrees of freedom, however it is noticed that the present invention can be provided in robot arms comprising less or more robot joints, and the robot joints can be connected directly to the neighbor robot joint or via a robot link. It is to be understood that the robot joints can be identical and/or different and that the robot joint gear may be omitted in some of the robot joints. The direction of gravity 123 is also indicated in the figure.

[0019] The robot arm comprises at least one robot controller 115 configured to control the robot joints by controlling the motor torque provided to the joint motors based on a dynamic model of the robot. The robot controller 115 can be provided as a computer comprising an interface device 117 enabling a user to control and program the robot arm. The controller can be provided as an external device as illustrated in fig. 1 or as a device integrated into the robot arm. The interface device can for instance be provided as a teach pendent as known from the field of industrial robots which can communicate with the controller via wired or wireless communication protocols. The interface device can for instance comprise a display 119 and a number of input devices 121 such as buttons, sliders, touchpads, joysticks, track balls, gesture recognition devices, keyboards etc. The display may be provided as a touch screen acting both as display and input device.

[0020] Fig. 2 illustrates a schematic cross-sectional view of a robot joint 203. The schematic robot joint 203 can reflect any of the robot joints 103a-103f of the robot 101 of fig. 1. The robot joint comprises a joint motor 209 having a motor axle 225. The motor axle 225 is configured to rotate an output axle 227 via a robot joint gear 229. The output axle 227 rotates around an axis of rotation 211 (illustrated by a dot-dash line) and can be connected to a neighbor part

(not shown) of the robot. Consequently, the neighbor part of the robot can rotate in relation to the robot joint 203 around the axis of rotation 211 as illustrated by rotation arrow 213. In the illustrated embodiment the robot joint comprises an output flange 231 connected to the output axle and the output flange can be connected to a neighbor robot joint or an arm section of the robot arm. However, the output axle can be directly connected to the neighbor part of the robot or by any other way enabling rotation of the neighbor part of the robot by the output axle.

[0021] The joint motor is configured to rotate the motor axle by applying a motor torque to the motor axle as known in the art of motor control, for instance based on a motor control signal 233 indicating the torque, $\tau_{control,\ motor}$, applied by said motor axle.

[0022] The robot joint gear 229 forms a transmission system configured to transmit the torque provided by the motor axle to the output axle for instance to provide a gear ratio between the motor axle and the output axle. The robot joint gear can for instance be provided as spur gears, planetary gears, bevel gears, worm gears, strain wave gears or other kind of transmission systems.

The robot joint comprises at least one joint sensor providing a sensor signal indicative of at least the angular position, q, of the output axle and an angular position, Θ, of the motor axle. For instance, the angular position of the output axle can be indicated by an output encoder 235, which provide an output encoder signal 236 indicating the angular position of the output axle in relation to the robot joint. Similarly, the angular position of the motor axle can be provided by an input encoder 237 providing an input encoder signal 238 indicating the angular position of the motor axle in relation to the robot joint. The output encoder 235 and the input encoder 237 can be any encoder capable of indicating the angular position, velocity and/or acceleration of respectively the output axle and the motor axle. The output/input encoders can for instance be configured to obtain the position of the respective axle based on the position of an encoder wheel 239 arrange on the respective axle. The encoder wheels can for instance be optical or magnetic encoder wheels as known in the art of rotary encoders. The output encoder indicating the angular position of the output axle and the input encoder indicating the angular position of the motor axle makes it possible to determine a relationship between the input side (motor axle) and the output side (output axle) of the robot joint gear.

[0023] The robot joints may optionally comprise one or more motor torque sensors 241 providing a motor torque signal 242 indicating the torque provided by the motor axle. For instance, the motor torque sensor can be provided as current sensors obtaining the current through the coils of the joint motor whereby the motor torque can be determined as known in the art of motor control. For instance, in connection with a multiphase motor, a plurality of current sensors can be provided in order to obtain the current through each of the phases of the multiphase motor and the motor torque can then be obtained based on the quadrature current obtained from the phase currents through a Park Transformation. Alternatively, the motor torque can be obtained using other kind of sensors for instance force-torque sensors, strain gauges etc.

[0024] Fig. 3 illustrates a model of a robot joint 303 connecting robot link 304i-1 and robot link 304i, where the joint motor 309i is arranged on robot link 304i-1 and rotates robot link 304i in relation to robot link 304i-1. The motor axle 325i of the joint motor is connected to an output axle 327i via robot joint gear 329i (illustrated in schematic form) and the robot link 304i rotates together with the output axle 327i. The robot joint gear provides a gear ratio between the motor axle and the output axle and in an ideal gear the rotation of the motor axle is immediately transformed into rotation of the output axle according to the gear ratio of the robot joint gear. However as described in the background of the invention flexibility exist in the types of robot joint gears used in the field of robot arms. The flexibility of a robot joint gear can be indicated by the gear stiffness of the robot joint gear which defines a relationship between torque through the robot joint gear and the deformation between the input side (motor axle) and the output side (output axle) of the robot joint gear. The flexibility of a robot joint gear can be represented as a spring 326 and a damper 328 coupled in parallel between the input side (motor axle) and the output side (output axle) of the robot joint gear. The spring constant K_i of the spring indicates the gear stiffness of the robot joint gear and the damping constant of the damper D_i indicates the damping of the robot joint gear. As described in the background of the invention the gear stiffness and damping of the robot joint gear can vary; consequently, K_i and D_i need not to be constants.

[0025] The non-infinite gear stiffness of the robot joint results in a deflection between the input side and the output side of the robot joint gear

when a torque is applied to the robot joint gear. The deflection of the robot joint gear can be indicated by a deflection variable indicating the differences between the angular position Θ of the motor axle and the angular position q of the of the output axle, thus the deflection variable is defined as:

eq. 1 $$\Phi_{joint,i} = \theta_i - q_i$$

[0026] The joint transmission torque $\tau_{joint,i}$ defines the torque that is transferred from the motor axle to the output axle via the robot joint gear and can be modeled as a function of the deflection variable Φ_{joint} and its time-derivative:

eq. 2 $$\tau_{joint,i}\left(\Phi_{joint,i}, \dot{\Phi}_{joint,i}\right) = \tau_{E,i}\left(\Phi_{joint,i}\right) + \tau_{D,i}(\dot{\Phi}_{joint,i})$$

where $\tau_{E,i}(\Phi_{\text{joint,i}})$ is a flexibility torque depending on the gear stiffness K_i and the deflection of the robot joint gear and $\tau_{\text{D,i}}(\dot{\Phi}_{\text{joint,i}})$ is damping torque depending on the damping coefficient D_i and the first time derivative of the deflection of the robot joint gear and the time derivative of the deflection of the robot joint gear.

The $\boldsymbol{\tau}_{\text{D,i}}(\dot{\Phi}_{\text{joint,i}})$ damping torque of the robot joint gear can for instance be obtained by following the steps:

- Fix the output axle of the robot joint gear;
- Apply a torque to the motor axle of the robot joint gear to yield a gear deflection;
- Keep the motor axle of the robot joint gear still and remove the applied torque from the motor axle of the robot joint gear;
- Observe the position of the motor axle of the robot joint gear over time as the motor axle of the robot joint gear undergoes a damped harmonic motion with an amplitude that decreases over time;

- The damping torque is a measure of the energy dissipation during the motion. Assuming an underdamped harmonic motion, the damping coefficient D_i can be obtained as:

eq. 3 $$D_i = \frac{-2\,B\,log_e\left(\frac{A_2}{A_1}\right)}{t_2 - t_1}$$

where B is the mass moment of inertia of the motor axle, A_1 and A_2 are, respectively, amplitudes of the first and second vibration, and t_1 and t_2 are, respectively, times for the first and second motion.

If the motion is not underdamped, a larger mass moment of inertia is added to the input axle.

[0027] The gear stiffness K_i of the robot joint gear can be characterized by how much the flexible torque τ_E causing the gear deflection changes as a function of the gear deflection. The gear stiffness can thus be expressed as:

eq. 4 $$K_i(\Phi_{joint,i}) = \frac{\delta\,\tau_E(\Phi_{joint,i})}{\delta\,\Phi_{joint,i}} \approx \frac{\Delta\,\tau_E(\Phi_{joint,i})}{\Delta\,\Phi_{joint,i}}$$

[0028] Assuming that that no flexibility torque exists for the undeformed transmission and that the transmission has the same behavior in compression and extension, thus:

eq. 5 $$\tau_{E,i}(0) = 0 \qquad \forall\,\Phi_{joint}, i$$

eq. 6 $$\tau_{E,i}(-\Phi_{joint,i}) = -\tau_E(\Phi_{joint,i}) \qquad \forall\,\Phi_{joint,i}$$

[0029] Fig. 4 illustrates a simplified structural diagram of a robot arm comprising a plurality of n number of robot joints 403i, 403i+1….403n. The robot arm can for instance be embodied like the robot arm illustrated in fig. 1 with a plurality of interconnected robot joints, where the robot joints can be embodied like the robot joint illustrated in fig. 2. It is to be understood that some of the robot joints and robot links between the robot joints have been omitted for sake of simplicity. The controller is connected to an interface device comprising a display 119 and a number of input devices 121, as described in

connection with fig.1. The controller 415 comprises a processor 443, a memory 445 and at least one input and/or output port enabling communication with at least one peripheral device.

[0030] The controller is configured to control the joint motors of the robot joints by providing motor control signals to the joint motors. The motor control signals 433i, 433i+1….433n are indicative of the motor torque $\tau_{control,motor,i}$, $\tau_{control,motor,i+1}$, and $\tau_{control,motor,n}$, that each joint motor shall provide by the motor axles. The motor control signals can indicate the desired motor torque, the desired torque provided by the output axle, the currents provided by the motor coils or any other signal from which the motor torque can be obtained. The motor torque signals can be sent to a motor control driver (not shown) configured to drive the motor joint with the motor current resulting in the desired motor torque. The robot controller is configured to determine the motor torque based on a dynamic model of the robot arm as known in the prior art. The dynamic model makes it possible for the controller to calculate which torque the joint motors shall provide to each of the joint motors to make the robot arm perform a desired movement and/or be arranged in a static posture. The dynamic model of the robot arm can be stored in the memory 445.

[0031] As described in connection with fig. 2 the robot joints comprise an output encoder providing output encoder signals 436i, 436i+1…436n indicating the angular position $q_{,i,}$ $q_{,i+1}$…$q_{,n}$ of the output axle in relation to the respective robot joint; an input encoder providing an input encoder signal 438i, 438i+1…438n indicating the angular position of the motor axle $\Theta_{,i,}$ $\Theta_{,i+1}$…$\Theta_{,n}$ in relation to the respective robot joint and a motor torque sensor providing a motor torque signal 442i,442i+1…442n indicating the torque $\tau_{actually,motor,i}$, $\tau_{actually,motor,i+1}$…$\tau_{actually,motor,n}$, provided by the motor axle of the respective robot joint. The controller is configured to receive the output encoder signal 436i, 436i+1…436n, the input encoder signal 438i, 438i+1…438n and the motor torque signals 442i,442i+1…442n.

[0032] The controller is further configured to obtain the gear stiffness of at least one of the robot joint gears of the robot joints of the robot arm by:

- applying a motor torque to the motor axle of the at least one robot joint using the joint motor;
- obtaining the angular position of the motor axle of the robot joint;

- obtaining the angular position of the output axle of the robot joint;

and determining the gear stiffness based on the motor torque applied to the motor axle, the angular position of the motor axle, the angular position of the output axle and the dynamic model of the robot arm.

[0033] The controller can for instance be configured to carry out the method of obtaining the gear stiffness of a robot joint gear obtained by the method illustrated in figs. 5-6 and described in following paragraphs [0034]-[0066].

[0034] Fig. 5 illustrates a flow chart of a method of obtaining the gear stiffness of a robot joint gear of a robot joint of a robot arm, where the robot joint is connectable to at least another robot joint and where the robot joint comprises a joint motor having a motor axle configured to rotate an output axle via the robot joint gear. The method can for instance be used to obtain the gear stiffness of the joint gears of the robot arm illustrated in figs. 1-4 and the method is described in view of the robot arm illustrated in figs. 1-4. It is noted that the method in the following is described in view of a method where the gear stiffness of all the robot joint gears of the robot arm are obtained, however it is to be understood that the method can be used to obtain the gear stiffness of a single robot joint gear or some of the robot joint gears.

[0035] The method comprises a step of initializing 550, a step 552 of applying a motor torque to the motor axles of the joint motors; a step 554 of obtaining the angular position of the motor axles of the joint motors; a step 556 of obtaining the angular position of the output axle of the robot joint gears and a step 560 of determining the gear stiffness of the robot joint gears based on the motor torques applied to the motor axles, the obtained angular positions of the motor axles, the obtained angular positions of the output axles and the dynamic model of the robot arm.

[0036] Step of initializing 550 comprises a step of obtaining the dynamic model D_{robot} of the robot arm and can be based on prior knowledge of the robot arm and robot joints, KoR [Knowledge of Robot], such as the dimensions and weight of robot joints and robot links; joint motor properties; information relating to an eventual payload attached to the robot arm, orientation of the

robot arm in relation to gravity and frictional properties of the robot arm and robot joints.

[0037] The dynamic model of the robot arm can be defined and pre-stored in the memory of the controller and the user can in some embodiment be allowed to modify the dynamic model op the robot arm, for instance by providing payload information of a payload attached to the robot arm or defining the orientation of the robot arm in relation to gravity.

[0038] The dynamic model of the robot arm can be obtained by considering the robot arm as an open kinematic chain having a plurality of (n+1) rigid robot links and a plurality of n revolute robot joints, comprising a joint motor configured to rotate at least one robot link. In this example the dynamic model is provided by making the following assumptions:

A1: The rotors of the joint motors are uniform bodies having their center of mass at the axis of rotation (motor axle);

A2: The joint motors are located on the robot links preceding the driven robot links; and

A3: The angular velocity of the rotors of the joint motors are due to their own spinning.

Assumption A1 is a basic requirement for long life of a joint motor such as electric motors and also implies that the dynamics of the robot joint will be independent of the angular position of the motor axle. The kinematic arrangement of joint motors and robot links described in assumption A2 is illustrated in fig. 3. It is to be understood that the assumption A2 may not be physically true when comparing with an actual robot where joint motor driving the robot links can be arrange at other positions of the robot arm, however there exist always a theoretical equivalent to this assumption. Assumption A3 is reasonable in connection with robot joint gears having large reduction ratios [18] typical in the order of 50-200, or more specific in the order of 100-150. The assumptions are equivalent to neglecting energy contributions due to the inertial couplings between the joint motor and the robot links and also implies that Coriolis and centripetal terms become independent of the rotor's angular velocity.

[0039] The configuration of robot arm can be characterized by the generalized coordinates $(\boldsymbol{q} \quad \boldsymbol{\Theta}) \in \mathbb{R}^{2N}$ where $\mathbf{q}$ is a vector comprising the angular position of the output axles of the robot joint gears and $\boldsymbol{\Theta}$ is a vector comprising the angular position of the motor axles as seen in "space" of the output side of the robot joint gear. Consequently:

$$\boldsymbol{\Theta} = \frac{\boldsymbol{\Theta}_{real}}{\boldsymbol{r}}$$

where $\boldsymbol{\Theta}_{real}$ is the real angular position of the motor axle (e.g. as measured by an encoder) and r the gear ratio of the robot joint gear. This is the notation used throughout this application.

[0040] Similar $\boldsymbol{\tau}_{\text{motor}}$ is a vector comprising the torques of the motor axles 4 as seen in "space" of the output side of the robot joint gear. Consequently:

$$\boldsymbol{\tau}_{\mathbf{motor}} = \mathbf{r} \cdot \boldsymbol{\tau}_{\text{motor real}}$$

where $\boldsymbol{\tau}_{\text{motor real}}$ is the real torque of the motor axles (e.g. as measured by sensors) and r the gear ratio of the robot joint gear. This is the notation used throughout this application.

[0041] Following assumptions 1-3, firstly the dynamic model as seen from the output side of the robot joint gears of the robot arm becomes [18]:

eq. 7 $$\boldsymbol{\tau}_{joint} = \boldsymbol{M}(\boldsymbol{q})\,\ddot{\boldsymbol{q}} + \boldsymbol{C}(\boldsymbol{q}, \dot{\boldsymbol{q}})\dot{\boldsymbol{q}} + \boldsymbol{G}(\boldsymbol{q}) + \boldsymbol{F}_{\boldsymbol{q}}(\dot{\boldsymbol{q}}) + \boldsymbol{\tau}_{\boldsymbol{ext}}$$

where $\boldsymbol{\tau}_{\text{joint}}$ is a vector comprising the transmission torques $\tau_{\text{joint,i}} \ldots \tau_{\text{joint,n}}$ of each of the robot joint gears; $\mathbf{q}$ is a vector comprising the angular position of the output axles of the robot joint gears; $\dot{\mathbf{q}}$ is a vector comprising the first time derivative of the angular position of the output axles of the robot joint gears and thus relates to the angular velocity of the output axles; $\ddot{\mathbf{q}}$ is a vector comprising the second time derivative of the angular position of the output axles of the robot joint gears and thus relates to the angular acceleration of the output axles. $\boldsymbol{M}(\mathbf{q})$ is the inertia matrix of the robot arm and indicates the mass moments of inertia of the robot arm as a function of the angular position of the output axles of the robot joint gears. $\mathbf{C}(\mathbf{q}, \dot{\mathbf{q}})\dot{\mathbf{q}}$ is the Coriolis and centripetal torques of the robot arm as a function of the angular position and angular

velocity of the output axle of the robot joint gears. $\mathbf{G}(\mathbf{q})$ is the gravity torques acting on the robot arm as a function of the angular position of the output axles of the robot joint gears.

[0042] $\boldsymbol{F_q}(\dot{\boldsymbol{q}})$ is a vector comprising the friction torques acting on the output axles of the robot joint gears. The friction torques acting on the output axle depends on angular velocity of the output axle ($\dot{\boldsymbol{q}}$); however it is to be understood the friction torques acting on the output axle also can depend on other parameters such as temperatures, type of lubricants, loads to robot arm, position/orientation of the robot arm etc. $\boldsymbol{F_q}(\dot{\mathbf{q}})$ can for instance be provided as linear or nonlinear functions or lookup tables (LUTs) with interpolation, and $\boldsymbol{F_q}(\dot{\mathbf{q}})$ can be defined based on for instance prior knowledge of the robot, experiments, and/or be adaptively updated during robot operation. For instance, the $\boldsymbol{F_q}(\dot{\boldsymbol{q}})$ can be obtained during calibration of the robot joints for instance by measuring the total friction torques of the robot joint gear and assuming that the friction torques act on the motor axle only thus $\boldsymbol{F_q}(\dot{\boldsymbol{q}})$=0. $\boldsymbol{\tau_{ext}}$ is a vector indicating the external torques acting on the output axles of the robot joint gears. The external torques can for instance be provided by external forces and/or torques acting on parts of the robot arm. For instance, if the tool flange of the robot is subject to external forces and/or torques described by $\boldsymbol{F_{ext}}$, the resulting torques at the output axles of the robot joints becomes:

eq. 8 $$\boldsymbol{\tau_{ext}} = \boldsymbol{J}^T(\boldsymbol{q})\, \boldsymbol{F_{ext}}$$

where $\boldsymbol{J}^T(\mathbf{q})$ is the transposed manipulator Jacobian of the robot arm and where $\boldsymbol{F_{ext}}$ is a vector describing the direction and magnitude of the external forces and torques in relation to the tool flange of the robot arm.

[0043] Secondly, the dynamic model as seen from the input side of the robot joint gears becomes [18]:

eq. 9 $$\boldsymbol{\tau_{motor}} = B\,\ddot{\boldsymbol{\Theta}} + \boldsymbol{F_{\Theta}}(\dot{\boldsymbol{\Theta}}) + \boldsymbol{\tau}_{joint}$$

where $\boldsymbol{\tau}_{\text{joint}}$ is a vector comprising transmission torque $\tau_{\text{joint,i}}$... $\tau_{\text{joint,n}}$ of each of the robot joint gears; $\ddot{\boldsymbol{\Theta}}$ is a vector comprising the second time derivative of the

angular position of the motor axle of the joint motor and thus relates to the angular acceleration of the motor axle. B is the positive-definite diagonal matrix indicating the mass moments of inertia of the joint motor's rotors. $\mathbf{F_\Theta}(\dot{\Theta})$ is a vector comprising the friction torques acting on the motor axles and $\boldsymbol{\tau}_{motor}$ is a vector indicating the torque generated by the joint motors.

[0044] $\boldsymbol{F_\theta}(\dot{\boldsymbol{\Theta}})$ is a vector comprising the friction torques acting on the input axles of the robot joint gears. The friction torques acting on the input axle depends on angular velocity of the input axle $(\dot{\boldsymbol{\Theta}})$; however, it is to be understood the friction torques acting on the input axle also can depend on other parameters such as temperatures, type of lubricants, loads to robot arm, position/orientation of the robot arm etc.

[0045] $\boldsymbol{F_\theta}(\dot{\boldsymbol{\Theta}})$ can for instance be provided as linear or nonlinear functions or lookup tables (LUTs) with interpolation, and $\boldsymbol{F_\theta}(\dot{\boldsymbol{\Theta}})$ can be defined based on for instance prior knowledge of the robot, experiments, and/or be adaptively updated during robot operation. For instance, $\boldsymbol{F_\theta}(\dot{\boldsymbol{\Theta}})$ can be obtained for each robot joint by running the robot joint gear at a constant angular velocity for at least one whole revolution of the output axle or any positive integer multiple of a revolution without the robot arm contacting external objects, while obtaining the motor torque of the robot joint motor. Under these conditions the inertia term of the robot arm $\boldsymbol{M}(\mathbf{q})\ddot{\boldsymbol{q}}$ is zero due to the constant angular velocity, the Coriolis and centripetal term $\mathbf{C}(\mathbf{q},\dot{\mathbf{q}})\dot{\mathbf{q}}$ cancels because only one robot joint is moved at the time, and the gravity term $\mathbf{G}(\mathbf{q})$ cancels out due to the full rotation of the output axle, and no external torques are provided to the robot arm. Consequently eq. 7 reduces to:

eq. 10 $$\boldsymbol{\tau}_{joint,average} = \boldsymbol{F}_{\boldsymbol{q},average}(\dot{\boldsymbol{q}})$$

where $\boldsymbol{\tau}_{joint,average}$ indicates the average joint transmission torque during one revolution of the output axle and $\boldsymbol{F}_{q,average}(\dot{\boldsymbol{q}})$ indicates the friction force acting on the output axle of the robot joint gear during one revolution of output axle. Further, under these conditions the inertia term of the joint motors $B\,\ddot{\boldsymbol{\Theta}}$ is zero due to the constant velocity. Consequently eq. 9 reduces to:

eq. 11 $$\boldsymbol{\tau}_{motor} = \boldsymbol{F_\theta}(\dot{\boldsymbol{\theta}}) + \boldsymbol{\tau}_{joint}$$

combining eq. 10 and eq. 11 makes it possible to obtain the friction torques acting on the motor axles as:

eq. 12 $$\boldsymbol{F_{\theta}}(\dot{\boldsymbol{\theta}}) = \boldsymbol{\tau}_{motor} - \boldsymbol{F}_{q,average}(\dot{\boldsymbol{q}})$$

[0046] The friction torque $\boldsymbol{F_{\theta}}(\dot{\boldsymbol{\Theta}})$ can also be mechanically modeled for instance as a Generalized Maxwell-Slip (GMS) model [19] which is based on three frictional properties

1) a Stribeck curve for constant velocities,

2) a hysteresis function with nonlocal memory in the pre-sliding regime, and

3) a frictional lag in the sliding regime.

The GMS model captures the behavior of hysteresis which often are seen in robot joint gears for instance strain wave gears, where the GMS model can be obtained based on the measured $\boldsymbol{F_{\theta}}(\dot{\boldsymbol{\Theta}})$.

[0047] For single robot joint gear, the GMS model can be visualized as a parallel connection of M massless block-spring models (illustrated in fig. 11) subject to the same input velocity $\omega = {}^{d\theta}/_{dt}$. The total friction force is given as the summation of friction forces for each element i, i.e.

eq. 13 $$F_{\Theta} = \sum_{i=1}^{M} F_i$$

The dynamics of each elementary model is represented by the equations (10) and (11). If the element is sticking:

eq. 14 $$\frac{d\,F_i}{dt} = k_i \omega$$

where k_i is the spring stiffness of the i^{th} element. The element remains sticking until $F_i > v_i s(\omega)$ where the fractional parameter v_i determines the maximum force F_i for each element during sticking. If the element is slipping

eq. 15 $$\frac{d\,F_i}{dt} = sign(\omega)\; C\; \left(v_i + \frac{F_i}{s(\omega)}\right)$$

The attraction parameter C determines how fast the total friction force approaches $s(\omega)$ in sliding.

The nonlinear static map

eq. 16 $$s(\omega) = sign(\omega)\left(F_C + (F_S - F_C)\cdot e^{-\left(|\omega|/v_S\right)^{\mu}}\right) + F_{V_1}\omega + F_{V_2}sign(\omega)\omega^2 + F_{V_3}\omega^3$$

captures the Stribeck effect and nonlinear viscous friction, where F_C, F_S, v_S and μ are, respectively, the Coulomb friction, the stiction, the Stribeck velocity, and the Stribeck shape factor, and F_{V_1}, F_{V_2}, F_{V_3} are viscous coefficients of friction.

[0048] Typically the robot controller is configured to control the movements/positions of the robot arm by determining the torques generated by the motor axles $\boldsymbol{\tau}_{motor}$ of the robot joint gears based on eq. 7 and eq. 9 and desired angular positions $\mathbf{q}$, angular velocity $\dot{\mathbf{q}}$ and/or desired angular accelerations $\ddot{\mathbf{q}}$ of the output axles of the robot joint gears. The desired angular positions $\mathbf{q}$, angular velocity $\dot{\mathbf{q}}$ and/or desired accelerations $\ddot{\mathbf{q}}$ of the output axles of the robot joint gears can for instance be provided via a robot program stored in the memory or via user inputs received through the input device. The angular positions $\mathbf{q}$, angular velocity $\dot{\mathbf{q}}$ and/or desired accelerations $\ddot{\mathbf{q}}$ of the output axles can be provided directly or as other parameter from which the parameters can be obtained for instance in form of coordinates of the robot tool flange in relation to the robot base or the like. The controller is then configured to control the joint motors by regulating the current through the joint motors.

[0049] Step 552 of applying a motor torque to the motor axles of the joint motors can for instance be carried out by the controller instructing the joint motor to apply a motor torque to the motor axles of the robot joint gears. For instance, the controller can be configured to provide motor torques that maintain the robot arm in a static posture, where the motor torques are sufficient to overcome the gravity on the robot arm or by providing motor torques moving parts of the robot. Consequently, the joint motors are driven in order to generate motor torques $\boldsymbol{\tau}_{\text{motor}}$ by the motor axles.

[0050] In one embodiment the step of applying a motor torque to the motor axle using the joint motor results in movement of at least a part of the robot arm. This can be achieved by driving the joint motors with current that results in rotation of the robot joints whereby at least a part of the robot arm

moves. For instance, the robot controller may be configured to apply a motor torque to the joint motors that result in movement of a part of the robot arm upward in relation to gravity and in such situation the applied motor torque is larger than the motor torque needed to compensate for gravity. Also, the robot controller may be configured to apply a motor torque to the joint motors that result in movement of a part of the robot arm downward in relation to gravity and in such situation the applied motor torque is smaller than the motor torque needed to compensate for gravity. However, it is to be understood that any motor torque resulting in movement in any direction of at least a part of the robot arm can be applied. Consequently, both the input axle of the robot joint gears and the output axle of the robot joint gears rotates. The dynamic terms of the dynamic models according to eq. 7 and eq. 9, which depends on the angular velocity $\dot{\boldsymbol{q}}$ of the output axle, the angular acceleration $\ddot{\boldsymbol{q}}$ of the output axle, the angular velocity $\dot{\boldsymbol{\Theta}}$ of the motor axle, and/or the angular acceleration $\ddot{\boldsymbol{\Theta}}$ of the motor axle can be obtained during movement of the robot arm. For instance the angular velocity $\dot{\mathbf{q}}$ of the output axle, the angular acceleration $\ddot{\mathbf{q}}$ of the output axle, the angular velocity $\dot{\boldsymbol{\Theta}}$ of the motor axle, the angular acceleration $\ddot{\boldsymbol{\Theta}}$ of the motor axle can be obtained as described in paragraphs [0053]-[0054]. This makes it possible to obtain the gear stiffness of the robot joint gear during movement and operation of the robot arm.

[0051] The method can comprise an optional step 535 of obtaining the actual motor torque $\tau_{actually}$ provided by the motor axles. The actual motor torques can for instance be obtained by obtaining the current through the joint motors whereby the actual motor torque can be obtained as known in the art of motor control. For instance, if the joint motors are provided as three-phase Permanent Magnet Synchronous Machines (PMSM) with dynamics much faster than that of the manipulator. If the joint motors are operated under their current saturation limit, the motor axle torque can be obtained by:

eq. 17
$$\boldsymbol{\tau}_{actually,motor} = \boldsymbol{K}_{\tau}\, \boldsymbol{I}_{motor}$$

where $\tau_{actually,motor}$ is a vector comprising the actual torque provided by the motor axles of the joint motors (seen in the output space of the robot joint gear), K_{τ} is the positive-definite diagonal matrix of torque constants and $\mathbf{I}_{motor}$ is a vector

comprising the torque-generating (quadrature) current obtained from the phase currents of the joint motors using the Park Transform.

[0052] The actual torque of the motor axle can also be obtained by using force/torque sensors such as strain gauges indicating the actual torque of the motor axle. Obtaining the actual torque $\tau_{actually}$ generated by the motor axles provides a more accurate gear stiffness as eventual deviation between the desired motor signal and the actual torque can be eliminated.

[0053] Step 554 of obtaining the angular position of the motor axles of the joint motors can be obtained by measuring the angular position of the motor axle for instance by using an encoder such as optical/magnetic encoders as known in the art of robotics. The angular position of the motor axles $\boldsymbol{\Theta}$ can be stored in a memory for later usage for instance in order to store a number of angular positions of the motor axles obtained at different times. The angular position of the motor axles can for instance be used to obtain the angular velocity and/or angular acceleration of the motor axles for instance by differentiation and double differentiation of the angular position with respect to time. The angular velocity of the motor axles and angular acceleration of the motor axles can then be used to obtain the robot joint gear stiffness using the dynamic terms of the dynamic model of the robot arm. Consequently, the gear stiffness of the robot joint gear can be obtained during movement and operation of the robot arm. It is to be understood that the angular velocity of the motor axles and/or angular acceleration other motor axles alternatively can be obtained using sensors/encoders measuring the actual parameters.

[0054] Step 556 of obtaining the angular position of the output axle of the robot joint gears can be obtained by measuring the angular position of the output axle for instance by using encoders such as optical/magnetic encoders as known in the art of robotics. The angular position of the output axles $\mathbf{q}$ can be stored in a memory for later usage, for instance a number of angular positions of the output axles obtained at different times can be stored in a memory. Alternatively, the angular position of the output axles of the robot joint gears can be obtained as the desired angular position of the output axles upon which the controller is generating the motor torques. This makes it possible to estimate the angle of the output axles in robot joints that does not comprise

encoders for measuring the angular position of the output axles. The angular position of the output axle of the robot joint gears can for instance be used to obtain the angular velocity and/or angular acceleration of the output axle of the robot joint gears for instance by differentiation and double differentiation of the angular position with respect to time. The angular velocity of the output axles and angular acceleration of the output axles can then be used to obtain the robot joint gear stiffness using the dynamic terms of the dynamic model of the robot arm. Consequently, the gear stiffness of the robot joint gear can be obtained during movement and operation of the robot arm. It is to be understood that the angular velocity of the output axles and/or angular acceleration of motor axles alternatively can be obtained using sensors/encoders measuring the actual parameters.

[0055] Step 560 of determining the gear stiffness of the robot joint gears can be embodied by considering the model of the flexibility of the robot joint illustrated in fig. 3 and described in paragraphs [0024]-[0028]. The dynamic model of the robot arm can be further specified by replacing $\boldsymbol{\tau}_{\text{joint}}$ of eq. 7 and eq. 9 with the right hand side of eq. 2 and thereafter isolating the nonlinear flexibility $\boldsymbol{\tau}_{\mathbf{E}}(\boldsymbol{\Phi}_{\text{joint}})$:

eq. 18 $$\boldsymbol{\tau}_{\boldsymbol{E}}(\boldsymbol{\Phi}_{joint}) = M(\boldsymbol{q})\,\ddot{\boldsymbol{q}} + C(\boldsymbol{q},\dot{\boldsymbol{q}})\boldsymbol{q} + \boldsymbol{G}(\boldsymbol{q}) + \boldsymbol{F}_{\boldsymbol{q}}(\dot{\boldsymbol{q}}) + \boldsymbol{\tau}_{ext} - \boldsymbol{\tau}_{D}(\dot{\boldsymbol{\Phi}}_{joint})$$

eq. 19 $$\boldsymbol{\tau}_{\boldsymbol{E}}(\boldsymbol{\Phi}_{joint}) = \boldsymbol{\tau}_{motor} - B\,\ddot{\boldsymbol{\theta}} - \boldsymbol{F}_{\boldsymbol{\theta}}(\dot{\boldsymbol{\theta}}) - \boldsymbol{\tau}_{D}(\dot{\boldsymbol{\Phi}}_{joint})$$

where $\boldsymbol{\Phi}_{\text{joint}}$ is a vector comprising the deflection of each robot joint gear, $\dot{\boldsymbol{\Phi}}_{\text{joint}}$ is a vector comprising the first-order time derivative of the deflection of each robot joint and $\boldsymbol{\tau}_{\text{D}}(\dot{\boldsymbol{\Phi}}_{\text{joint}})$ is a vector comprising the damping torque for each robot joint gear as a function of the time derivative of the deflection of the robot joints and $\boldsymbol{\tau}_{\mathbf{E}}(\boldsymbol{\Phi}_{\text{joint}})$ is a vector comprising the flexibility torque of each of the robot joint gears as a function of the deflection of the robot joint gears.

[0056] Step 560 of determining the gear stiffness of the robot joint gears comprise thus a step 562 of obtaining the deflection $\boldsymbol{\Phi}_{\text{joint}}$ of the robot joint

gears based on the angular position $\boldsymbol{\Theta}$ of the motor axles and the angular position $\mathbf{q}$ of the output axles, where the deflection $\boldsymbol{\Phi}_{\text{joint}}$ of the robot joint gears can be indicated as the difference between the angular position Θ of the motor axle and the angular position q of the output axle as indicated by eq. 1. It is to be understood that the deflection alternatively also can be indicated as the difference between the angular position of the output axle and the angular position of the motor axle. Step 560 of determining the gear stiffness of the robot joint gears comprise a step 564 of obtaining a flexibility torque of the robot joint gear at the deflection of the robot joint gear based on at least the angular position of the motor axle, the angular position of the output axle and a dynamic model of said robot arm. The flexibility torque $\boldsymbol{\tau}_{\mathbf{E}}(\boldsymbol{\Phi}_{\text{joint}})$ of the robot joint gear at the deflection of the robot joint gear can be obtained based on eq. 18, with the angular position of the motor axles $\boldsymbol{\Theta}$ and the angular position $\mathbf{q}$ of the output axles as input variables, as the remaining parts of eq. 18 have been obtained during the initialization and for instance stored the memory. It is noted that $\boldsymbol{\tau}_{\text{ext}}$ is zero in situations where no external forces/torques are acting on the robot arm, however if for instance an external force is acting on the robot tool flange the external forces/torques can then be obtained based on eq. 8. Further the contribution from external forces can also be obtained by using force/torques sensors. Additionally, or alternatively $\boldsymbol{\tau}_{\mathbf{E}}(\boldsymbol{\Phi}_{\text{joint}})$ can be obtained based on eq. 19 with the angular position of the motor axles $\boldsymbol{\Theta}$, the angular position $\mathbf{q}$ of the output axles and motor torques $\boldsymbol{\tau}_{\text{motor}}$ by the motor axles as input variables. It is thus to be understood that the motor torques $\boldsymbol{\tau}_{\text{motor}}$ by the motor axles can be provided as an additional/optional input to step 564. In the embodiment comprising step 553 the motor torques $\boldsymbol{\tau}_{\text{motor}}$ can be replaced by the actual motor torques $\boldsymbol{\tau}_{\text{actually}}$ obtained in step 553 when obtaining the gear stiffness of the robot joint gear using eq. 19. The motor torques $\boldsymbol{\tau}_{\text{motor}}$ and the actual motor torques $\boldsymbol{\tau}_{\text{actually}}$ is indicated in brackets [] and () in fig 5 in order to illustrate that they can be provided as additional parameters to step 564.

[0057] In step 566 the gear stiffness of the robot joint gears can be obtained based on the deflection of the robot joint gear obtained in step 562 and the flexibility torque $\boldsymbol{\tau}_{\mathbf{E}}(\boldsymbol{\Phi}_{\text{joint}})$ of the robot joint gear obtained in step 564. Considering the eq. 4, eq. 5 and eq. 6 makes it possible to obtain the gear stiffness as:

eq. 20 $$\boldsymbol{K}_i(\boldsymbol{\Phi}_{joint}) = \frac{\delta\,\boldsymbol{\tau}_E}{\delta\,\boldsymbol{\Phi}_{joint}} \approx \frac{\Delta\,\boldsymbol{\tau}_E}{\Delta\,\boldsymbol{\Phi}_{joint}}$$

where $\boldsymbol{\tau}_{\mathbf{E}}(\boldsymbol{\Phi}_{\text{joint}})$ can be obtained based on eq. 18 or eq. 19 as described in connection with step 564.

[0058] The gear stiffness $\mathbf{k}_{\text{i}}(\boldsymbol{\Phi}_{\text{joint}})$ obtained by eq. 20 provides can be used to obtain the average gear stiffness between a certain deflection of the robot joint gear and the situation where deflection of the robot joint gear is zero, which is typically when no motor torque is provided to the robot joint gears. In such situation eq. 20 can be simplified to

eq. 21 $$\boldsymbol{K}_{i,average}(\boldsymbol{\Phi}_{joint}) = \frac{\boldsymbol{\tau}_E(\boldsymbol{\Phi}_{joint}) - \boldsymbol{\tau}_E(0)}{\boldsymbol{\Phi}_{joint} - 0} = \frac{\boldsymbol{\tau}_E(\boldsymbol{\Phi}_{joint})}{\boldsymbol{\Phi}_{joint}}$$

[0059] Additionally or alternatively the gear stiffness of the robot joint gears can be indicated as the flexibility torque $\boldsymbol{\tau}_{\mathbf{E}}(\boldsymbol{\Phi}_{\text{joint}})$, where a high flexibility torque at a given deflection of the robot joint gear indicates a high gear stiffness, as a higher flexibility torque is needed to achieve the deflection of the robot joint gear; reversely a low flexibility torque at a given deflection of the robot joint gear indicates a low gear stiffness as a smaller flexibility torque is needed to achieve the deflection of the robot joint gear. The gear stiffness of the robot joint gears can thus be indicated based eq. 18 and/or eq. 19.

[0060] The method can comprise an optional step 570 of comparing the obtained gear stiffness $\mathbf{k}_{\text{i}}(\boldsymbol{\Phi}_{\text{joint}})$ with prior knowledge of the robot joint gear stiffness $\mathbf{k}_{\text{i,limit}}(\boldsymbol{\Phi}_{\text{joint}})$ and provide a status $\mathbf{S}_{\text{joint}}$ of the robot joint gears based on the obtained gear stiffness and said prior knowledge of the robot gear stiffness. For instance, the average gear stiffness can be obtained at different times during the life time of the robot and be compared a threshold value of the gear stiffness, where the threshold value has been determined based on knowledge about the evolution of the gear stiffness in relation to wear of the robot joint gear. The status of the robot joint gear can thus be used to indicate the wear of the robot joint gears. Typically, the gear stiffness of a robot joint gears tend to decrease before the robot joint gears breaks, as material is worn off at the gear meshing. Consequently, the controller can be adapted to provide a warning when the gear stiffness reaches a threshold value, whereby the robot joint gear can be sent

for repair or replaced before the gear breaks. This makes it possible to avoided failure of the robot joint gear and thereby avoid downtime of the robot arm.

[0061] The method can comprise an optional step 580 of controlling the robot arm based on the obtained gear stiffness of the robot joint gears by providing a control signal $\boldsymbol{\tau}_{\text{control}}$ indicative of a desired motor torque $\boldsymbol{\tau}_{\text{motor}}$ of the motor axle. The desired motor torque $\boldsymbol{\tau}_{\text{motor}}$ can for instance be obtained based on the gear stiffness of the robot joint gears by modifying the dynamic model of the robot to include the stiffness of the robot joint gears and then update the dynamic model of the robot based on the gear stiffness obtained in step 560.

[0062] Fig. 6 illustrates a flow chart of the method of obtaining the gear stiffness of a robot joint gear of a robot joint of a robot arm. The method is like the method illustrated in fig. 5 and similar steps have been given the same reference numbers as in fig. 5 and will not be described further.

[0063] In this embodiment the methods comprise a step 665 (illustrated as an arrow) of repeating the following steps:

- step 552 of applying a motor torque to the motor axle using the joint motor;
- step 554 of obtaining the angular position of the motor axle;
- step 556 of obtaining the angular position of the output axle;
- step 562 of obtaining the deflection of the robot joint gear based on the angular position of the motor axle and the angular position of the output axle; and
- step 564 of obtaining a flexibility torque of the robot joint gear at the deflection of the robot joint gear based on at least the angular position of the motor axle, the angular position of the output axle and a dynamic model the of robot arm.

The steps are repeated a plurality of times and the deflection $\boldsymbol{\Phi}_{\text{joint}}$ of the robot gears obtained in step 562 and the flexibility torque of the robot joint gears obtained in step 564 are stored for each repetition. Consequently, a data set comprising a plurality of data points $(\boldsymbol{\Phi}_{\text{joint}}; \boldsymbol{\tau}_{\mathbf{E}}(\boldsymbol{\Phi}_{\text{joint}}))$ can be obtained and the flexibility torque of the robot joint gears can be obtained for different deflections of the robot joint gears. During the repetitions motor torque applied to the motor

axle of the robot joint gears can be varied in step 552 whereby it is possible to obtain the flexibility torque of the robot joint gears over a range of robot joint gear deflections. This makes it possible to map the flexibility torque of the robot joint gears as a function of the robot joint gear deflection and the gear stiffness of the robot joint gear can be obtained as function of the robot joint gear deflection.

[0064] Step 667 is a step of fitting the obtained data points comprising the flexibility torques of the robot joint gears and the corresponding robot joint gear deflection with a mathematical function. For instance, the obtained data points for a single robot joint can be fitted to polynomial function having a linearly parametrized polynomial basis:

eq. 22 $$\tau_{E,i}(\Phi_{joint,i}) = \boldsymbol{\Psi}^T(\Phi_{joint,i})\ \boldsymbol{\alpha}_i$$

where $\boldsymbol{\Psi}^T(\boldsymbol{\Phi}_{\text{joint}})$ is the linear polynomial basis of the deflection variable Φ_{joint}, $\boldsymbol{\alpha}_{\text{i}}$ is a vector comprising the constants for polynomial basis functions of the i^{th} robot joint. Based on the symmetry assumptions in eq. 5 and eq. 6 the regressor $\boldsymbol{\Psi}^T(\boldsymbol{\Phi}_{\text{joint}})$ can be specified to contain only odd powers of $\boldsymbol{\Phi}_{\text{joint}}$, thus:

eq. 23 $$\boldsymbol{\Psi}^T(\boldsymbol{\Phi}_{joint}) = \boldsymbol{\Phi}_{joint}{}^{2p-1}, \qquad p = 1,2,\ldots\ldots,P$$

In summation form the polynomial function can be written as:

eq. 24

$$\tau_{\text{E,i}}(\Phi_{\text{joint,i}}) = \sum_{p=1}^{P} \boldsymbol{\alpha}_{p,i} \cdot \Phi_{\text{joint,i}}{}^{2\text{p}-1}$$

where $\boldsymbol{\alpha}_{\boldsymbol{p,i}}$ is a vector comprising the constants for the polynomial basis functions for the i^{th} robot joint. In a robot arm comprising a plurality of robot joints a polynomial function and corresponding vector of constants can be provided for each robot joint.

[0065] As described in paragraph [0027] and stated by eq. 4 the stiffness of the robot joint gear can then be determined as the change of flexibility torque of the robot joint gears with respect to the robot joint gear deflection. The method can comprise a step 668 of obtaining the gear stiffness of the robot joint robot by obtaining the slope of the flexibility torque with respect to the deflection of said robot joint gear. For instance, the slope can be determined between at least two of the data points indicated by eq. 20 and by eq. 21 for the situation where no flexibility torque exists at a deflection of zero. The slope can also be indicated by differentiation of the mathematical function fitted to the data points. In case of a polynomial function this corresponds to differentiation of eq. 24

eq. 25

$$K_i(\Phi_{joint}) = \frac{\delta\, \tau_E(\Phi_{joint,i})}{\delta\, \Phi_{joint,i}} = \sum_{p=1}^{P} (2p-1)\boldsymbol{\alpha}_{p,i} \cdot {\Phi_{joint,i}}^{2p-2}$$

[0066] The method of obtaining the gear stiffness of the robot joint gears of a robot joint have been demonstrated on a robot arm by obtaining the flexibility torque of a single robot joint gear as a function of robot joint gear deflection using both a method according to the present invention and an alternative method. The experiments have been performed using a UR5e robot arm provided by Universal Robots and the results are discussed in the following paragraphs.

[0067] Fig. 7 illustrates the robot arm 701 in configuration used in the experimental analysis. The robot arm is a six-axis robot comprising robot base 705 carrying the robot arm. A base joint 703a is directly connected to the shoulder joint 703b and is configured to rotate the robot arm around a base axis 711a (illustrated by a dashed dotted line) as illustrated by rotation arrow 713a. The shoulder joint 703b is connected an elbow joint 703c via a robot link 704b and is configured to rotate the robot arm around a shoulder axis 711b as illustrated by rotation arrow 713b. The elbow joint 703c connected to a first wrist joint 703d via a robot link 704c and is configured to rotate the robot arm around an elbow axis 711c as illustrated by rotation arrow 713c. The first wrist joint 703d connected to a second wrist joint 703e and is configured to rotate

the robot arm around a first wrist axis 711d as illustrated by rotation arrow 713d. The second wrist joint 703e is connected to a robot tool joint 703f and is configured to rotate the robot arm around a second wrist axis 711e as illustrate by rotation arrow 713e. The robot tool joint 703f comprising the robot tool flange 707, which is rotatable around a tool axis 711f as illustrated by rotation arrow 713f.

[0068] During the experiments the robot arm 701 is arranged in a pose where the base axis 711A is parallel with the direction of gravity 723 and the shoulder axis 711b, the elbow axis 711c, the first wrist axis 711d, the second wrist axis 711e and the tool axis 711b are perpendicular to the direction of gravity 723. The base joint 703a is the only joint which is rotated during the experiment and the shoulder joint 703b, the elbow joint 703c, the first wrist joint 703d, the second wrist joint 703e and the tool joint 703b are thus fixed during the experiments.

[0069] The gear stiffness of the robot joint gear of the base joint 703a is obtained in the experiments. Firstly, the friction and the stiffness characteristics for the base joint 703a of the UR5e Robot arm is obtained using an alternative method.

[0070] The steady-state friction torque is identified by imposing different signals of constant velocity on the base joint while measuring the robot joint current. For constant velocity eq. 7, eq. 9 and eq. 17 yield $F_\theta + F_q = \mathrm{K}_\tau I$. The steady-state friction torque is illustrated in fig. 8. Fig. 8 illustrates a graph of the measured friction torques at varying angular velocity of the motor axle, where the horizontal axis indicates the angular velocity 881 of the motor axle and the vertical axis indicates the friction torque 882. The experimental data points comprising an angular velocity and corresponding friction torque 883 are illustrated as triangles. The parameters in eq. 16 are fitted to the data points using a Quasi-Newton method with a cubic line search procedure and updating the Hessian matrix approximation by the Broyden-Fletcher-Goldfarb-Shanno (BFGS) method and the fit have been illustrated by solid line 884. The fit of to the data points is 98,6 % using a normalized Root Mean Squared Error (NRMSE) method.

[0071] The flexibility torque of the robot joint gear of the base joint is obtained in a static setting by locking the input axle (motor axle) of the robot joint gear and imposing a set of known torques on the output axle using a Sauter

FH–S 500 digital force gage while measuring the deformation of the robot joint gear using the output and input encoders of the robot. Fig. 9 illustrates a graph where the vertical axis indicates flexibility torque of the robot joint gear 987 and the horizontal axis indicated the deflection of the robot joint gear 986. The experimental data points comprise a robot joint deflection and corresponding flexibility torque and are illustrated as triangles 988. The data points have been fitted to a linearly parametrized polynomial basis 989 (Static POLY fit) as described in eq. 24 with P=2 and is illustrated as a solid line. The fit of the polynomial bases to the data points is 96,9% using a normalized Root Mean Squared Error (NRMSE) method.

[0072] The flexibility torque of the robot joint gear of the base joint is obtained dynamically based on the method according to the present invention by rotating the base joint according to the bang-coast-bang joint space trajectory generated with randomly generated waiting times and angular positions, velocities, and accelerations in intervals ranging from 30 % to 100 % of the maximum allowed values. Fig. 10 illustrates graphs of the joint space trajectory used to drive the base joint of the robot, where the horizontal axis 1093 indicates time in seconds; graph 1093 illustrates the angular position of the base joint output axle; graph 1094 illustrates the angular velocity of the base joint output axle; graph 1095 illustrates the angular acceleration of the base joint output axle.

[0073] During the experiment the angular position of the output axle of the base joint, the angular position of motor axle of base joint, and the current trough the base joint motor are measured while the robot arm moves according the joint space trajectory illustrated in fig. 10. The flexible torque is the obtained based on the measured angular position of the output axle of the base joint, the angular position of motor axle of base joint and the current trough the base joint motor using eq. 19 and eq. 17.

[0074] Fig. 12 illustrates a graph where the vertical axis indicates flexibility torque of the robot joint gear 987 and the horizontal axis indicated the deflection of the robot joint gear 986. The experimental data points comprise a robot joint deflection and corresponding flexibility torque and are illustrated as triangles 1288. The experimental data points have been fitted to linearly parametrized polynomial basis (dynamic POLY fit 1290 illustrated in dashed line)

with P=2 using a Recursive Lease Squares (RLS) approach [20] as described in the next paragraph. The fit of the polynomial bases to the data points is 96,7% using a normalized Root Mean Squared Error (NRMSE) method.

[0075] Estimating time-varying parameters with the Recursive Least Squares (RLS) approach is obtained by incorporating a forgetting factor discounting past data. In the present example, the incoming information (the transmission deformation) is nonuniformly distributed over the parameter space. Tracking can only happen in some direction if there is an excitation in that same direction, hence the estimation algorithm tracks time-varying parameters only within the excited subspace. In particular, inspired by the results in [21], by a suitable notion of excitation subspace, the parameter vector in eq. 22 is estimated by the procedure:

eq. 26: $$\varepsilon(k) = \tau_E(k) - \mathbf{\Psi}^{\mathsf{T}}(k)\,\hat{\boldsymbol{\alpha}}(k-1)$$

eq. 27 $$r(k) = \mathbf{\Psi}^{\mathsf{T}}(k)\,P(k-1)\,\mathbf{\Psi}(k)$$

eq. 28 $$\mathbf{L}(k) = \frac{P(k-1)\,\mathbf{\Psi}(k)}{1+r(k)}$$

eq. 29 $$\hat{\boldsymbol{\alpha}}(k) = \hat{\boldsymbol{\alpha}}(k-1) + \mathbf{L}(k)\,\varepsilon(k)$$

eq. 30 $$\beta(k) = \begin{cases} \mu - \frac{1-\mu}{r(k)}, & \mu \in [0;1] \quad \text{if } r(k) > 0 \\ 1 & \text{if } r(k) = 0 \end{cases}$$

eq. 31 $$P(k) = P(k-1) - \frac{P(k-1)\,\mathbf{\Psi}(k)\,\mathbf{\Psi}^{\mathsf{T}}(k)\,P(k-1)}{\beta(k)^{-1} + r(k)} + \delta\, I$$

where $\delta > 0$ enforces an increment of the covariance matrix P improving the algorithm alertness. More alertness is achieved by decreasing μ at the price of an increased sensitivity to disturbances. By setting $\mu = 1$ and $\delta = 0$, eq. 31 reduces to the standard RLS algorithm.

[0076] The fit of the polynomial bases (static POLY fit 989) of the flexible torque obtained statically as descried in paragraph [0063] have also been included in the fig. 12. There is very good alignment between the flexibility torque obtained by the two methods. Thus, it is possible to obtain the flexibility torque and/or stiffness of the robot joint gear based on the method according

to the present invention under dynamic conditions where the output axle of the robot joint gear rotates. For instance, by obtaining the angular position of the input axle, the angular position of the output axle and the motor torque applied to the input axle. Where the motor torque applied to the input axle for instance can be obtained based on the phase currents through the coils of the joint motors (provided as PMSM).

[0077] Fig. 13 illustrates the obtained joint stiffness obtained by differentiation of the static POLY fit 989 and dynamic POLY fit graphs 1290 in fig. 12. The vertical axis indicates gear stiffness of the robot joint gear 1397 and the horizontal axis indicated the deflection of the robot joint gear 986. The gear stiffness as obtained via the static measurements illustrated as solid line 1398 (static POLY stiffness) and is obtained by differentiation of the linearly parametrized polynomial basis 989 with respect the robot joint deflection. The gear stiffness as obtained via the dynamic measurements illustrated as dashed line line 1397 (dynamic POLY stiffness) and is obtained by differentiation of the linearly parametrized polynomial basis 1290 with respect the robot joint deflection. The variations of gear stiffness as function of the robot joint deflection obtained by the two methods are very good aligned.

[0078] The present invention makes it thus possible to obtain the flexibility torque and the gear stiffness of the robot joint gears of a robot arm online during ordinary usage of the robot arm, where the robot arm typically performs a number of movements for instance in connection with a production setup.

BRIEF DESCRIPTION OF FIGUR REFERENCES

101	robot arm
103a-103f, 203, 303, 403i; 403i+1; 401n	robot joint
104b, 104c, 104d, 304i; 304i-1	robot link
105	robot base
107	robot tool flange
209, 309	joint motor
111a-111f, 211	axis of rotation
113a-113f:, 213	rotation arrow
115, 415	robot controller
117	interface device
119	display
121	input device
123	direction of gravity

225, 325i	motor axle
326	spring connecting input side and output side
227, 327i	output axle
328	damper connecting input side and output side
229, 329i	robot joint gear
231	output flange
233, 433i; 433i+1; 433n	motor control signal
235	output encoder
236, 436i; 436i+1; 436n	output encoder signal
237	motor encoder
238, 438i; 438i+1; 438n	output encoder signal
239	encoder wheel
241	motor torque sensor
242	motor torque signal
443	Processor
445	memory
550	Initializing
552	Apply motor torque to motor axle
653	obtain actual motor torque
554	obtain motor axle position
556	obtain output axle position
560	obtain stiffness of joint gear
562	obtain deflection of robot joint gears
564	Obtain flexibility torque of robot joint gears
665	Repeat
566, 666	determine gear stiffness
667	Fit data points with mathematical function
668	determine slope of fit
570	compare gear stiffness
580	Control robot based on gear stiffness
881	Angular velocity of motor axle
882	friction torque
883	data points comprising an angular velocity and corresponding friction torque
884	BRGS fit
986	flexibility torque of the robot joint gear
987	deflection of the robot joint gear
988, 1288	data points comprise a robot joint deflection and corresponding flexibility torque
989	static POLY fit
1290	dynamic POLY fit
1092	time

1093	angular position of base joint output axle
1094	angular velocity of base joint output axle
1095	angular acceleration of base joint output axle
1397	gear stiffness of robot joint gear
1398	static POLY stiffness
1399	dynamic POLY stiffness

REFERENCES

[1] T. W. Nye, ”Harmonic Drives: Determining Wear Life Based on Stiffness Considerations,” in Proc. of the International Power Transmission and Gearing Conference, Chicago, April 25-28, 1989.

[2] M. R. Johnson et al., ”Life Test Failure of Harmonic Gears in a Two-Axis Gimbal for the Mars Reconnaissance Orbiter Spacecraft,” Proceedings of the 38th Aerospace Mechanisms Symposium, Langley Research Center, May 17-19, 2006.

[3] J. Mobley and J. Parker, ”Harmonic Drive™ Gear Material Selection and Life Testing,” Proceedings of the 41th Aerospace Mechanisms Symposium, Jet Propulsion Laboratory, May 16-18, 2012.

[4] A. Albu-Schäffer and G. Hirzinger, ”Parameter identification and passivity based joint control for a 7DOF torque controlled light weight robot,” in Proc. of IEEE International Conference on Robotics & Automation (ICRA), Seoul, Korea, May 21-26, 2001, pp. 2852–2858.

[5] M. T. Pham et al., ”Identification of joint stiffness with bandpass filtering,” in Proc. of IEEE International Conference on Robotics & Automation (ICRA), Seoul, Korea, May 21-26, 2001, pp. 2867–2872.

[6] M. Östring et al., ”Closed-loop identification of an industrial robot containing flexibilities,” in Control Engineering Practice, vol. 11, 2003, pp. 291–300.

[7] M. Gautier et al., ”Dynamic Identification of flexible joint manipulators with an efficient closed loop output error method based on motor torque output data,” in IEEE International Conference on Robotics and Automation (ICRA), Karlsruhe, Germany, May 6-10, 2013, pp. 2949–2955.

[8] C. Dumas et al., ”Joint stiffness identification of six-revolute industrial serial robots,” in Robotics and Computer-Integrated Manufacturing, vol. 27, 2011, pp. 881–888.

[9] A. Klimchick and A. Pashkevich, “Robotic manipulators with double encoders: accuracy improvement based on advanced stiffness modeling and intelligent control,” in IFAC PapersOnLine, vol. 51, no. 11, 2018, pp. 740–745.

[10] A. Jubien et al., ”Joint Stiffness Identification of a Heavy Kuka Robot with a Low-cost Clamped End-effector Procedure,” in Proc. Of International Conference on Informatics in Control, Automation and Robotics (ICINCO), Vienna, Austria, Sept. 1-3, 2014, pp. 585–591.

[11] A. Jafari et al., ”AwAS-II: A new Actuator with Adjustable Stiffness based on the novel principle of adaptable pivot point and variable lever ratio,” in Proc. of IEEE International Conference on Robotics & Automation (ICRA), Shanghai, China, May 9-13, 2011, pp. 4638–4643.

[12] M. Grebenstein et al., ”The DLR Hand Arm System,” in Proc. Of IEEE International Conference on Robotics & Automation (ICRA), Shanghai, China, May 9-13, 2011, pp. 3175–3182.

[13] F. Flacco and A. De Luca, ”Residual-based Stiffness Estimation in Robots with Flexible Transmissions,” in Proc. of IEEE International Conference on Robotics & Automation (ICRA), Shanghai, China, May 9 - 13, 2011, pp. 5541–5547.

[14] F. Flacco and A. De Luca, ”Robust Estimation of Variable Stiffness in Flexible Joints,” in Proc. of IEEE/RSJ International Conference on Intelligent Robots and Systems, San Francisco, CA, USA, September 25-30, 2011, pp. 4026–4033.

[15] F. Flacco and A. De Luca, ”A Pure Signal-Based Stiffness Estimation for VSA Devices,” in Proc. of IEEE International Conference on Robotics & Automation (ICRA), Hong Kong, China, May 31 – June 7, 2014, pp. 2418–2423.

[16] T. Ménard et al., ”A real time robust observer for an Agonist-Antagonist Variable Stiffness Actuator,” in Proc. of IEEE International Conference on Robotics & Automation (ICRA), Karlsruhe, Germany, May 6-10, 2013, pp. 3988–3993.

[17] A. Cirillo et al., "A mechatronic approach for robust stiffness estimation of variable stiffness actuators," in IEEE/ASME International Conference on Advanced Intelligent Mechatronics, Wollongong, Australia, July 9-12, 2013, pp. 399–404.

[18] M. W. Spong, "Modeling and Control of Elastic Joint Robots," Journal of Dynamic Systems, Measurement, and Control, vol. 109, no. 4, 1987, pp. 310–319.

[19] V. Lampaert et al., A Generalized Maxwell-Slip Friction Model appropriate for Control Purposes," in IEEE International Conference for Physics and Control, St. Petersburg, Russia, Proceedings, pp. 1170–1177, 2003.

[20] S. Bittanti et al., "Recursive Least-Squares Identification Algorithms with Incomplete Excitation: Convergence Analysis and Application to Adaptive Control," IEEE Trans. Automatic Control, vol. 35, pp. 1371–1373, 1990.

[21] S. Bittanti et al., "Convergence and Exponential Convergence of Identification Algorithms with Directional Forgetting Factor," Automatica, Vol. 26, No. 5, pp. 929–932, 1990.

CLAIMS

1. A method of obtaining the gear stiffness of a robot joint gear of a robot joint of a robot arm, where said robot joint is connectable to at least another robot joint, said robot joint comprises a joint motor having a motor axle, said motor axle is configured to rotate an output axle via said robot joint gear, said method comprises the steps of:

- applying a motor torque to said motor axle using said joint motor;
- obtaining the angular position of said motor axle;
- obtaining the angular position of said output axle;
- determining said gear stiffness based on at least said angular position of said motor axle, said angular position of said output axle and a dynamic model of said robot arm, where said dynamic model of said robot arm defines a relationship between forces acting on said robot arm and resulting accelerations of said robot arm.

2. The method according to claim 1 wherein said step of determining said gear stiffness is further based on said motor torque applied to said motor axle.

3. The method according to any one of claims 1-2, wherein said step of applying a motor torque to said motor axle using said joint motor results in movement of at least a part of said robot arm.

4. The method according to any one of claims 1-3 wherein said step of determining said gear stiffness comprises the steps of:

- obtaining the deflection of said robot joint gear based on said angular position of said motor axle and said angular position of said output axle; and
- obtaining a flexibility torque of said robot joint gear at said deflection of said robot joint gear based on at least said angular position of said motor axle, said angular position of said output axle and said dynamic model of said robot arm.

5. The method according to claim 4 wherein said step of obtaining said gear stiffness comprises a step of repeating a plurality of times said steps of:

- applying a motor torque to said motor axle using said joint motor;
- obtaining the angular position of said motor axle;
- obtaining the angular position of said output axle;
- obtaining the deflection of said robot joint gear based on said angular position of said motor axle and said angular position of said output axle; and
- obtaining a flexibility torque of said robot joint gear at said deflection of said robot joint gear based on at least said angular position of said motor axle, said angular position of said output axle and said dynamic model of said robot arm;

and for each repetition store said deflection of said robot joint gear and said flexibility torque of said robot joint gear at said deflection of said robot joint gear.

6. The method according to claim 5 wherein said step of determining said gear stiffness of said robot joint gear comprises a step of fitting said obtained flexibility torques and said deflection of said robot joint gears with a mathematical function.

7. The method according to claim 6 wherein said mathematical function is a polynomial function obtained based on a recursive least squares estimation.

8. The method according to any one of claims 5-7 wherein said gear stiffness of said robot joint gear is obtained as the slope of said flexibility torque with respect to said deflection of said robot joint gear.

9. The method according to any one of claim 1-8 wherein said method comprises a step of comparing said obtained gear stiffness with prior knowledge of the robot gear stiffness and provide a status indication of the robot joint gears based

on the obtained gear stiffness and said prior knowledge of the robot gear stiffness.

10. The method according to anyone of claims 1-9 wherein said dynamic model of said robot arm comprises information modeling a parallel spring and damper coupling between said motor axle of said robot joint and said output axle of said robot joint.

11. A method of controlling a robot arm, said robot arm comprising a plurality of robot joints connecting a robot base and a robot tool flange, said method comprises the steps of controlling said robot joints based on a dynamic model, and the gear stiffness of a robot joint gear of at least one of said robot joints, where said at least one robot joint is connectable to at least another robot joint, said at least one robot joint comprises a joint motor having a motor axle*,* said motor axle is configured to rotate an output axle via said robot joint gear, where said dynamic model of said robot arm defines a relationship between forces acting on said robot arm and resulting accelerations of the robot arm **characterized in** that said method comprises a step of obtaining said gear stiffness comprising the method according to any one of claims 1-11.

12. The method according to claim 11 wherein said method comprises a step of modifying said dynamic model based on said obtained gear stiffness.

13. A robot arm comprising a plurality of robot joints connecting a robot base and a robot tool flange, said robot arm comprises at least one controller configured to control said robot joints based on a dynamic model of said robot arm, where at least one of said robot joint comprises a joint motor having a motor axle*,* said motor axle is configured to rotate an output axle via said robot joint gear, where said dynamic model of said robot arm defines a relationship between forces acting on said robot arm and resulting accelerations of said robot arm **characterized in** that said controller is configured to obtain the gear stiffness of said robot joint gear by:

- applying a motor torque to said motor axle using said joint motor;
- obtaining the angular position of said motor axle;
- obtaining the angular position of said output axle;
- determining said gear stiffness based on at least said angular position of said motor axle, said angular position of said output axle and said dynamic model of said robot arm, where said dynamic model of said robot arm defines a relationship between forces acting on said robot arm and resulting accelerations of said robot arm.

14. The robot arm according to claim 13 **characterized in** that said controller is configured to control said robot joints based on said obtained gear stiffness of said robot joint gear.

15. The robot arm according to any one of claims 13-14 **characterized in** that said motor torque applied to said motor axle causes movement of at least at part of said robot arm.

16. The robot arm according to any one of claims 13-15 **characterized in** that said robot arm comprises at least one of:

- an output encoder configured to indicate said angular position of said output axle;
- an input encoder configured to indicate said angular position of said motor axle.

17. The robot arm according to any one of claims 13-16 **characterized** in that said controller is configured to:

- compare said obtained gear stiffness with a threshold value of said gear stiffness;
- provide a status signal relating to said robot joint gear based on said comparison of said obtained gear stiffness with said threshold value of said gear stiffness.

18. The robot arm according to any one of claims 13-17 **characterized in** that said robot arm comprises a memory comprising instructions instructing said controller to obtain said gear stiffness by performing the method according to any one of claims 1-10.

5

ABSTRACT

A method of obtaining the gear stiffness of a robot joint gear of a robot joint of a robot arm, where the robot joint is connectable to at least another robot joint. The robot joint comprises a joint motor having a motor axle configured to rotate an output axle via the robot joint gear. The method comprises the steps of: -applying a motor torque to the motor axle using the joint motor; -obtaining the angular position of the motor axle; -obtaining the angular position of the output axle; -determining the gear stiffness based on at least the angular position of the motor axle, the angular position of the output axle and a dynamic model of the robot arm.

1/10

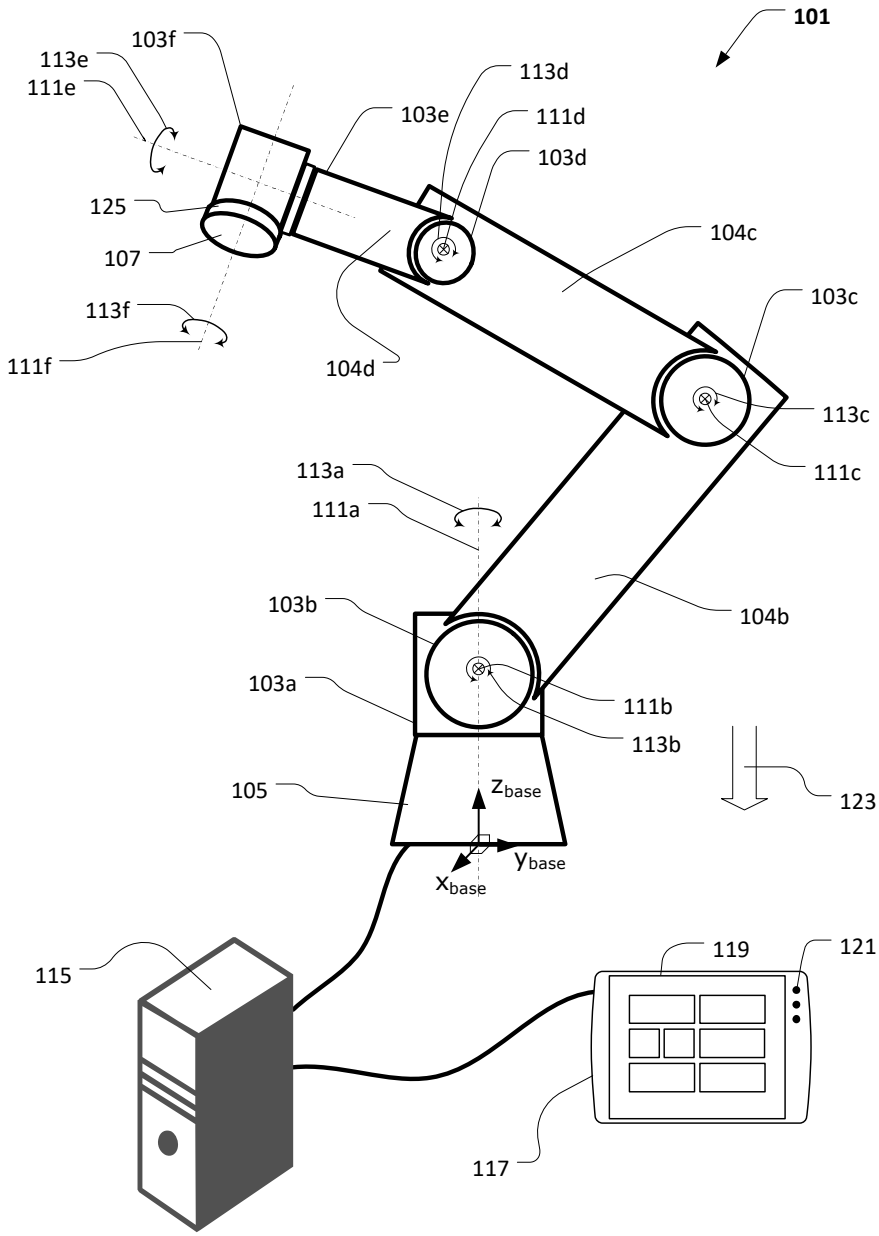
101
103f
113e
111e
113d
103e
111d
103d
125
107
104c
103c
113f
111f
104d
113c
111c
113a
111a
104b
103b
103a
111b
113b
105
z_{base}
y_{base}
x_{base}
123
115
119
121
117

FIG. 1

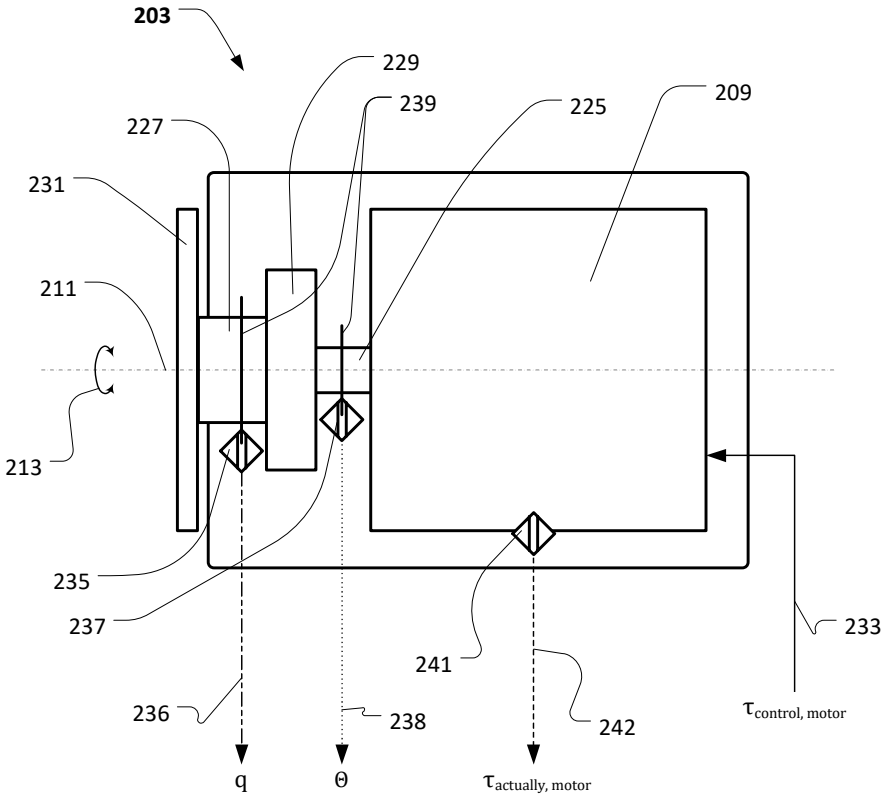
203
229
239
225
209
227
231
211
213
235
237
241
233
236
238
242
q
Θ
$\tau_{actually,\ motor}$
$\tau_{control,\ motor}$

FIG. 2

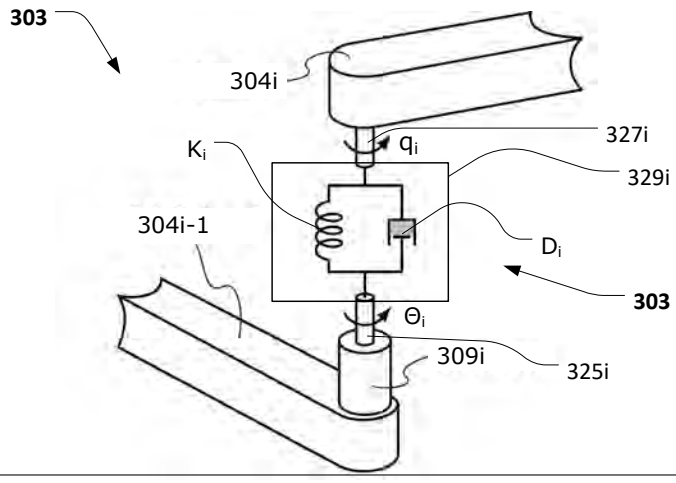
303
304i
327i
K_i
q_i
329i
304i-1
D_i
303
Θ_i
309i
325i

FIG. 3

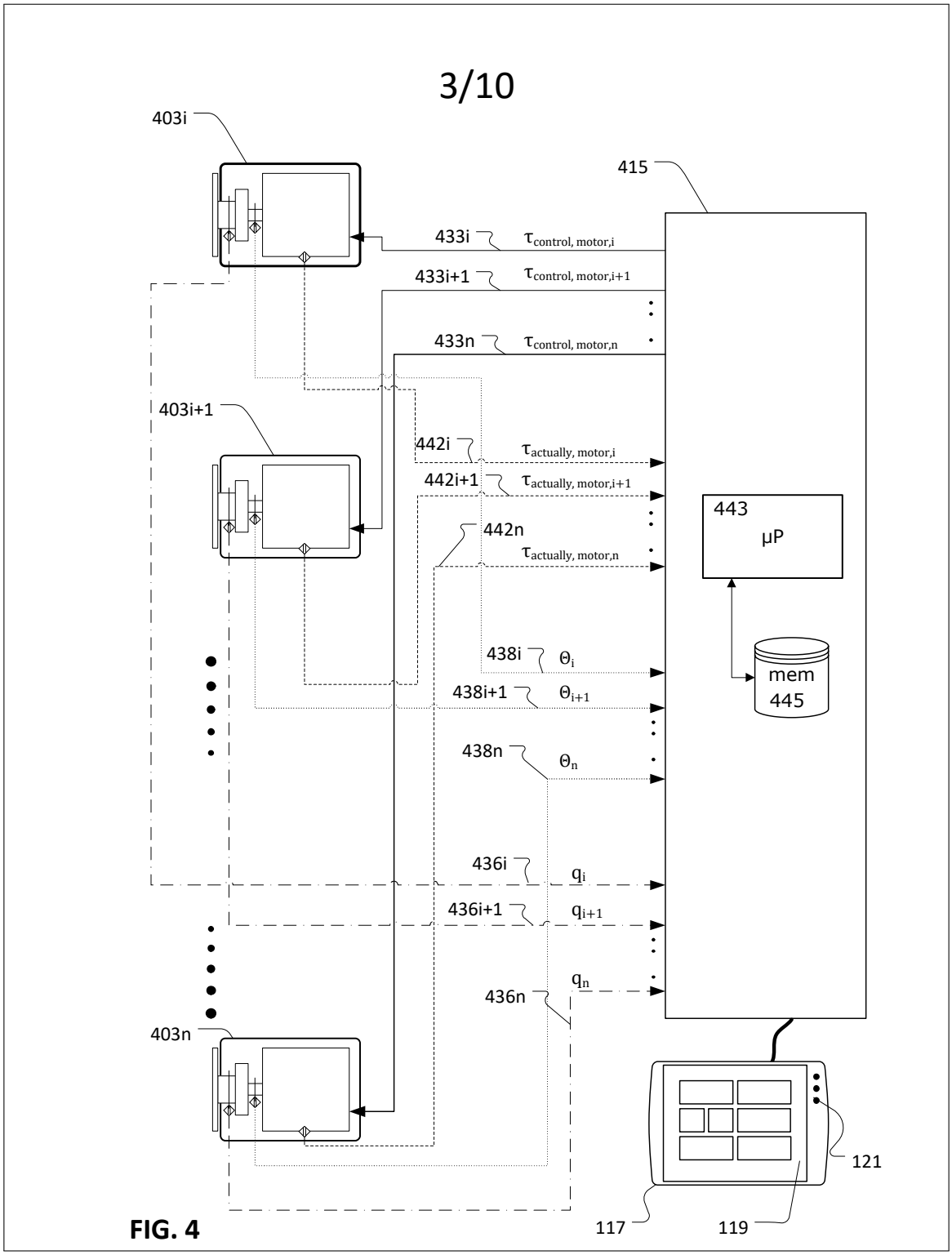
3/10
403i
415
433i
$\tau_{control,\ motor,i}$
433i+1
$\tau_{control,\ motor,i+1}$
433n
$\tau_{control,\ motor,n}$
403i+1
442i
$\tau_{actually,\ motor,i}$
442i+1
$\tau_{actually,\ motor,i+1}$
442n
$\tau_{actually,\ motor,n}$
443
µP
mem
445
438i
Θ_i
438i+1
Θ_{i+1}
438n
Θ_n
436i
q_i
436i+1
q_{i+1}
q_n
436n
403n
121
117
119

FIG. 4

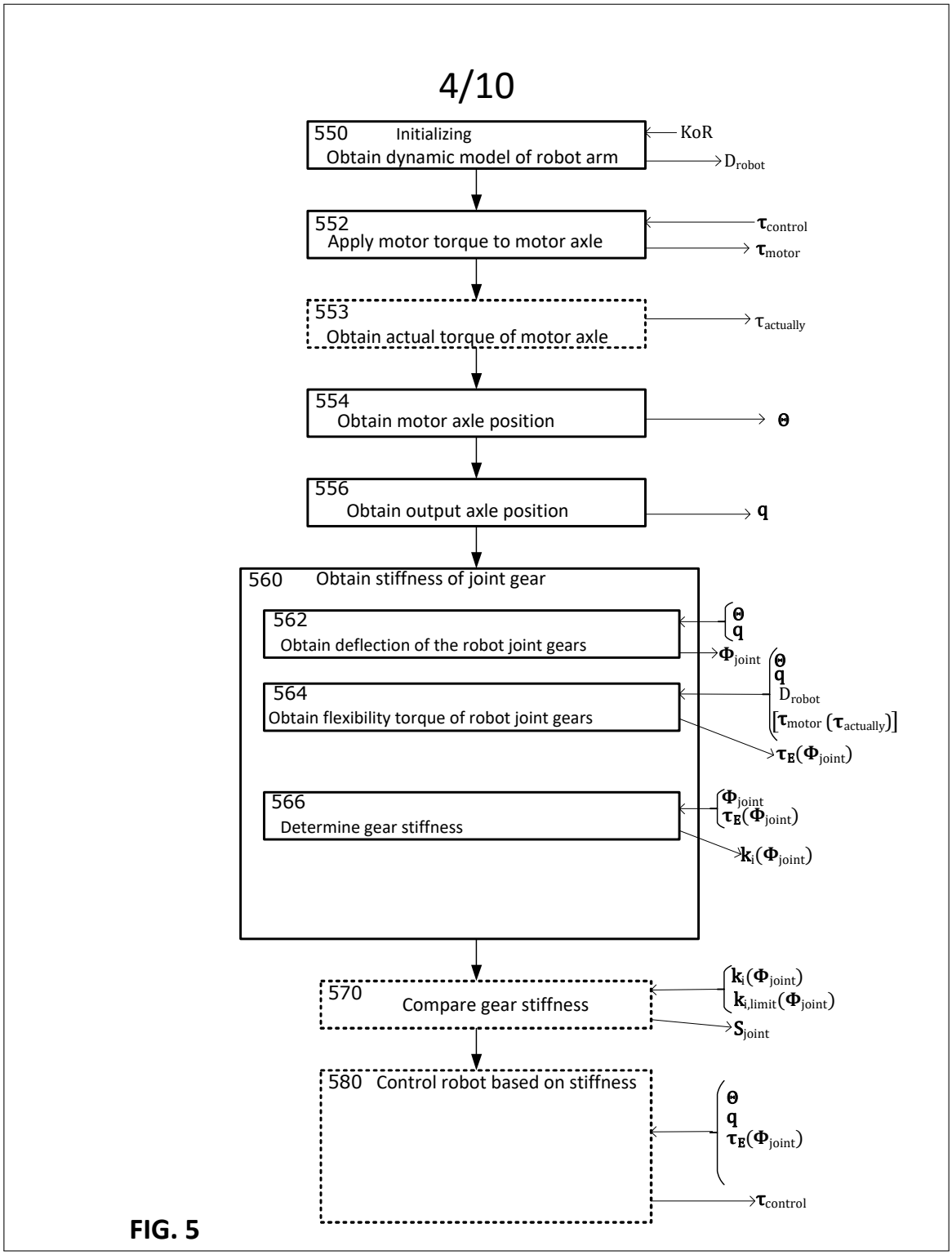
4/10
550 Initializing
Obtain dynamic model of robot arm
KoR
D_{robot}
552
Apply motor torque to motor axle
$\tau_{control}$
τ_{motor}
553
Obtain actual torque of motor axle
$\tau_{actually}$
554
Obtain motor axle position
Θ
556
Obtain output axle position
q
560 Obtain stiffness of joint gear
562
Obtain deflection of the robot joint gears
Θ
q
Φ_{joint}
564
Obtain flexibility torque of robot joint gears
Θ
q
D_{robot}
$[\tau_{motor}(\tau_{actually})]$
$\tau_E(\Phi_{joint})$
566
Determine gear stiffness
Φ_{joint}
$\tau_E(\Phi_{joint})$
$k_i(\Phi_{joint})$
570
Compare gear stiffness
$k_i(\Phi_{joint})$
$k_{i,limit}(\Phi_{joint})$
S_{joint}
580 Control robot based on stiffness
Θ
q
$\tau_E(\Phi_{joint})$
$\tau_{control}$

FIG. 5

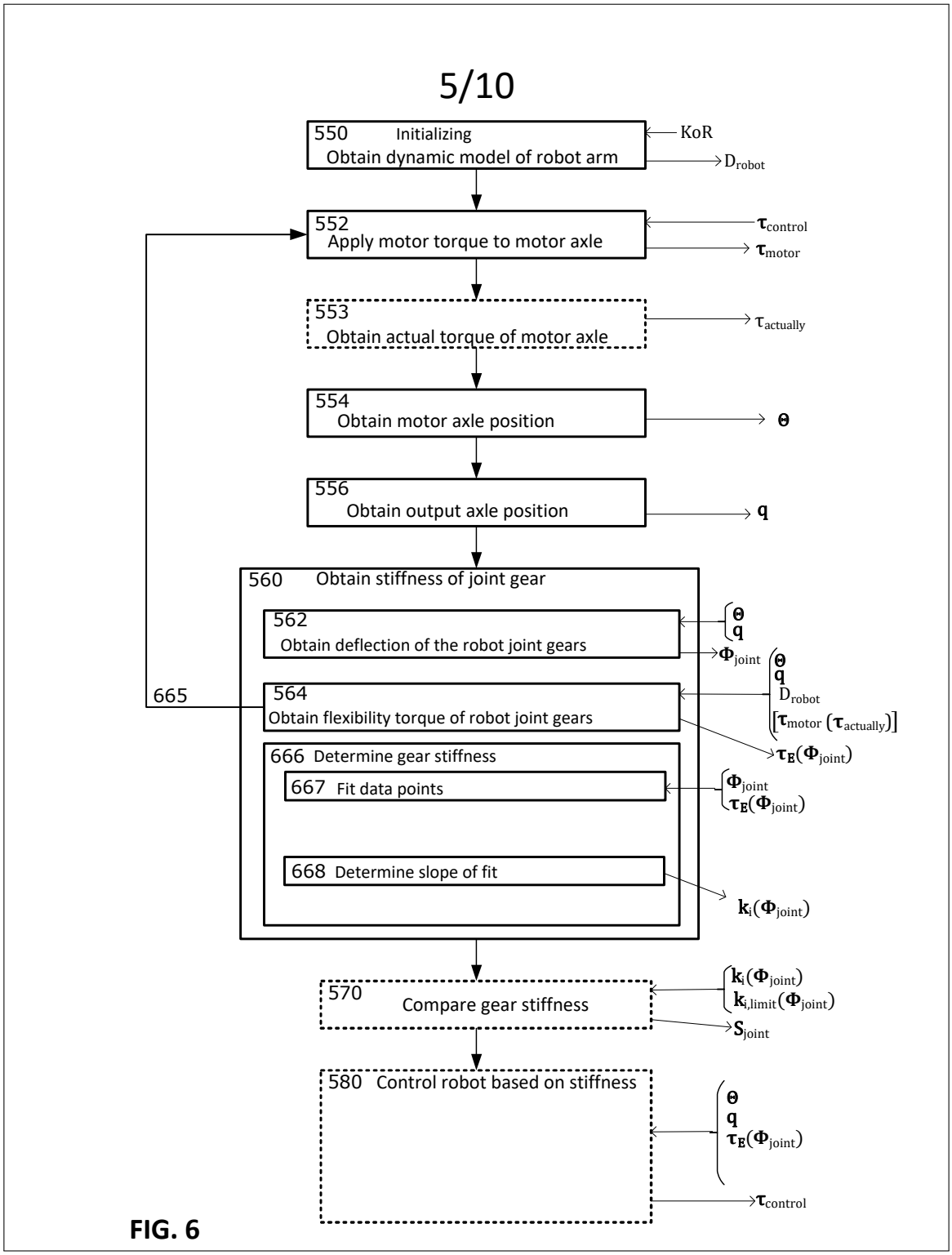
5/10
550 Initializing
Obtain dynamic model of robot arm
KoR
D_{robot}
552
Apply motor torque to motor axle
$\tau_{control}$
τ_{motor}
553
Obtain actual torque of motor axle
$\tau_{actually}$
554
Obtain motor axle position
Θ
556
Obtain output axle position
q
560 Obtain stiffness of joint gear
562
Obtain deflection of the robot joint gears
Θ
q
Φ_{joint}
665
564
Obtain flexibility torque of robot joint gears
Θ
q
D_{robot}
$[\tau_{motor}(\tau_{actually})]$
$\tau_E(\Phi_{joint})$
666 Determine gear stiffness
667 Fit data points
Φ_{joint}
$\tau_E(\Phi_{joint})$
668 Determine slope of fit
$k_i(\Phi_{joint})$
570
Compare gear stiffness
$k_i(\Phi_{joint})$
$k_{i,limit}(\Phi_{joint})$
S_{joint}
580 Control robot based on stiffness
Θ
q
$\tau_E(\Phi_{joint})$
$\tau_{control}$

FIG. 6

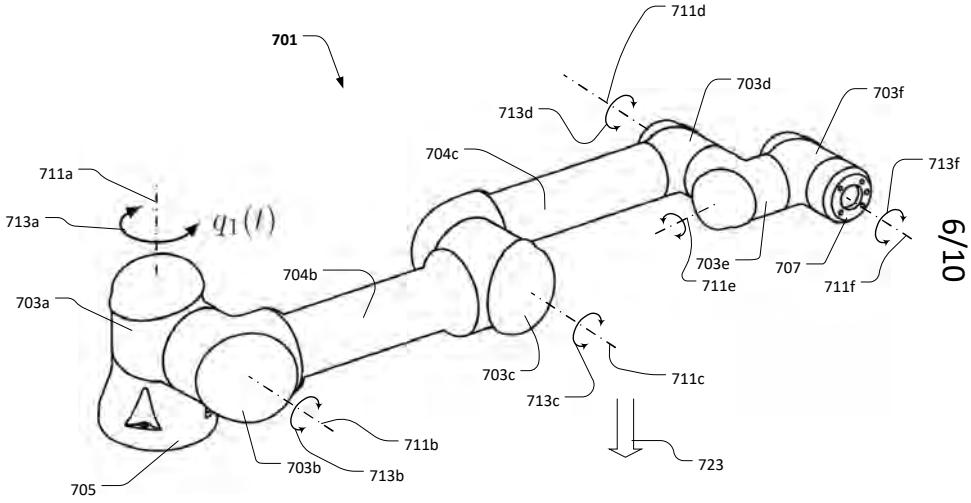
701
711d
703d
703f
713d
704c
711a
713f
713a
$q_1(l)$
703e
707
711e
711f
704b
703a
703c
711c
713c
711b
723
703b
713b
705

FIG. 7

7/10

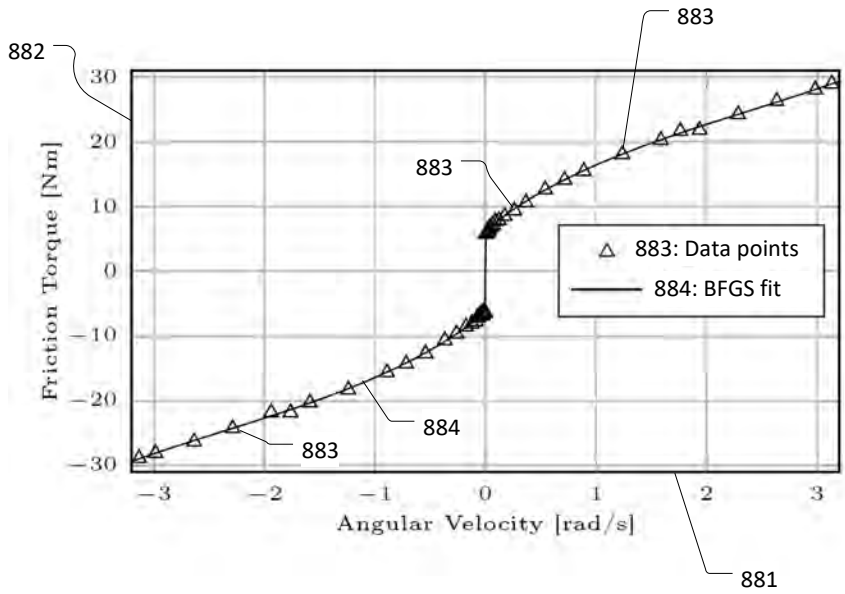

FIG. 8

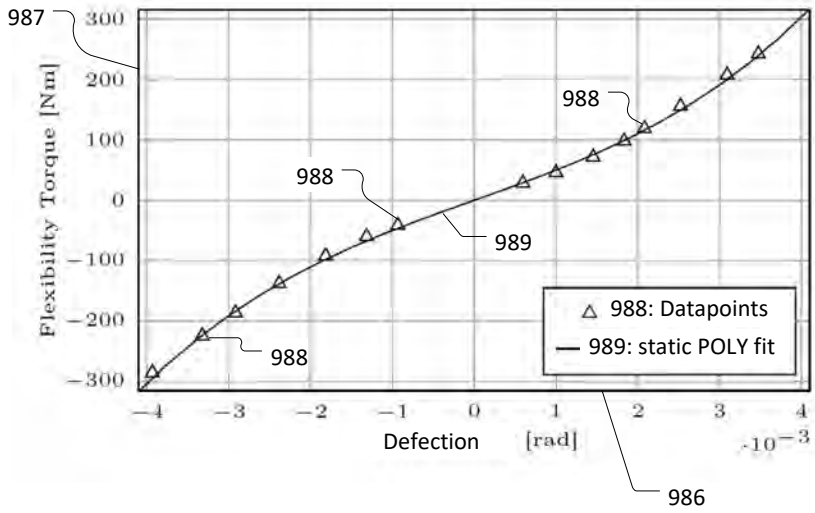

FIG. 9

8/10

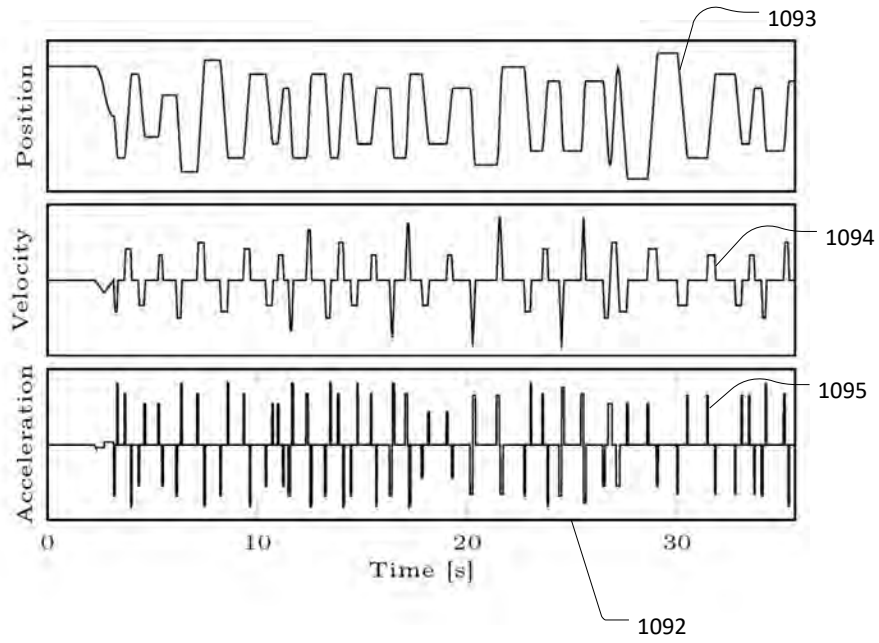

FIG. 10

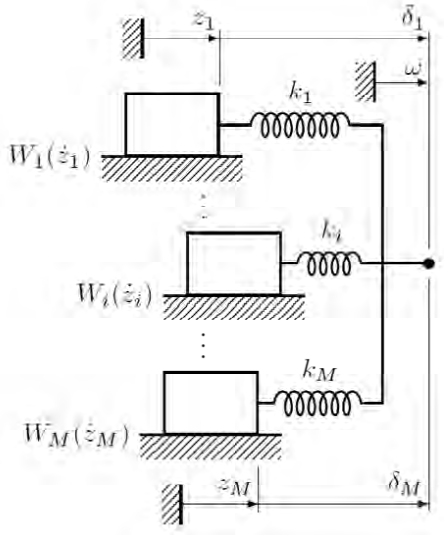

FIG. 11

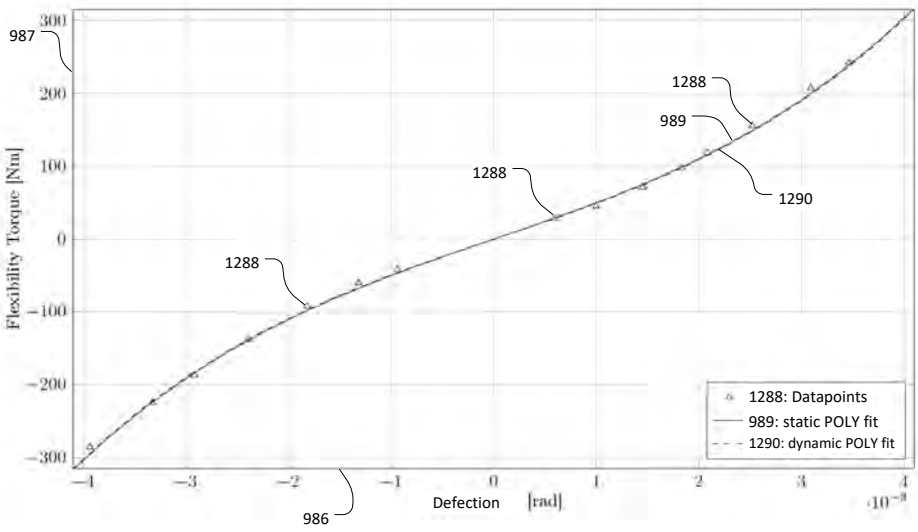
987
1288
989
1288
1290
1288
986
Flexibility Torque [Nm]
Defection [rad]
1288: Datapoints
989: static POLY fit
1290: dynamic POLY fit

9/10

FIG. 12

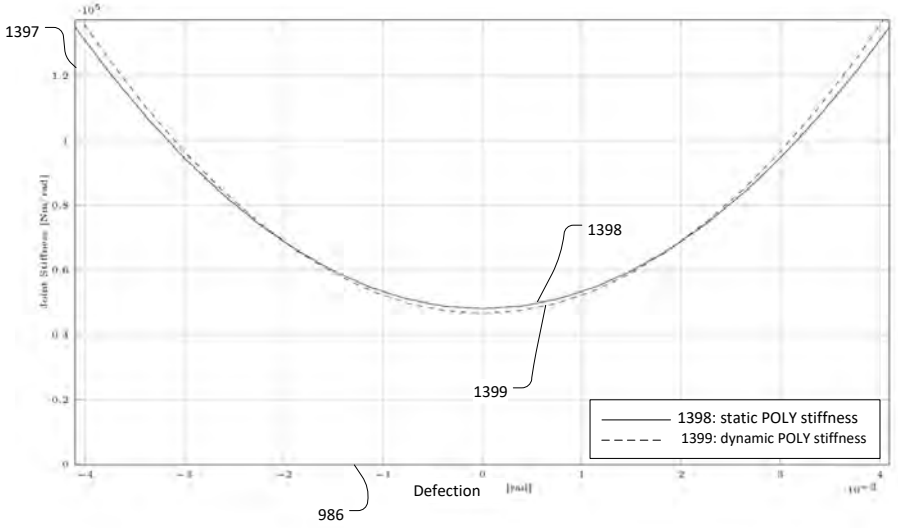
1397
1398
1399
986
Defection
1398: static POLY stiffness
1399: dynamic POLY stiffness

FIG. 13

Appendix B

Patent Application: Torque Control [Pat. App. 2]

Method of Controlling a Robot Arm Based on Adaptive Friction

Title	METHOD OF CONTROLLING A ROBOT ARM BASED ON ADAPTIVE FRICTION
Danish App. No.	PA/2019/00470
Priority Date	April 17, 2019
Applicant	Universal Robots A/S
Inventor	Emil Madsen
Agent	Morten Fruelund

B.1 Contribution

The author developed and described the methods and performed experiments and data processing. The agent prepared the application by instruction from the author.

METHOD OF CONTROLLING A ROBOT ARM BASED ON ADAPTIVE FRICTION

FIELD OF THE INVENTION

[0001] The present invention relates to methods of controlling a robot arm comprising a plurality of robot joints connecting a robot base and a robot tool flange, where at least one of the robot joints is a rotational robot joint comprising a joint motor having a motor axle, where the motor axle is configured to rotate an output axle of the rotational robot joint via a robot joint transmission.

BACKGROUND OF THE INVENTION

[0002] Robot arms comprising a plurality of robot joints and links where motors can rotate the joints in relation to each other are known in the field of robotics. Typically, the robot arm comprises a robot base which serves as a mounting base for the robot arm and a robot tool flange where to various tools can be attached. A robot controller is configured to control the robot joints to move the robot tool flange in relation to the base. For instance, in order to instruct the robot arm to carry out a number of working instructions.

[0003] Typically, the robot controller is configured to control the robot joints based on a dynamic model of the robot arm, where the dynamic model defines a relationship between the forces acting on the robot arm and the resulting accelerations of the robot arm. Often, the dynamic model comprises a kinematic model of the robot arm, knowledge about inertia of the robot arm and other parameters influencing the movements of the robot arm. The kinematic model defines a geometric relationship between the different parts of the robot arm and may comprise information of the robot arm such as, length, size of the joints and links and can for instance be described by Denavit-Hartenberg parameters or the like. The dynamic model makes it possible for the controller to determine which torques the joint motors shall provide in order to move the robot joints for instance at specified positions, velocities, and accelerations.

[0004] On many robot arms it is possible to attach various end effectors to the robot tool flange, such as grippers, vacuum grippers, magnetic grippers, screwing machines, welding equipment, dispensing systems, visual systems etc.

[0005] In some robots the robot joint comprises a joint motor having a motor axle configured to rotate an output axle, for instance via a transmission system. The robot joint transmission system is configured to transmit torque provided by the motor axle to the output axle. Typically, the output axle is connected to and configured to rotate parts of the robot arm in relation to each other. The robot joint transmission system can for instance comprise a robot joint gear or a direct drive mechanism. The robot joint gear can for instance be provided as a spur gears, planetary gears, bevel gears, worm gears, strain wave gears or other kind of transmission systems.

[0006] Commonly flexibility and friction exist in the various types of transmissions. Taking into account the friction of the transmission in the dynamic model makes the dynamic model more accurately resemble the dynamics of the real robot arm because the robot joint friction originating from the transmission system can be known and thereby compensated in the robot controller. The art of compensating the effects of friction in the controller is well known in the field of motor control {1}. A more accurate dynamic model can for instance allow the robot controller to control the robot arm with greater accuracy and precision. A more accurate dynamic model can also allow the robot controller to more accurately identify external disturbances, for instance human interference which is of great concern in terms of safety.

[0007] One issue when taking into account the robot joint friction in the robot controller design is that the friction changes in a manner that is difficult to predict accurately. For instance, friction is known to change with quantities such as temperature and wear that are hardly measurable on most industrial robots. The friction's temperature dependency is caused for instance by the thermal expansion of mechanical parts in contact and/or temperature-dependent lubricant properties. The friction's wear dependency is caused for instance by material being worn off at contacting surfaces such as for instance at the gear meshing in a robot joint gear.

[0008] Due to the variation of the robot joint friction it is desired to estimate the friction on-line, such that the friction can be compensated more accurately in the robot controller. The art of adaptive friction compensation is well known within the field of motor control. Adaptive friction compensation has been accomplished through various strategies by several researchers {2}, {3}, {4}.

[0009] There are several robot control strategies that utilizes the knowledge on the dynamic model of the industrial robot to compute the control action. The control strategy Joint Torque Feed-back (JTF) has been widely used to improve the performance of robot motion and force control {5}, {6}, {7}. Implementation of JTF control requires to know the joint torque transmitted to the output axle from the transmission system. The joint transmission torque is most often obtained by measuring the deformation of an elastic member inside the transmission. If for instance strain wave transmissions are used as robot joint gears the joint transmission torque can be obtained for instance by mounting strain gauges on the flex spline {8}, {9}, {10}. Another option is to measure the angular position of both the input axle and the output axle in the robot joint. The difference between these position measurements defines the deformation of the transmission system. This deformation combined with an accurate mathematical model of the transmission system can yield an estimate of the robot joint transmission torque as shown in {11}, {12}, {13}. However, while these works demonstrate sufficient accuracy in the experimental test systems during a maximum period of 80 seconds, the methods are deemed to fail if applied to industrial robots where changes in ambient conditions or changes in the temperature or wear level of the robot joint transmission system occurs and influences the industrial robot's friction characteristics.

REFERENCES

{1} B. Bona and M. Indri (2005). "Friction Compensation in Robotics: An Overview," Proc. *44th IEEE Conference on Decision and Control*, Seville, Spain, Dec 15, 2005.

{2} C. Canudas-de-Wit et al. (1987). "Adaptive friction compensation in dc-motor drives," *IEEE Journal on Robotics and Automation*, Vol. 3, No. 6, pp. 681-685.

{3} C. Canudas-de-Wit et al. (1991). "Adaptive Friction Compensation in Robot Manipulators: Low Velocities," *The International Journal of Robotics Research*, Vol. 10, No. 3, pp. 189-199.

{4} W. Susanto et al. (2008). "Adaptive Friction Compensation: Application to a Robotic Manipulator," *IFAC Proceedings Volumes*, Vol. 41, No. 2, pp. 2020-2024.

{5} F. Aghili and M. Buehler and J. M. Hollerbach (2001). "Motion control systems with /spl Hscr//sup /spl infin// positive joint torque feedback," *IEEE Transactions on Control Systems Technology*, Vol. 9, No. 5, pp. 685-695.

{6} L. Le Tien et al. (2008). "Friction observer and compensation for control of robots with joint torque measurement," *IEEE/RSJ International Conference on Intelligent Robots and Systems*, Nice, France, Sep 22-26, 2008, pp. 3789-3795.

{7} A. Albu-Schäffer et al. (2007). "The DLR lightweight robot: design and control concepts for robots in human environments," *Industrial Robot: An International Journal*, Vol. 34, No. 5, pp. 376-385.

{8} M. Hashimoto et al. (1993). "A Torque Sensing Technique for Robots with Harmonic Drives," *IEEE Transactions on Robotics and Automation*, Vol. 9, No. 1, pp. 108-116.

{9} W.-H. Zhu et al. (2006). "Adaptive Control of Harmonic Drives," *Journal of Dynamic Systems, Measurement, and Control*, Vol. 129, No. 2, pp. 182-193.

{10} J. W. Sensinger and R. F. ff. Weir (2006). "Improved Torque Fidelity in Harmonic Drive Sensors Through the Union of Two Existing Strategies," *IEEE/ASME Transactions on Mechatronics*, Vol. 11, No. 4, pp. 457-461.

{11} T. Kawakami et al. (2010). "High-Fidelity Joint Drive System by Torque Feedback Control Using High Precision Linear Encoder," *IEEE International Conference on Robotics & Automation*, Anchorage, Alaska, USA, May 3-8, 2010.

{12} H. Zhang et al. (2013). "Torque Estimation Technique of Robotic Joint with Harmonic Drive Transmission," *IEEE International Conference on Robotics & Automation*, Karlsruhe, Germany, May 6-10, 2013.

{13} H. Zhang et al. (2015). "Torque Estimation for Robotic Joint with Harmonic Drive Transmission Based on Position Measurements," *IEEE Transactions on Robotics*, Vol. 31, No. 2, pp. 322-330.

{14} M. W. Spong (1987). "Modeling and Control of Elastic Joint Robots," *Journal of Dynamic Systems, Measurement, and Control*, vol. 109, no. 4, pp. 310–319.

{15} Gene F. Franklin, J. David Powell, and Abbas Emami-Naeini. "Feedback Control of Dynamic Systems", 8th Edition. Pearson, 2018.

SUMMARY OF THE INVENTION

The objective of the present invention is to address the above described limitations with the prior art or other problems of the prior art. This is achieved by a method of a method of controlling a robot arm with robot joints, where the joint motors of the joints are controlled based a signal generated based on the friction $\hat{F}$ of at least one of the input/outside of the robot joint transmission and the robot joint transmission torque $\hat{\tau}_J$ between the input side and the output side of the transmission. The friction is determined based on: at least two of the angular position of the motor axle; the angular position of the output axle and/or the motor torque provided to the motor axle by the joint motor. The robot joint transmission torque is determined based on: at least one of the angular positions of the output axle; the angular position of the output axle and/or the angular position of the motor axle; the angular position of the motor axle and the motor torque provided to the motor axle by the joint motor. This makes it possible to prove a more accurate control of a robot arm as the friction of he joint transmissions can adaptive obtained and used to generate the controls signals of the robot joint motors. Further the objective of the present invention is addressed a robot arm based comprising a plurality of robot joints and a robot controller where the root controller is configured to control the robot arm based on ad adaptive obtained friction of the robot joint transmission. The dependent claims describe possible embodiments of the method according to the present invention. The advantages and benefits of the present invention are described in the detailed description of the invention

BRIEF DESCRIPTION OF THE DRAWINGS

Fig. 1 illustrates a robot arm configured according to the present invention;

fig. 2 illustrates a schematic cross-sectional view of a rotational robot joint;

fig. 3 illustrates a model of a rotational robot joint gear;

fig. 4 illustrates a simplified structural diagram of a robot arm configured according to the present invention;

fig. 5 illustrates a flow chart of a method of controlling a robot arm according to the present invention where the robot arm is controlled based on adaptive friction of a rotational robot joint;

fig. 6 illustrates a structural diagram of a robot controller system controlling robot arm where the robot arm is controlled based on adaptive friction of a rotational robot joint;

fig. 7 illustrates a flow chart of a method of controlling a robot arm according to the present invention, where the robot arm is controlled based on an adaptive friction depending transmission torque of a rotational robot joint;

fig. 8 illustrates a structural diagram of a robot controller system controlling robot arm where the robot arm is controlled based on an adaptive friction depending transmission torque of a rotational robot joint;

fig. 9 illustrates a flow chart of a method of controlling a robot arm according to the present invention where the robot arm is controlled based on adaptive friction dependent feed-forward;

fig. 10 illustrates a structural diagram of a robot controller system controlling robot arm where the robot arm is controlled based on adaptive friction dependent feed-forward controller;

fig. 11 illustrates a structural diagram of an adaptive friction module of a robot controller system controlling robot arm where the adaptive friction module provides the friction of the robot joint transmission.

DETAILED DESCRIPTION OF THE INVENTION

[0010] The present invention is described in view of exemplary embodiments only intended to illustrate the principles of the present invention. The skilled person will be able to provide several embodiments within the scope of the claims. Throughout the description, the reference numbers of similar elements providing similar effects have the same last two digits. Further it is to be understood that in the case that an embodiment comprises a plurality of the same features then only some of the features may be labeled by a reference number.

[0011] The invention can be embodied into a robot arm and is described in view of the robot arm illustrated in fig. 1. The robot arm 101 comprises a plurality of robot joints 103a, 103b, 103c, 103d, 103e, 103f and robot links 104b, 104c, 104d connecting a robot base 105 and a robot tool flange 107. A base joint 103a is connected directly with a shoulder joint and is configured to rotate the robot arm around a base axis 111a (illustrated by a dashed dotted line) as illustrated by rotation arrow 113a. The shoulder joint 103b is connected to an elbow joint 103c via a robot link 104b and is configured to rotate the robot arm around a shoulder axis 111b (illustrated as a cross indicating the axis) as illustrated by rotation arrow 113b. The elbow joint 103c connected to a first wrist joint 103d via a robot link 104c and is configured to rotate the robot arm around an elbow axis 111c (illustrated as a cross indicating the axis) as illustrated by rotation arrow 113c. The first wrist joint 103d connected to a second wrist joint 103e via a robot link 104d and is configured to rotate the robot arm around a first wrist axis 111d (illustrated as a cross indicating the axis) as illustrated by rotation arrow 113d. The second wrist joint 103e is connected to a robot tool joint 103f and is configured to rotate the robot arm around a second wrist axis 111e (illustrated by a dashed dotted line) as illustrate by rotation arrow 113e. The robot tool joint 103f comprising the robot tool flange 107, which is rotatable around a tool axis 111f (illustrated by a dashed dotted line) as illustrated by rotation arrow 113f. The illustrated robot arm is thus a six-axis robot arm with six degrees of freedom, however it is noticed that the present invention can be provided in robot arms comprising less or more robot

joints, and the robot joints can be connected directly to the neighbor robot joint or via a robot link. In the illustrated embodiment the robot joints are illustrated as rotational robot joints where a the rotational robot joint rotates one part of the robot arm in relation to another part of the robot joint, however it is to be understood that some of the robot joint may be provided as translational robot joints where the robot joint is configured to move a part of the robot arm in relation to another part of a robot arm via a translational movement. For instance, such translational robot joint may be provided as a prismatic robot joint. It is to be understood that the robot joints can be identical and/or different. The direction of gravity 123 is also indicated in the figure.

[0012] The robot arm comprises at least one robot controller 115 configured to control the robot joints by controlling the motor torque provided to the joint motors based on a dynamic model of the robot. The robot controller 115 can be provided as a computer comprising an interface device 117 enabling a user to control and program the robot arm. The controller can be provided as an external device as illustrated in fig. 1 or as a device integrated into the robot arm. The interface device can for instance be provided as a teach pendent as known from the field of industrial robots which can communicate with the controller via wired or wireless communication protocols. The interface device can for instance comprise a display 119 and a number of input devices 121 such as buttons, sliders, touchpads, joysticks, track balls, gesture recognition devices, keyboards etc. The display may be provided as a touch screen acting both as display and input device.

[0013] Fig. 2 illustrates a schematic cross-sectional view of a rotational robot joint 203. The schematic robot joint 203 can reflect any of the robot joints 103a-103f of the robot 101 of fig. 1. The robot joint comprises a joint motor 209 having a motor axle 225. The motor axle 225 is configured to rotate an output axle 227 via a robot joint transmission 229. The robot joint transmission can be any device transferring the rotation of the motor axle to the output axle and may for instance be provide as a direct drive where the motor axle is directly coupled with the output axle and the motor axle and output may thus be the

same. The robot joint transmission may also be provided as a robot joint gear providing ratio between the motor axle and the output axle, for instance in order to increase the rotational torque provided by the output axle. The robot joint gear can be provided as any kind of gear mechanism such as strain wave gears, planet gears, epicyclic gears, spur gears, bevel gears etc. and may be provided as single stager or multi stage gear systems. The output axle 227 rotates around an axis of rotation 211 (illustrated by a dot-dash line) and can be connected to a neighbor part (not shown) of the robot arm. Consequently, the neighbor part of the robot arm can rotate in relation to the robot joint 203 around the axis of rotation 211 as illustrated by rotation arrow 213. In the illustrated embodiment the robot joint comprises an output flange 231 connected to the output axle and the output flange can be connected to a neighbor robot joint or an arm section of the robot arm. However, the output axle can be directly connected to the neighbor part of the robot arm or by any other way enabling rotation of the neighbor part of the robot by the output axle.

[0014] The joint motor 209 is configured to rotate the motor axle by applying a motor torque to the motor axle as known in the art of motor control, for instance based on a motor control signal 233 indicating the torque, $\tau_{control}$ applied by the motor axle, for instance by driving the joint motor with a motor current i_{motor} proportional with a motor torque. The robot transmission 229 is configured to transmit the torque provided by the motor axle to the output axle for instance to provide a gear ratio between the motor axle and the output axle. The robot joint comprises at least one joint sensor providing a sensor signal indicative of at least the angular position, q, of the output axle and an angular position, Θ, of the motor axle. For instance, the angular position of the output axle can be indicated by an output encoder 235, which provide an output encoder signal 236 indicating the angular position of the output axle in relation to the robot joint. Similar, the angular position of the motor axle can be provided by an input encoder 237 providing an input encoder signal 238 indicating the angular position of the motor axle in relation to the robot joint. The output encoder 235 and the input encoder 237 can be any encoder capable of indicating the angular position, velocity and/or acceleration of respectively the output axle and the motor axle. The output/input encoders can for instance

be configured to obtain the position of the respective axle based on the position of an encoder wheel 239 arrange on the respective axle. The encoder wheels can for instance be optical or magnetic encoder wheels as known in the art of rotary encoders. The output encoder indicating the angular position of the output axle and the input encoder indicating the angular position of the motor axle makes it possible to determine a relationship between the input side (motor axle) and the output side (output axle) of the robot joint gear.

[0015] The robot joints may optionally comprise one or more motor torque sensors 241 providing a motor torque signal 242 indicating the torque provided by the motor axle. For instance, the motor torque sensor can be provided as current sensors obtaining the current i_{motor} through the coils of the joint motor whereby the motor torque can be determined as known in the art of motor control. For instance, in connection with a multiphase motor, a plurality of current sensors can be provided in order to obtain the current through each of the phases of the multiphase motor and the motor torque can then be obtained based on the obtained currents. For instance, in a three-phase motor the motor torque may be obtained based on quadrature current obtained from the phase currents through a Park Transformation. Alternatively, the motor torque can be obtained using other kind of sensors for instance force-torque sensors, strain gauges etc.

[0016] Fig. 3 illustrates a model of a rotational robot joint 303 connecting robot link 304i-1 and robot link 304i, where the joint motor 309i is arranged on robot link 304i-1 and rotates robot link 304i in relation to robot link 304i-1. The motor axle 325i of the joint motor is connected to an output axle 327i via robot joint transmission 329i (illustrated in schematic form) and the robot link 304i rotates together with the output axle 327i. The robot joint transmission provides a transmission ratio between the motor axle and the output axle and in an infinitely stiff transmission the rotation of the motor axle is immediately transformed into rotation of the output axle according to the transmission ratio of the robot joint transmission. However as described in the background of the invention flexibility exist in the types of robot joint transmissions used in the

field of robot arms. The flexibility of a robot joint transmission can be indicated by the transmission stiffness of the robot joint transmission which defines a relationship between torque through the robot joint transmission and the deformation between the input side (motor axle) and the output side (output axle) of the robot joint transmission. The flexibility of a robot joint transmission can be represented as a spring 326 and a damper 328 coupled in parallel between the input side (motor axle) and the output side (output axle) of the robot joint transmission. The stiffness K_i of the spring indicates the transmission stiffness of the robot joint transmission and the damping D_i of the damper indicates the damping of the robot joint transmission.

[0017] Fig. 4 illustrates a simplified structural diagram of a robot arm comprising a plurality of n number of robot joints 403i, 403i+1….403n. The robot arm can for instance be embodied like the robot arm illustrated in fig. 1 with a plurality of interconnected robot joints, where at the robot joints can be embodied like the rotational robot joint illustrated in fig. 2. It is to be understood that some of the robot joints and robot links between the robot joints have been omitted for sake of simplicity. The controller is connected to an interface device comprising a display 119 and a number of input devices 121, as described in connection with fig.1. The robot controller 415 comprises a processor 443, a memory 445 and at least one input and/or output port enabling communication with at least one peripheral device.

[0018] The robot controller is configured to control the robot arm based on a dynamic model of the robot arm D_{robot}. The dynamic model of the robot arm can be defined and pre-stored in the memory 445 of the controller and the user can in some embodiment be allowed to modify the dynamic model op the robot arm, for instance by providing payload information of a payload attached to the robot arm or defining the orientation of the robot arm in relation to gravity.

[0019] The configuration of the robot arm can be characterized by the generalized coordinates $(\mathbf{q} \quad \boldsymbol{\Theta}) \in \mathbb{R}^{2N}$ where $\mathbf{q}$ is a vector comprising the angular positions of the output axles of the robot joint transmissions and $\boldsymbol{\Theta}$ is a

vector comprising the angular positions of the motor axles as seen in the output side of the robot joint transmission. Consequently:

eq. 1 $$\boldsymbol{\Theta} = \frac{\boldsymbol{\theta}'}{\boldsymbol{r}}$$

where $\boldsymbol{\Theta}'$ is the actual angular position of the motor axle, which can for instance be measured by a rotary encoder, and $\mathbf{r}$ the gear ratio of the robot joint transmission. This is the notation used throughout this application.

Alternatively, it is noted that $\mathbf{q}$ can be indicated in the input side of the robot joint gear:

eq. 2 $$\boldsymbol{q} = \boldsymbol{q}' \boldsymbol{r}$$

where $\mathbf{q}'$ is the actual angular position of the output axle, which can for instance be measured by a rotary encoder.

[0020] The transmission flexibility of the robot joint results in a deflection between the input side and the output side of the robot joint transmission when a torque is applied to the robot joint transmission. The deflection of the robot joint transmission can be indicated by a joint transmission deformation variable $\boldsymbol{\Phi}_{\mathbf{joint}}$ indicating the differences between the angular position $\boldsymbol{\Theta}$ of the motor axle and the angular position $\mathbf{q}$ of the output axle, thus the joint transmission deformation for robot joint i is defined as:

eq. 3 $$\Phi_{joint,i} = \Theta_i - q_i$$

[0021] The joint transmission torque $\tau_{joint,i}$ defines the torque that is transferred from the motor axle to the output axle via the robot joint transmission and can be modeled as a function of the joint transmission deformation $\boldsymbol{\Phi}_{\mathbf{joint}}$ and its time-derivative:

eq. 4 $$\tau_{joint,i}\left(\Phi_{joint,i}, \dot{\Phi}_{joint,i}\right) = \tau_{E,i}\left(\Phi_{joint,i}\right) + \tau_{D,i}\left(\dot{\Phi}_{joint,i}\right)$$

where $\tau_{E,i}(\Phi_{\text{joint},i})$ is a flexibility torque depending on the robot joint transmission stiffness K_i and the joint transmission deformation of the robot joint transmission and $\tau_{D,i}(\dot{\Phi}_{\text{joint},i})$ is a damping torque depending on the damping D_i and the first time derivative of the joint transmission deformation of the robot joint transmission.

[0022] The transmission stiffness K_i of the robot joint transmission can be characterized by how much the flexibility torque $\tau_{E,i}(\Phi_{\text{joint},i})$ causing the joint transmission deformation changes as a function of the joint transmission deformation. The transmission stiffness can thus be expressed as:

eq. 5 $$K_i(\Phi_{joint,i}) = \frac{\partial\, \tau_{E,i}(\Phi_{joint,i})}{\partial\, \Phi_{joint,i}} \approx \frac{\Delta\, \tau_{E,i}(\Phi_{joint,i})}{\Delta\, \Phi_{joint,i}}$$

The flexibility torque $\tau_{E,i}(\Phi_{\text{joint},i})$ of the robot joint transmission can be obtained experimentally, for instance by following these steps:

- Impose a set of different known torques around the rotational axis (111a-111f, 211) of the robot joints and for each torque obtain the resulting joint transmission deformation $\boldsymbol{\Phi_{joint}}$ based on obtained/measured the angular positions of the input axle and output axle using eq. 3. The torques can be exerted to the robot joint for instance by;
  - orienting the joint rotation axis parallel to the direction of the gravitational acceleration such that there will be no torque resulting from gravity, and then;
    - using a device capable of measuring force to exert a force on the robot arm, the force being exerted at a position with a known distance between the applied force and the joint axis, the distance being perpendicular to the direction of the exerted force and perpendicular to the joint rotation axis, and then calculating the torque as force times distance;

- letting part of the robot, for instance the tool flange, exert a force/torque on its surroundings and using the kinematic properties of the robot arm and the actual configuration of the robot arm to calculate the torque around the joint rotation axis.

Based on the experimental results a mathematical model of the relationship between the joint transmission deformation and the flexibility torque for joint i can be constructed, for instance a polynomial of odd powers in $\Phi_{joint,i}$ can be used to describe the relationship between the joint transmission deformation and the flexibility torque for joint i, thus

eq. 6

$$\tau_{E,i}(\Phi_{joint,i}) = \begin{bmatrix} \Phi_{joint,i} & \Phi_{joint,i}^3 & \cdots & \Phi_{joint,i}^{2P-1} \end{bmatrix} \cdot \begin{bmatrix} k_{1,i} \\ k_{2,i} \\ \vdots \\ k_{P,i} \end{bmatrix}$$

where $k_{j,i}$ is j^{th} polynomial coefficient and P is the total number of polynomial coefficients.

[0023] The $\tau_{D,i}(\dot{\Phi}_{\text{joint},i})$ damping torque of the robot joint transmission can, if assumed linear in the time-derivative of joint transmission deformation, for instance be obtained by following the steps:

- Fix the output axle of the robot joint transmission;
- Apply a torque to the motor axle of the robot joint transmission to yield a transmission deflection of the joint transmission;
- Keep the motor axle of the robot joint transmission still and remove the applied torque from the motor axle of the robot joint transmission;
- Observe the position of the motor axle of the robot joint transmission over time as the motor axle of the robot joint transmission undergoes a damped harmonic motion with an amplitude that decreases over time.
- The damping torque is a measure of the energy dissipation during the motion. Assuming an underdamped harmonic motion, the damping coefficient $\mathrm{D_i}$ can be obtained as:

eq. 7

$$D_i = \frac{-2\,B\,log_e\left(\frac{A_2}{A_1}\right)}{t_2 - t_1}$$

where B is the mass moment of inertia of the motor axle, A_1 and A_2 are, respectively, amplitudes of the first and second vibration, and t_1 and t_2 are, respectively, times for the first and second motion.

If the motion is not underdamped, a larger mass moment of inertia is added to the input axle.

[0024] The output-side friction torque $\mathbf{F_q}$ of the transmissions of robot joints can be obtained experimentally, for instance by following these steps for each of the robot joints independently:

- Orient the rotation axis (111a-111f, 211) of a robot joint parallel to the direction of the gravitational acceleration.
- Apply motor torque such as to rotate the output axle of the robot joint with different known constant angular velocities in a known period of time while measuring the joint transmission deformation.
- The output-side friction is obtained as the joint transmission deformation mapped to flexibility torque during the constant angular velocity motion of the output axle, thus

eq. 8 $$F_{q,i} = \tau_{E,i}\left(\Phi_{joint,i}\right)$$

[0025] The input-side friction torque $\mathbf{F_\theta}$ of the robot joint transmission can be obtained experimentally, for instance by following these steps for each of the robot joints independently:

- Orient the robot joint axis rotation axis (111a-111f, 211) parallel to the direction of the gravitational acceleration;
- Apply motor torque such as to rotate the motor axle of the robot joint with a known constant angular velocity in a known period of time while obtaining the joint motor torque, for instance based on motor currents.

- The input-side friction is obtained as the joint motor torque during the constant angular velocity motion of the motor axle as a function of the flexibility torque, thus

eq. 9 $$F_{\theta,i} = \tau_{motor,i} - \tau_{E,i}(\Phi_{joint,i})$$

[0026] Facing fig. 4 the controller is configured to control the joint motors of the robot joints by providing motor control signals to the joint motors. The motor control signals 433i, 433i+1….433n are indicative of the motor torque $\tau_{control,i}$, $\tau_{control,i+1}$, and $\tau_{control,n}$, that each joint motor shall provide to the motor axles; alternatively, the motor control signal may be provided as the current $i_{control,i}$, $i_{control,i+1}$, and $i_{,control,n}$ that each joint motor shall provide. The motor control signals can indicate the desired motor torque, the desired torque provided by the output axle, the currents provided by the motor coils or any other signal from which the motor torque can be obtained. The motor torque signals can be sent to a motor control driver (not shown) configured to drive the motor joint with the motor current resulting in the desired motor torque. The robot controller is configured to determine the motor torque based on a dynamic model of the robot arm as known in the prior art. The dynamic model makes it possible for the controller to calculate how much torque the joint motors shall provide to each of the motor axels to make the robot arm perform a desired movement and/or be arranged in a static posture. The dynamic model of the robot arm can be stored in the memory 445.

[0027] As described in connection with fig. 2 the robot joints comprise an output encoder providing output encoder signals 436i, 436i+1…436n indicating the angular position $q_{,i}$, $q_{,i+1}$…$q_{,n}$ of the output axle in relation to the respective robot joint; an input encoder providing an input encoder signal 438i, 438i+1…438n indicating the angular position of the motor axle $\Theta_{,i}$, $\Theta_{,i+1}$…$\Theta_{,n}$ in relation to the respective robot joint and a motor torque sensors providing an motor torque signal 442i,442i+1…442n indicating the torque $\tau_{motor,i}$, $\tau_{motor,i+1}$…$\tau_{motor,n}$, provided by the motor axle of the respective robot joint; alternatively the motor torque signals may be provided as the current $i_{control,i}$,

$i_{control,i+1}$, and $i_{control,n}$ that is provided to each joint. The controller is configured to receive the output encoder signal 436i, 436i+1…436n, the input encoder signal 438i, 438i+1…438n and the motor torque signals 442i,442i+1…442n.

[0028] The controller can for instance be configured to carry out the method of controlling the robot arm as illustrated in figs. 5, 7 and 9 and be structured as illustrated in figs. 6, 8 and 10 as described forwardly.

[0029] Fig. 5 illustrates a flow diagram of a method of controlling a robot arm comprising a plurality of robot joints connecting a robot base and a robot tool flange, where at least one of the robot joints is a rotational robot joint comprising a joint motor having a motor axle, where the motor axle is configured to rotate an output axle of the rotational robot joint via a robot joint transmission. The method comprises a step of initializing 550, a step 552 of obtaining the angular position of the motor axles of the joint motors; a step 554 of obtaining the angular position of the output axle of the robot joint and a step 556 of obtaining the motor torque provided by the robot motors, a step 558 of obtaining the friction of the robot joint transmission, step 560 of obtaining the transmission torque between the input side and output side of the robot joint transmission and a step 562 of generating control signals for the joint motors.

[0030] Step of initializing 550 comprises a step of obtaining the dynamic model D_{robot} of the robot arm and can be based on prior knowledge of the robot arm and robot joints, KoR [Knowledge of Robot], such as the dimensions and weight of robot joints and robot links; joint motor properties; information relating to an eventual payload attached to the robot arm, orientation of the robot arm in relation to gravity and frictional properties of the robot arm and robot joints. The dynamic model of the robot arm can be defined and pre-stored in the memory of the controller and the user can in some embodiment be allowed to modify the dynamic model of the robot arm, for instance by providing payload information of a payload attached to the robot arm or defining the orientation of the robot arm in relation to gravity. The dynamic model of the robot arm can be obtained by considering the robot arm as an open kinematic

chain having a plurality of (n+1) rigid robot links and a plurality of n revolute robot joints, comprising a joint motor configured to rotate at least one robot link.

[0031] For instance, the dynamic model as seen from the output side of the robot joint transmissions of the robot arm be characterized by {14}:

eq. 10 $$\boldsymbol{\tau}_{joint} = M(\boldsymbol{q})\,\ddot{\boldsymbol{q}} + C(\boldsymbol{q},\dot{\boldsymbol{q}})\dot{\boldsymbol{q}} + \boldsymbol{g}(\boldsymbol{q}) + \boldsymbol{F}_{\boldsymbol{q}} + \boldsymbol{\tau}_{\boldsymbol{ext}}$$

where $\boldsymbol{\tau}_{\text{joint}}$ is a vector comprising the transmission torques $\tau_{\text{joint,i}}$... $\tau_{\text{joint,n}}$ of each of the robot joint transmissions; $\mathbf{q}$ is a vector comprising the angular position of the output axles of the robot joint transmissions; $\dot{\mathbf{q}}$ is a vector comprising the first time derivative of the angular position of the output axles of the robot joint transmissions and thus relates to the angular velocity of the output axles; $\ddot{\mathbf{q}}$ is a vector comprising the second time derivative of the angular position of the output axles of the robot joint transmissions and thus relates to the angular acceleration of the output axles. $M(\mathbf{q})$ is the inertia matrix of the robot arm and indicates the mass moments of inertia of the robot arm as a function of the angular position of the output axles of the robot joint transmissions. $C(\mathbf{q},\dot{\mathbf{q}})\dot{\mathbf{q}}$ is the Coriolis and centripetal torques of the robot arm as a function of the angular position and angular velocity of the output axle of the robot joint transmissions. $\mathbf{g}(\mathbf{q})$ is the gravity torques acting on the robot arm as a function of the angular position of the output axles of the robot joint transmissions.

[0032] $\mathbf{F}_{\mathbf{q}}$ is a vector comprising the friction torques acting on the output axles of the robot joint transmissions. The $\mathbf{F}_{\mathbf{q}}$ can be obtained during calibration of the robot joints for instance by as described in paragraph [0024]. $\boldsymbol{\tau}_{\mathbf{ext}}$ is a vector indicating the external torques acting on the output axles of the robot joint transmissions. The external torques can for instance be provided by external forces and/or torques acting on parts of the robot arm. For instance, if the tool flange of the robot is subject to external forces and/or torques described by $\mathbf{F}_{\mathbf{ext}}$, the resulting torques at the output axles of the robot joints becomes:

eq. 11 $$\boldsymbol{\tau_{ext}} = J^{T}(\boldsymbol{q})\, \boldsymbol{F_{ext}}$$

where $J^{\mathrm{T}}(\mathbf{q})$ is the transposed manipulator Jacobian of the robot arm and where $\mathbf{F_{ext}}$ is a vector describing the direction and magnitude of the external forces and torques in relation to the tool flange of the robot arm.

[0033] Secondly, the dynamic model as seen from the input side of the robot joint transmissions becomes {14}:

eq. 12 $$\boldsymbol{\tau_{motor}} = B\, \ddot{\boldsymbol{\Theta}} + \boldsymbol{F_{\Theta}} + \boldsymbol{\tau_{joint}}$$

where $\boldsymbol{\tau}_{\mathrm{joint}}$ is a vector comprising transmission torque $\tau_{\mathrm{joint,i}}$... $\tau_{\mathrm{joint,n}}$ of each of the robot joint transmissions; $\ddot{\boldsymbol{\Theta}}$ is a vector comprising the second time derivative of the angular position of the motor axle of the joint motor and thus relates to the angular acceleration of the motor axle. B is the positive-definite diagonal matrix indicating the mass moments of inertia of the joint motors' rotors. $\mathbf{F_{\Theta}}$ is a vector comprising the friction torques acting on the motor axles and $\boldsymbol{\tau}_{\mathrm{motor}}$ is a vector indicating the torque generated by the joint motors. $\mathbf{F_{\Theta}}$ can be obtained for each robot joint as described in paragraph [0025].

[0034] Step 552 of obtaining the angular position of the motor axles of the joint motors can be obtained by measuring the angular position of the motor axle for instance by using an encoder such as optical/magnetic encoders as known in the art of robotics. The angular position of the motor axles $\boldsymbol{\Theta}$ can be stored in a memory for later usage for instance in order to store a number of angular positions of the motor axles obtained at different times.

[0035] Step 554 of obtaining the angular position of the output axle of the robot joint transmission can be obtained by measuring the angular position of the output axle for instance by using encoders such as optical/magnetic

encoders as known in the art of robotics. The angular position of the output axles $\mathbf{q}$ can be stored in a memory for later usage, for instance a number of angular positions of the output axles obtained at different times can be stored in a memory. Alternatively, the angular position of the output axles of the robot joint transmissions can be obtained as the desired angular position of the output axles upon which the controller is generating the motor torques. This makes it possible to estimate the angle of the output axles in robot joints that does not comprise encoders for measuring the angular position of the output axles or the One could also estimate the output axle angular position based on the motor axle angular position for instance by estimating the output axle based on the gear ratio of the robot joint transmission.

[0036] The step 556 of obtaining the actual motor torque τ_{motor} provided by the joint motors can for instance be obtained by obtaining the current i_{motor} through the joint motors whereby the actual motor torque can be obtained as known in the art of motor control. For instance, if the joint motors are provided as three-phase Permanent Magnet Synchronous Machines (PMSM) with dynamics much faster than that of the manipulator and if the joint motors are operated under their current saturation limit, the motor axle torque can be obtained by:

eq. 13 $$\boldsymbol{\tau}_{motor} = K_{\tau}\, \boldsymbol{i}_{motor}$$

where τ_{motor} is a vector comprising, the actual torque provided by the motor axles of the joint motors (seen in the output space of the robot joint gear), K_{τ} is the positive-definite diagonal matrix of torque constants and $\mathbf{i}_{motor}$ is a vector comprising the torque-generating (quadrature) current obtained from the phase currents of the joint motors using the Park Transformation.

[0037] The actual motor torque can also be obtained by using force/torque sensors such as strain gauges indicating the actual torque of the motor axle, as in many cases it can be assumed the motor torque is transferred to the motor axle.

[0038] Step 558 of obtaining the friction $\hat{\mathbf{F}}$ of the input side and/or the output of joint transmission can be obtained based on least two of:

- the angular position Θ of the motor axle;
- the angular position q of the output axle;
- the motor torque τ_{motor}/i_{motor} provided to the motor axle by the joint motor;

by using any method or a combination of methods within the field of Digital Signal Processing (DSP) or an adaptive observer method known in the art of adaptive state estimation in the field of control theory. This makes it possible to provide an online estimation of the friction of the robot joint transmission whereby it becomes possible to take varying friction of the robot joint transmission due to wear and changes in ambient working conditions into account when providing a control system for the robot arm. Consequently, a more accurate control of a robot arm can be provided. Further in many robots arms the angular position of the motor axle, the angular position of the output axle and the motor torque are already obtainable by various sensors and thus no additional sensors need to be provided in such robots. The adaptive filtering methods include for instance;

- Least Mean Squares (LMS) filter; and
- Recursive Least Squares (RLS) filter;

And the observer methods include for instance;

- Luenberger Observer (LO);
- Kalman Filter (KF), including also Extended Kalman Filter (EKF) and Uncented Kalman Filter (UKF);
- Sliding Mode Observer (SMO), including also the Super-Twisting Sliding-Mode Observer (STSMO);
- High-Gain Observer (HGO);
- Fuzzy Observer (FO);
- Artificial Neural Network (ANN);

where at least two of the angular position Θ of the motor axle; the angular position q of the output axle; and the motor torque τ_{motor}/i_{motor} provided to the motor axle by the joint motor serves as inputs of the observers.

[0039] For instance, adaptive friction estimation can be conducted to obtain an estimate of the input-side and/or output-side friction torque(s) of the robot transmissions based on the position of the motor axles of the robot joints, and/or the position of the output axles of the robot joints, and the motor torques, for instance by describing the friction torque by the linearly parametrizable model

eq. 14 $$\widehat{\boldsymbol{F}} = \widehat{\boldsymbol{F}}_{\boldsymbol{C}}\, sgn(\boldsymbol{\omega}) + \widehat{\boldsymbol{F}}_{\boldsymbol{V}}\, \boldsymbol{\omega} = [sgn(\boldsymbol{\omega}) \quad \boldsymbol{\omega}] \cdot \begin{bmatrix} \widehat{\boldsymbol{F}}_{\boldsymbol{C}} \\ \widehat{\boldsymbol{F}}_{\boldsymbol{V}} \end{bmatrix}$$

where $\boldsymbol{\omega}$ is the angular velocity of the motor axle and/or output axle, $\hat{\mathbf{F}}_{\mathbf{C}}$ is the vector of estimated Coulomb friction coefficients, and $\hat{\mathbf{F}}_{\mathbf{V}}$ is the vector of estimated viscous friction coefficients. Due to the linear parametrization it is possible to estimate the unknown and assumed slowly changing coefficients by Recursive Least Squares (RLS) methods with some forgetting scheme discounting past data.

[0040] Assuming that data for each robot joint is sampled at times $t_k = k\,T_S$, where T_S is the sampling time and k an incrementing integer denoting the specific sample, and that the dynamic friction residual $F_i(k) = \tau_{motor,i}(k) - B_i\,\ddot{\theta}_i(k) - \tau_{J,i}\left(\phi_i(k), \dot{\phi}_i(k)\right)$, the RLS method works by estimating the unknown filter coefficients $\hat{\alpha} = \left[\hat{F}_{C,i} \quad \hat{F}_{V,i}\right]^{\mathrm{T}}$ through the following procedure for each sample as

eq. 15 $$\Psi(k) = \left[sgn\left(\omega_i(k)\right) \quad \omega_i(k)\right]$$

eq. 16 $$P(k) = \frac{1}{\lambda}\left(P(k-1) - \frac{P(k-1)\Psi(k)\Psi^T(k)P(k-1)}{\lambda + \Psi^T(k)P(k-1)\Psi(k)}\right)$$

eq. 17 $$Q(k) = \frac{P(k)}{\lambda + \Psi^T(k)P(k)\Psi(k)}$$

eq. 18 $$L(k) = Q(k)\Psi(k)$$

eq. 19 $$\hat{F}(k) = \Psi^T(k)\,\hat{\alpha}(k-1)$$

eq. 20 $$\hat{\alpha}(k) = \alpha(k-1) + L(k)\left(F(k) - \hat{F}(k)\right)$$

[0041] where λ is the forgetting factor. A forgetting factor of $\lambda = 1$ is chosen to estimate time-invariant (constant) parameters, and a forgetting factor $\lambda < 1$ is chosen to estimate time-varying parameters. A smaller forgetting factor will make the RLS method forget parameters faster.

[0042] Estimating for instance the input-side friction torque through the use of an observer can be obtained using for instance the observer structure shown in fig. 11 illustrating an adaptive friction module 1174, which can be implemented as the adaptive friction module 674 of the robot system illustrated in figs. 6, 8 and 10. Here, the difference between a model-based estimate of the angular velocity $\hat{\dot{\boldsymbol{\theta}}}$ of the motor axle and the measured velocity $\dot{\boldsymbol{\theta}}$ obtained by time-differentiation of the motor axle angular position $\boldsymbol{\theta}$ signal is used to estimate the friction torque. The observer gain L is used to tune the observer. Based on the angular position of the motor axle $\boldsymbol{\theta}$ and the angular position of the output axle $\mathbf{q}$, the joint transmission deformation $\boldsymbol{\Phi}_{\mathbf{joint}}$ is determined by a joint transmission deformation module 1190 based on *eq. 3*. The time-derivative of the joint transmission deformation $\dot{\boldsymbol{\Phi}}_{\mathbf{joint}}$ is obtained by a joint transmission deformation differentiating module 1191 by differentiating the joint transmission deformation $\boldsymbol{\Phi}_{\mathbf{joint}}$. Based on the joint transmission deformation and the time-derivative of the joint transmission deformation, the joint torque $\boldsymbol{\tau}_{\mathbf{J}}$ is obtained by a joint torque obtaining module 1192 based on *eq. 4*. The dynamic model as seen from the input side of the robot joint transmissions (*eq. 12*) is used by a motor axle inertia torque estimation module 1193 to obtain the torque from the angular acceleration of the motor axle. An estimate of the angular acceleration of the motor axle $\hat{\ddot{\boldsymbol{\theta}}}$ obtained by a motor axle angular

acceleration estimation module 1194 by dividing the torque obtained from 1193 with the rotor inertia B. An estimate of the motor axle angular velocity $\hat{\dot{\boldsymbol{\theta}}}$ is obtained by a motor axle angular velocity estimation module 1195 based on the estimate of the angular acceleration of the motor axle. Based on the angular position $\boldsymbol{\theta}$ of the motor axle, the angular velocity of the motor axle $\dot{\boldsymbol{\theta}}$ is obtained by a motor axle position differentiating module 1196. The difference between the estimated angular velocity $\hat{\dot{\boldsymbol{\theta}}}$ of the motor axle and the angular velocity of the motor axle $\dot{\boldsymbol{\theta}}$ is obtained by a motor axle angular velocity difference module 1197 and multiplied by the observer gain L and the rotor inertia B in the inertia module 1198 to generate the input-side friction torque estimate $\hat{\mathbf{F}}_{\boldsymbol{\theta}}$. The estimated input-side friction torque is also fed back to 1193.

[0043] In another embodiment the adaptive friction module 674 can also be is configured to provide an estimate of the input-side and/or output-side friction torque(s) of the robot transmissions based on the position of the motor axles of the robot joints, and/or the position of the output axles of the robot joints, and the motor torques. The adaptive friction module can for instance be obtained by describing the friction torque by the linearly parametrizable model

eq. 21
$$\widehat{\boldsymbol{F}} = \widehat{\boldsymbol{F}}_{\boldsymbol{C}}\, sgn(\boldsymbol{\omega}) + \widehat{\boldsymbol{F}}_{\boldsymbol{V}}\, \boldsymbol{\omega} = [sgn(\boldsymbol{\omega}) \quad \boldsymbol{\omega}] \cdot \begin{bmatrix} \widehat{\boldsymbol{F}}_{\boldsymbol{C}} \\ \widehat{\boldsymbol{F}}_{\boldsymbol{V}} \end{bmatrix}$$

where $\boldsymbol{\omega}$ is the angular velocity of the motor axle and/or output axle, $\hat{\mathbf{F}}_{\mathbf{C}}$ is the vector of estimated Coulomb friction coefficients, and $\mathbf{F}_{\mathbf{V}}$ is the vector of estimated viscous friction coefficients. Due to the linear parametrization it is possible to estimate the unknown and assumed slowly changing coefficients by Recursive Least Squares (RLS) procedures as known in the art of adaptive control.

[0044] Step 560 of obtaining the transmission torque $\hat{\boldsymbol{\tau}}_{\mathbf{J}}$ between input side and the output side of the joint transmissions can be obtained based on at least one of:

- the angular position (q) of the output axle;
- the angular position (q) of the output axle and the angular position (Θ) of the motor axle;
- the angular position (Θ) of the motor axle and the motor torque (τ_{motor}) provided to the motor axle by the joint motor;

for instance, based on the angular position (q) of the output axle using eq. 10, where $\mathbf{F_q}$ have be obtained for each robot joint as described in paragraph [0024]; or by using *eq. 4*, where the joint transmission deformation Φ_{joint} and its time-derivative have been obtained based on the angular position (Θ) of the motor axle and the angular position (q) of the output axle using equation eq. 3. Alternatively, the transmission torque can be obtained based on the angular position (Θ) of the motor axle and the motor torque (τ_{motor}) provided to the motor axle by the joint motor using eq. 12, where $\mathbf{F_\Theta}$ have been obtained for each robot joint as described in paragraph [0025]. It is noted that in one embodiment the $\mathbf{F_q}$ and/or $\mathbf{F_\Theta}$ can be obtained based on the friction $\hat{\mathbf{F}}$ of the input side and/or the output obtained in step 558. Further it is to be understood the transmission torque $\hat{\boldsymbol{\tau}}_J$ can be obtained based on two or more of the data sets described above and where the transmission torque is obtained as any combination of the transmission torques obtained using the different methods.

[0045] Step 562 of generating motor control signal indicative of a desired motor torque $\tau_{control}$ for at least one of the joint motors is based on at least:

- the friction $\hat{\mathbf{F}}$ of the input side of the robot joint transmission and/or the output side of the robot joint transmission;
- the robot joint transmission torque τ_J between the input side and the output side of the robot joint transmission;

where the friction $\hat{\mathbf{F}}$ have been obtained as descried in step 558 and where the robot joint transmission torque has been obtained as described in step 560. In addition to the friction $\hat{\mathbf{F}}$ and the joint transmission torque $\boldsymbol{\tau}_J$, the desired motor torque is also obtained based on a desired motion $\mathbf{M}_d$, at least a part of the robot

arm, and a dynamic model of the robot arm D_{robot}. For instance, the desired motor torque can be obtained using dynamic model of the robot arm as expressed by eq. 12 where the second time derivative of the angular position of the motor axle $\ddot{\boldsymbol{\Theta}}$ has been obtained based on the angular position Θ of the motor axle obtained in step 552, the friction torques $\mathbf{F_\Theta}$ acting on the motor axles have been obtained in step 558 and the transmission torque $\boldsymbol{\tau_j}$ have been obtained in step 560 based on eq. 10, and based on desired motion of the robot arm. In eq. 10 the desired motion parameter is provided as desired angular positions $\mathbf{q}_d$, desired angular velocities $\dot{\mathbf{q}}_d$, and desired angular accelerations $\ddot{\mathbf{q}}_d$ of the output axles of the robot joint transmissions. The friction torques $\mathbf{F_\Theta}$ are adaptively obtained in step 558 and consequently the motor control signals indicating the desired motor toques are generated based on adaptive friction of the robot joint transmissions whereby a more accurate control of the robot joints can be provided.

[0046] Fig. 6 illustrates a structural diagram of a robot system 600 comprising a user interface 617, a robot control system 615 controlling a robot arm (not illustrated) by controlling the robot joints 603. The robot arm is like the robot arm illustrated in figs. 1-4 and comprises at least one rotational robot joint like the robot joint illustrated in fig. 2. The rotational robot joint comprises an input encoder 637 indicating the angular position of the motor axle Θ, and output encoder 635 indicating the angular position q of the output axle and a motor torque sensor 641 indicating the motor torque provided by the joint motor. In the illustrated embodiment the motor torque is provided as a current sensor indicating the motor current i_{motor} of the joint motor. The robot control 615 system is configured to control the robot joints based on the method of controlling a of the robot arm obtained according to the present invention. The user interface enables 617 a user to communicate with the robot controller system for instance in order to program the robot arm to perform various tasks. The user interface may be provided as described in connection with fig. 1.

[0047] The robot controller system 615 comprises a motion planner module 670, an adaptive friction module 674, a transmission torque module 676, a motor controller module 680 and optional a motor torque obtaining module 678.

[0048] The motion planner module 670 is configured to provide the desired motions of the robot arm, for instance by generating trajectories of parts of the robot arm. The trajectories can for instance be generated based on a robot program instructing the robot arm to perform various tasks. In the illustrated embodiment the motion planner module provides a desired motion $\mathbf{M}_d$ of parts of the robot arm. The desired motion of parts of the robot arm can for instance be indicated as motions properties of the robot joints, such as angular position $\boldsymbol{q_d}$ of output axles of the joint transmissions, a desired angular velocity $\dot{\boldsymbol{q}}_{\boldsymbol{d}}$ of output axles of the joint transmissions, a desired angular acceleration $\ddot{\boldsymbol{q}}_{\boldsymbol{d}}$ of the robot transmission. It is noted that the desired motion of part of the robot arm also can be indicated a position of various parts of the robot arm in relation a reference point, for instance the desired motion may be indicated as position, velocity and/or acceleration of the robot tool flange in relation to the robot base.

[0049] The desired motion $\mathbf{M}_d$ is provided to the motor controller module 680. The motor controller module 680 is configured to generate at least one motor control signal 633 to the joint motors, for instance in form of a signal indicating the motor torque $\tau_{control}$ that each joint motor shall provide to the motor axles or a current signal indicating the current $i_{control,}$ that each joint motor shall provide. The motor controller module 680 is configured to generate the motor control signal 633 based on:

- the desired motion $\mathbf{M}_d$;
- a dynamic model of the robot arm $D_{robot;}$
- the friction $\hat{F}$ of at the input side of the robot joint transmission and/or the output side of the robot joint transmission;
- the robot joint transmission torque τ_J between the input side and the output side of the robot joint transmission;

where the friction $\hat{F}$ is obtained by the adaptive friction module 674, the robot joint transmission torque τ_J is obtained by transmission torque is module 676 and the dynamic model of the robot arm D_{robot} in a memory 645. The motor controller module can for instance be configured to generate the motor control signal 633 by carrying out step 562 of the method described in fig. 5. As indicated by dotted lines the motor controller module may additionally also be configured to generate the motor control signal 633 based on:

- the angular position q of the output axle;
- the angular position Θ of the motor axle;
- the motor torque τ_{motor} provided to the motor axle by the joint motor.

[0050] The optional motor torque obtaining module 678 is configured to obtain the motor torque provided by the joint motors based on the current i_{motor} as known in the art and to provide the motor torque τ_{motor} to the adaptive friction module 674 and optionally to the transmission torque module and the motor controller module 680. However, it is noted the motor torque obtaining module 678 also can be provided as a part of the adaptive friction module 674, the transmission torque module and/or the motor controller module whereby the current i_{motor} is provided directly to the various modules. Further the motor torque obtaining module may also be provided as an external module to the robot controller system 615.

[0051] The adaptive friction module 674 is configured to provide the friction $\hat{F}$ at the input side of the robot joint transmission and/or the output side of the robot joint transmission based can be obtained based on least two of:

- the angular position Θ of the motor axle;
- the angular position q of the output axle;
- the motor torque τ_{motor}/i_{motor} provided to the motor axle by the joint motor;

and is configured to carry out step 558 of the method described in fig. 5. The friction $\hat{F}$ is provided the motor controller module as an adaptive parameter, further additionally the friction $\hat{F}$ may also be provided to the transmission torque module as an adaptive parameter.

[0052] The transmission torque module 676 is configured to provide the transmission torque $\hat{\tau}_j$ between input side and the output side of the joint transmissions can be obtained based on at least one of:

- the angular position q of the output axle (illustrated in solid line);
- the angular position q of the output axle (illustrated in dotted line) and the angular position Θ of the motor axle;
- the angular position (Θ) of the motor axle and the motor torque (illustrated in dotted line) provided to the motor axle by the joint motor.

The transmission torque module is configured to carry out step 560 of the method described in fig. 5. The transmission torque is then provided to the motor controller module.

[0053] The robot system 600 illustrated in fig. 6 makes it possible to provide a robot arm comprising where the friction of the robot joint transmissions is dynamically adapted whereby a more accurately control of the robot arm can be provided.

[0054] Fig. 7 illustrates a flow diagram of another method of controlling a robot arm comprising a plurality of robot joints connecting a robot base and a robot tool flange, where at least one of the robot joints is a rotational robot joint comprising a joint motor having a motor axle, where the motor axle is configured to rotate an output axle of the rotational robot joint via a robot joint transmission. The method is like the method illustrated and described in fig. 5

and similar steps and features have been given the same reference numbers as in fig. 5 and will not be described further.

[0055] In this embodiment step 760 of obtaining the transmission torque $\hat{\tau}_J$ between the input side and output side of the robot joint transmission is further obtained based on the friction $\hat{\mathbf{F}}$. Consequently, the transmission torque is obtained based on the adaptive friction whereby the transmission torque $\hat{\tau}_J(\hat{\mathbf{F}})$ can be obtained and adapted according the adaptive friction. For instance, the transmission torque $\hat{\tau}_J(\hat{\mathbf{F}})$ can be obtained by using eq. 10, where $\mathbf{F_q}$ have be obtained for each robot have been obtained in step 558 or by using eq. 12, where $\mathbf{F_\theta}$ each robot have been obtained in step 558.

[0056] In this embodiment step 762 of generating control signals for the joint motors is based the joint transmission torque $\hat{\tau}_J(\hat{\mathbf{F}})$ obtained in step 760 and since the joint transmission torque $\hat{\tau}_J(\hat{\mathbf{F}})$ in step 760 is obtained based on the friction $\hat{\mathbf{F}}$ of at the input side of the robot joint transmission and/or the output side of the robot joint transmission the control signals of for the joint motor will in step 762 indirectly also be obtained based the friction $\hat{\mathbf{F}}$. In addition, as described the desired motor torque are also obtained based on a desired motion $\mathbf{M}_d$ at least a part of the robot arm and a dynamic model of the robot arm D_{robot}.

[0057] Fig. 8 illustrates a structural diagram of a robot system 800. The robot system is like the robot system illustrated and described in fig. 6 and similar elements and features have been given the same reference numbers as in fig. 6 and will not be described further.

[0058] In transmission torque module 876 is configured to provide the transmission torque $\hat{\tau}_J$ between the input side and output side of the robot joint transmission is based on the friction $\hat{\mathbf{F}}$. Consequently, the transmission torque is obtained based on the adaptive friction whereby the transmission torque $\hat{\tau}_J(\hat{\mathbf{F}})$ can be obtained and adapted according the adaptive friction. For instance, the

transmission torque $\hat{\tau}_J(\hat{\mathbf{F}})$ can be obtained by using eq. 10, where $\mathbf{F_q}$ have be obtained for each robot have been obtained in step 558 or by using eq. 12, where $\mathbf{F_\theta}$ each robot have been obtained in step 558.

[0059] The motor controller module 880 is configured to generate generating control signals for the joint motors is based the joint transmission torque $\hat{\tau}_J(\hat{\mathbf{F}})$ obtained in step 760 and since the joint transmission torque $\hat{\tau}_J(\hat{\mathbf{F}})$ in step 760 is obtained based on the friction $\hat{\mathbf{F}}$ of at the input side of the robot joint transmission and/or the output side of the robot joint transmission the control signals of rate joint motor will in step 762 indirectly also be obtained based the friction $\hat{\mathbf{F}}$. In addition, as described the desired motor torque are also obtained based on a desired motion $\mathbf{M}_d$ at least a part of the robot arm and a dynamic model of the robot arm D_{robot}.

[0060] Fig. 9 illustrates a flow diagram of another method of controlling a robot arm comprising a plurality of robot joints connecting a robot base and a robot tool flange, where at least one of the robot joints is a rotational robot joint comprising a joint motor having a motor axle, where the motor axle is configured to rotate an output axle of the rotational robot joint via a robot joint transmission. The method is like the method illustrated and described in fig. 5 and similar steps and features have been given the same reference numbers as in fig. 5 and will not be described further.

[0061] In this embodiment step 962 of generating motor control signals comprises:

- a step 963 of determining a desired transmission torque $\tau_{J,d}$;
- a step 964 of determining a desired feed-forward motor torque $\tau_{m,FF}$;
- a step 965 of determining a transmission torque error correction motor torque $\tau_{m,torque\text{-}err}$;
- a step 967 of determining a resulting motor torque τ_r;
- a optional step 966 of determining an error correction motor torque;

- a step 968 of generating a motor control signal indicative of a motor control current.

[0062] Step 963 of determining a desired transmission torque $\tau_{J,d}$ indicative of desired transmission torque of the robot joint transmission can be based on:

- a dynamic model of the robot D_{robot};
- at least one motion parameter M_d, q_d, $\dot{q}_d$, $\ddot{q}_d$ indicating a desired motion of at least a part of the robot arm; and
- the friction $\hat{F}$ of at least one of the input side of the robot joint transmission and the output side of the robot joint transmission.

This makes it possible to obtain a more accurate desired transmission torque $\tau_{J,d}$ as the friction term adaptively can be determined and this more correct be incorporate into the dynamic model of the robot. For instance the desired transmission torque $\tau_{J,d}$ may be obtained by using eq. 10 and the desired transmission torque $\tau_{J,d}$ may in step 965 be used to obtain a transmission torque error correction motor torque $\tau_{m,torque-err}$.

[0063] Step 965 of determining the transmission torque error correction motor torque $\tau_{m,torque-err}$ indicating a motor torque minimizing differences between the desired transmission torque $\tau_{J,d}$ and the robot joint transmission torque $\hat{\tau}_J$ can be based on desired transmission torque $\tau_{J,d}$; and the robot joint transmission torque $\hat{\tau}_J$. This makes it possible to compare the actual transmission torque $\hat{\tau}_J$ obtained in step 560 with the desired transmission torque $\tau_{J,d}$ and provide a determine a transmission torque error correction motor torque which can correct eventual differences as known in the art of feed-back control systems.

[0064] Step 964 of determining a desired feed-forward motor torque $\tau_{m,FF}$ indicating a desired motor torque of the joint motor can based on:

- a dynamic model of the robot D_{robot};
- at least one motion parameter M_d, q_d, $\dot{q}_d$, $\ddot{q}_d$ indicating a desired motion of at least a part of the robot arm; and
- the friction ($\hat{F}$) of at least one of the input side of the robot joint transmission and the output side of the robot joint transmission.

This makes it possible to obtain a more accurate desired feed-forward motor torque $\tau_{m,FF}$ as the friction term adaptively can be determined and thus be correct when incorporate into the dynamic model of the robot. For instance the desired feed-forward motor torque $\tau_{m,FF}$ may be obtained by using eq. 10 and eq. 12 and desired feed-forward motor torque $\tau_{m,FF}$ may in be used to generate the motor control signal as known in the art of feed-forward control mechanisms.

[0065] Step 966 of determining error correction motor torque $\tau_{m,err}$ indicating a motor torque minimizing errors between at least one of:

- a desired motion parameter of the robot arm and actual motion parameter of the robot arm;
- a desired angular position q_d of the output axle and the angular position q of the output axle;
- a desired angular velocity $\dot{q}_d$ of the output axle and the angular velocity $\dot{q}$ of the output axle;
- a desired angular acceleration $\ddot{q}_d$ of the output axle and the angular acceleration velocity $\ddot{q}$ of the output axle;
- a desired angular position Θ_d of the motor axle and the angular position Θ of the motor axle;
- a desired angular velocity $\dot{\Theta}_d$ of the motor axle and the angular velocity $\dot{\Theta}$ of the motor axle;
- a desired angular acceleration $\ddot{\Theta}_d$ of the motor axle and the angular acceleration velocity $\ddot{\Theta}$ of the motor axle;
- a desired torque $\tau_{motor,d}$ provided to the motor axle by the joint motor and the motor torque τ_{motor}) provided to the motor axle by the joint motor.

This makes it possible to compare the parameters of the robot arm with corresponding desired parameters of the robot arm and determine a correction parameters which can be used to correct eventual errors between desired parameters and actual parameters as known in the art of feed-back control systems for instance as described in {15}

[0066] Step 967 of determining a resulting motor torque τ_r indicative of the resulting motor torque to be applied by the joint motor can be based on at least one of:

- the transmission torque error correction motor torque $\tau_{m,torque\text{-}err}$;
- desired feed-forward motor torque $\tau_{m,FF;}$ and
- error correction motor torque $\tau_{m,err}$;

where the motor control signal is generated based on the resulting motor torque. This makes is possible to generate the motor control signals for the joint motors based one both feed-forward parameters and feed-back parameters where the fiction op the robot joint transmissions are adapted according to the operation of the robot arm.

[0067] Fig. 10 illustrates a structural diagram of a robot system 1000. The robot system is like the robot system illustrated and described in fig. 6 and similar elements and features have been given the same reference numbers as in fig. 6 and will not be described further. The robot controller system 1070 comprises a motion planner module 1070, an adaptive friction module 674, a transmission torque module 676, a motor controller module 1080 and optional a motor torque obtaining module 678.

[0068] The motion planner module 1070 is configured to provide the desired motions of the robot arm, for instance by generating trajectories of parts of the robot arm. The trajectories can for instance be generated based on a robot program instructing the robot arm to perform various tasks. In the illustrated embodiment the desired motions M_d provided to the motor controller

module 1080 are a desired angular position $\boldsymbol{q_d}$ of the output axles of the joint transmissions, a desired angular velocity $\dot{\boldsymbol{q}}_{\boldsymbol{d}}$ of output axles of the joint transmissions and a desired angular acceleration $\ddot{\boldsymbol{q}}_{\boldsymbol{d}}$ of the robot transmission.

[0069] The motor controller module comprises a feed-forward controller module 1082, a torque feed-back module 1084, a motor current controller 1086 and an optional a feed-back controller module 1080.

[0070] The feed-forward controller module 1082 is configured to determine a desired transmission torque $\tau_{J,d}$ indicative of desired transmission torque of the robot joint transmission based on:

- a dynamic model of the robot D_{robot};
- at least one motion parameter M_d, q_d, $\dot{q}_d$, $\ddot{q}_d$ indicating a desired motion of at least a part of the robot arm; and
- the friction ($\hat{F}$) of at least one of the input side of the robot joint transmission and the output side of the robot joint transmission.

The feed-forward controller module can for instance be configured to carry our step 963 of the method illustrated in fig. 9 and similar advantages are archived by the feed-forward controller.

[0071] The feed-forward controller module 1082 can also be configured to determine a desired feed-forward motor torque $\tau_{m,FF}$ indicating a desired motor torque of the joint motor based on:

- a dynamic model of the robot D_{robot};
- at least one motion parameter M_d, q_d, $\dot{q}_d$, $\ddot{q}_d$ indicating a desired motion of at least a part of the robot arm; and
- the friction $\hat{F}$ of at least one of the input side of the robot joint transmission and the output side of the robot joint transmission.

The feed-forward controller module can for instance be configured to carry our step 964 of the method illustrated in fig. 9 and similar advantages are archived by the feed-forward controller.

[0072] The torque feed-back controller module 1084 is configured to determine a transmission torque error correction motor torque $\tau_{m,torque\text{-}err}$ indicating a motor torque minimizing differences between the desired transmission torque $\tau_{J,d}$ and the robot joint transmission torque ($\hat{\tau}_J$), where the transmission torque error correction motor torque $\tau_{m,torque\text{-}err}$ is determined based on:

- the desired transmission torque $\tau_{J,d}$; and
- the robot joint transmission torque $\hat{\tau}_J$.

The torque feed-back controller module 1084 can for instance be configured to carry our step 965 of the method illustrated in fig. 9 and similar advantages are archived by torque feed-back controller module 1084.

[0073] The robot controller comprises a feed-back controller module 1088 configured to determine determining an error correction motor torque $\tau_{m,err}$ indicating a motor torque minimizing errors between at least one of:

- a desired motion parameter of the robot arm and actual motion parameter of the robot arm;
- a desired angular position q_d of the output axle and the angular position q of the output axle;
- a desired angular velocity $\dot{q}_d$ of the output axle and the angular velocity $\dot{q}$ of the output axle;
- a desired angular acceleration $\ddot{q}_d$ of the output axle and the angular acceleration velocity $\ddot{q}$ of the output axle;
- a desired angular position Θ_d of the motor axle and the angular position Θ of the motor axle;
- a desired angular velocity $\dot{\Theta}_d$ of the motor axle and the angular velocity $\dot{\Theta}$ of the motor axle;

- a desired angular acceleration $\ddot{\Theta}_d$ of the motor axle and the angular acceleration velocity $\ddot{\Theta}$ of the motor axle;
- a desired torque $\tau_{motor,d}$ provided to the motor axle by the joint motor and the motor torque τ_{motor} provided to the motor axle by the joint motor.

The feed-back controller module 1088 can for instance be configured to carry our step 966 of the method illustrated in fig. 9 and similar advantages are archived feed-back controller module 1088.

[0074] The motor current controller module 1086 is configured to generate a motor control signal indicating a motor current $i_{control}$ for the robot joint based on a resulting motor torque τ_r indicative of a resulting motor torque to be applied by the joint motor where the resulting motor torque τ_r is determined based on at least one of:

- the transmission torque error correction motor torque $\tau_{m,torque-err}$;
- desired feed-forward motor torque $\tau_{m,FF;}$ and
- error correction motor torque $\tau_{m,err}$.

[0075] The motor current controller may be providing as any motor control driver driving and controlling motors base on a desired torque. Typically, such motor control divers generate signal indicative of the current to be provided to the motor coil. In some embodiment the motor control driver generates the currents directly. It is to be understood that an adaptive or non-adaptive system can be configured to provide smoothed estimates of the position of the motor axles and/or output axles of the robot joints based on noisy measurements.

[0076] The invention comprises an adaptive control system having an adaptive feed-forward control command and a computation of the torque through the robot joint transmission in at least one of the robot joints. The present invention can for instance be provided at a robot comprising a robot

control system which monitors and controls the robot joint, whereby the position error is reduced when the robot is subject to changes in ambient conditions, wear, etc. This is achieved by providing control of robot joint torque based on an adaptive observer estimating the robot joint friction adaptively and the robot joint torque.

BRIEF DESCRIPTION OF FIGURE REFERENCES

600, 800, 1000	Robot system
101	robot arm
103a-103f, 203, 303, 403i, 403i+1, 403n, 603	robot joint
104b, 104c, 104d, 304i; 304i-1	robot link
105	robot base
107	robot tool flange
209, 309	joint motor
111a-111f, 211	axis of rotation
113a-113f:, 213	rotation arrow
115, 415	robot controller
117, 617	interface device
119	display
121	input device
123	direction of gravity
225, 325i	motor axle
326	spring connecting input side and output
227, 327i	output axle
328	damper input side and output
229, 329i	robot joint transmission
231	output flange
233, 433i; 433i+1; 433n, 633	motor control signal
235, 635	output encoder
236, 436i; 436i+1; 436n	output encoder signal
237, 637	input encoder
238, 438i; 438i+1; 438n	output encoder signal
239	encoder wheel
241, 641	motor torque sensor
242, 442i; 442i+1; 442n	motor torque signal
443	Processor
445, 645	memory
550	Step of initializing
552	Step of obtaining the angular position of motor axle
554	Step of obtaining the angular position of output axle
556	Step of obtaining the actual motor torque
558	Step of obtaining the friction of joint transmission
560, 760	Step of obtaining the transmission torque between input side and the output side of the joint transmissions

562, 762, 962	Step of generating motor control signal indicative of a desired motor torque
963	Step of determining a desired transmission torque
964	Step of determining a desired feed-forward motor torque
965	Step of determining a transmission torque error correction motor torque
966	Step of determining an error correction motor torque
967	Step of determining resulting motor torque
968	step of generating a motor control signal indicating desired motor current
670	motion planner
674, 1174	adaptive friction module
676, 876	transmission torque module
678	motor torque module
680, 880, 1080	motor controller module
1082	Feed-forward controller module
1084	torque feed-back controller module
1086	a current controller
1088	feed-back controller module
1190	joint transmission deformation module
1191	joint transmission deformation differentiating module
1192	joint torque obtaining module
1193	motor axle inertia torque estimation module
1194	motor axle angular acceleration estimation module
1195	motor axle angular velocity estimation module
1196	motor axle position differentiating module
1197	obtained by an motor axle angular velocity difference module
1198	A gain and inertia module

CLAIMS

1. A method of controlling a robot arm comprising a plurality of robot joints connecting a robot base and a robot tool flange, where at least one of said robot joints is a rotational robot joint comprising a joint motor having a motor axle, where said motor axle is configured to rotate an output axle of said rotational robot joint via a robot joint transmission, said method comprises the steps of:

- obtaining (552) the angular position (Θ) of said motor axle;
- obtaining (554) the angular position (q) of said output axle;
- obtaining (556) the motor torque (τ_{motor}) provided to said motor axle by said joint motor;
- determine (558) the friction ($\hat{F}$) of at least one of:
    - the input side of said robot joint transmission; and
    - the output side of said robot joint transmission

  based on at least two of
    - said angular position (Θ) of said motor axle;
    - said angular position (q) of said output axle;
    - said motor torque (τ_{motor}/i_{motor}) provided to said motor axle by said joint motor;
- determining (560) a robot joint transmission torque ($\hat{\tau}_j$) between the input side and the output side of said robot joint transmission based on at least one of:
    - said angular position (q) of said output axle;
    - said angular position (q) of said output axle and said angular position (Θ) of said motor axle;
    - said angular position (Θ) of said motor axle and said motor torque (τ_{motor}) provided to said motor axle by said joint motor;
- generating (562) a motor control signal for said at least one joint motor of said rotational joint based on:
    - said friction ($\hat{F}$) of at least one of said input side of said robot joint transmission and said output side of said robot joint transmission;

- said robot joint transmission torque ($\hat{\tau}_J$) between the input side and the output side of said robot joint transmission.

2. The method according to claim 1 wherein said motor control signal is further generated based on at least one of:

- said angular position (Θ) of said motor axle;
- said angular position (q) of said output axle;
- said motor torque (τ_{motor}) provided to said motor axle by said joint motor;
- a dynamic model of said robot (D_{robot});
- at least one motion parameter (M_d, q_d, $\dot{q}_d$, $\ddot{q}_d$) indicating a desired motion of at least a part of said robot arm.

3. The method according to any one of claims 1-2 wherein said step of determining said robot joint transmission torque is further based on said friction ($\hat{F}$) of at least one of said input side of said robot joint transmission and said output side of said robot joint transmission.

4. The method according to any one of claims 1-3 wherein said step of generating a motor control signal for said at least one joint motor of said rotational joint comprises a step (963) of determining a desired transmission torque ($\tau_{J,d}$) indicative of desired transmission torque of said robot joint transmission based on:

- a dynamic model of said robot (D_{robot});
- at least one motion parameter (M_d, q_d, $\dot{q}_d$, $\ddot{q}_d$) indicating a desired motion of at least a part of said robot arm; and
- said friction ($\hat{F}$) of at least one of said input side of said robot joint transmission and said output side of said robot joint transmission.

5. The method according to claim 5 wherein said step of generating a motor control signal for said at least one joint motor of said rotational joint comprises a step (965) of determining a transmission torque error correction motor torque ($\tau_{m,torque\text{-}err}$) indicating a motor torque minimizing differences between said desired transmission torque ($\tau_{J,d}$) and said robot joint transmission torque ($\hat{\tau}_J$), where said transmission torque error correction motor torque ($\tau_{m,torque\text{-}err}$) is determined based on :

- said desired transmission torque ($\tau_{J,d}$); and
- said robot joint transmission torque ($\hat{\tau}_J$).

6. The method according to any one of claims 1-5 wherein said step of generating a motor control signal for said at least one joint motor of said rotational joint comprises a step (964) of determining a desired feed-forward motor torque ($\tau_{m,FF}$) indicating a desired motor torque of said joint motor based on:

- a dynamic model of said robot (D_{robot});
- at least one motion parameter (M_d, q_d, $\dot{q}_d$, $\ddot{q}_d$) indicating a desired motion of at least a part of said robot arm; and
- said friction ($\hat{F}$) of at least one of said input side of said robot joint transmission and said output side of said robot joint transmission.

7. The method according to any one of claims 1-6 wherein said step of generating a motor control signal for said at least one joint motor of said rotational joint comprises a step (966) of determining error correction motor torque ($\tau_{m,err}$) indicating a motor torque minimizing errors between at least one of:

- a desired motion parameter of said robot arm and actual motion parameter of said robot arm;

- a desired angular position (q_d) of said output axle and said angular position (q) of said output axle;
- a desired angular velocity ($\dot{q}_d$) of said output axle and the angular velocity ($\dot{q}$) of said output axle;
- a desired angular acceleration ($\ddot{q}_d$) of said output axle and the angular acceleration velocity ($\ddot{q}$) of said output axle;
- a desired angular position (Θ_d) of said motor axle and said angular position (Θ) of said motor axle;
- a desired angular velocity ($\dot{\Theta}_d$) of said motor axle and the angular velocity ($\dot{\Theta}$) of said motor axle;
- a desired angular acceleration ($\ddot{\Theta}_d$) of said motor axle and the angular acceleration velocity ($\ddot{\Theta}$) of said motor axle;
- a desired torque ($\tau_{motor,d}$) provided to said motor axle by said joint motor and said motor torque (τ_{motor}) provided to said motor axle by said joint motor.

8. The method according to any one of claims 4-7 wherein said step of generating a motor control signal for said at least one joint motor of said rotational joint comprises a step (967) of determining a resulting motor torque (τ_r) indicative of a resulting motor torque to be applied by said joint motor based on at least one of:

- said transmission torque error correction motor torque ($\tau_{m,torque\text{-}err}$);
- desired feed-forward motor torque ($\tau_{m,FF}$); and
- error correction motor torque ($\tau_{m,err}$);

where said motor control signal is generated based on said resulting motor torque.

9. A robot system comprising a robot arm controlled by a robot controller configured to control said robot arm, said robot arm comprising a plurality of robot joints connecting a robot base and a robot tool flange, where at least one

of said robot joints is a rotational robot joint comprising a joint motor having a motor axle, where said motor axle is configured to rotate an output axle of said rotational robot joint via a robot joint transmission, said robot controller is configured to control said robot arm by providing a motor control signal for said at least one joint motor of said rotational joint and said robot controller is configured to generate said motor control signal based on:

- the angular position (Θ) of said motor axle;
- the angular position (q) of said output axle;
- the motor torque (τ_{motor}) provided to said motor axle by said joint motor;

characterized in that said robot controller comprises:

- an adaptive friction module (674) configured to determine the friction ($\hat{F}$) of at least one of said input side of said robot joint transmission and said output side of said robot joint transmission based on at least two of:
  - said angular position (Θ) of said motor axle;
  - said angular position (q) of said output axle;
  - said motor torque (τ_{motor}/i_{motor}) provided to said motor axle by said joint motor;
- a transmission torque module (676) configured to determine the robot joint transmission torque ($\hat{\tau}_J$) between the input side and the output side of said robot joint transmission based on at least one of:
  - said angular position (q) of said output axle;
  - said angular position (q) of said output axle and said angular position (Θ) of said motor axle;
  - said angular position (Θ) of said motor axle and said motor torque (τ_{motor}) provided to said motor axle by said joint motor;

and robot controller is configured to generate said motor control signal based on friction ($\hat{F}$) of at least one of said input side of said robot joint transmission and said output side of said robot joint transmission and said robot joint transmission torque ($\hat{\tau}_J$) between the input side and the output side of said robot joint transmission.

10. The robot system according to claim 9 comprising at least one of:

- an encoder (237,637) configured to obtain the angular position (Θ) of said motor axle;
- an encoder (235,635) configured to obtain the angular (q) of said output axle;
- a sensor (241,641) configured to obtaining the motor torque (τ_{motor}) provided to said motor axle by said joint motor.

11. The robot system according to any one of claims 9-10 wherein said robot controller comprises a feed-forward controller module (1082) configured to determine a desired transmission torque ($\tau_{J,d}$) indicative of desired transmission torque of said robot joint transmission based on:

- a dynamic model of said robot (D_{robot});
- at least one motion parameter (M_d, q_d, $\dot{q}_d$, $\ddot{q}_d$) indicating a desired motion of at least a part of said robot arm; and
- said friction ($\hat{F}$) of at least one of said input side of said robot joint transmission and said output side of said robot joint transmission.

12. The robot system according to claim 12 wherein said robot controller comprises a torque feed-back controller module (1084) configured to determine a transmission torque error correction motor torque ($\tau_{m,torque\text{-}err}$) indicating a motor torque minimizing differences between said desired transmission torque ($\tau_{J,d}$) and said robot joint transmission torque ($\hat{\tau}_J$), where said transmission torque error correction motor torque ($\tau_{m,torque\text{-}err}$) is determined based on:

- said desired transmission torque ($\tau_{J,d}$); and
- said robot joint transmission torque ($\hat{\tau}_J$).

13. The robot system according to any one of claims 9-12 wherein said robot controller comprises a feed-forward controller module (1082) configured to

determine a desired feed-forward motor torque ($\tau_{m,FF}$) indicating a desired motor torque of said joint motor based on:

- a dynamic model of said robot (D_{robot});
- at least one motion parameter (M_d, q_d, $\dot{q}_d$, $\ddot{q}_d$) indicating a desired motion of at least a part of said robot arm; and
- said friction ($\hat{F}$) of at least one of said input side of said robot joint transmission and said output side of said robot joint transmission.

14. The robot system according to any one of claims 9-14 wherein said robot controller comprises a feed-back controller (1088) configured to determine determining a error correction motor torque ($\tau_{m,err}$) indicating a motor torque minimizing errors between at least one of:

- a desired motion parameter of said robot arm and actual motion parameter of said robot arm;
- a desired angular position (q_d) of said output axle and said angular position (q) of said output axle;
- a desired angular velocity ($\dot{q}_d$) of said output axle and the angular velocity ($\dot{q}$) of said output axle;
- a desired angular acceleration ($\ddot{q}_d$) of said output axle and the angular acceleration velocity ($\ddot{q}$) of said output axle;
- a desired angular position (Θ_d) of said motor axle and said angular position (Θ) of said motor axle;
- a desired angular velocity ($\dot{\Theta}_d$) of said motor axle and the angular velocity ($\dot{\Theta}$) of said motor axle;
- a desired angular acceleration ($\ddot{\Theta}_d$) of said motor axle and the angular acceleration velocity ($\ddot{\Theta}$) of said motor axle;
- a desired torque ($\tau_{motor,d}$) provided to said motor axle by said joint motor and said motor torque (τ_{motor}) provided to said motor axle by said joint motor.

15. The robot system according to any one of claims 11-14 wherein said robot controller comprises motor controller module (1086) configured to generate a motor control signal indicating a motor current ($i_{control}$) for said robot joint based on a resulting motor torque (τ_r) indicative of a resulting motor torque to be applied by said joint motor where said resulting motor torque (τ_r) is determined based on at least one of:

- said transmission torque error correction motor torque ($\tau_{m,torque\text{-}err}$);
- desired feed-forward motor torque ($\tau_{m,FF}$); and
- error correction motor torque ($\tau_{m,err}$).

16. The robot system according to any one of claims 9-15 wherein said robot controller is configured to control said robot arm based on a motor control signal for said at least one joint motor of said rotational joint based, wherein said robot controller is configured to generate said motor control signal by carrying out the method according to claims 1-8.

ABSTRACT

A method of controlling a robot arm with robot joints, where the joint motors of the joints are controlled based a signal generated based on the friction $\hat{F}$ of at least one of the input/outside of the robot joint transmission and the robot joint transmission torque $\hat{\tau}_J$ between the input side and the output side of the transmission. The friction is determined based on: at least two of the angular position of the motor axle; the angular position of the output axle and/or the motor torque provided to the motor axle by the joint motor. The robot joint transmission torque is determined based on: at least one of the angular position of the output axle; the angular position of the output axle and/or the angular position of the motor axle; the angular position of the motor axle and the motor torque provided to the motor axle by the joint motor.

1/10

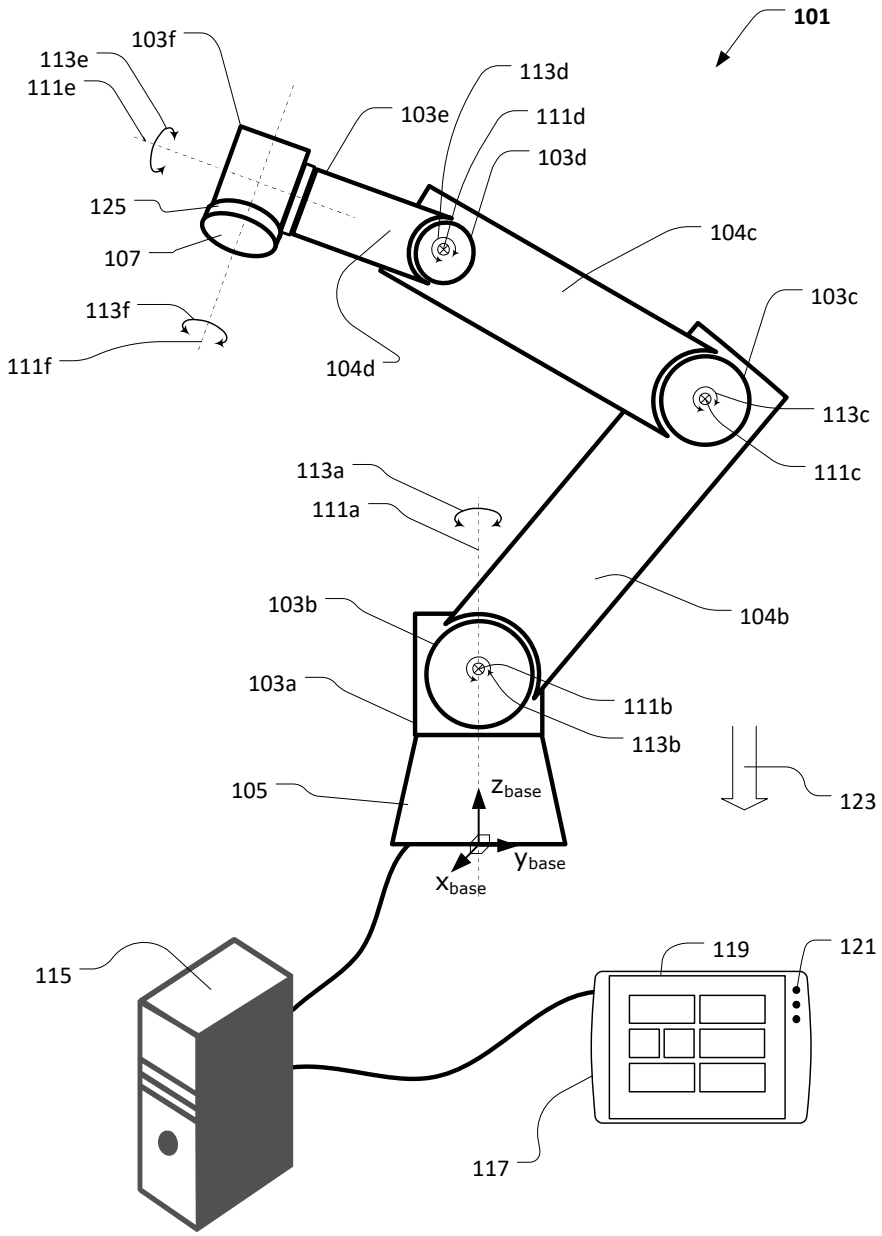
101
103f
113e
111e
113d
103e
111d
103d
125
107
104c
103c
113f
111f
104d
113c
111c
113a
111a
104b
103b
103a
111b
113b
105
z_{base}
y_{base}
x_{base}
123
115
119
121
117

FIG. 1

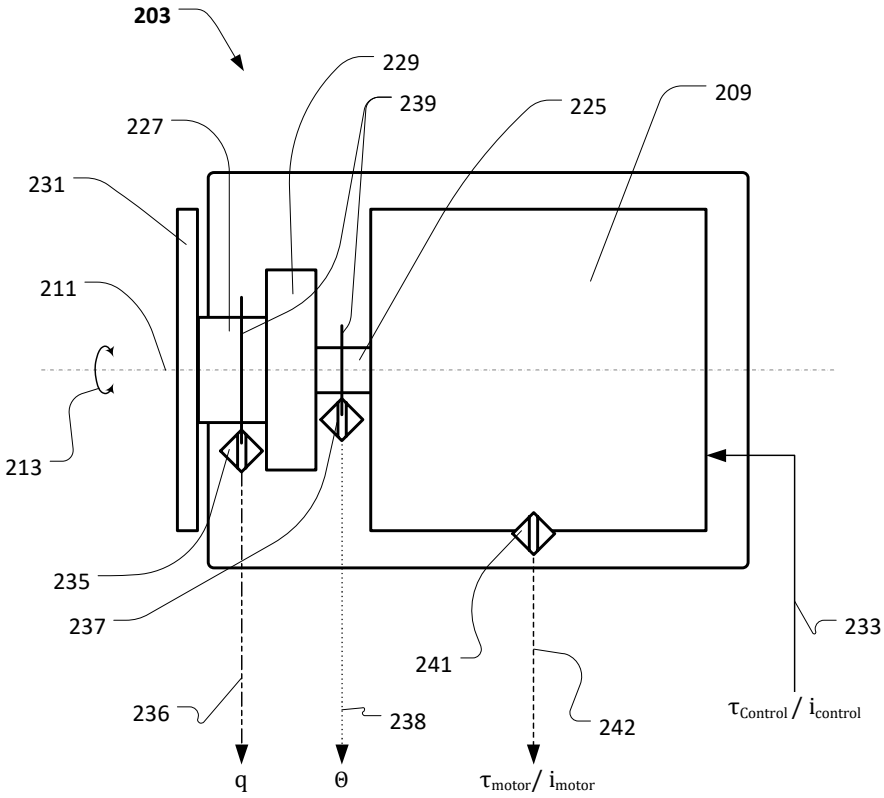
203
229
239
225
209
227
231
211
213
235
237
241
233
236
238
242
q
Θ
τ_{motor}/ i_{motor}
$\tau_{Control}$ / $i_{control}$

FIG. 2

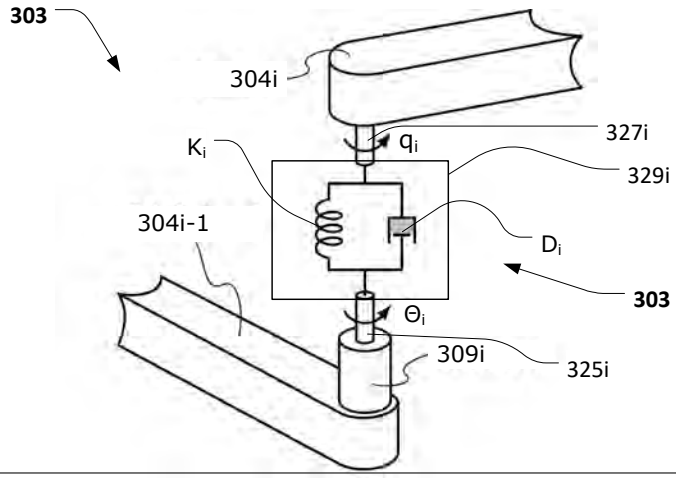
303
304i
327i
q_i
K_i
329i
304i-1
D_i
303
Θ_i
309i
325i

FIG. 3

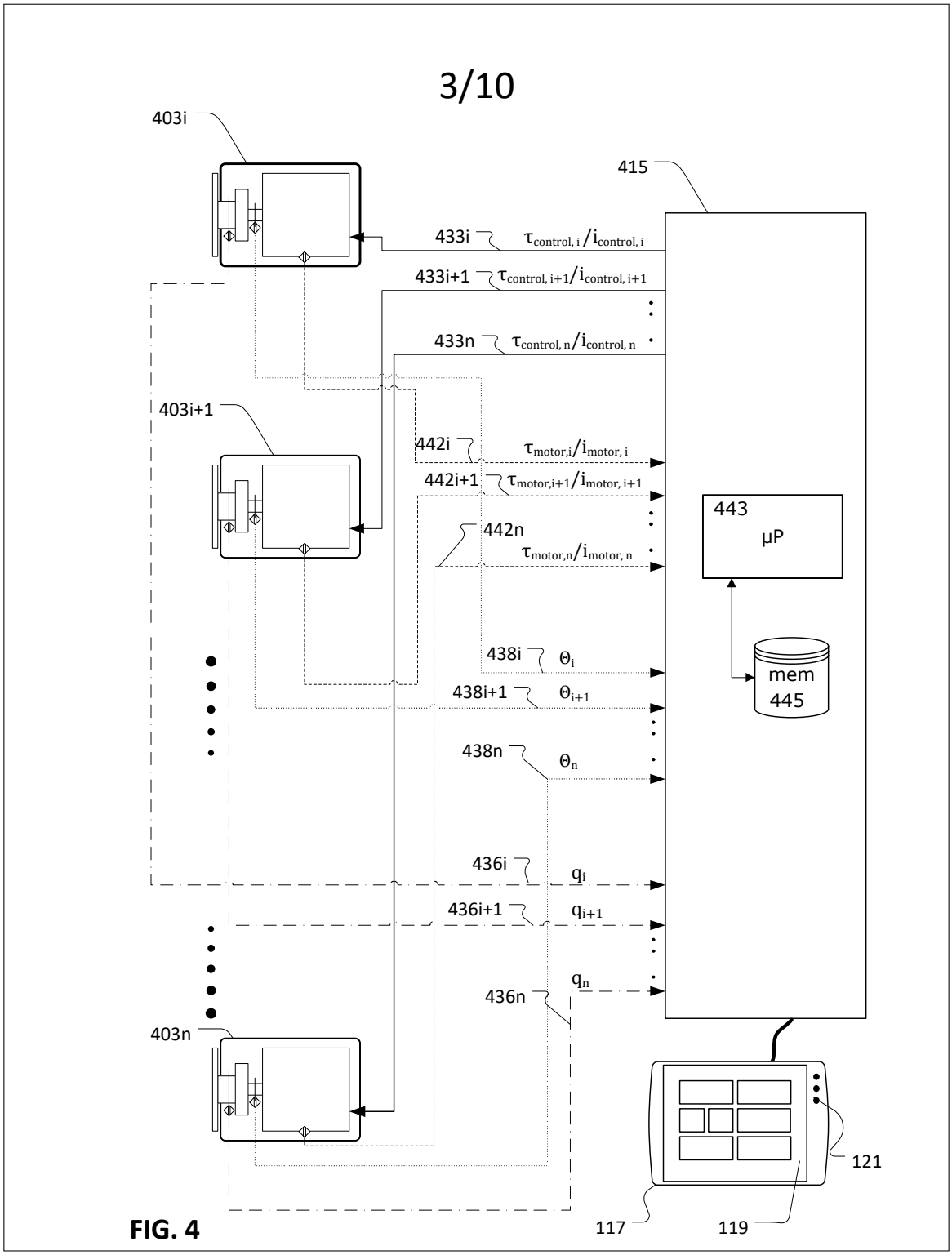
3/10
403i
415
433i
$\tau_{control,\,i}/i_{control,\,i}$
433i+1
$\tau_{control,\,i+1}/i_{control,\,i+1}$
433n
$\tau_{control,\,n}/i_{control,\,n}$
403i+1
442i
$\tau_{motor,i}/i_{motor,\,i}$
442i+1
$\tau_{motor,i+1}/i_{motor,\,i+1}$
442n
$\tau_{motor,n}/i_{motor,\,n}$
443
µP
mem
445
438i
Θ_i
438i+1
Θ_{i+1}
438n
Θ_n
436i
q_i
436i+1
q_{i+1}
q_n
436n
403n
121
117
119

FIG. 4

4/10

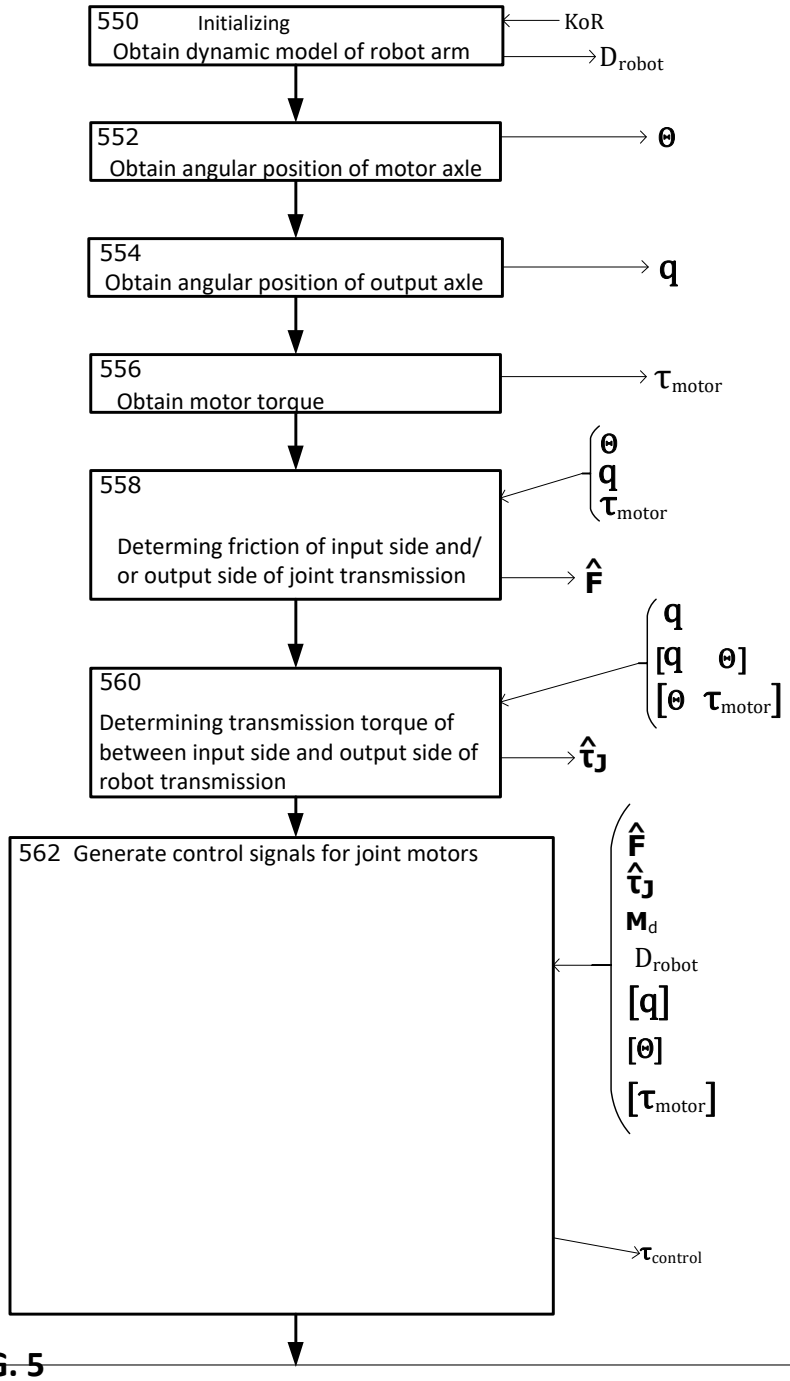
550 Initializing
Obtain dynamic model of robot arm
KoR
D_{robot}
552
Obtain angular position of motor axle
Θ
554
Obtain angular position of output axle
q
556
Obtain motor torque
τ_{motor}
558
Determing friction of input side and/ or output side of joint transmission
Θ
q
τ_{motor}
$\hat{F}$
560
Determining transmission torque of between input side and output side of robot transmission
q
$[q \quad \Theta]$
$[\Theta \quad \tau_{motor}]$
$\hat{\tau}_J$
562 Generate control signals for joint motors
$\hat{F}$
$\hat{\tau}_J$
M_d
D_{robot}
$[q]$
$[\Theta]$
$[\tau_{motor}]$
$\tau_{control}$

FIG. 5

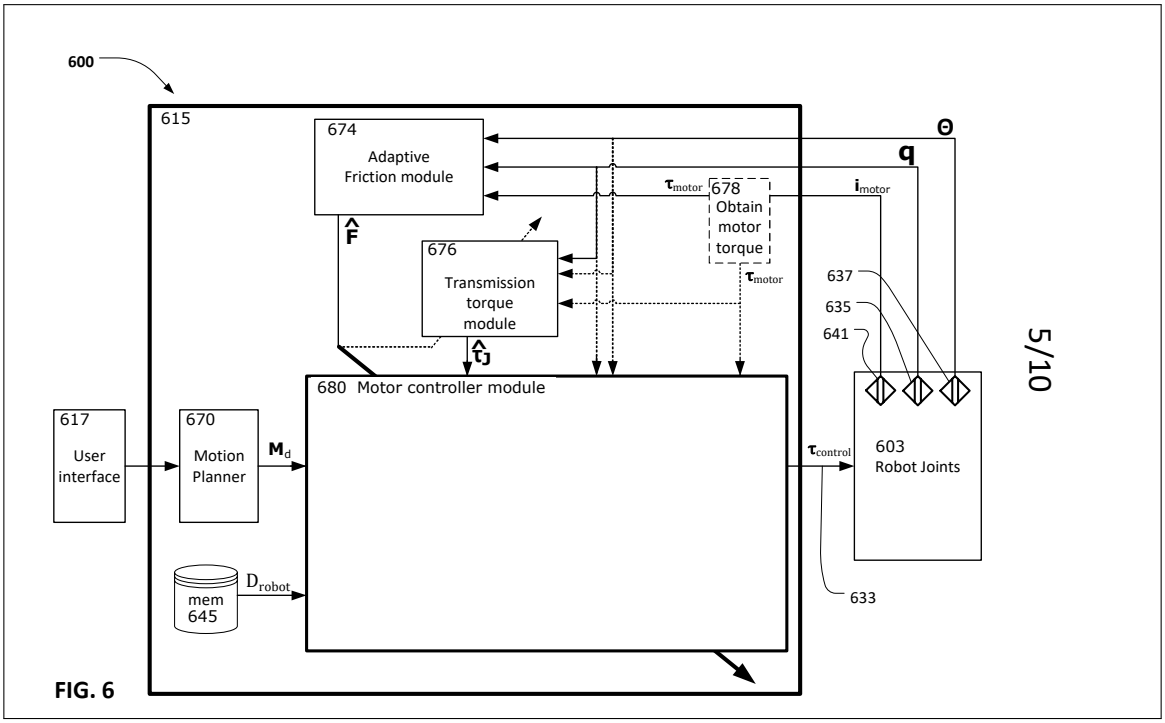
600
615
674
Adaptive
Friction module
Θ
q
τmotor
678
Obtain
motor
torque
imotor
F̂
676
Transmission
torque
module
τmotor
637
635
641
τ̂J
680 Motor controller module
617
User
interface
670
Motion
Planner
Md
τcontrol
603
Robot Joints
mem
645
Drobot
633
FIG. 6

6/10

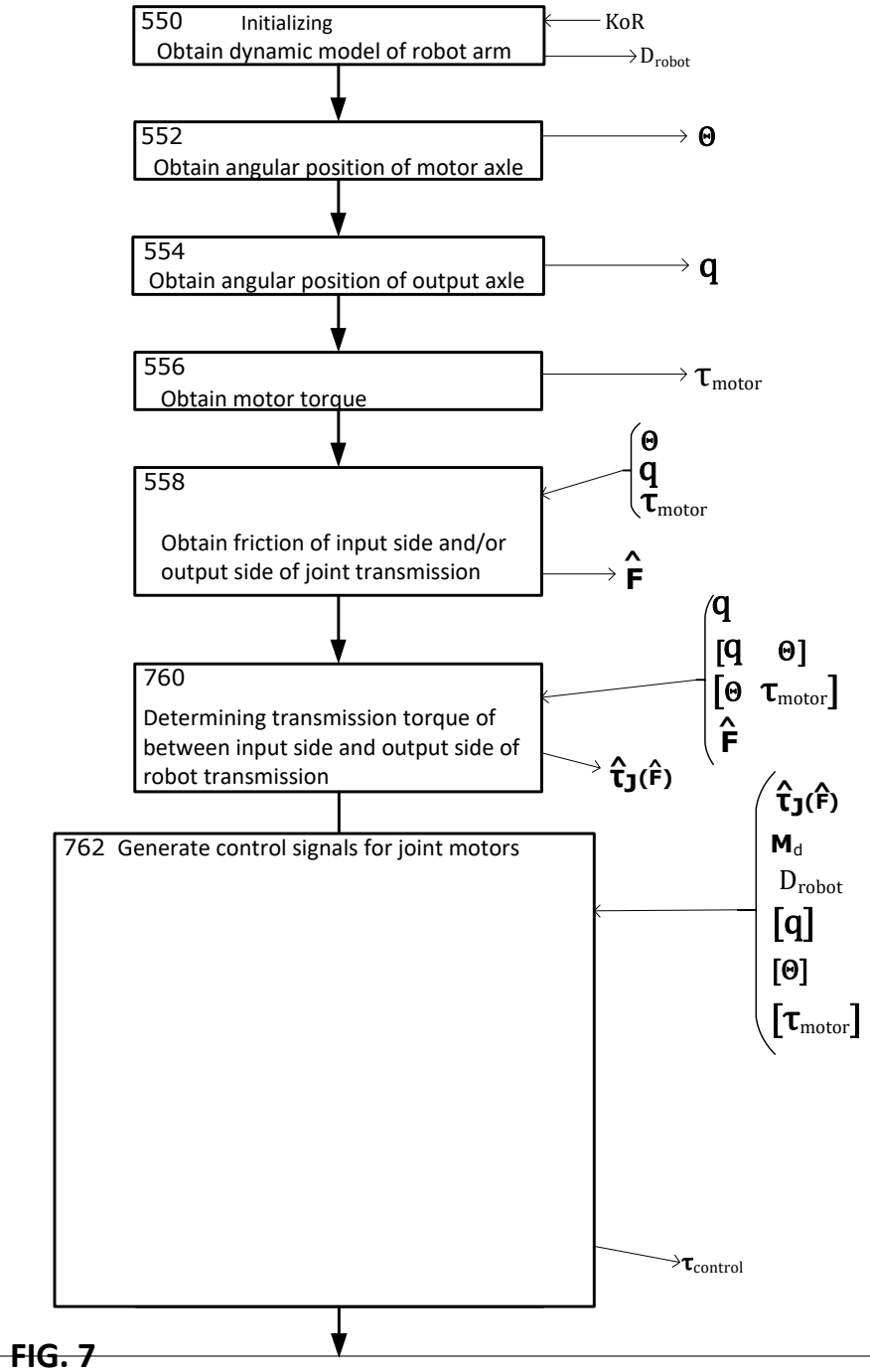
550 Initializing
Obtain dynamic model of robot arm
KoR
D_{robot}
552
Obtain angular position of motor axle
Θ
554
Obtain angular position of output axle
q
556
Obtain motor torque
τ_{motor}
558
Obtain friction of input side and/or output side of joint transmission
Θ
q
τ_{motor}
$\hat{F}$
760
Determining transmission torque of between input side and output side of robot transmission
q
$[q \quad \Theta]$
$[\Theta \quad \tau_{motor}]$
$\hat{F}$
$\hat{\tau}_J(\hat{F})$
762 Generate control signals for joint motors
$\hat{\tau}_J(\hat{F})$
M_d
D_{robot}
$[q]$
$[\Theta]$
$[\tau_{motor}]$
$\tau_{control}$

FIG. 7

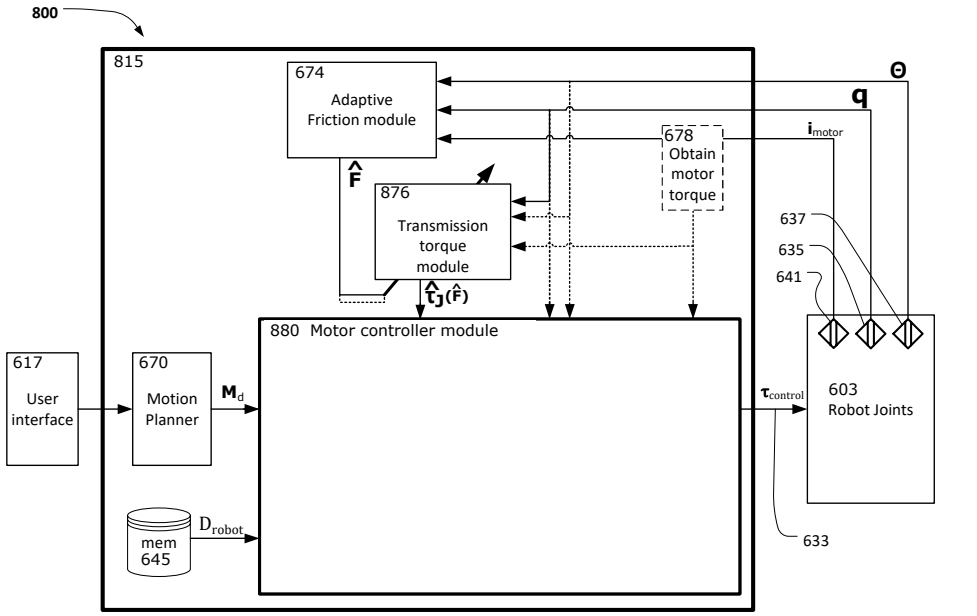
800
815
674
Adaptive
Friction module
Θ
q
i_{motor}
678
Obtain
motor
torque
$\hat{F}$
876
Transmission
torque
module
$\hat{\tau}_J(\hat{F})$
637
635
641
880 Motor controller module
617
User
interface
670
Motion
Planner
M_d
$\tau_{control}$
603
Robot Joints
mem
645
D_{robot}
633

FIG. 8

8/10

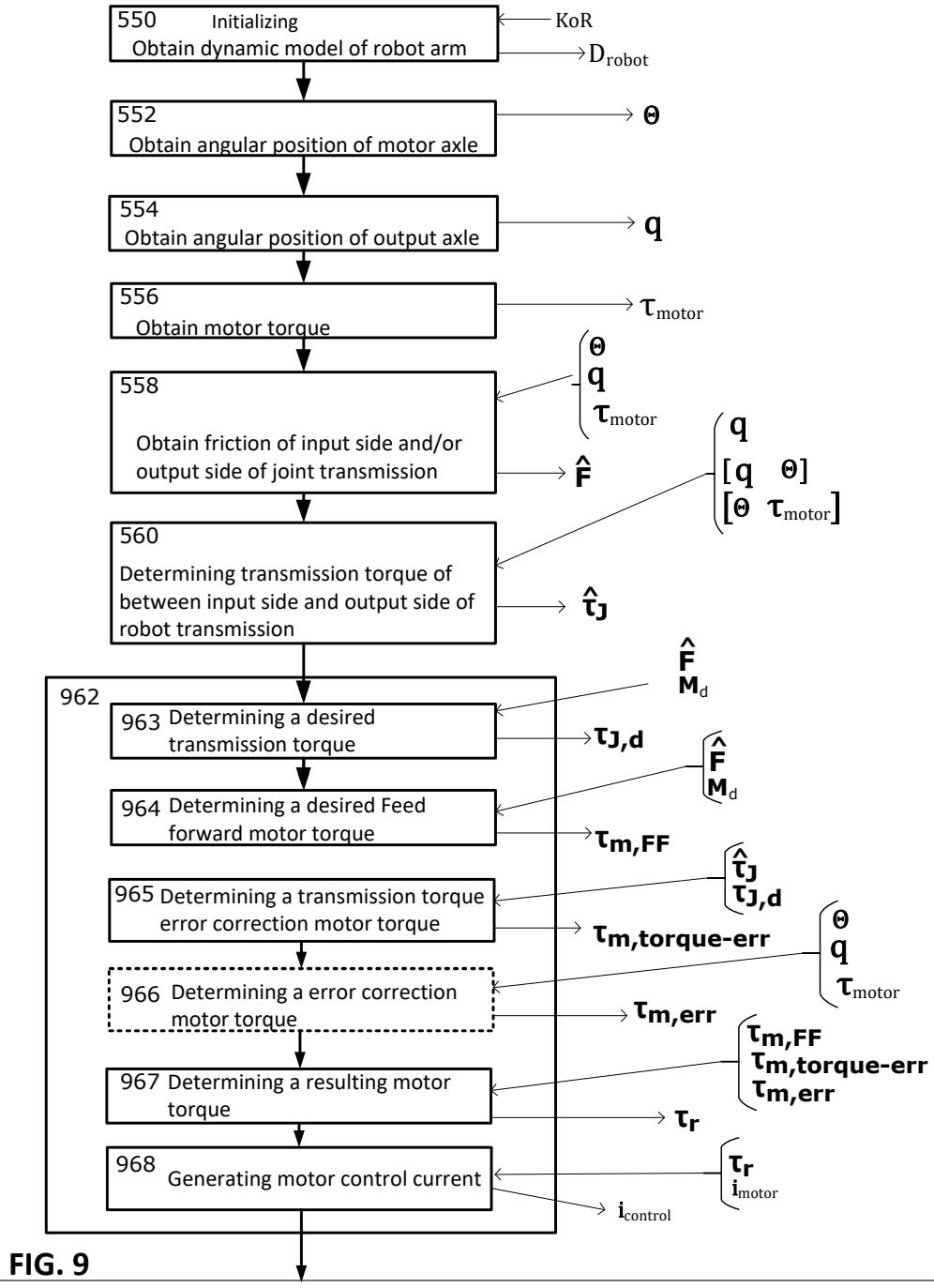
550 Initializing
Obtain dynamic model of robot arm
KoR
D_{robot}
552
Obtain angular position of motor axle
Θ
554
Obtain angular position of output axle
q
556
Obtain motor torque
τ_{motor}
558
Obtain friction of input side and/or output side of joint transmission
Θ
q
τ_{motor}
$\hat{F}$
q
[q Θ]
[Θ τ_{motor}]
560
Determining transmission torque of between input side and output side of robot transmission
$\hat{\tau}_J$
962
963 Determining a desired transmission torque
$\hat{F}$
M_d
$\tau_{J,d}$
964 Determining a desired Feed forward motor torque
$\hat{F}$
M_d
$\tau_{m,FF}$
965 Determining a transmission torque error correction motor torque
$\hat{\tau}_J$
$\tau_{J,d}$
$\tau_{m,torque-err}$
966 Determining a error correction motor torque
Θ
q
τ_{motor}
$\tau_{m,err}$
967 Determining a resulting motor torque
$\tau_{m,FF}$
$\tau_{m,torque-err}$
$\tau_{m,err}$
τ_r
968 Generating motor control current
τ_r
i_{motor}
$i_{control}$

FIG. 9

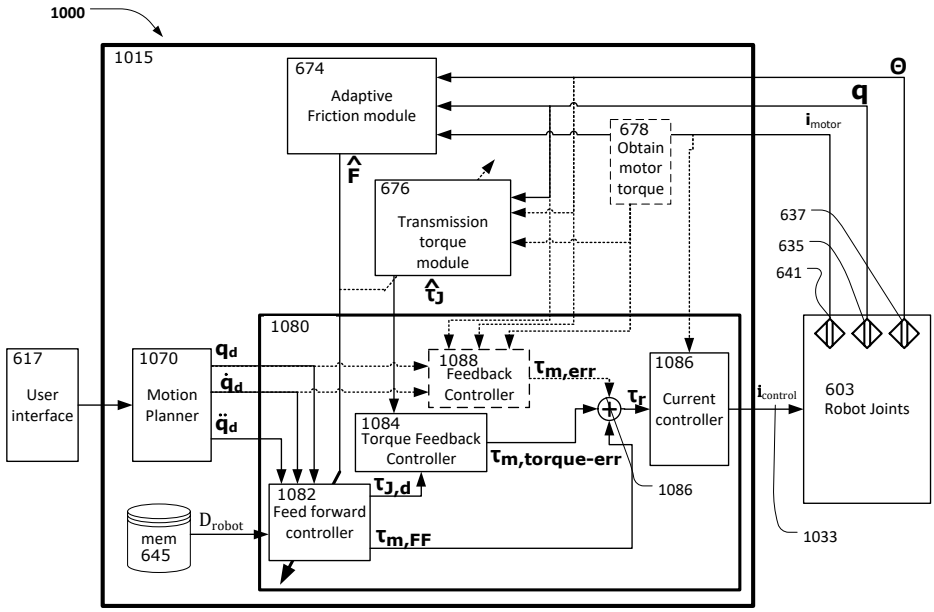
1000
1015
674
Adaptive
Friction module
678
Obtain
motor
torque
676
Transmission
torque
module
637
635
641
1080
617
User
interface
1070
Motion
Planner
1088
Feedback
Controller
1086
Current
controller
603
Robot Joints
1084
Torque Feedback
Controller
1086
1082
Feed forward
controller
mem
645
1033

FIG. 10

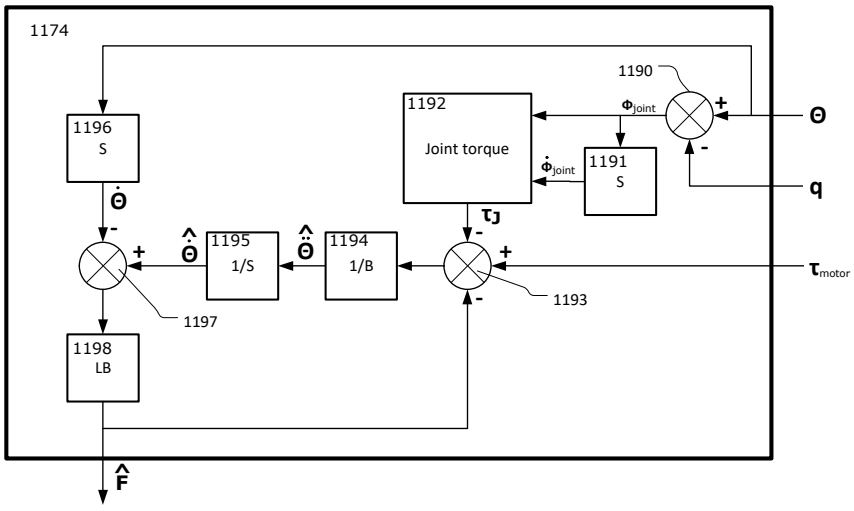
1174
1190
1192
Joint torque
1191
S
1196
S
1195
1/S
1194
1/B
1193
1197
1198
LB
Θ
q
τ_motor
τ_J
Φ_joint
10/10

FIG. 11

PhD Dissertation
Author: Emil Madsen

Supervisor: Xuping Zhang
Department of Engineering
Aarhus University, Denmark

Company Supervisor: David Brandt
Company Co-Supervisor: Oluf Skov Rosenlund
Universal Robots A/S, Denmark